JAERI-Data/Code
97-043

LIGHT WATER REACTOR FUEL ANALYSIS CODE FEMAXI-IV (VER. 2) —DETAILED STRUCTURE AND USER'S MANUAL—

November 1997

Motoe SUZUKI and Hiroaki SAITOU*

日本原子力研究所
Japan Atomic Energy Research Institute

本レポートは，日本原子力研究所が不定期に公刊している研究報告書です。
入手の問合わせは，日本原子力研究所研究情報部研究情報課（〒319-11　茨城県那珂郡東海村）あて，お申し越しください。なお，このほかに財団法人原子力公済会資料センター（〒319-11　茨城県那珂郡東海村日本原子力研究所内）で複写による実費頒布をおこなっております。

This report is issued irregularly.
Inquiries about availability of the reports should be addressed to Research Information Division, Department of Intellectual Resources, Japan Atomic Energy Research Institute, Tokai-mura, Naka-gun, Ibaraki-ken 319-11, Japan.

編集兼発行　日本原子力研究所
印　　刷　㈱高野高速印刷

JAERI－Data/Code 97－043

Light Water Reactor Fuel Analysis Code FEMAXI-IV(Ver.2) —Detailed Structure and User's Manual—

Motoe Suzuki and Hiroaki Saitou*

Department of Reactor Safety Research
Nuclear Safety Research Center
Tokai Research Establishment
Japan Atomic Energy Research Institute
Tokai-mura, Naka-gun, Ibaraki-ken

(Received October 8, 1997)

A light water reactor fuel behavior analysis code FEMAXI-IV(Ver.2) was developed as an improved version of FEMAXI-IV.

Development of FEMAXI-IV has been already finished in 1992, though a detailed structure and input manual of the code have not been open to users yet.

Here, the basic theories and structure, the models and numerical solutions applied to FEMAXI-IV(Ver.2), and the material properties adopted in the code are described in detail.

In FEMAXI-IV(Ver.2), programming bugs in previous FEMAXI-IV were eliminated, renewal of the pellet thermal conductivity was performed, and a model of thermal-stress restraint on FP gas release was incorporated.

For facilitation of effective and wide-ranging application of the code, methods of input/output of the code are also described in detail, and sample output is included.

Keywords: LWR, Fuel, FEM, Pellet, Cladding, PCMI, Cladding, PCMI, FP Gas Release

*CRC Research Institute Inc.,

軽水炉燃料解析コードFEMAXI-IV(Ver.2)
—詳細構造とユーザーズマニュアル—

日本原子力研究所東海研究所安全性試験研究センター原子炉安全工学部
鈴木　元衛・斉藤　裕明*

(1997年10月8日受理)

軽水炉燃料のふるまい解析コードFEMAXI-IVの改良バージョンとしてFEMAXI-IV(Ver.2)を開発した。FEMAXI-IVは、開発が1992年に既に終了しているが、その詳細構造及び入力マニュアルはユーザーに未公開であった。

本報告は、FEMAXI-IV(Ver.2)の基本理論と構造、モデルと数値解法、採用した物性値を詳述したものである。FEMAXI-IV(Ver.2)では、バグフィックスがされ、ペレット熱伝導率の更新および熱応力によるFP放出抑制モデルの追加がされた。さらに、本コードの有効かつ広範な利用を可能とするため、入出力の種類と方法を詳しく説明し、具体的なサンプル出力を添えた。

東海研究所：〒319-11　茨城県那珂郡東海村白方白根2－4
*CRC総合研究所

Contents

目　　次

1. Introduction

Light water reactors are currently expected to serve as major facilities for nuclear power generation for quite a long period. Therefore it is important to ensure the reliability of fuel rods, and a fuel behavior analysis code is one of the indispensable tools.

Development of a fuel behavior analysis code FEMAXI-IV[1], which is an extended version of FEMAXI-III[2], has been already finished in 1992, though a detailed description of the code has not been open to users yet. FEMAXI-IV has been evaluated for its prediction performance using data from the Battelle High Burnup Experiment Program and Halden Project, etc[1),(3)-(9)].

Thereafter, FEMAXI-IV(ver.2) was developed as an improved version of FEMAXI-IV.

Here, in addition to the explanation of improvements in FEMAXI-IV(ver.2), the present report describes the structure and methods that have been inherited to the ver.2 as a basic frame from FEMAXI-IV.

1.1 Outline of the Code

FEMAXI-IV analyzes the thermal and mechanical behavior of a single fuel rod in the steady and transient states, while accident conditions are not within the scope of analysis of the code. The transient states include power ramp and load-following operation, etc.

In the present Ver. 2 of FEMAXI-IV, facilitation of use has been greatly enhanced by the following improvements and by this manual which describes details of the structure and input/output method.

(1) Bug elimination

Programming bugs have been eliminated throughout the code.

(2) Pellet material properties

Thermal conductivity of UO_2 pellet decreases with burnup. Therefore, we have adopted some representative empirical equations for the burnup dependence of pellet thermal conductivity. In addition, the empirical equations representing densification and swelling of

pellet have been modified, and the hot-press* model has been improved.

(* Shrinkage of a porous pellet caused by static pressure.)

(3) Model of thermal-stress restraint on FP gas release

Upon an increase in the power, thermal stress is generated inside the pellet. Recent findings have revealed that the FP gas release behavior is affected by this stress generation. A model of this phenomenon has been incorporated in the Ver.2.

(4) Others

Additional input parameters and a function to simulate changes in the gas composition inside the fuel rod have been installed. In addition, the input data format has been improved.

Table 1.1 lists the phenomena analyzed by the code. Material properties adopted in the present code are obtained from as many literatures as available.

MOX fuels and UO_2 fuels containing Gd can be analyzed by designating materials properties.

Table 1.1 Phenomena analyzed by FEMAXI-IV.

	Thermal process determining temperature distribution	Process with mechanical displacement
Pellet	Thermal conduction (depending on flux distribution) FP gas release (depending on temperature and burnup level)	Thermal expansion, elasticity, plasticity, creep, cracking, initial relocation, densification, swelling (solid FP, gas bubble), hot-press
Cladding	Thermal conduction	Thermal expansion, elasticity, plasticity, creep, irradiation growth in the axial direction
Fuel rod	Gap thermal conduction (mixed gas, contact, radiation), cladding surface heat transfer, gap gas flow	Mechanical interaction between pellet and cladding, friction

1.2 Basic structure

(1) Whole structure

FEMAXI-IV consists of two parts: one for analyzing the temperature distribution, thermally induced deformation, and FP gas release etc. (hereafter called "thermal analysis part"), and the other for analyzing the mechanical behavior of the fuel rod (hereafter called

"mechanical analysis part"). Figure 1.1 outlines the entire code structure.

In the thermal analysis part, calculation always covers an entire length of a fuel rod. Namely, the temperature distribution is calculated as a one-dimensional axisymmetrical problem in the radial direction, in which the change in gap width between pellet and cladding, FP gas release, gap gas flow in the axial direction, and their feedback effects on gap thermal conduction are analyzed. For analysis of the power distributions in the axial direction, a fuel rod is divided into a maximum of 12 axial segments, and iteration is performed until thermal feedback among these segments converges for the entire length of the rod.

In the mechanical analysis part, users can select either analysis of the entire length of a fuel rod, or analysis of one pellet length. In the former, the axisymmetrical finite element method (FEM) is applied to the entire length of the rod; in the latter, the axisymmetrical FEM is applied to half the pellet length, and mechanical interaction between pellet and cladding is analyzed.

In the mechanical analysis, the magnitude of pellet strain caused by thermal expansion, densification, swelling and relocation is calculated first, and a stiffness equation is formulated with consideration given to cracking, elasticity/plasticity and creep of pellet.

Then, stress and strain of pellet and cladding are calculated by solution of the stiffness equation with boundary conditions corresponding to the pellet-cladding contact mode. When pellet-cladding mechanical interaction occurs and states of pellet-cladding contact change, calculation is re-started with the new boundary conditions of contact from the time when the change occurs.

In the analysis of the entire length of a fuel rod, evaluation is possible for the axial force on a lower axial segment which is in contact with an upper segment. Also, the finite element method used is simplified to reduce the total number of degrees of freedom.

(2) Method treating the inter-dependency between thermal analysis and mechanical analysis

As stated above, FEMAXI-IV consists of the thermal analysis part and mechanical analysis part. Since temperature and stress/strain and displacement distributions obtained from the two analysis parts physically depend on each other, strictly speaking, simultaneous

equations of thermal conduction and mechanical deformation should be solved.

For example, in order to obtain convergence in the calculation of the temperature distribution of a pellet in the thermal analysis part, it is necessary to introduce the mechanical analysis to predict gap width into the calculation of gap thermal conduction.

Accordingly, introduction of the mechanical analysis into the convergence calculation loop is required. Therefore, a model which can perform the gap width calculation within a short time is desired to facilitate the large number of iterations.

Meanwhile, it is almost impossible to perform detailed stress/strain and displacement analysis, which is the original objective of the mechanical analysis part, within a short time.

To avoid this contradiction, the mechanical analysis part of FEMAXI-IV is divided into two parts. One is a detailed mechanical analysis part which is used for an accurate prediction of stress/strain and displacement distribution, and the other is a simple mechanical analysis part which is developed to solve simultaneous equations of the relationship between temperature and stress/strain required in the thermal analysis part.

These two mechanical analysis parts use common material properties and empirical equations. Results of the analyses are not necessarily identical, but the overall tendencies are quite similar, and the absence of problems which might appear in estimation of temperature, stress/strain, and displacement distribution is confirmed.

The method of the simple mechanical analysis part is explained in section 2.1.3, Contact-force estimation model. The method of the detailed mechanical analysis part is explained in section 2.2, Mechanical Behavior over Entire Length of Fuel Rod (Analysis I), and in section 2.3, Local Mechanical Behavior (Analysis II).

1.3 Features of numerical method and modelling

The main features of the code are as follows.

(1) FEM element characteristics

Storage region and calculation time are reduced by introduction of rectangular 3-degrees-of-freedom elements into the FEM analysis in order to perform mechanical calculation for the

entire length of the fuel rod.

(2) Creep solution

Through use of an implicit procedure, the numerical solution stability for high creep rate is improved.

(3) Matrix solution

The coefficient matrix of simultaneous equations of the FEM (stiffness equations) is a diagonal symmetrical matrix having a large number of zero elements, as shown in the figure below. Therefore, the skyline method has been adopted to solve the equations, and the memory method of nonzero elements in the matrix, as well as the calculation procedure, has been improved, in order to reduce the size of the storage region and calculation time.

In the skyline method, only the elements under the solid line in the figure below are stored. In the FP gas release model, the procedure has been improved so that the number of computing steps for the matrix becomes a minimum.

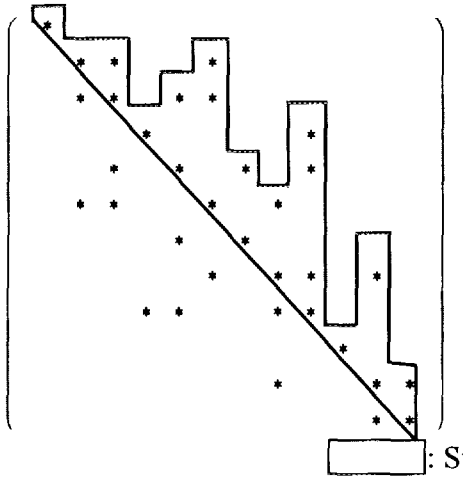

*: Nonzero element

: Storage region in the skyline method

(4) Nonequilibrium residue

In order to avoid accumulation of non-equilibrium residue generated at each time step during solution of a nonlinear problem, equilibrium condition equations are formulated not in an incremental manner but in a form which maintains the total balance of loads and stresses.

(5) Contact problem

Three contact states are dealt with as the contact conditions between pellet and cladding: open gap state, clogged gap state and sliding state. In the FEM, contact conditions at each

node pair of pellet and cladding are determined, and the boundary conditions are set in accordance with the conditions.

(6) Behavior of cracked pellet

Cracking of a pellet is modeled using a decreased stiffness approximation method, similar to the case for FEMAXI-III. In order to describe behavior of the cracked pellet which is relocated under PCI, recovery of the stiffness during compression is expressed as a function of the amount of relocation.

(7) FP gas release model

An equivalent sphere model is adopted to simulate the FP gas release. This model allows prediction outside the range of experimental data, which cannot be obtained by an empirical model.

(8) Gap gas diffusion–flow model

Gap gas-diffusion flow is modeled, and effects of the released FP gas on gap thermal conductance are carefully evaluated.

(9) Nonsteady phenomena analysis

The fuel behavior in a nonsteady state can be analyzed by mechanistic treatment of a nonsteady heat transfer model, gap gas flow model and FP gas release model. Also, the accuracy of prediction is improved and calculation time is reduced through use of independent time-step controls in each model.

(10) Simplification of calculation

In the FP gas release model, when the same type of calculations are performed both in a low-temperature region and a high-temperature region, calculation results obtained for elements in one region are used for calculation in another region in order to avoid carrying out similar calculations twice. Also, physical properties and other values which are frequently referred to are stored in a data table, and use of special mathematical functions is avoided.

By means of the above-mentioned procedures, FEMAXI-IV can give highly accurate solutions within a shorter calculation time.

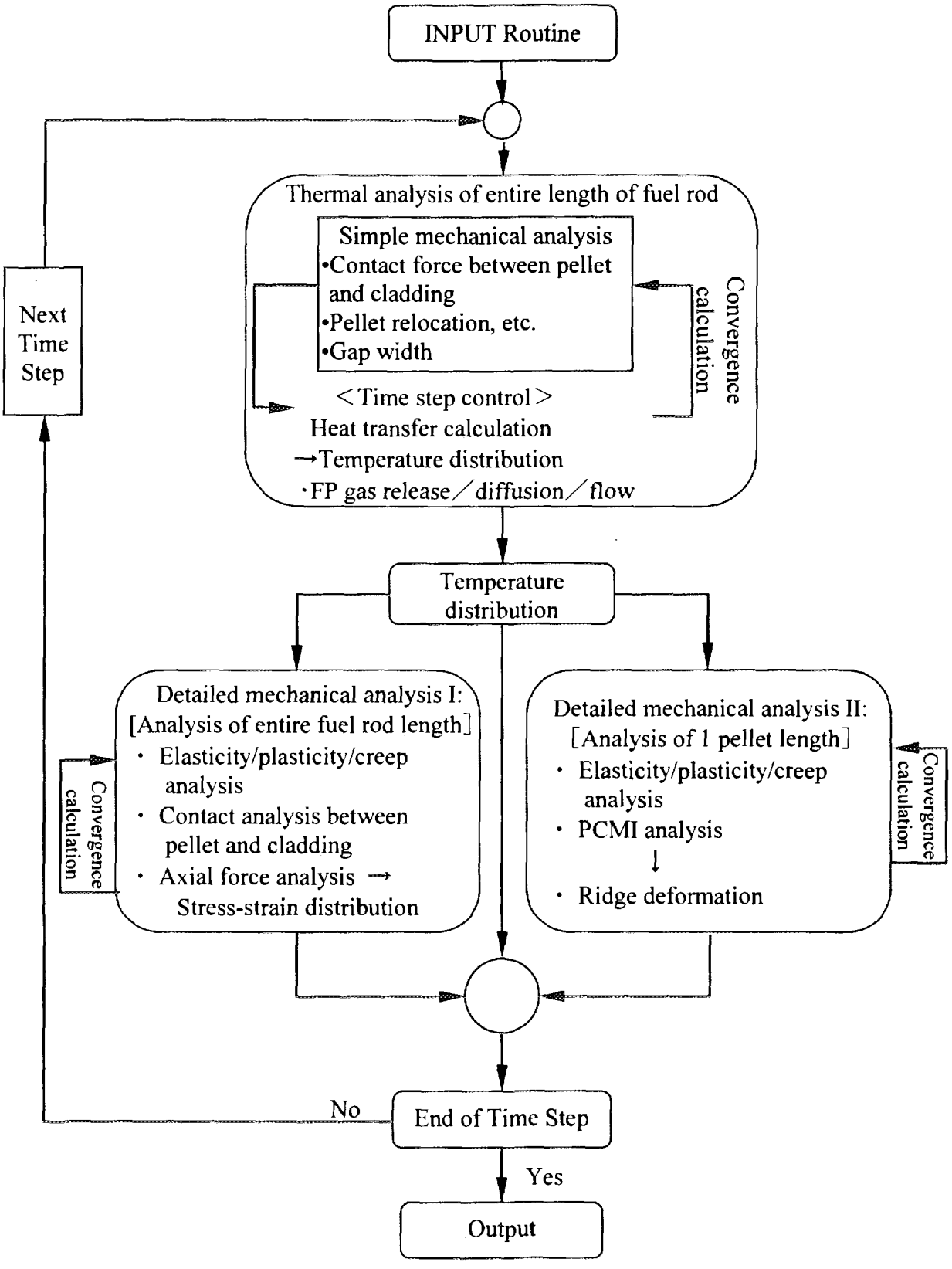

Fig. 1.1 Entire code structure of FEMAXI-IV

2. Analytical Theory and Functions

In this chapter, analytical theory and functions used in FEMAXI-IV are explained. The thermal analysis part is explained in section 2.1, the mechanical analysis part for the entire length of a fuel rod is explained in section 2.2, and the local mechanical analysis part is explained in section 2.3. Materials properties are described in section 2.4.

2.1 Thermal Behavior

In the thermal analysis part, temperature distribution of a fuel rod is calculated with the boundary condition determined by coolant temperatures. The basic assumption and calculation procedure are as follows.

(1) The temperature and state of coolant at every axial segment at current time step are calculated from the inlet temperature, inlet pressure, flow velocity, and heat flux from a fuel rod, independently from the coolant state progress by the former time step. While, in a strict sense, this method can hold only when fuel rod and coolant are in a steady state relationship, FEMAXI-IV applies this method not only to the steady state, but also to such transient states as power ramp and load following operation, because these transients are substantially slow enough to be approximated with a steady state model.

(2) Specifically, coolant temperature at each axial segment is calculated from the coolant temperature at the lower adjacent segment and the coolant temperature rise which is given by the thermal power, i.e. heat flux, generated at the lower segment. This calculation begins with the inlet coolant temperature. Thus, the coolant temperature distribution in the axial direction is determined.

(3) Cladding surface temperature is calculated by the cladding surface heat transfer model using the coolant temperature as a starting point.

(4) The temperature distribution in the area between the center of the pellet and the cladding surface is calculated using a one-dimensional finite difference method in the radial direction, with the results of (3) as boundary conditions.

(5) Axial heat conduction of a fuel rod is neglected. Heat conduction caused by the axial power difference of the rod is substantially limited by such thermal resisitance as dish or gap in the pellet end surface, so that axial temperature gradient is much smaller in comparison with the radial gradient inside the pellet.

The above-mentioned methods will be explained in section 2.1.1. Such models determining temperature distribution in the radial direction, as a gap thermal conduction model, contact force model and FP gas release model, will be described in sections 2.1.2, 2.1.3, and 2.1.4, respectively.

2.1.1 Temperature distribution

(1) Fuel rod surface heat transfer model

(1)-1 Assumptions and methods

Enthalpy is used as a primary variable in the calculation of the coolant temperature distribution, taking into consideration the phase change of water. Calculation is performed in terms of either single-phase flow (subcooled water) or two-phase flow (nucleate boiling state). The basic assumptions and methods are:

① Regarding the increase in coolant enthalpy, a steady-state model is applied in accordance with the above assumption(1). Here, it is not required that inlet temperature and flow velocity be uniform throughout the analysis period, but they can be input as time-dependent variables.

② State variables are calculated by interpolation from data obtained from the simplified steam table which is incorporated in the code.

③ Pressure and mass flow rate are assumed to be constant in the axial direction. Slip between steam and water is assumed to be zero.

(1)-2 Enthalpy of the coolant

In the system defined as shown in Fig. 2.1 based on the above assumptions, enthalpy of the coolant (water or steam) is sequentially obtained using the equation below, starting from the inlet.

$$h_{n+1} - h_n = \frac{2\pi r \overline{\phi}_n l_n}{GS} \tag{2.1.1}$$

Here,

h_n : specific enthalpy of node n (J/kg)

r : outer radius of fuel rod (m)

l_n : length of axial segment n (m)

G : mass flow rate $(=\rho v)$ $(kg/m^2 \cdot s)$

S : flow area (cross-sectional area of channel) (m^2)

$\overline{\phi_n}$: heat flux of axial segment n $(J/m^2 \cdot s)$.

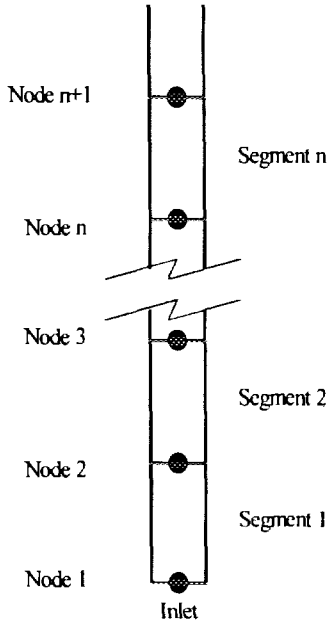

Fig. 2.1 Model system.

A flowchart of the calculation is shown in Fig. 2.2, where 'representative entahlpy of each segment' is the average value of the two enthalpies at upper and lower nodes of one segment.

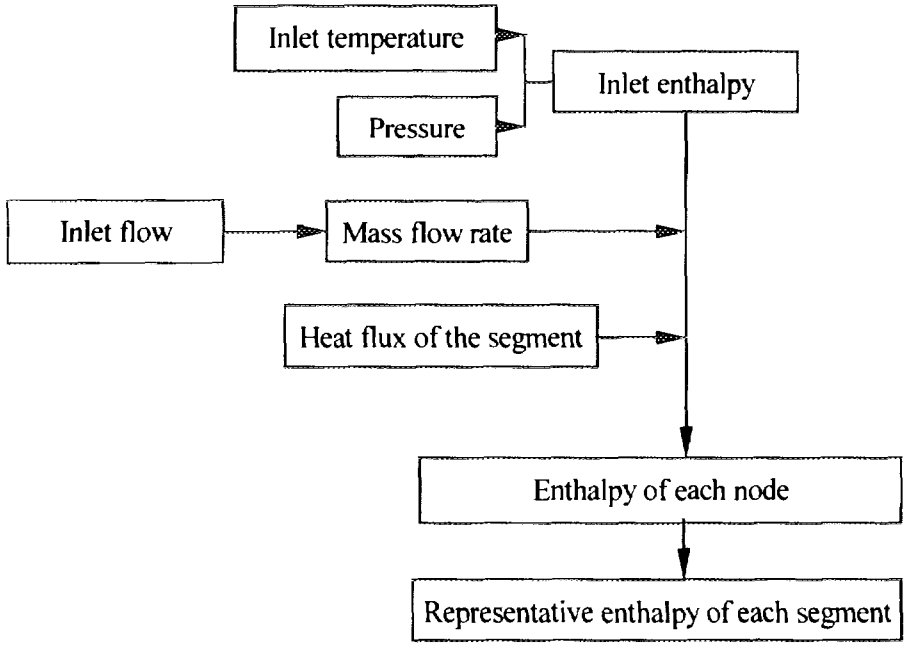

Fig. 2.2 Calculation flowchart.

(1)-3 Calculation of state quantities using the steam table

State quantities required in the calculation described in (1)-2 and in the heat transfer

calculation to be described in (1)-4 are specific enthalpy, specific volume, viscosity coefficient, heat transfer coefficient, and Prandtl number.

Regarding the coolant states in FEMAXI-IV, subcooled water and a two-phase region close to liquid phase are considered. The latter is indicated by hatched area of Fig.2.3

The calculation method is explained below, where T is temperature, P is pressure and h is enthalpy.

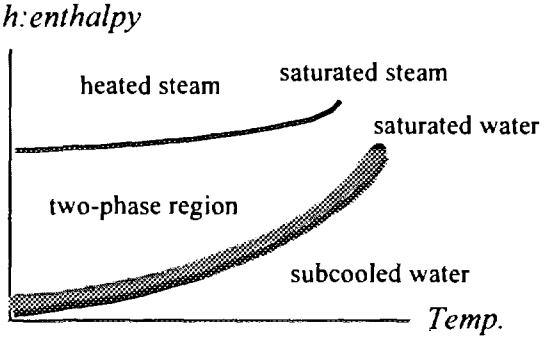

Fig. 2.3 Relationship among status of coolant water.

[1] Enthalpy and temperature

The enthalpy of the subcooled water depends weakly on pressure, but changes significantly with substantial change in pressure. Therefore, in the table showing $h(P,T)$ in subcooled regions, data are obtained for a large pressure interval of 30 atm, and used for interpolation as follows.

① Calculation of inlet enthalpy h from T and P

1) Determination of the state

First, saturation temperature T_s is obtained by interpolation from data in a $T_s(P)$ diagram in terms of coolant pressure, and it is compared with water temperature T. Here, the $T_s(P)$ diagram is constructed for the pressure range of 1 bar to 180 bar.

2) Calculation of enthalpy

a. In the case of $T<T_s$ (subcooled water)

Using the $h(P,T)$ table (T: 20°C, P: 30 atm intervals), h is obtained by interpolation from the first constant pressure datum which is higher than the coolant pressure at T (interpolation is not performed in terms of pressure).

b. In the case of $T=T_s$ (two-phase state, within an allowable range of $T_s \pm 0.1$°C)

Even though this is a two-phase state, the enthalpy of the saturated water in the water phase is assumed to be $h=h_f$.

c. In the case of $T>T_s$ (overheated steam)

Overheated steam is not in the analysis range of FEMAXI-IV. When $T>T_s$ +0.1°C, execution of the program is terminated.

② Calculation of T from P and h (calculation of representative temperature of each segment)

After the enthalpy of each axial elevation is obtained using eq. (2.1.1), a representative enthalpy h of axial segment n is obtained as $h = \frac{1}{2}(h_n + h_{n+1})$.

1) Determination of the state

Enthalpies of saturated water h_f and saturated steam h_g are obtained by interpolation from data in $h_f(P)$ and $h_g(P)$ diagrams in terms of pressure, respectively. Here, $h_f(P)$ and $h_g(P)$ diagrams have a pressure range of 1 to 180 bar.

2) Determination of T

a. In the case of $h \leqq h_f$

In the $h(P,T)$ table (T: 20°C, P: 30 atm intervals), T is obtained by interpolation from the enthalpy datum for the P_l-row pressure which is the first value higher than P (interpolation is not performed in terms of pressure).

b. In the case of $h_f < h < h_g$ (two-phase region)

Water-phase temperature is adopted and $T=T_s$ is assumed.

[2] Other state variables

In FEMAXI-IV, density, viscosity coefficient, thermal conductivity and Prandtl number of water are used only in the Dittus-Boelter equation[10]. Since these quantities do not depend much on pressure, they are determined using data from the tables of $\rho_S(T)$, $\mu_S(T)$, $k_S(t)$ and $Pr_S(T)$ for saturated water. Data in these tables are obtained at 10°C intervals in terms of T.

Figures 2.4 through 2.10 show a $H_S(P)$ diagram, $T_S(P)$ diagram, and $h(P,T)$ diagram,

and density, viscosity coefficient, thermal conductivity and Prandtl number of water, respectively. In these diagrams, data represented by open triangles (△) correspond to data in the table of material properties incorporated in FEMAXI-IV.

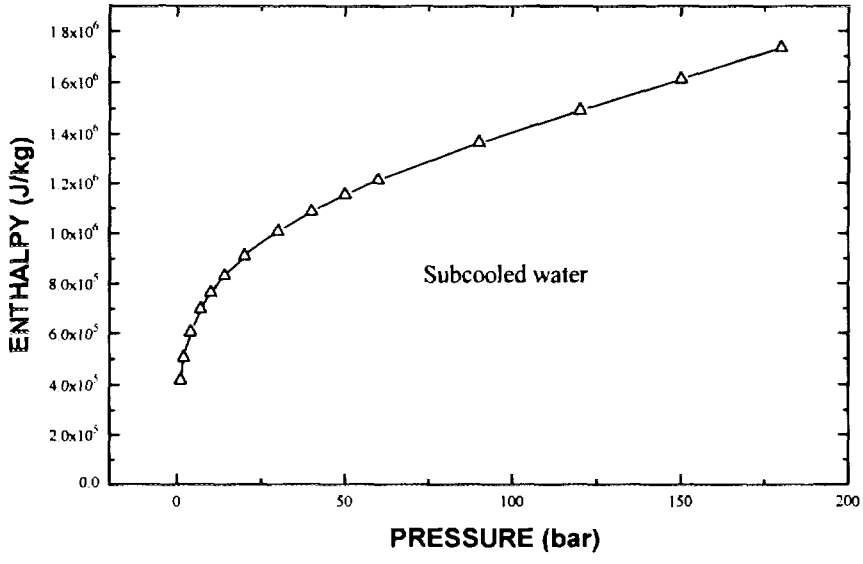

Fig. 2.4 $H_S(P)$ Diagram.

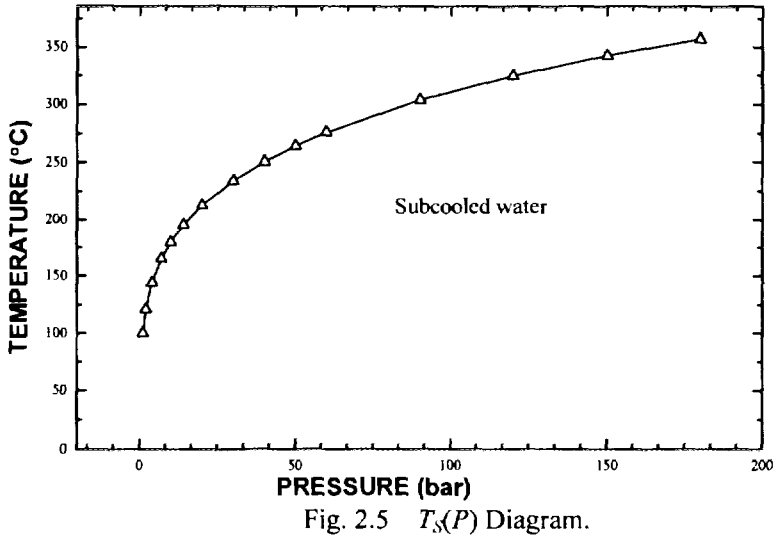

Fig. 2.5 $T_S(P)$ Diagram.

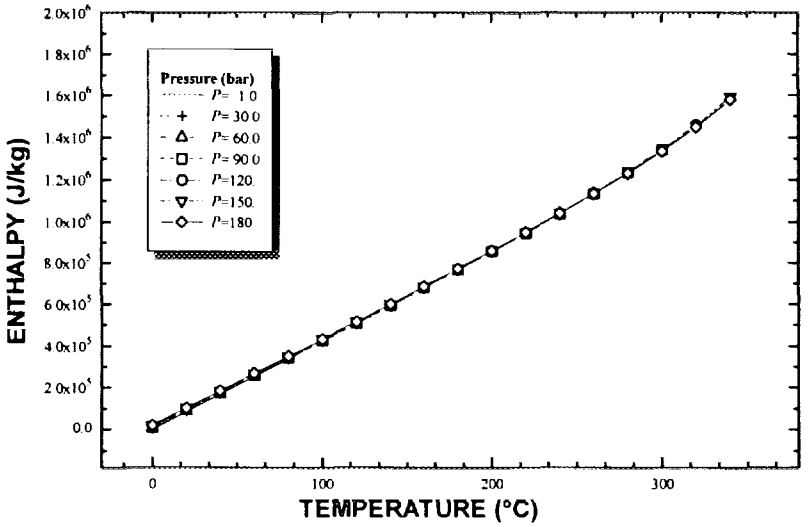

Fig. 2.6 $h(P,T)$ Diagram.

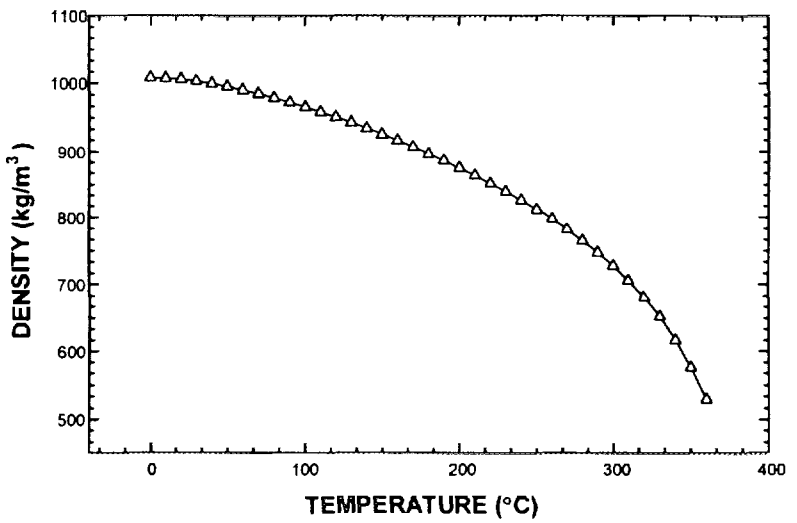

Fig. 2.7 Density of water.

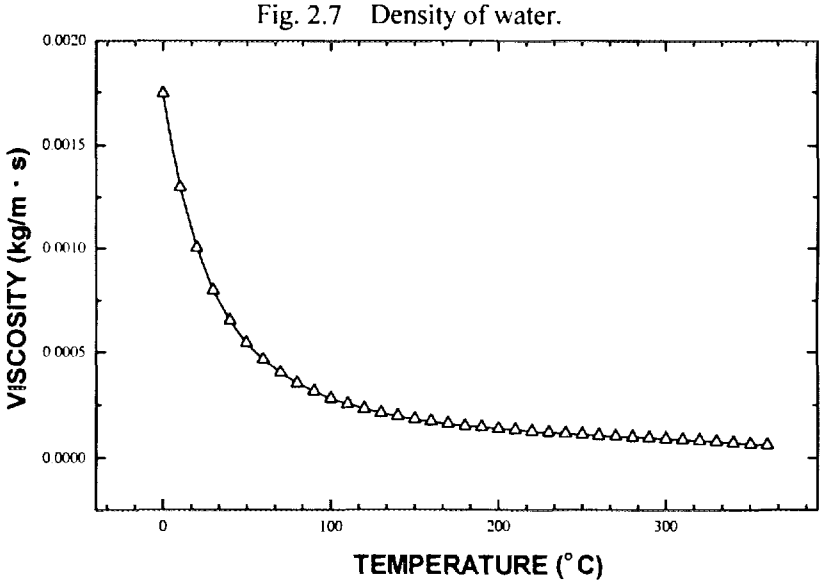

Fig. 2.8 Viscosity coefficient of water.

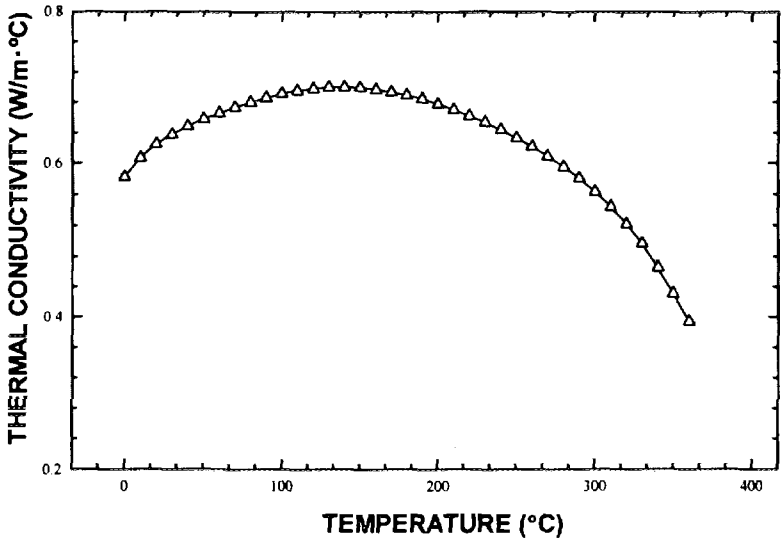

Fig. 2.9 Thermal conductivity of water.

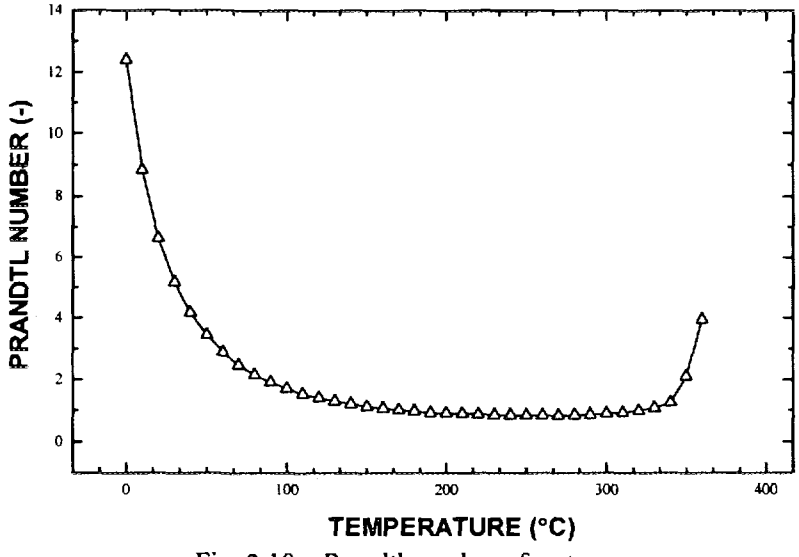

Fig. 2.10 Prandtl number of water.

(1)-4 Cladding surface temperature (heat transfer model)

In FEMAXI-IV, the following equation is obtained from the heat transfer differential equation for the fuel (see item (3)).

$$\phi_N = AT_N + B \tag{2.1.2}$$

Here,

ϕ_N : cladding surface heat flux (W/m^2)

T_N : cladding surface temperature (K)

N : mesh-point number of the cladding surface

A, B : coefficients obtained from heat transfer differential equation.

Surface temperature T_N can be obtained from eq. (2.1.2), the Dittus-Boelter equation[10] regarding the cladding surface heat transfer coefficient (see item (1)-5) and the Jens-Lottes equation[11] (see (1)-5). A method of obtaining T_N for each state of the coolant is described below.

[1] Subcooled state 1 (cladding surface temperature < saturation temperature)

In this case, the Dittus-Boelter equation shown as eq. (2.1.14) is used. When the coolant temperature is T_B, heat flux of the cladding surface is obtained as:

$$\phi_N = h_W (T_N - T_B) \tag{2.1.3}$$

Here,

ϕ_N : cladding surface heat flux (W/m^2)

h_W : heat transfer coefficient obtained by the Dittus-Boelter equation ($W/m^2 \cdot K$)

T_N : cladding surface temperature (K)

T_B : coolant temperature (K).

T_N is obtained by eliminating ϕ_N from eqs. (2.1.2) and (2.1.3).

[2] Subcooled state 2 (cladding surface temperature > saturation temperature)

T_N is obtained by simultaneously solving the heat transfer equation for subcooled water and the heat transfer equation for the two-phase state. Cladding surface heat flux ϕ_N can be obtained as the sum of the heat flux ϕ_{N1} of the subcooled state heat transfer and ϕ_{N2} of the two-phase state heat transfer,

$$\phi_N = \phi_{N1} + \phi_{N2}. \tag{2.1.4}$$

Heat flux ϕ_{N1} of the subcooled state can be expressed as follows, using the heat transfer coefficient h_{W1} obtained from the Dittus-Boelter equation (eq. (2.1.14)).

$$\phi_{N1} = h_{W1} (T_N - T_B) \tag{2.1.5}$$

Similarly, heat flux ϕ_{N2} of the two-phase state can be expressed using the Jens-Lottes equation shown as eq. (2.1.15). Here, in eq. (2.1.15), heat transfer coefficient h_{W2} is given as a function of ϕ_{N2}. Accordingly, when eq. (2.1.15) is simply expressed as $h_{W2} = \alpha^* \phi_{N2}^{3/4}$,

the term ϕ_{N2} can be expressed as

$$\begin{aligned}\phi_{N2} &= h_{W2}(T_N - T_S) \\ &= \alpha^* \phi_{N2}^{3/4}(T_N - T_S).\end{aligned} \tag{2.1.6}$$

Solving this equation in terms of ϕ using

$$\begin{aligned}\phi_{N2}^{1/4} &= \alpha^*(T_N - T_S) \\ \phi_{N2} &= \alpha^{*4}(T_N - T_S)^4,\end{aligned}$$

we obtain

$$\phi_{N2} = \alpha(T_N - T_S)^4, \quad \alpha = \alpha^{*4}. \tag{2.1.7}$$

By substituting eqs. (2.1.5) and (2.1.6) into eq. (2.1.4), the following equation for T_N is obtained.

$$AT_N + B = h_{W1}(T_N - T_B) + \alpha(T_N - T_S)^4 \tag{2.1.8}$$

In FEMAXI-IV, eq. (2.1.8) is converted to be solved by Newton's method.

Terms in eq. (2.1.8) are transpositioned as

$$(A - h_{W1})T_N + B + h_{W1}T_B = \alpha(T_N - T_S)^4.$$

Here, $\tilde{T} = T_N - T_S$, $T_N = \tilde{T} + T_S$, and the following equations hold.

$$\begin{aligned}&(A - h_{W1})(\tilde{T} + T_S) + B + h_{W1}T_B = \alpha\tilde{T}^4 \\ &(A - h_{W1})\tilde{T} + (A - h_{W1})T_S + B + h_{W1}T_B = \alpha\tilde{T}^4\end{aligned} \tag{2.1.9}$$

By setting

$$a = (A - h_{W1})/\alpha, \quad b = \{(A - h_{W1})T_S + B + h_{W1}T_B\}/\alpha\ , \tag{2.1.10}$$

the equation for $\tilde{T}$ holds as follows.

$$a\tilde{T} + b = \tilde{T}^4 \tag{2.1.11}$$

By solving this equation to obtain $\tilde{T}$ using Newton's method and substituting the result into

$$T_N = \tilde{T} + T_S\ , \tag{2.1.12}$$

T_N is obtained.

[3] Two-phase state

Since the coolant temperature is saturated in the two-phase state, using the heat transfer coefficient h_W of the Jens-Lottes eq. (2.1.14), the following equation holds.

$$\phi_N = h_W (T_N - T_S) \tag{2.1.13}$$

Here,

ϕ_N : cladding surface heat flux (W/m^2)

h_W : heat transfer coefficient obtained from the Jens-Lottes equation (W/m^2・K)

T_N : cladding surface temperature (K)

T_S : saturation temperature (K).

T_N is obtained by eliminating ϕ_N from eqs. (2.1.2) and (2.1.13).

(1)-5 Cladding surface heat transfer coefficient

Dittus-Boelter equation[10]

$$h_W = 0.023 \frac{k}{D_e} \left(\frac{D_e V \rho}{\mu} \right)^{0.2} Pr^{0.4} \tag{2.1.14}$$

k : coolant water thermal conductivity (W/m・K)

D_e : equivalent diameter (m)

V : coolant water velocity (m/s)

ρ : coolant water density (kg/m^3)

μ : coolant water viscosity (kg/m・s)

Pr : Prandtl number

The equivalent diameter D_e will be explained in section (1)-7.

Jens-Lottes empirical equation[11]

$$h_W = 0.1263 \cdot \exp\left(\frac{P_W}{6.201 \times 10^6} \right) \phi_N^{0.75} \tag{2.1.15}$$

h_W : surface heat transfer coefficient (W/cm^2・K)

P_W : coolant water pressure (N/m^2)

ϕ_N : cladding outer surface heat flux (W/cm^2)

Fitting parameter AKFAC

The cladding surface heat transfer coefficient is adjusted using the following equation. $h_W = h_W \times AKFAC$

(1)-6 Flowchart of the heat transfer analysis:

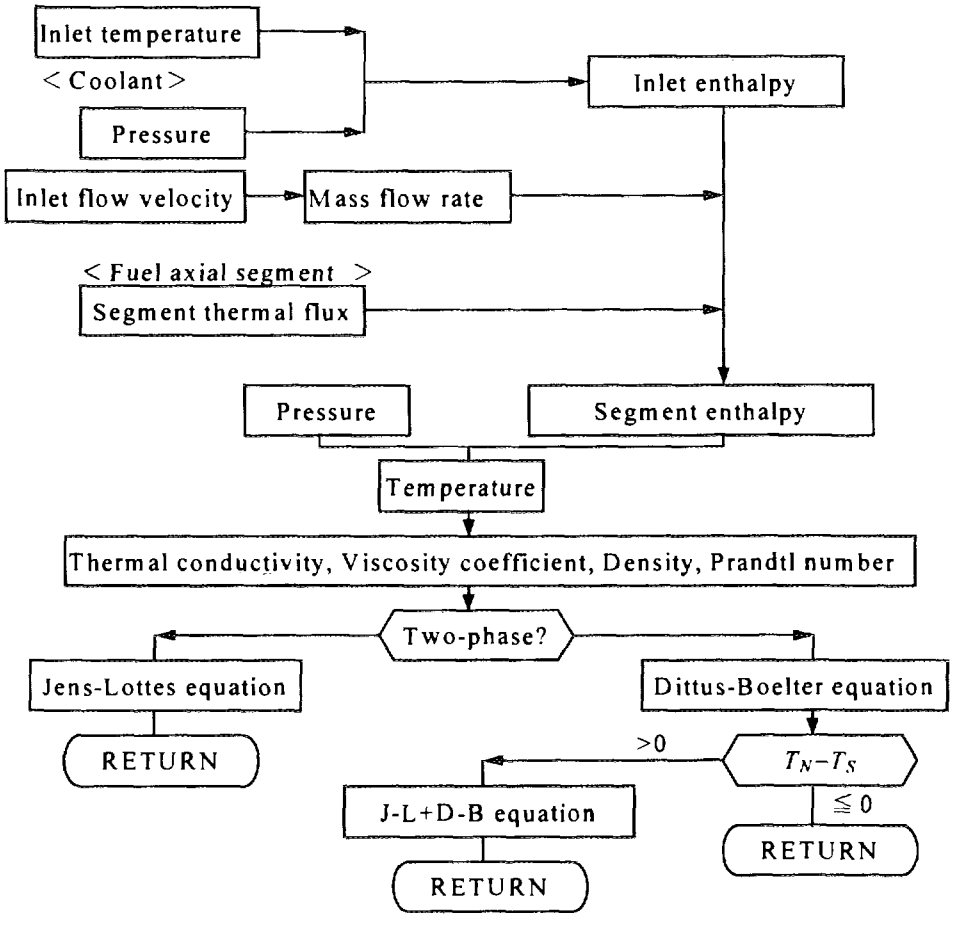

Fig. 2.11 Flowchart of the heat transfer analysis

(1)-7 Equivalent diameter and cross-sectional area of flow channel

Equivalent diameter and cross-sectional area of the coolant flow channel are the parameters required for obtaining cladding surface temperature. The equivalent diameter D_e is the diameter of a virtual column when the shape of a coolant channel around the fuel rod is converted to a column. D_e is used in eq. (2.1.14) to determine the cladding surface heat transfer coefficient, and the cross-sectional area of the channel is used in eq. (2.1.1) to calculate the enthalpy of each axial node.

Usually these two parameters are directly set by input; in the case that one of them is not set or none of them is set, a method of converting one value to the other or of calculating both values using the pitch between fuel rods is incorporated in FEMAXI-IV. These methods are explained below.

[1] Equivalent diameter of the channel

1) When D_e is specified by input data, the input value is used.

2) When D_e is not input but the cross-sectional area of the channel is input, D_e is obtained

using

$$D_e = \frac{4S}{2\pi\bar{r}}, \tag{2.1.16}$$

where

S : cross-sectional area of the channel,

$\bar{r}$: fuel rod outer radius.

3) When neither the equivalent diameter D_e nor the cross-sectional area S is input, these values are calculated using the pitch between fuel rods. Assuming channel ③ in Fig. 2.12, S is given by

$$S = 4l^2 - \pi\bar{r}^2, \tag{2.1.17}$$

where l is half of the pitch between fuel rods.

D_e is calculated using eq. (2.1.16) after obtaining S.

[2] Cross-sectional area of the channel, S

1) When S is specified by input data, the input value is used.

2) When S is not input but D_e is input, S is obtained using the following equation.

$$S = \frac{2\pi\bar{r}D_e}{4} \tag{2.1.18}$$

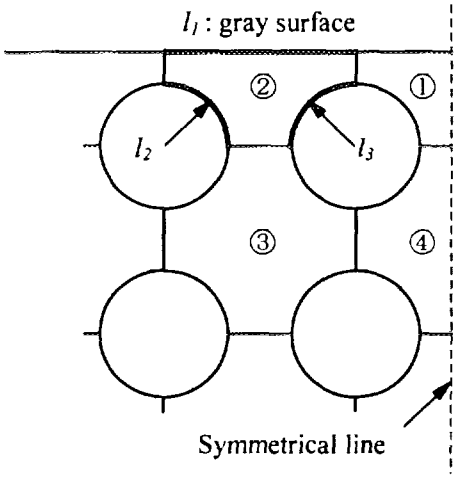

Fig. 2.12 Channel model.

3) When neither D_e nor S is input, S is calculated from eq. (2.1.17) using the pitch between fuel rods.

Input values
Cross-sectional area of the channel, equivalent diameter of the channel and pitch between fuel rods are input as the following variables. PITCH ···Pitch between fuel rods (cm) FAREA···Cross-sectional area of the channel (cm^2) DE ···Equivalent diameter of the channel (cm)

(2) One-dimensional radial-direction temperature model

In the analysis of radial temperature gradient at each axial segment, one-dimensional radial-direction thermal conduction equations are used, while the thermal conduction in the axial direction is neglected. It is assumed that the thermal properties of the fuel at each mesh are dependent on temperature, and that the gap heat transfer coefficient and cladding surface temperature change at each axial segment. The radial mesh divisions are the same

as those used in the mechanical analysis I. (See section 2.2, Figs.2.29 and 2.31)

Based on these assumptions, thermal conduction is described as follows.

$$\frac{\partial}{\partial t}\left[c_v(T,r)T(r,t)\right] = \nabla k(T,r)\cdot\nabla T(r,t) + q(r,t) \qquad (2.1.19)$$

Here,

T : temperature (K)

r : coordinate in the radial direction (m)

t : time (s)

C_v : volume specific heat (J/m^3)

k : thermal conductivity (W/m·K)

q : heat generation per unit volume ($J/m^3 \cdot s$).

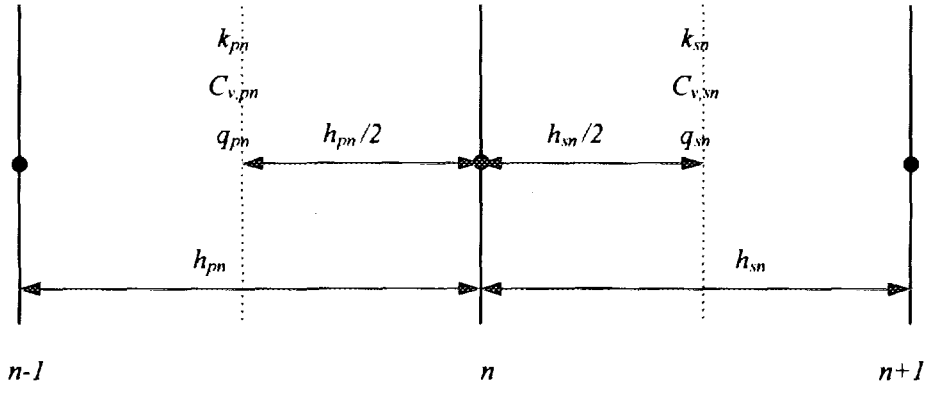

Fig. 2.13 Mesh model.

Volume integration is performed with eq. (2.1.19). Here, the volume to be integrated is the volume enclosed by the dotted lines in Fig. 2.13.

$$\iiint_V \frac{\partial}{\partial t} C_v(T,r)T(r,t)dV = \iiint_V \nabla k(T,r)\cdot\nabla T(r,t)dV + \iiint_V q(r,t)dV \qquad (2.1.20)$$

Since this is a one-dimensional problem, dimensions of the volume are set as 1 except for the radial direction. Eliminating the common factor 2π and using the forward finite difference method for time differentiation, the first term of eq. (2.1.20) is expressed as

$$\iiint_V \frac{\partial}{\partial t}\left[C_v(T,r)T(r,t)\right]dV \approx \iiint_V C_v(T,r)\frac{\partial T}{\partial t}(r,t)dV$$
$$\approx \frac{\left(T_n^{m+1}-T_n^m\right)}{h_{pn}}\left[C_{v,pn}\frac{h_{pn}}{2}\left(r_n-\frac{h_{pn}}{4}\right)+C_{v,sn}\frac{h_{sn}}{2}\left(r_n+\frac{h_{sn}}{4}\right)\right], \tag{2.1.21}$$

where T_n^m is the temperature at coordinate r_n and time t_m, and T_n^{m+1} is the temperature at coordinate r_n and time t_{m+1}. The second term of eq. (2.1.20) is expressed as

$$\iiint_V \nabla k(T,r)\cdot\nabla T(r,t)dV = \iint_S k(T,r)\nabla T(r,t)\cdot d\vec{S}$$
$$\approx -\frac{k_{pn}\left(T_n^{m+1/2}-T_{n-1}^{m+1/2}\right)}{h_{pn}}\left(r_n-\frac{h_{pn}}{2}\right)+\frac{k_{sn}\left(T_{n+1}^{m+1/2}-T_n^{m+1/2}\right)}{h_{sn}}\left(r_n+\frac{h_{sn}}{2}\right). \tag{2.1.22}$$

Here, continuous conditions of the heat flux at the inner boundary are used for evaluation of the plane integration along the boundary surface.

The following terms are defined.

$$h_{pn}^V=\frac{h_{pn}}{2}\left(r_n-\frac{h_{pn}}{4}\right),\quad h_{sn}^V=\left(r_n+\frac{h_{sn}}{4}\right)$$
$$h_{pn}^S=\frac{1}{h_{pn}}\left(r_n-\frac{h_{pn}}{2}\right),\quad h_{sn}^S=\frac{1}{h_{sn}}\left(r_n+\frac{h_{sn}}{2}\right) \tag{2.1.23}$$
$$D_n=C_{v,pn}h_{pn}^V+C_{v,sn}h_{sn}^V$$

Then the heat generation term $q(r,t)$ of the third term in eq. (2.1.20) is separated with variables as

$$q(r,t)=Q(r)P_f\,P(t).$$

Here, $Q(r)$ is the relative power distribution in the radial direction, P_f is the standard value of the heat generation density, and $P(t)$ is the relative change against time. Then the third term of eq. (2.1.20) is expressed as

$$\iiint_V q(r,t)dV \approx \left(Q_{pn}h_{pn}^V+Q_{sn}h_{sn}^V\right)P_f\,P\left(t_{m+1/2}\right). \tag{2.1.24}$$

By adding the right sides of eqs.(2.1.21), (2.1.22) and (2.1.24) which are approximate expressions of the terms in eq.(2.1.20), eq.(2.1.20) is converted into the difference approximation equation for the nth mesh point as follows.

$$\frac{\left(T_{n+1}-T_n^n\right)D_n}{\Delta t}=-\left(T_n^{m+\frac{1}{2}}-T_{n-1}^{m+\frac{1}{2}}\right)k_{pn}h_{pn}^s+\left(T_{n+1}^{m+\frac{1}{2}}-T_n^{m+\frac{1}{2}}\right)k_{sn}h_{sn}^s$$
$$+\left(Q_{pn}h_{pn}^V+Q_{sn}h_{sn}^V\right)P_fP\left(t_{n+\frac{1}{2}}\right) \tag{2.1.25}$$

Upon application of the Crank-Nicholson method to eq. (2.1.25), the following equation holds.

$$\frac{\left(T_n^{m+1}-T_n^m\right)D_n}{\Delta t}=\left(\frac{\left(T_n^{m+1}+T_n^m\right)}{2}-\frac{\left(T_{n-1}^{m+1}+T_{n-1}^m\right)}{2}\right)k_{pn}h_{pn}^s$$
$$+\left(\frac{T_{n+1}^{m+1}+T_{n+1}^m}{2}-\frac{T_n^{m+1}+T_n^m}{2}\right)k_{sn}h_{sn}^s \tag{2.1.26}$$
$$+\left(Q_{pn}h_{pn}^V+Q_{sn}h_{sn}^V\right)P_f\frac{P(t_{m+1})+P(t_m)}{2}$$

Here, T^{m+1} and T^m are obtained using the average temperature at mesh points n-1 and n, as well as the average temperature at mesh points n and n+1.

Through modification of eq. (2.1.26), the differential equation at mesh point n in the medium region is given as

$$a_nT_{n-1}^{m+1}+b_nT_n^{m+1}+c_nT_{n+1}^{m+1}=d_n^m,$$

where

$$a_n=-\frac{k_{pn}h_{pn}^s\Delta t}{2},\quad c_n=-\frac{k_{sn}h_{sn}^s\Delta t}{2}$$
$$b_n=D_n-a_n-c_n$$
$$d_n^m=-a_nT_{n-1}^m+\left(D_n+a_n+c_n\right)T_n^m-c_nT_{n+1}^m \tag{2.1.27}$$
$$+\Delta t\left(Q_{pn}h_{pn}^V+Q_{sn}h_{sn}^V\right)P_f\left\{\frac{P(t_{m+1})+P(t_m)}{2}\right\}.$$

The gap region is shown in Fig. 2.14.

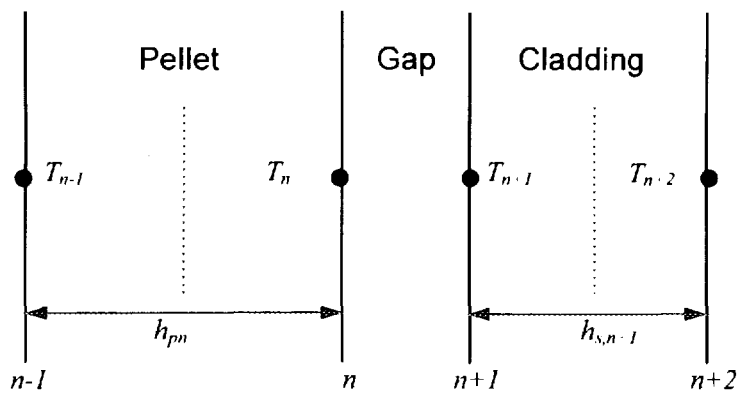

Fig. 2.14 Gap thermal conductance model.

For the gap region, the following equations hold by means of difference approximation, as in the case of eq. (2.1.25).

$$\frac{\left(T_n^{m+1}-T_n^m\right)D_n'}{\Delta t}=-\left(T_n^{m+\frac{1}{2}}-T_{n-1}^{m+\frac{1}{2}}\right)k_{pn}h_{pn}^s+\left(T_{n+1}^{m+\frac{1}{2}}-T_n^{m+\frac{1}{2}}\right)h_g + Q_{pn}h_{pn}^V P_f P\left(t_{m+\frac{1}{2}}\right) \tag{2.1.28}$$

$$\frac{\left(T_{n+1}^{m+1}-T_{n+1}^m\right)D_{n+1}''}{\Delta t}=-\left(T_{n+1}^{m+\frac{1}{2}}-T_n^{m+\frac{1}{2}}\right)h_g+\left(T_{n+2}^{m+\frac{1}{2}}-T_{n+1}^{m+\frac{1}{2}}\right)k_{s,n+1}h_{s,n+1}^s + Q_{s,n+1}P_f P\left(t_{m+\frac{1}{2}}\right) \tag{2.1.29}$$

Here, $D_n'=C_{v,pn}h_{pn}^V$, $D_{n+1}''=C_{v,s,n+1}h_{s,n+1}^V$, and h_g is gap thermal conductance. The center region of the fuel rod is shown in Fig. 2.15, and the cladding surface region is shown in Fig. 2.16.

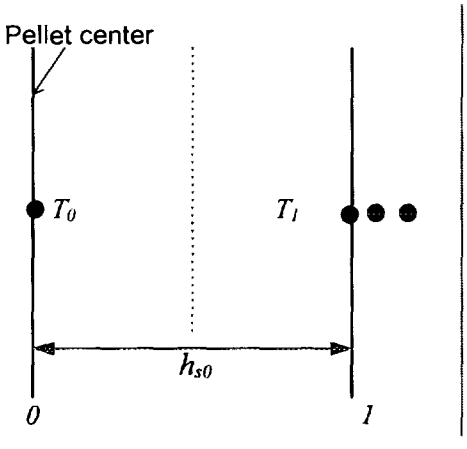

Fig. 2.15 Fuel rod center model.

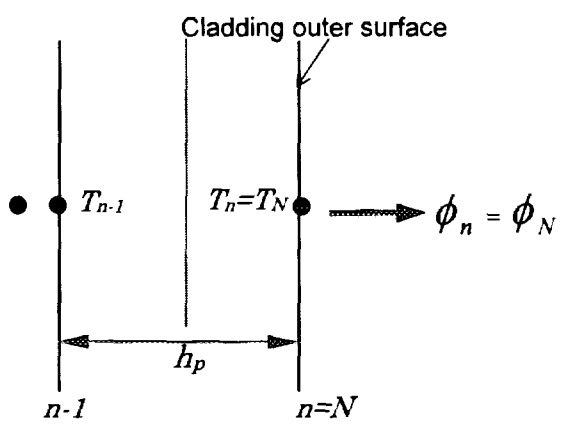

Fig. 2.16 Cladding surface model.

For the center of the fuel rod, eq. (2.1.20) is transformed by the difference approximation as follows.

$$\frac{\left(T_0^{m+1}-T_0^m\right)}{\Delta t}C_{v,s0}=\left(T_1^{m+\frac{1}{2}}-T_0^{m+\frac{1}{2}}\right)k_{s0}h_{s0}^s+Q_{s0}h_{s0}^V P_f P\left(t_{m+\frac{1}{2}}\right) \tag{2.1.30}$$

The boundary equation for the cladding surface region is

$$\frac{\left(T_n^{m+1}-T_n^m\right)}{\Delta t}C_{v,pn}h_{pn}^V=-\left(T_n^{m+\frac{1}{2}}-T_{n-1}^{m+\frac{1}{2}}\right)k_{pn}h_{pn}^s-r_n\phi_n+Q_{pn}h_{pn}^V P_f P\left(t_{m+\frac{1}{2}}\right). \tag{2.1.31}$$

The difference approximation equation (2.1.31) is expressed as

$$a_n T_{n-1}^{m+1} + b_n T_n^{m+1} = d_n . \tag{2.1.32}$$

Then the coefficients a_n, b_n and d_n are given as

$$a_n = -\frac{k_{pn} h_{pn}^{s} \Delta t}{2} \tag{2.1.33}$$

$$b_n = C_{v,pn} h_{pn}^{V} - a_n \tag{2.1.34}$$

$$\begin{aligned} d_n &= -a_n T_{n-1}^{m} + \left(C_{V,pn} h_{pn}^{V} - a_n\right) T_n^{m} \\ &\quad - \Delta t\, r_n \left(\frac{\phi_n^{m+1} + \phi_n^{m}}{2}\right) + \Delta t Q_{pn} h_{pn}^{V} P_f \left\{\frac{P(t_{m+1}) + P(t_m)}{2}\right\} \\ &= d_n' + d_n'' \phi_n^{m+1} . \end{aligned} \tag{2.1.35}$$

Here, ϕ_n is the cladding surface heat flux.

Heat flux $\phi_n{}^m$ at time t_m in eq. (2.1.35) is given as follows in the steady-state calculation.

$$\phi_n{}^m = q^m / 2\pi r_n , \tag{2.1.36}$$

where

q : linear heat rate (W/m).

This equation is used to avoid that difference errors generated by remeshing are accumulated in the calculated heat flux.

Now, unknown variables in eqs.(2.1.32) to (2.1.35) are T_{n-1}^{m+1}, T_n^{m+1} and ϕ^{m+1}.

Next, using coefficients expressed as E and F, which are obtained using the forward elimination of the Gaussian elimination method starting from the first point to the $(n+1)$th point, the following equation is derived.

$$T_{n-1}^{m+1} = -E_{n-1} T_n^{m+1} + F_{n-1} \tag{2.1.37}$$

By substituting eqs.(2.1.33) to (2.1.35) and (2.1.37) into eq. (2.1.32), we obtain

$$A_1 T_n^{m+1} + B_1 = \phi^{m+1} \tag{2.1.38}$$

where

$$A_1 = \left(b_n - a_n E_{n-1}\right) / d_n'' \tag{2.1.39}$$

$$B_1 = \left(a_n F_{n-1} - d_n'\right) / d_n'' . \tag{2.1.40}$$

Therefore, A_1 and B_1 are known values.

However, eq. (2.1.38) is equal to eq. (2.1.2), and A and B in eq. (2.1.2) are known values; thus T_n^{m+1} is obtained as described in section (1)-4.

Therefore, using the backward substitution of the Gaussian elimination method, T^{m+1} is sequentially obtained.

Two methods are available for designating the distribution function $Q(r)$. One is to designate it by input as a function of burnup, and the other is to use the Robertson formula (Halden experimental equation) [12] which is incorporated in the code.

$$Q_1(R) = I_0(k \cdot R) + \frac{I_1(k \cdot R_1)}{K_1(k \cdot R_1)} \cdot K_0(k \cdot R) \tag{2.1.41}$$

Here,

I : first transformed Bessel function

R_1 : pellet center hole radius

K : second transformed Bessel function

R : radial coordinate in pellet

k : Inverse of the neutron diffusion distance (cm^{-1}).

Here, k is calculated using

$$k = 0.328(E \cdot D)^{0.8} + 0.54\left(\frac{0.5}{R_p}\right)^{0.82} \cdot (E \cdot D)^{0.19}, \tag{2.1.42}$$

where

E : ^{235}U enrichment (%)

D : pellet theoretical density ratio (–)

R_p : pellet diameter (cm).

The distribution function (2.1.41) can be approximated by the following function :

$$Q_2(r) = \frac{(b+2)(1-h^2)[(1-a)r^b + (a-h^b)]}{b(1-h^2)(a-h^b) + 2(1-h^b)(1-ah^2)}, \tag{2.1.43}$$

where

r : normalized pellet radius $(0 \le r \le 1)$

a : heat generation density ratio of inner surface to outer surface of the pellet (–)

b : shape factor of the heat generation density function $Q(r)$ (–)

h : normalized inner radius of the pellet (–).

In the case of Halden reactor, the shape factor in eq. (2.1.43) can be set as b=2, since eq. (2.1.43) can be well approximated with a quadratic function. The heat generation density ratio a is expressed as follows using eq. (2.1.41).

$$a = \frac{Q_1(R_1)}{Q_1(R_p)} \tag{2.1.44}$$

Selection of option IFLX	The heat generation density distribution is selected using IFLX as follows.

IFLX>0: Designated by input as a function of burnup. The heat generation density distribution between the input burnup is obtained by interpolation in terms of burnup.

FLX=0: Robertson formula is used.

2.1.2 Gap thermal conduction

Gap thermal conductance is represented by the following equation which is modified from the Ross and Stoute model.[13]

$$h = \frac{\lambda_{gas}}{C(R_{eff} + R_2) + (g_1 + g_2) + \delta} + \frac{\lambda_m \cdot P_c}{0.5 \cdot R^{1/2} \cdot H} + h_r \qquad (2.1.46)$$

The first term on the right side of the equation is the gas conduction component, the second term is that due to solid contact, and the third term is that due to radiation.

Here,

$$C = 2.77 - 2.55 \times 10^{-8} \cdot P_c$$

$$\lambda_m = \frac{2\lambda_p(T_{po}) \cdot \lambda_c(T_{ci})}{\lambda_p(T_{po}) + \lambda_c(T_{ci})} \quad (\mathrm{W/cm \cdot K})$$

$$h_r = \left[\frac{1}{\varepsilon_p} + \frac{1}{\varepsilon_c} - 1\right]^{-1} \cdot \sigma \cdot \frac{T_{po}^4 - T_{ci}^4}{T_{po} - T_{ci}}$$

T_{po} : pellet outer surface temperature (K)

T_{ci} : cladding inner surface temperature (K)

λ_p : pellet thermal conductivity (W/cm·K)

λ_c : cladding thermal conductivity (W/cm·K)

λ_{gas} : thermal conductivity of the mixed gas (W/cm·K)

P_c : contact pressure between pellet and cladding (Pa)

R_{eff} : apparent surface roughness of the pellet (cm)

R_2 : cladding surface roughness (cm)

$g_1 + g_2$: temperature jump distance between solid phase and liquid phase (cm)

GAP : radial gap width (cm)

R : $\sqrt{\dfrac{R_{eff}^{\ 2} + R_2^{\ 2}}{2}}$

H : cladding Mayer's hardness (Pa) ($H = 2.8\sigma_Y$ [9])

σ_Y : yield stress (Pa)

σ : Stefan-Boltzmann constant (W/cm·K^4) $\left(\sigma = 5.67 \times 10^{-12}\right)$

ε_p : pellet emissivity (–), ε_c : cladding black oxide emissivity (–).

Fitting parameter R_{eff}, R2	The roughness R_{eff} and R2 can be designated by the input parameters R1 and R2(μm), respectively. The default values are 1.0 μm.

Equations for describing λ_{gas} and $g_1 + g_2$ are as follows.

(1) Thermal conductivity of mixed gas

This value can be represented as follows using the MATPRO-09 model. [14]

$$\lambda_{gas} = \sum_{i=1}^{n} \left(\frac{\lambda_i}{1 - \sum_{\substack{j=1 \\ i \neq j}}^{n} \phi_{ij} \frac{x_j}{x_i}} \right) \tag{2.1.47}$$

Here, the equation

$$\phi_{ij} = \frac{\left[1 + \left(\frac{\lambda_i}{\lambda_j} \right)^{\frac{1}{2}} \left(\frac{M_i}{M_j} \right)^{\frac{1}{4}} \right]^2}{2^{\frac{3}{2}} \left(1 + \frac{M_i}{M_j} \right)^{\frac{1}{2}}} \left[1 + \frac{2.41 \left(M_i - M_j \right) \left(M_i - 0.142 M_j \right)}{\left(M_i + M_j \right)^2} \right] \tag{2.1.48}$$

holds, where

x_i : molar ratio of gas i

λ_i : thermal conductivity of gas i (W/cm･K)

M_i : molar mass of gas i.

The gases dealt with here are Helium, Nitrogen, Krypton and Xenon. Naturally, gas composition depends on FP gas release, which will be explained in section 2.1.4.

(2) Temperature jump distance

The temperature jump distance is given by

$$g_1 + g_2 = \sum_{i=1}^{n} \left(g_1 + g_2 \right)_i \cdot \frac{10^5}{P_{gas}} \tag{2.1.49}$$

Here,

$(g_1 + g_2)$: jump distance of gas i between solid phase and liquid phase (cm)

P_{gas} : gas pressure (Pa).

According to the Ross and Stoute model, the values of (g_1+g_2) for Helium, Nitrogen,

Krypton and Xenon are 10×10^{-4}, 5×10^{-4}, 1×10^{-4} and 1×10^{-4}(cm), respectively.

Calculation of P_{gas} is explained later using eq. (2.1.217).

Selection of option IGAPCN
Designation of IGAPCN allows selection of gap conduction models other than those described in section 2.1.2. (See section 2.4, Material Properties.) IGAPCN = 0: Modified Ross and Stoute model, = 1: MATPRO-09 model, = 2: Ross and Stoute model, = 3: Modified Dean model.

2.1.3 Contact-force estimation model

[Simple mechanical model for thermal analysis]

To calculate the gap thermal conductance by eq.(2.1.46), the contact pressure between pellet and cladding P_c must be obtained. For this purpose, FEMAXI-IV incorporates a contact-force estimation model which is independent of the analysis of the mechanical behavior of the entire fuel rod described in sections 2.2 and 2.3.

Features of this model are

- Creep is taken into consideration in the calculation of radial displacements of pellet and cladding.
- Calculation of the contact force utilizes a pellet stiffness recovery model.

(1) Radial displacement of pellet

Radial displacement of pellet is given by the following equation, taking creep into consideration.

$$u_f = u^{rel} + \sum_{i=1}^{10}\left(\varepsilon_i^{th} + \varepsilon_i^{den} + \varepsilon_i^{ss} + \varepsilon_i^{u} + \varepsilon_i^{c}\right)\Delta r_i \qquad (2.1.50)$$

Here,

u_f : radial displacement (cm)

u_{rel} : radial displacement due to relocation (cm)

ε_i^{th} : thermal strain of ring i (–)

ε_i^{den} : densification of ring i (–)

ε_i^{ss} : solid FP (constrained) swelling of ring i (–)

ε_i^{u} : gas FP (unconstrained) swelling of ring i (–)

ε_i^{c} : creep strain of ring i (–)

Δr_i : width of ring i, radial mesh (cm)

i : ring number (total of 10 radial rings).

Among the above items, ε_i^{th}, ε_i^{den} and ε_i^{ss} are the strains which can be determined independent of the contact condition, while ε_i^{u} and ε_i^{c} are those that can be determined depending on the contact condition. It is assumed that pellet swelling by gas FP can be generated only under the unconstrained condition (i.e., contact force = 0), and that compressive creep of pellet is induced under contact force.

Fitting parameter XRELOC The initial relocation value of peller, u^{rel} is designated by u^{rel} =[initial radial gap width]×XRELOC. The default value of XRELOC is 0.2.

The following MATPRO-09 equation is used[14] as the creep equation of pellet,

$$\dot{\bar{\varepsilon}}^c = \frac{(A_1 + A_2 F)\bar{\sigma} e^{-Q_1/RT}}{(A_3 + f_d)G^2} + \frac{A_4 \bar{\sigma}^{4.5} e^{-Q_2/RT}}{(A_6 + f_d)} + A_7 \bar{\sigma} F e^{-Q_3/RT} \qquad (2.1.51)$$

Here,

$A_1 = 9.728 \times 10^6$, $Q_1 = 90{,}000$

$A_2 = 3.240 \times 10^{-12}$, $Q_2 = 132{,}000$

$A_3 = -87.7$, $Q_3 = 5{,}200$

$A_4 = 1.376 \times 10^{-4}$, $A_6 = -90.5$

$A_7 = 9.24 \times 10^{-28}$

$\dot{\bar{\varepsilon}}^c$: equivalent creep strain rate (hr^{-1})

F : fission rate ($=10^{19}$ fissions/m^3·s is designated by FEMAXI-IV)

$\bar{\sigma}$: equivalent stress (psi)

R : gas constant (1.987cal/mol·K)

Q : activation energy (cal/mol)

T : temperature (K)

f_d : theoretical density ratio (%)

G : grain diameter (μm).

Fitting parameter TCRMX
The upper limit of the temperature used for the creep strain velocity is given by TCRMX. The default value of TCRMX is 1773.15 (K).

However, when the pellet temperature exceeds the designated temperature TCRMX, the creep strain rate is calculated with TCRMX. Since the present model assumes the plane

stress condition and therefore the equivalent stress is $\sigma_z = 0$, $\bar{\sigma} = P_{fc}$ holds when $\sigma_r \approx \sigma_\theta = -P_{fc}$ (contact force) is assumed.

In this condition, the creep strain rate components can be given as

$$\begin{Bmatrix} \dot{\varepsilon}^c_{r,t} \\ \dot{\varepsilon}^c_{z,t} \\ \dot{\varepsilon}^c_{\theta,t} \end{Bmatrix} = \dot{\bar{\varepsilon}}^c_t \frac{1}{2\bar{\sigma}} \begin{Bmatrix} 2\sigma_r - \sigma_\theta \\ -\sigma_r - \sigma_\theta \\ 2\sigma_\theta - \sigma_r \end{Bmatrix} = \dot{\bar{\varepsilon}}^c_t \begin{Bmatrix} -\frac{1}{2} \\ 1 \\ -\frac{1}{2} \end{Bmatrix} \tag{2.1.52}$$

and the creep rate in the circumferential direction is

$$\dot{\varepsilon}^c_{\theta,t} = -\frac{1}{2}\dot{\bar{\varepsilon}}^c_t . \tag{2.1.53}$$

(2) Radial displacement of cladding

In the calculation of the cladding radial displacement, the creep strain in addition to the elastic strain and thermal strain is considered. It is given by

$$u = \frac{r_{ci}}{E}\left[\frac{\left(P_{gas} + P_{fc}\right)\left(r_{ci}^2 + r_{co}^2\right) - 2P_w r_{co}^2}{r_{co}^2 - r_{ci}^2} + \nu P_{gas}\right] + \left(\varepsilon^{th} + \varepsilon^c\right)\frac{r_{co} + r_{ci}}{2}. \tag{2.1.54}$$

Here,

u : cladding radial displacement (cm)

E : Young's modulus of cladding (Pa)

r_{ci} : cladding inner diameter (cm)

r_{co} : cladding outer diameter (cm)

P_{gas} : internal pressure (Pa)

P_{fc} : contact pressure between pellet and cladding (Pa)

P_w : coolant water pressure (Pa)

ν : Poisson's ratio of cladding

ε^{th} : cladding thermal strain

ε^c : cladding creep strain.

Circumferential and axial components of cladding stress are given as follows using the thin cylindrical shell model:

$$\sigma_\theta = \frac{r_{ci}\left(P_{fc} + P_{gas}\right) - r_{co}P_w}{r_{co} - r_{ci}} \tag{2.1.55}$$

$$\sigma_z = \frac{r_{ci}^2\left(P_{fc} + P_{gas}\right) - r_{co}^2 P_w}{r_{co}^2 - r_{ci}^2}. \tag{2.1.56}$$

However, $P_{fc} = 0$ in the non-contact condition.

Here, since this model does not taken into account the shearing components, the equivalent stress is expressed as

$$\bar{\sigma} = \left[\frac{1}{2}\left\{\left(\sigma_\theta - \sigma_z\right)^2 + \sigma_\theta^2 + \sigma_z^2\right\}\right]^{\frac{1}{2}}. \tag{2.1.57}$$

Using this $\bar{\sigma}$, the equivalent creep strain increment of cladding is expressed as

$$d\bar{\varepsilon}^c = f\left(\bar{\sigma}, T, \phi, \bar{\varepsilon}^c\right) \cdot dt. \tag{2.1.58}$$

Here, determination of the function f requires a creep equation of cladding. This creep equation is selected from either MATPRO-09 equation[14] or NENANSEN equation[15]. The concrete form of these equations are described in section 2.4.2.

The function $f = \dot{\bar{\varepsilon}}^c$ does not contain time explicitly. Therefore, time t is eliminated from the formulation of $\dot{\bar{\varepsilon}}^c$ by transforming the creep equation :

1) MATPRO-09 equation has a form:

$$\dot{\varepsilon} = K\phi\left(\sigma + B\exp(C\sigma)\right)\exp(-10000/RT)t^{-0.5} \qquad ①$$

Integrating eq.① with t gives

$$\varepsilon = 2K\phi\left(\sigma + B\exp(C\sigma)\right)\exp(-10000/RT)t^{0.5}. \qquad ②$$

Since eq.② is a primary creep equation which has non-unity power of t,

$\varepsilon_H = \varepsilon$ (total creep strain)

holds. Eliminating t from the eqs.① and ② gives

$$\dot{\varepsilon} = 2\{K\phi\left(\sigma + B\exp(C\sigma)\right)\exp(-10000/RT)\}^2 / \varepsilon$$

Consequently,

$$f = \dot{\bar{\varepsilon}}^c = 2\{K\phi\left(\sigma + B\exp(C\sigma)\right)\exp(-10000/RT)\}^2 / \bar{\varepsilon}^c \tag{2.1.59}$$

holds, where

$\dot{\bar{\varepsilon}}^c$: equivalent creep strain rate of cladding (s^{-1})

$\bar{\varepsilon}^c$: equivalent creep strain of cladding

$C_1 = 5.129 \times 10^{-29}$, $Q_1 = 10{,}000$

$C_2 = 7.252 \times 10^{2}$, $Q_2 = 4.967 \times 10^{-8}$

ϕ : fast neutron flux (n/m^2/s)

$\bar{\sigma}$: equivalent stress (Pa)

T : temperature (K)

R : gas constant (1.987 cal/mol·K).

2) NENANSEN equation has the following form:

creep strain rate: $\dot{\varepsilon}^c = \dot{\varepsilon}^c_{th} + \dot{\varepsilon}^c_{irr}$ (2.1.60)

$$\dot{\varepsilon}^c_{th} = mK^{\frac{1}{m}}\varepsilon_H^{(1-\frac{1}{m})} \tag{2.1.61}$$

$$\dot{\varepsilon}^c_{irr} = 6.64 \times 10^{-25}\phi^{1.23}\sigma_{eq}^{1.34}, \tag{2.1.62}$$

so that it is not necessary to eliminate time t, and

$f = \dot{\bar{\varepsilon}}^c$ holds.

The creep strain increments in the circumferential and axial directions are

$$d\varepsilon^c_\theta = \frac{1}{2\bar{\sigma}}\left(2\sigma_\theta - \sigma_z\right)\cdot d\bar{\varepsilon}^c \tag{2.1.63}$$

$$d\varepsilon^c_z = \frac{1}{2\bar{\sigma}}\left(2\sigma_z - \sigma_\theta\right)\cdot d\bar{\varepsilon}^c. \tag{2.1.64}$$

Here, $\bar{\varepsilon}^c$ in eq. (2.1.58) is expressed as

$$\bar{\varepsilon}^c = \bar{\varepsilon}^c_n + \theta\cdot d\bar{\varepsilon}^c \quad \left(\theta = \frac{1}{2}\right),$$

and $\dot{\bar{\varepsilon}}^c$ is obtained by iteration of convergence calculation.

Also, with the time-step number designated as m and the time-step number of the current step as $n+1$, ε^c in eq. (2.1.54) is given by

$$\varepsilon^c = \varepsilon^c_{\theta,n+1} = \sum_{m=1}^{n+1} d\varepsilon^c_{\theta,m} \tag{2.1.65}$$

(5) Pellet crack migration model

Crack shape in the pellet changes with burnup. This change is modeled as follows.

At the beginning-of-life, cracks develop in radial directions, and void spaces generated by cracking and relocation are present near the center of the pellet as shown in Fig. 2.17.

As the burnup progresses, these radial cracks gradually become circumferentially oriented, and as a result, circumferentially oriented cracks are formed as shown in Fig. 2.18.

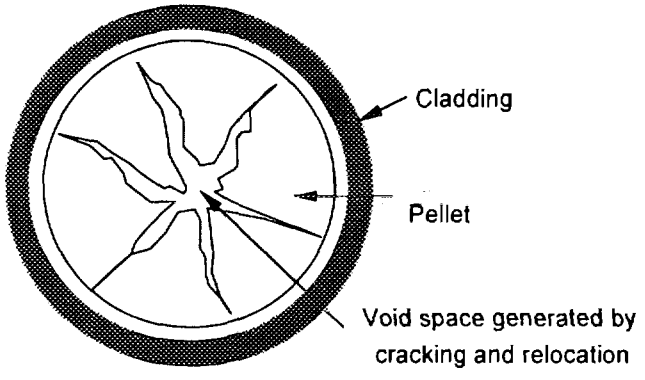

Fig. 2.17 Cracks in pellet at the beginning-of-life.

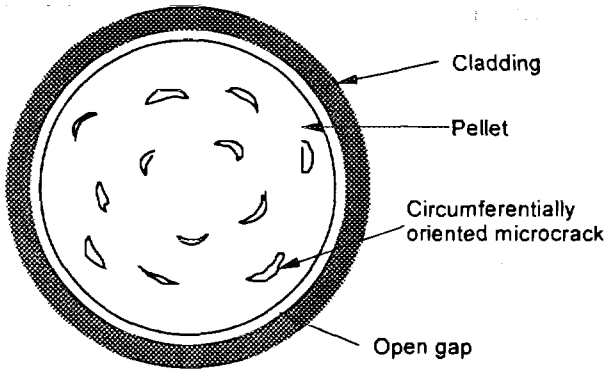

Fig. 2.18 Cracks at extended burnup

In FEMAXI-IV, it is assumed that this migration of cracks begins at a certain stage and is completed at another stage of burnup, and that the volumes of pellet, cladding, cracks and gaps change linearly with burnup during the migration process, as shown in Fig. 2.19.

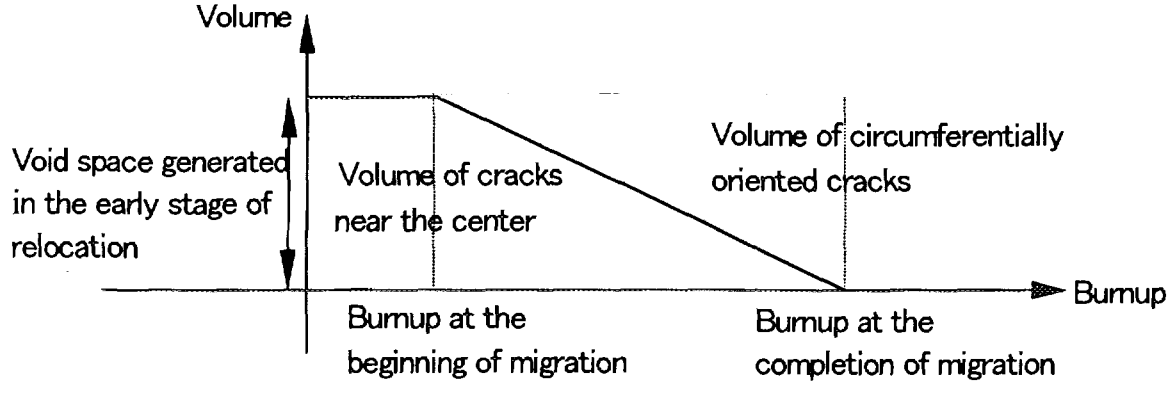

Fig. 2.19 Change of crack volume with burnup.

Also, it is assumed that when the pellet and cladding make contact, the decrease in pellet volume due to contact force is accommodated only by the decrease in volume of the

circumferentially oriented cracks, and the contact force does not affect the volume of radial cracks near the pellet center. It follows that, in a burnup region before the beginning of crack migration, no apparent change in stiffness due to cracking of the pellet is assumed and the original Young's modulus is used. The contact force between pellet and cladding increases in proportion to the imaginary overlap width, δ_{fc}, of the pellet and cladding.

In the burnup region after the beginning of crack migration, the apparent change in stiffness due to pellet cracking, which is in proportion to the amount of increase in the volume of circumferentially oriented cracks, should be dealt with. Namely, the model of varying Young's modulus of pellet is used.

When the burnup reaches the level at which migration is completed, the apparent change in stiffness due to pellet cracking becomes most moderate.

In FEMAXI-IV, burnup levels of beginning and completion of crack migration are designated by input parameters. The present model is applied only to the contact force prediction in the thermal analysis, and is similar but not identical to that used in the mechanical analysis, which will be described later.

Fitting parameters BUMIN and BUMAX	Burnup levels of beginning and copmletion of crack migration can be input as BUMIN and BUMAX, respectively. Default values of BUMIN and BUMAX are 0(Mwd/t-U). Namely, in the default condition, crack migration is already completed at the beginning-of-life.

(4) Recovery of stiffness of cracked pellet

Pellet cracks are described using a 'Stiffness Recovery model' in which the pellet Young's modulus is varied. The Young's modulus of the cracked pellet is represented by a linear function of the elastic strain as follows[2].

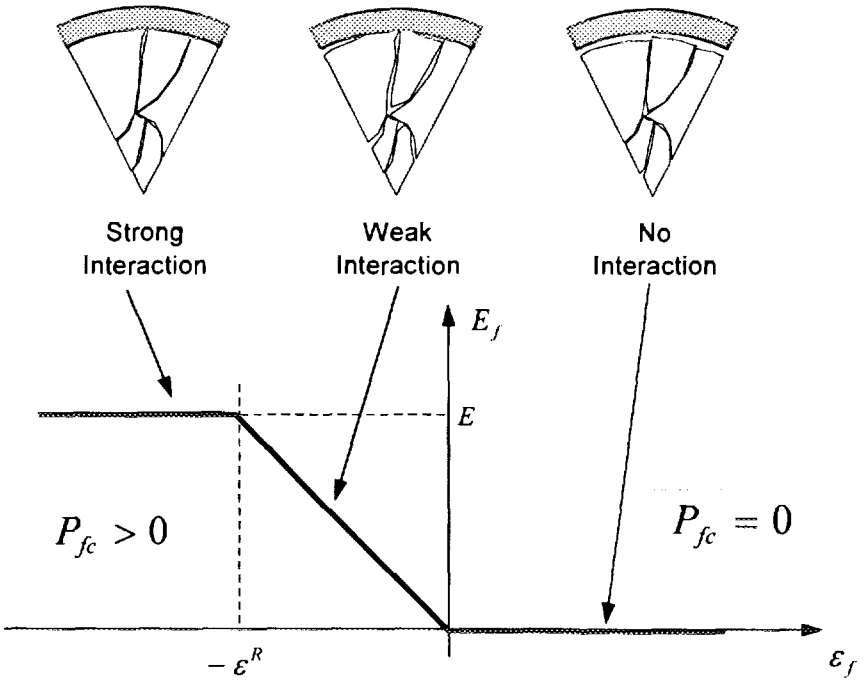

Fig. 2.20 Young's modulus of the cracked pellet.

Assuming that the pellet radial displacement by relocation is δ_{crk} which is generated by circumferentially oriented cracks, the radial displacement of pellet which is caused when pellet is compressed by cladding in the radial direction is $\delta_f (>0)$, the model assumes that the pellet stiffness recovers to its original value when $\delta_f = 2\delta_{crk}$. (See eq.(2.1.74))

As shown in Fig. 2.20, Young's modulus in the radial direction is given by the equations

$$E_f = \begin{cases} 0_c & \left(0 \le \varepsilon_f\right) \\ -\dfrac{E}{\varepsilon_R}\varepsilon_f & \left(-\varepsilon_R < \varepsilon_f < 0\right) \\ E & \left(\varepsilon_f \le -\varepsilon_R\right) \end{cases} \tag{2.1.66}$$

Here,

E_f : apparent Young's modulus of pellet

ε_f : radial compressive strain of pellet which is caused when pellet is compressed by contact force from cladding (ε_f <0)

E : original Young's modulus of pellet

ε_R: pellet radial strain due to pushed-back portion of pellet displacement when stiffness of pellet is completely recovered

Therefore,

$$\varepsilon_f = -\frac{\delta_f}{r_{po}} \tag{2.1.67}$$

holds, where

r_{po} : pellet initial outer radius,

and pellet radial displacement is expressed as,

$$\delta_{crk} = r_{po}\varepsilon_{crk} \tag{2.1.68}$$

ε_R(>0) is determined as follows:

$-\varepsilon_R$ = (lost portion of strain of circumferentially oriented crack<0)

+ (elastic compressive strain <0)

namely,

$$-\varepsilon_R = \bar{\varepsilon}_{crk} + \frac{\sigma_R}{E} \tag{2.1.69}$$

holds, where

$\bar{\varepsilon}_{crk}$: $= -\varepsilon_{crk}$, lost portion of strain due to circumferentially oriented crack,

σ_R : compressive stress imposed by cladding when stiffness of pellet completely recovered.

(See Fig.2.21.)

Here, as shown in section (3), $\bar{\varepsilon}_{crk}$, or the lost portion of strain due to circumferentially oriented crack is given as a function of burnup and relocation strain,

$$\bar{\varepsilon}_{crk} = \begin{cases} 0 & (Bu \le Bu_{\min}) \\ -\dfrac{Bu - Bu_{\min}}{Bu_{\max} - Bu_{\min}}\varepsilon_{rel} & (Bu_{\min} < Bu < Bu_{\max}) \\ -\varepsilon_{rel} & (Bu_{\max} \le Bu) \end{cases}$$

where

Bu : burnup,

$Bu_{\min}$: burnup at the beginning of crack migration

$Bu_{\max}$: burnup at the completion of crack migration

ε_{rel} : relocation strain = XRELOC $\cdot \dfrac{\delta_0}{r_{po}}$

δ_0 :initial radial gap width.

As shown in eq.(2.1.66), ε_f affects the determination of E_f only within the range of $-\varepsilon_R < \varepsilon_f < 0$. Therefore, using the relationship $\dfrac{d\sigma_f}{d\varepsilon_f} = E_f$,

$$\sigma_f = -\frac{E}{\varepsilon_R}\frac{\varepsilon_f^2}{2} \qquad \left(-\varepsilon_R < \varepsilon_f < 0\right) \tag{2.1.70}$$

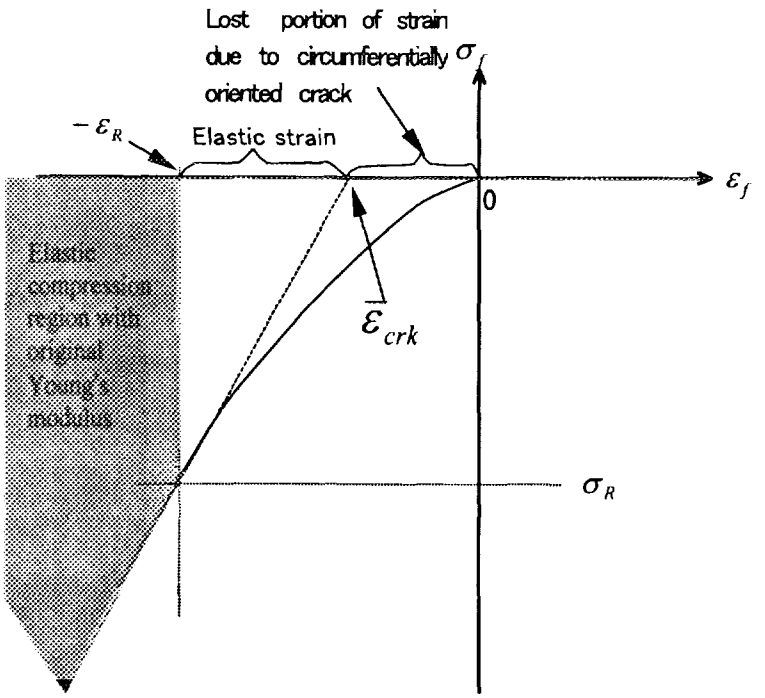

Fig.2.21 Relationship between stress and strain of cracked pellet

Solving eq.(2.1.70) for $\varepsilon_f < 0$, the following equation is obtained.

$$\varepsilon_f = -\sqrt{\frac{2\varepsilon_R(-\sigma_f)}{E}} \tag{2.1.71}$$

Substituting eq.(2.1.71) into eq.(2.1.66) in the range of $-\varepsilon_R < \varepsilon_f < 0$ and solving eq.(2.1.66) in terms of E_f,

$$E_f = \sqrt{\frac{2E(-\sigma_f)}{\varepsilon_R}} \tag{2.1.72}$$

holds.

When $\varepsilon_f = -\varepsilon_R$, σ_R is obtained as follows substituting the relationship $E_f = E$ into eq.(2.1.70),

$$\sigma_R = -\frac{E\varepsilon_R}{2} \tag{2.1.73}$$

Substituting eq.(2.1.73) into eq.(2.1.69),

$$\varepsilon_R = 2\varepsilon_{crk} \tag{2.1.74}$$

Substituting eqs.(2.1.67) and (2.1.73) into eq.(2.1.66), E_f is obtained as

$$E_f = \frac{E}{2\varepsilon_{crk}} \cdot \frac{\delta_f}{r_{po}} \quad \left(-\varepsilon_R < \varepsilon_f, \quad \text{i.e.,} \quad \delta_f < 2r_{po}\varepsilon_{crk}\right)$$
$$E_f = E \qquad \left(\varepsilon_f \le \varepsilon_R, \quad \text{i.e.,} \quad \delta_f \ge 2r_{po}\varepsilon_{crk}\right) \tag{2.1.75}$$

(5) Gap width and contact force

Here, method to calculate pellet-cladding contact force P_{fc} is explained on the basis of the imaginary overlap quantity δ_{fc} of pellet and cladding radial displacements and on the assumption of the stiffness recovery model described in section (4).

The contact force P_{fc} is force that is generated across the contact surface to eliminate the imaginary overlap δ_{fc} by counter-pushing and balancing when pellet and cladding make a contact at the start of a time step.

The contact force P_{fc} can be obtained as the force with which cladding pushes pellet and vise versa, if radial displacement of cladding in contact with pellet is known, from such quantities as inner and outer radii, thickness, and Young's modulus of cladding.

The gap width between pellet and cladding is expressedas

$$\delta = \delta_o + u_c - u_f \tag{2.1.76}$$

where

δ : radial gapwidth (m)
δ_o : initial gap width (m)
u_c : radial displacement of cladding (m)
u_f : radial displacement of pellet (m)

When δ is calculated to be negative at the start of a time step, it is judged that the pellet is in contact with the cladding and P_{fc} is calculated. At this time of numerical calculation, the pellet and cladding have an imaginary overlap with each other by width

$$\delta_{fc} = -\delta = -\left(\delta_o + u_c - u_f\right) > 0 \tag{2.1.77}$$

Namely, δ_{fc} is known at the start of the time step.

It is assumed that, when δ_{fc} is positive, cladding pushes pellet and vice versa until δ_{fc} becomes 0. In this situation, setting the pellet push-back displacement caused by cladding

pushing inward as δ_f, and setting the cladding push-out displacement caused by pellet pushing outward as δ_c,

$$\delta_{fc} = \delta_f + \delta_c \tag{2.1.78}$$

holds.

At the pellet side, when $\varepsilon_r = \varepsilon_\theta$, using δ_f, radial strain ε_r and contact force P_{fc} are

$$\varepsilon_r = \varepsilon_\theta = \frac{\delta_f}{r_{ci}}$$

and

$$P_{fc} = E_f\left(\frac{\delta_f}{r_{ci}}\right) \tag{2.1.79}$$

Here,

E_f : pellet apparent (effective) Young's modulus

r_c : cladding inner radius(=pellet outer radius (r_{po}) in contact with cladding)

At the cladding side, since $\varepsilon_\theta = \delta_c / r_{ci}$ holds, setting E_c as cladding Young's modulus,

$$\sigma_\theta = E_c \varepsilon_\theta = E_c \frac{\delta_c}{r_{ci}} \tag{2.1.80}$$

$$P_{fc} = \sigma_r = \sigma_\theta \frac{t}{r_{ci}} = E_c \frac{\delta_c}{r_{ci}} \cdot \frac{t}{r_{ci}} \tag{2.1.81}$$

($t = r_{co} - r_{ci}$: cladding thickness)

Namely,

$$P_{fc} = E_c \frac{\delta_c (r_{co} - r_{ci})}{r_{ci}^2} \tag{2.1.82}$$

holds.

Simultaneously solving eqs. (2.1.78)-(2.1.82) in terms of δ_f and δ_c and eliminating P_{fc}, we obtain

$$\delta_f = \frac{E_c (r_{co} - r_{ci})}{E_c (r_{co} - r_{ci}) + E_f r_{ci}} \delta_{fc} \tag{2.1.83}$$

$$\delta_c = \frac{E_f r_{ci}}{E_c (r_{co} - r_{ci}) + E_f r_{ci}} \delta_{fc} \tag{2.1.84}$$

However, eqs.(2.1.83) and (2.1.84) do not hold in a strict sense, since they are derived on

the basis of the balance of force and δ_{fc} contains 'displacement for the lost portion of strain due to circumferentially oriented crack'.

Here, pellet apparent Young's modulus E_f, i.e. one of the unknown variables, is expressed as follows from eqs.(2.1.66) and (2.1.75).

① When $\delta_f = 0$, $E_f = 0$

② When $0 < \delta_f < 2\delta_{crk}$, $E_f = \dfrac{\delta_f}{2\delta_{crk}} E$ (2.1.85)

③ When $\delta_f \geq 2\delta_{crk}$, $E_f = E$ (original property value)

Now, equations are defined taking 'the displacement due to circumferentially oriented crack' which is contained in δ_{fc} of eqs.(2.1.83) and (2.1.84) into consideration by using the above relationship.

When $\delta_f \geq 2\delta_{crk}$, pellet loses entirely the radial displacement δ_{crk} due to circumferentially oriented crack and $E_f = E$ holds, eqs.(2.1.83) and (2.1.84) are rewritten as

$$\delta_f = \frac{E_c(r_{co} - r_{ci})}{E_c(r_{co} - r_{ci}) + Er_{ci}}\left(\delta_{fc} - \delta_{crk}\right) + \delta_{crk} \tag{2.1.86}$$

$$\delta_c = \frac{Er_{ci}}{E_c(r_{co} - r_{ci}) + Er_{ci}}\left(\delta_{fc} - \delta_{crk}\right) \tag{2.1.87}$$

When $\delta_f = 2\delta_{crk}$, δ_{fc} is calculated as follows.

Using the relationship $\delta_{fc} = \delta_f + \delta_c = 2\delta_{crk} + \dfrac{Er_{ci}}{E_c(r_{co} - r_{ci}) + E \quad r_{ci}}\left(\delta_{fc} - \delta_{crk}\right)$,

$$\delta_{fc} = 2\delta_{crk} + \frac{Er_{ci}}{E_c(r_{co} - r_{ci})}\delta_{crk} \tag{2.1.88}$$

holds.

Therefore, in the range of ③ in eq.(2.1.75), i.e., $\delta_{fc} \geq 2\delta_{crk} + \dfrac{Er_{ci}}{E_c(r_{co} - r_{ci})}\delta_{crk}$,

eq.(2.1.87) gives δ_c.

Next, derivation of δ_c in the range of ② in eq.(2.2.85), i.e.,

$o < \delta_{fc} < 2\delta_{crk} + \dfrac{Er_{ci}}{E_c(r_{co} - r_{ci})}\delta_{crk}$ is explained. In this range, in the same manner as eqs.(2.1.86) and (2.1.87), eqs.(2.1.83) and (2.1.84) are rewritten as

$$\delta_f = \frac{E_c(r_{co} - r_{ci})}{E_c(r_{co} - r_{ci}) + E_f r_{ci}}\left(\delta_{fc} - \tilde{\delta}_{crk}\right) + \tilde{\delta}_{crk} \tag{2.1.89}$$

$$\delta_c = \frac{E_f r_{ci}}{E_c(r_{co} - r_{ci}) + E_f r_{ci}}\left(\delta_{fc} - \tilde{\delta}_{crk}\right) \tag{2.1.90}$$

Here, $\tilde{\delta}_{crk}$ is the lost relocation displacement.

$\tilde{\delta}_{crk}$ corresponds to the value which is obtained from r_{po} times the distance between the origin and intersection point of the tangential line of stress-strain curve with ε_f -axis shown in Fig.2.21.

$\tilde{\delta}_{crk}$ is calculated in the following method. Using the strain $\tilde{\varepsilon}_{crk}$ due to circumferentially oriented crack,

$$\sigma_f = E_f\left(\varepsilon_f + \tilde{\varepsilon}_{crk}\right) \tag{2.1.91}$$

holds, where $\tilde{\varepsilon}_{crk} = \frac{\tilde{\delta}_{crk}}{r_{po}}$.

Substituting eqs.(2.1.66) and (2.1.70) into this equation,

since $$-\frac{E}{\varepsilon_R}\frac{\varepsilon_f^2}{2} = -\frac{E}{\varepsilon_R}\varepsilon_f\left(\varepsilon_f + \tilde{\varepsilon}_{crk}\right)$$

$$\tilde{\varepsilon}_{crk} = -\frac{\varepsilon_f}{2} \tag{2.1.92}$$

is obtained. Multiplying the both sides of eq.(2.1.92) by $-r_{po}$ gives

$$\tilde{\delta}_{crk} = \frac{\delta_f}{2} \tag{2.1.93}$$

Substituting eqs.(2.1.85) and (2.1.93) into eq.(2.1.89), we obtain

$$\delta_f = \frac{E_c(r_{co} - r_{ci})}{E_c(r_{co} - r_{ci}) + \dfrac{\delta_f}{2\delta_{crk}} E r_{ci}}\left(\delta_{fc} - \frac{\delta_f}{2}\right) + \frac{\delta_f}{2}$$

Rearranging this equation in terms of δ_f,

$$E r_{ci}\delta_f^2 + 4\delta_{crk}E_c(r_{co} - r_{ci})\delta_f - 4\delta_{crk}E_c(r_{co} - r_{ci})\delta_{fc} = 0$$

is derived. Solving this in terms of $\delta_f\,(>0)$, we obtain

$$\delta_f = \frac{-2\delta_{crk}E_c(r_{co} - r_{ci}) + \sqrt{4\delta_{crk}^2 E_c^2(r_{co} - r_{ci})^2 + 4\delta_{crk}E E_c r_{ci}(r_{co} - r_{ci})\delta_{fc}}}{E r_{ci}} \tag{2.1.94}$$

Substituting eq.(2.1.94) into eqs.(2.1.85) and (2.1.93), E_f and $\bar{\delta}_{rel}$ is obtained.

Rearranging in terms of δ_c using the above relationship,

$$\delta_c = \begin{cases} \dfrac{E_f r_{ci}}{E_c(r_{co}-r_{ci})+E_f r_{ci}}\left(\delta_{fc}-\dfrac{\delta_f}{2}\right) & \left(0 \le \delta_{fc} < 2\delta_{crk}+\dfrac{Er_{ci}}{E_c(r_{co}-r_{ci})}\delta_{crk}\right) \\ \dfrac{E\, r_{ci}}{E(r_{co}-r_{ci})+Er_{ci}}\left(\delta_{fc}-\delta_{crk}\right) & \left(2\delta_{crk}+\dfrac{Er_{ci}}{E_c(r_{co}-r_{ci})}\delta_{crk} \le \delta_{fc}\right) \end{cases} \tag{2.1.95}$$

hold. δ_f is known from eq.(2.1.94), therefore the contact force can be determined by substituting δ_c which is determined by eq.(2.1.95) into eq.(2.1.82).

It is assumed that, after cladding yields, contact force does not exceeds the value obtained when cladding yields. Namely, when the equivalent stress of cladding exceeds the yield stress σ_y, the following equation is used instead of eq. (2.1.57).

$$\bar{\sigma} = \sigma_Y$$

Here, the equation below is used to obtain σ_y of the cladding in the case of recrystallized annealed materials.[2]

$$\sigma_Y = 21.60 - 0.0213 \times T + \Delta\sigma_{Y_o}{}^{irr}, \tag{2.1.96}$$

where

σ_y : 0.2% proof stress (kg/mm^2)

T : temperature (°C).

In the cases of stress-relieved materials, the equation below is used.[2]

$$\sigma_Y = 31.32 - 0.0213 \times T + \Delta\sigma_{YO}{}^{irr} \tag{2.1.97}$$

For the increase in yield stress $\Delta\sigma_{YO}{}^{irr}$ due to irradiation hardening, the following equation is used. [2]

$$\Delta\sigma_{YO}{}^{irr} = 33.4\left[1-\exp(-c\phi t)\right]^{\frac{1}{2}} \tag{2.1.98}$$

Here,

c : $2.92 \times 10^{-21} \exp(-1.6 \times 10^{-14}\phi)$

ϕ : fast neutron flux (n/cm^2/s)

t : time (s).

2.1.4 Generation and release of FP gas

In FEMAXI-IV, generation and release of FP gas are calculated with the pellet stack which is divided into a maximum of 12 axial segments, and each axial segment is divided into 10 concentric zones (ring element) in the radial direction. Either a mechanistic model or a temperature zone model is selected in the FP gas release analysis.

Selection of option IGASP	FP gas release model option
IGASP=0: Mechanistic model, =1: Temperature zoning model.	

(1) Generation rate

The FP gas generation rate in the axial segment j and radial zone i is represented by

$$P^{ij} = \frac{Y \cdot f^{ij} \cdot q^{j}}{E_f \cdot N_A}. \tag{2.1.99}$$

Here,

P^{ij} : FP gas generation rate per unit length in zone ij (mol/cm・s)

$$f^{ij} = 2\pi \int_{-\frac{1}{2}}^{+\frac{1}{2}} \phi(r) r dr$$

$\phi(r)$: heat generation density distribution function in the radial direction, eq. (2.1.24)

q^j : average heat generation density of axial segment j $= \dfrac{P^j_{LHR}}{\pi(1-h^2)}$

P^j_{LHR} : linear heat rate of axial segment j (W/cm)

h : normalized radius of the center hole of pellet (–)

E_f : energy generated per one fission, 3.204×10^{-11} J (=200 MeV)

Y : fission yield of FP gas (K_r + K_e), = 0.3

N_A : Avogadro's number, 6.02×10^{23}.

(2) FP gas release model (mechanistic model)

(2)–1 Assumptions of the release mechanism

The gas produced in UO_2 grains is transported to grain boundaries through the two mechanisms described below, and that there it forms bubbles which accumulate there.

1) Gas atom diffusion within grains

2) Sweeping of gas atoms to grain boundaries by grain growth

When the amount of FP gas in the intergranular gas bubbles reaches a certain saturation value, a number of bubbles connect and a tunnel which leads to a free surface of pellet is formed. After the tunnel is formed, additional gas which has diffused from within grains to the grain boundaries enters the tunnel and is immediately released to the free surface. The gas accumulated at the grain boundaries also re-dissolves into the grains at a constant rate.

Analysis for the intragranular gas atoms includes trapping of the gas by the intragranular bubbles, or re-dissolution of the gas from the bubbles into the matrix.

(2)-2 Diffusion accompanied by trapping

Figure 2.22 shows states of intragranular gas bubbles and intergranular gas bubbles in a pellet, and Fig. 2.23 shows an ideal model of crystal grains of a pellet.

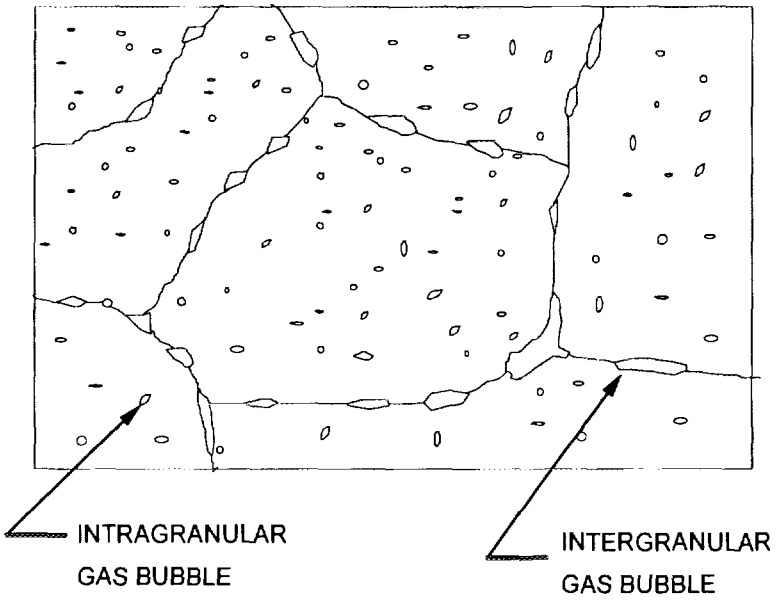

Fig. 2.22 Schematics of intragranular and intergranular gas bubbles in a pellet.

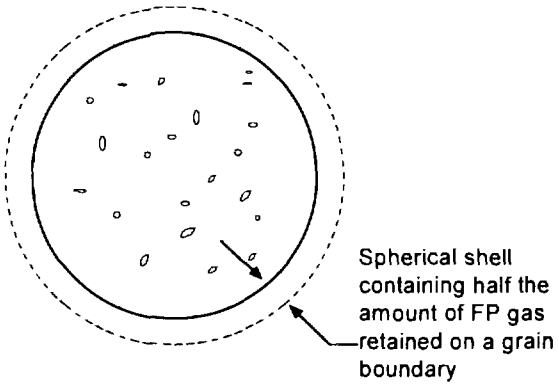

Fig. 2.23 Ideal model of crystal grains of a pellet.

The grain shown in Fig. 2.23 is illustrated as if it were covered with a spherical shell blanket boundary. However, an actual grain boundary is a thin membrane layer separating adjacent crystal grains.

The relative amounts of gas dissolved in the matrix and present in intragranular bubbles depend on the equilibrium between trapping and re-dissolution. The gas dissolved in the matrix moves toward the grain boundary by concentration-gradient diffusion.

The gas diffusion rate in a spherical solid matrix with a radius of a is given by the following equation in which trapping and re-dissolution are taken into consideration[16].

$$\frac{\partial c}{\partial t} = D\left(\frac{\partial^2 c}{\partial r^2} + \frac{2}{r}\frac{\partial c}{\partial r}\right) - gc + b'm + \beta \qquad (2.1.100)$$

Here,

c : number of gas atoms dissolved per unit volume of solid matrix (atoms/cm^3)

D : diffusion coefficient of gas atoms (cm^2/s)

g : rate of trapping of gas by intragranular bubbles (s^{-1})

b' : rate of re-dissolution of gas into solid phase (s^{-1})

m : number of gas atoms per unit bubble volume (atoms/cm^3)

β : generation rate of the gas per unit volume of pellet (atoms/cm^3/s).

The gas equilibrium between trapping and re-dissolution is

$$\frac{\partial m}{\partial t} = gc - b'm. \qquad (2.1.101)$$

When the time-course change of m can be neglected in the equilibrium state,

eq.(2.1.101) is simplified as

$$gc = b'm . \tag{2.1.102}$$

Addition of eqs. (2.1.100) and (2.1.101) gives

$$\frac{\partial(c+m)}{\partial t} = D\left(\frac{\partial^2 c}{\partial r^2} + \frac{2}{r}\frac{\partial c}{\partial r}\right) + \beta . \tag{2.1.103}$$

In the meantime, the following equation is obtained from eq. (2.1.102).

$$c + m = \frac{b' + g}{b'} c \tag{2.1.104}$$

Substituting the above equation into eq. (2.1.103),

$$\frac{\partial(c+m)}{\partial t} = \frac{Db'}{b'+g}\left(\frac{\partial^2(c+m)}{\partial r^2} + \frac{2}{r}\frac{\partial(c+m)}{\partial r}\right) + \beta \tag{2.1.105}$$

is obtained. Setting the sum of the number of gas atoms in the solid matrix and the number of those in the intra-granular bubbles as

$$\Psi = c + m , \tag{2.1.106}$$

the diffusion equation in the intra-granular spherical coordinate system, including trapping, is

$$\frac{\partial \Psi}{\partial t} = +D'\left(\frac{\partial^2 \Psi}{\partial r^2} + \frac{2}{r}\frac{\partial \Psi}{\partial r}\right) + \beta . \tag{2.1.107}$$

Here,

$$D' = \frac{b'D}{b'+g} , \tag{2.1.108}$$

and Ψ represents the apparent average number of gas atoms per unit intragranular volume regardless of the location of the gas (i.e., whether it is present in the matrix or in the intragranular bubbles). D' is the apparent diffusion coefficient, which includes the trapping effect.

Next, to solve eq.(2.1.107), first g and b' are obtained. Assuming that N intragranular gas bubbles with an average radius of $\overline{R}$ are present per unit volume, $\overline{R}$ and N are related as follows in an equilibrium state during irradiation[17].

$$N = 1.52\alpha / \pi\lambda\left(\overline{R} + Z_o\right)^2 \tag{2.1.109}$$

Here,

N : intragranular bubble density (bubbles/cm^3)

$\overline{R}$: average radius of intragranular bubbles (cm)

Z_0 : affected zone (cm)

α : bubble generation rate (= 24 bubbles/fission fragment)

λ : range (6×10^{-4} cm).

Fitting parameter APORE

The affected zone of fission Z_0 is given as the input parameter APORE. The default value of APORE is 0.0 (cm).

The rate of trapping by intra-granular bubbles, g, is given by [18]

$$g = 4\pi D\overline{R}N \tag{2.1.110}$$

$\overline{R}$: average intragranular bubble radius (cm)

N : intragranular bubble density (bubbles/cm^3)

The rate of re-dissolution of the gas into the matrix is given by

$$b' = 3.03F\pi\lambda\left(\overline{R} + Z_0\right)^2. \tag{2.1.111}$$

Here,

F : fission rate (fissions/cm^3/s)

λ : range (= 6×10^{-4}cm)

Z_0 : affected zone (cm).

Fitting parameter BFCT

The rate of redissolution in the solid phase is controlled using BFCT.
$b' = b' \times$ BFCT (Default value: 1.0)

$\overline{R}$ is obtained using van der Waals' state equation, which is

$$\left(P_0 + \frac{2\gamma}{\overline{R}}\right)\left(V - m^* B\right) = m^* kT, \tag{2.1.112}$$

where

$\overline{R}$: average intragranular bubble radius (cm)

P_0 : external force applied on intragranular bubbles (dyn/cm^2)

γ : surface tension (626 erg/cm^2)

V : intragranular bubble volume (= $\frac{4}{3}\pi\overline{R}^3$ cm^3)

B : van der Waals' constant (= 8.5×10^{-23} cm^3/atom)

m^* : number of gas atoms per unit bubble volume (atoms/bubble)

k : Boltzmann's constant (= 1.38×10^{-16} erg/K)

T : temperature (K).

Since $\overline{R}$ is very small, less than 1 nm, $2\gamma/\overline{R} \gg P_0$ holds and P_0 can be neglected. Setting P_0=0, eq. (2.1.112) is solved in terms of m^* as

$$m^* = \frac{8\pi\gamma\overline{R}}{3\left(2\gamma B + kT\overline{R}\right)}. \tag{2.1.113}$$

In the denominator of eq. (2.1.113), since $kT\overline{R}$ is smaller than $2\gamma B$, when $kT\overline{R}$ is neglected,

$$m^* = \frac{4\pi\gamma\overline{R}}{3B} \tag{2.1.114}$$

is obtained.

Meanwhile, from the equation describing the phase equilibrium between trapping and re-dissolution,

$$gc = b'm \tag{2.1.102}$$

is converted to the following equation of m^* using $m=m^*N$ and $c = \Psi - m$.

$$\left(b' + g\right)m^* N = g\Psi \tag{2.1.115}$$

By substituting eqs.(2.1.110), (2.1.111) and (2.1.114) into eq.(2.1.115), the following equation is obtained.

$$\left(3.03F\pi\lambda\left(\overline{R} + Z_0\right)^2 + 4\pi D\overline{R}N\right)\frac{\overline{R}^2}{3B} = D\Psi \tag{2.1.116}$$

Then, by substituting eq. (2.1.109) and rearranging the equation, the following equation of $\overline{R}$ is obtained.

$$\frac{3.03F\pi\lambda\left(\overline{R} + Z_0\right)^2\overline{R}^2}{3B} + \frac{4D \cdot 1.52\alpha\overline{R}^3}{3B\lambda\left(\overline{R} + Z_0\right)^2} - D\Psi = 0 \tag{2.1.117}$$

The diffusion coefficient D is given by the following equation derived by Turnbull.[19]

$$D = 7.6 \times 10^{-10} \exp\left(-7 \times 10^4 / RT\right) + S^2 jvV + 2 \times 10^{-40} F \quad (\mathrm{m^2/s}) \tag{2.1.118}$$

Here,

R : gas constant＝1.987 cal/mol/K

T : temperature (K)

S : atomic jump distance＝$\Omega^{\frac{2}{3}}$

Ω : atomic volume＝4.09×10^{-29} (m^2/s)

Fitting parameter FACD

The diffusion coefficient is controlled using FACD. $D = D \times$ FACD (Default value: 1.0)

$$jv = 10^{13} \exp\left(-5.52 \times 10^4 / RT\right)$$

$$V = \frac{\left(\partial_s S^2 + ZV_o\right)}{2Z}\left[\left(1 + \frac{4K'Z}{jv\left(\partial_s S^2 + ZV_o\right)^2}\right)^{\frac{1}{2}} - 1\right]$$

∂_s : sink strength=10^{15} (m^{-2})

Z : number of loss points=2

K' : loss ratio per atom=10^4

$V_0 = \exp\left(-5.52 \times 10^4 / RT\right)$

F : fission rate = 10^{19} (fission/m^3/s).

Figure 2.24 shows the temperature dependence of the diffusion coefficient.

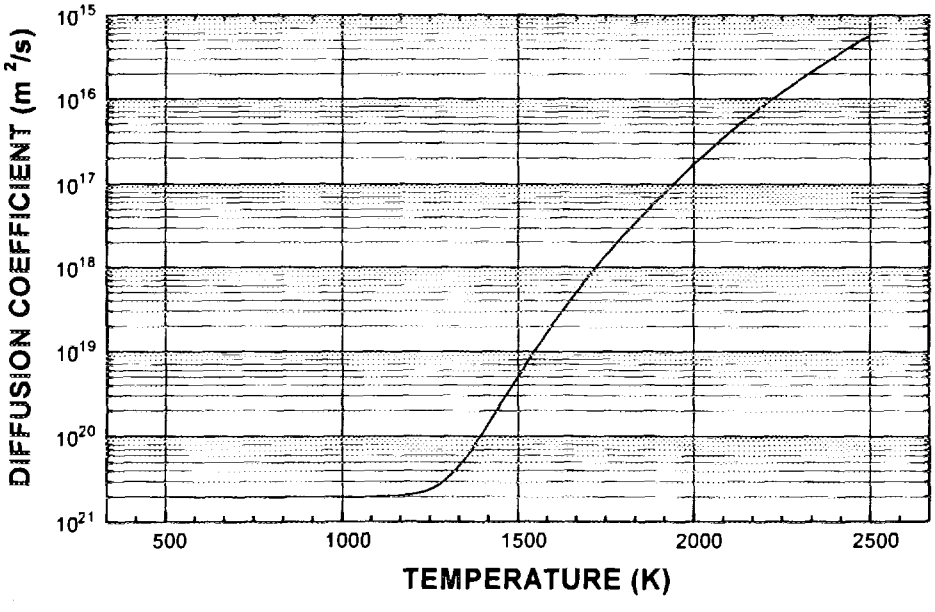

Fig. 2.24 Temperature dependence of the diffusion coefficient.

(2)－3 Solution of partial differential equation

To solve the partial differential equation (2.1.107), the weighted residuals finite element method developed by Galerkin is used. Equation (2.1.107) can be rewritten as

$$\frac{\partial \Psi}{\partial t} - D'\nabla^2\Psi - \beta = 0, \tag{2.1.119}$$

where an approximation function of the function $\Psi(t,r)$ is set as follows.

$$\Psi(t,r) \approx \hat{\Psi}(t,r) = \sum_j \Psi_j(t)\phi_j(r)$$

Here, $\phi_j(r)$ is an arbitrary known function called the basic function, and Ψ_j is an unknown coefficient, where the residuals are represented as

$$R_\Psi(t,r) = \frac{\partial \hat{\Psi}}{\partial t} - D'\nabla^2\hat{\Psi} - \beta.$$

The coefficient $\{\Psi_j\}$ which provides the minimum residuals is determined. The coefficient $\{\Psi_j\}$ can be determined by requiring a condition in which weighted integration becomes zero. When the basic function is selected as a weight function, this requirement can be satisfied by the equation

$$\int_V R_\Psi(t,r)\phi_i dv = 0. \tag{2.1.120}$$

To satisfy eq. (2.1.120) for an arbitrary weight function of ϕ_j, $R_\Psi(t,r)=0$ must be satisfied. Therefore, eq. (2.1.120) is equivalent to eq. (2.1.119). Integrating eq. (2.1.120),

$$\int_V \left(\frac{\partial \hat{\Psi}}{\partial t} - D'\nabla^2\hat{\Psi} - \beta\right)\phi_i dv = 0$$

$$\int_V \left(\frac{\partial \hat{\Psi}}{\partial t} - \beta\right)\phi_i dv - \int_V D'\nabla^2\hat{\Psi}\phi_i dv = 0 \tag{2.1.121}$$

are obtained. The second term of eq. (2.1.121) can also be expressed as

$$\begin{aligned} -\int_V D'\nabla^2\hat{\Psi}\phi_i dv &= -D'\left[\int_V \nabla\cdot\left(\phi_i\nabla\hat{\Psi}\right)dv - \int_V \left(\nabla\hat{\Psi}\right)\cdot\left(\nabla\phi_i\right)dv\right] \\ &= -D'\int_{\partial V}\phi_i\nabla\hat{\Psi}\cdot d\vec{s} + D'\int_V \left(\nabla\hat{\Psi}\right)\cdot\left(\nabla\phi\right)_i dv. \end{aligned}$$

Here, when a weight function which satisfies $\phi_j=0$ at the grain boundary ∂V is selected, the

surface integration term is eliminated and eq. (2.1.121) is expressed as

$$\int_{V_e}\left(\frac{\partial\hat{\Psi}}{\partial t}-\beta\right)\phi_i dv + D'\int_{V_e}\left(\nabla\hat{\Psi}\right)\cdot\left(\nabla\phi_i\right)dv = 0. \tag{2.1.122}$$

When a pellet grain is divided into finite elements, eq. (2.1.122) is expressed for a certain element V_e as

$$\sum_j\left(\dot{\Psi}_j E_{ji} + D'\Psi_j A_{ji}\right) - \beta H_i = 0, \tag{2.1.123}$$

where

$$E_{ji} = \int_{V_e}\phi_j\phi_i dv$$
$$A_{ji} = \int_{Ve}\frac{\partial\phi_i}{\partial r}\frac{\partial\phi_i}{\partial r}dv\int_{Ve}$$
$$H_i = \int_{V_e}\phi_i dv.$$

The following quadratic functions are adopted as basic functions ϕ_j.

$$\begin{aligned}\phi_1(\xi) &= -\frac{1}{2}\xi(1-\xi)\\ \phi_2(\xi) &= 1-\xi^2\\ \phi_3(\xi) &= \frac{1}{2}(1+\xi)\xi\end{aligned} \tag{2.1.124}$$

Using these basic functions, E_{ji}, A_{ji} and H_i in eq.(2.1.123) are represented using R_k, i.e., coordinates of the midpoint of element Ve, and ΔR , i.e., half-width of the element, as follows.

$$\begin{aligned}E_{ji} &= \int_{Ve}\phi_j\phi_i dv = 4\pi\int_{R_K-\Delta R}^{R_K+\Delta R}\phi_j\phi_i r^2 dr\\ &= 4\pi\Delta R\int_{-1}^{1}\phi_j\phi_i\left(R_k+\Delta R\xi\right)^2 d\xi\end{aligned}$$

$$\begin{aligned}A_{ji} &= \int_{Ve}\frac{\partial\phi_i}{\partial r}\frac{\partial\phi_j}{\partial r}dv = 4\pi\int_{R_k-\Delta R}^{R_k+\Delta R}\frac{\partial\phi_i}{\partial r}\frac{\partial\phi_j}{\partial r}r^2 dr\\ &= \frac{4\pi}{\Delta R}\int_{-1}^{1}\frac{\partial\phi_i}{\partial\xi}\frac{\partial\phi_j}{\partial\xi}\left(R_k+\Delta R\xi\right)^2 d\xi\end{aligned} \tag{2.1.125}$$

$$H_i = \int_{Ve}\phi_i dv = 4\pi\int_{R_k-\Delta R}^{R_k+\Delta R}\phi_i r^2 dr = 4\pi\Delta R\int_{-1}^{1}\phi_j\left(R_k+\Delta R\xi\right)^2 d\xi$$

Next, eq. (2.1.123) is represented by an implicit formula (Q is a constant).

$$\sum_j \left\{ \frac{\Psi_j^{n+1} - \Psi_j^n}{\Delta t} E_{ij} + D^* \left((1-\theta)\Psi_j^n + \theta \Psi_j^{n+1} \right) A_{ji} \right\} - \beta^* H_i = 0 \qquad (2.1.126)$$

Here,

$$D^* = (1-\theta) D'^n + \theta D'^{n+1}$$

$$\beta' = (1-\theta)\beta^n + \theta \beta^{n+1}.$$

Through rearrangement of the unknown and known values of eq. (2.1.126),

$$\sum_j \left(\frac{1}{\Delta t} E_{ij} + D^* \theta A_{ji} \right) \Psi_j^{n+1} = \sum_j \left(\frac{1}{\Delta t} E_{ij} - D^* (1-\theta) A_{ji} \right) \Psi_j^n + \beta^* H_i \qquad (2.1.127)$$

is obtained. Therefore, the element matrix W_{ij} and the element vector Q_i are

$$W_{ij} = \frac{1}{\Delta k} E_{ij} + D^* \theta A_{ji} \qquad (2.1.128)$$

$$Q_i = \sum_j \left(\frac{1}{\Delta t} E_{ij} - D^* (1-\theta) A_{ji} \right) \Psi_j^n + \beta^* H_i . \qquad (2.1.129)$$

Through superimposition of the equations for all elements and setting of the condition of $\Psi^{n+1} = 0$ on the surface, $\left\{ \Psi_j^{n+1} \right\}$ can be obtained by solving the simultaneous equations below.

$$\left[W_{ij} \right] \left\{ \Psi_j^{n+1} \right\} = \left\{ Q_i \right\} \qquad (2.1.130)$$

(2)－4 Sweeping of gas into grain boundary by grain growth, and re-dissolution of the gas from inter-granular gas bubbles into grains

During grain growth, the gas in grains is swept into the grain boundary. The rate of gas sweeping into the grain boundary is given as

$$f_g = \left(\frac{a^{n+1}}{a^n} \right)^3 - 1. \qquad (2.1.131)$$

Here,

a^{n+1} : grain size after grain growth (cm)

a^n : grain size before grain growth (cm).

Fitting parameter FGG
The rate of gas sweepings is controlled with FGG as $f_g = f_g \times$ FGG.

Figure 2.25 shows a conceptual schematic of the grain growth. The gas present in the region with diagonal lines is released at the grain boundary during grain growth.

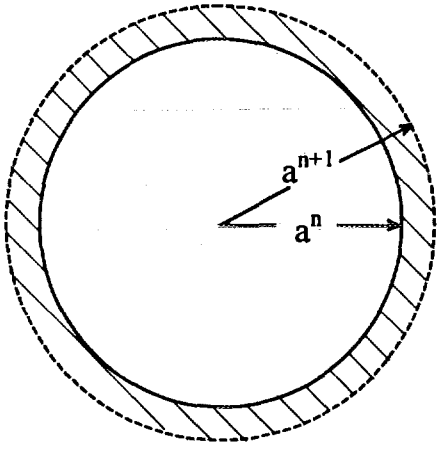

Fig. 2.25 Conceptual diagram of grain growth.

The grain growth model uses the following Itoh's equation as a representative one.[20]

$$\frac{da}{dt} = K\left(\frac{1}{a} - \frac{1 + N_f / N_f^{\max}}{a_m}\right) \text{ (μm/h)} \qquad (2.1.132)$$

$$K = 5.24 \times 10^7 \exp\left(-2.67 \times 10^5 / RT\right) \text{ (μm}^2\text{/h)}$$

a : grain size at current time step (μm)

a_m : maximum grain size $\left(= 2.23 \times 10^3 \exp(-7620 / T)\right)$ (μm)

R : gas constant (=8.314 J/mol/K)

N_f : gas atom density at grain boundary (atoms/cm^2)

N_f^{max} : saturation value of the gas atom density at grain boundary (atoms/cm^2)

Fitting parameters AG and GRWF

The grain growth rate can be controlled using AG and GRWF as follows.
1) Control of the gas atom density: $N_f = N_f \times$ AG (Default value: AG=1.5)
2) Grain growth rate: $\frac{da}{dt} = \frac{da}{dt} \times$ GRWF (Default value: GRWF=1.0)

Selection of option IGRAIN The option of the grain growth model can be selected using IGRAIN as follows. IGRAIN=0: Itoh's model(default), =1: Ainscough model, =2: MacEwan model, =3: Lyons model, =4: MATPRO-09 model.

Each grain consists of a maximum of 5 elements. The outermost element is the boundary layer, which is a special element for consideration of re-dissolution. When grain growth occurs during time step from n to n+1, elements (mesh) in the grains are re-meshed.

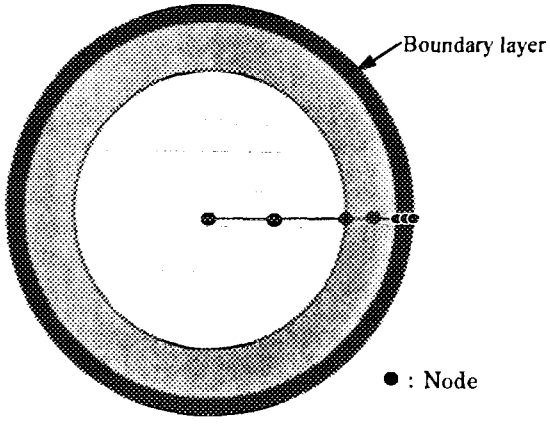

Fig. 2.26 Meshing of a pellet grain.

Setting the boundary layer width as $2\Delta R$, coordinates r at the node of the first and second elements are given as

$$r^{n+1} = \frac{a^{n+1} - 2\Delta R}{a^n - 2\Delta R} r^n, \tag{2.1.133}$$

where

r^{n+1} : coordinates at the node point after grain growth

r^n : coordinates at the node point before grain growth.

Coordinates at the three node points in the outermost boundary layer are given as $a^{n+1} - 2\Delta R$, $a^{n+1} - \Delta R$ and a^{n+1}.

Model parameters NODEG and RREL The number of elements in grains is designated by NODEG. The default value is 3, and the maximum value is 5. The width of layers other than the outermost layer, namely the elements of NODEG-1, is designated by the ratio RREL. The default value is 5, 1, which means that the ratio of the width of the first to second layers is 5:1.

The FP gas concentration Ψ at a given set of coordinates after re-meshing is given by

$$\Psi^{n+1,0}(r) = \Psi^n(r) \qquad (0 \leqq r \leqq a^n) \tag{2.1.134}$$

$$\Psi^{n+1,0}(r) = 0 \qquad (a^n \leqq r \leqq a^{n+1}),$$

where

$\Psi^{n+1,0}(r)$: initial concentration distribution of FP gas after grain growth

$\Psi(r)$: FP gas concentration distribution before grain growth.

Namely, it is assumed that sweeping of the gas into the grain boundary due to grain growth occurs instantaneously. Therefore, the initial value of the FP gas atom density per unit area at the grain boundary during grain growth is set as $N_f^{n+1,0}$ in calculation of its change between time step n and time step (n+1), and the following equation holds.

$$\left(\frac{a^{n+1}}{a^n}\right)^3\left(\overline{\Psi}^n_{total}+4\pi a^{n^2}N_f^n\right)=\overline{\Psi}^n_{total}+4\pi a^{n+1^2}N_f^{n+1,0} \tag{2.1.135}$$

Here,

$\overline{\Psi}^n_{total}$: number of FP gas atoms in grain before grain growth (atoms)

N_f^n : FP gas atom density per unit area at the grain boundary before grain growth (atoms/cm^2), and $N_f^0=0$.

Equation (2.1.135) is solved in terms of $N_f^{n+1,0}$, and the equation

$$N_f^{n+1,0}=\frac{f_g\overline{\Psi}^n_{total}}{4\pi a^{n+1^2}}+\frac{a^{n+1}}{a^n}N_f^n \tag{2.1.136}$$

holds.

Thus, the initial value for determination of the FP gas concentrations of both intragrain and intergrain at time step (n+1) is obtained. Using the initial value and eq. (2.1.134), the FP gas concentration at the time step (n+1) during grain growth will be calculated.

(2)－5 FP gas redissolution

In the model of FP gas atom re-dissolution from grain boundary into grains, since the grain boundary separates adjacent crystal grains, we assume that half of the FP gas per unit area of the grain boundary is re-dissolved. Namely,

$$\frac{bN_f}{2}\cdot(\mathrm{ADDF})\ (\mathrm{atoms/cm^2/s}) \tag{2.1.137}$$

where b : rate of re-dissolution (10^{-6}/s).

Model parameter RB	RB is a parameter for controlling the thickness of the boundary layer where FP gas redissolves. The default value of RB is 2×10^{-8} (cm).

Re-dissolution means physical transfer of FP gas from the grain boundary into grains, which is virtually equivalent to an additional generation of FP gas in grains. Therefore, when the thickness of regions where FP gas re-dissolves is assumed to be equal to the boundary layer thickness (200 Å), the apparent rate of FP gas generation β' in the boundary layer is determined.

> Fitting parameter ADDF
> The amount of gas redissolved is controlled using ADDF. The default value of ADDF is 9.0.

Therefore, β' is given by the following equation.

$$\beta' = \frac{b}{2}\left\{(1-\theta)N_f^n + \theta N_f^{n+1}\right\}\frac{1}{2\Delta R}(\cdot ADDF) \text{ (atoms/cm}^3\text{/·s)} \tag{2.1.138}$$

Here,

N_f^n : concentration of FP gas atoms in the grain boundary at time step n (atoms/cm^2)

N_f^{n+1} : concentration of FP gas atoms in the grain boundary at time step(n+1) (atoms/cm^2)

θ : interpolation parameter between time steps in the implicit solution,

where values of N_f^n and N_f^{n+1} do not depend on the occurrence of grain growth.

Accordingly, β in eq. (2.1.96) for the boundary layer is expressed as

$$\tilde{\beta} = \beta + \beta' \tag{2.1.139}$$

and $\tilde{\beta}$ is defined as the FP gas generation rate.

N_f^{n+1} is expressed as

$$N_f^{n+1} = \frac{a^{n+1}}{a^n}N_f{}^n + \frac{\left(1+f_g\right)\overline{\Psi}_{total}^n - \overline{\Psi}_{total}^{n+1} + \int_V \beta\Delta t dv}{4\pi a^{n+1^2}}. \tag{2.1.140}$$

Here,

$\overline{\Psi}_{total}^{n+1}$: number of FP gas atoms in grains at time step $n+1$ (atoms)

$\beta\Delta tvd$: amount of FP gas generated excluding the amount of re-dissolved atoms during the time step increment (atoms), where $\int_V dv = \frac{4}{3}\pi a^{n+1^3}$ holds.

$\overline{\Psi}_{total}^{n+1}$ is expressed as follows when the number of elements comprising each grain is 3.

$$\overline{\Psi}_{total}^{n+1} = \sum_{e=1}^{3}\int_r 4\pi r^2 \hat{\Psi}^{n+1}(r)dr, \tag{2.1.141}$$

$$\hat{\Psi}^{n+1}(r) = \sum_{j=1}^{3} \Psi_j^{n+1} \phi_j(r)$$

(2)-6 Gas release due to connection of intergranular gas bubbles

With irradiation, intergranular bubble density increases and the bubbles expand and become connected. Then, a certain point of the connected bubbles comes into contact with a crack or a channel which leads to a free space inside the fuel rod, and the bubble becomes an open bubble, i.e. non-isolated bubble, releasing the gas it contains into the free space.

The current model assumes that when the number of gas atoms per unit area at the grain boundary exceeds N_f^{max}, bubbles are connected and a tunnel leading to a free space is formed. It is also assumed that once the gas concentration at the grain boundary reaches a certain value, additional gas atoms diffused from grains are immediately released into the free space. N_f^{max} is given by the following equation.[17]

$$N_f{}^{max} = \frac{4 r_f f_f(\vartheta)}{3kT \sin^2 \vartheta} f_b \left\{ \frac{2\gamma}{r_f} + P_{ext} \right\} \qquad (2.1.142)$$

Here,

$$f_f(\vartheta) = 1 - \frac{3}{2}\cos\vartheta + \frac{1}{2}\cos^3\vartheta \qquad (2.1.143)$$

N_f^{max} : saturation value of the number of gas atoms per unit area at the grain boundary (atoms/cm^2)

r_f : intergranular gas bubble radius ($=0.5\times10^{-4}$cm)

$f_f(\delta)$: volume ratio of lenticular bubble to sphere bubble

ϑ : lenticular bubble angle (=50°)

k : Boltzmann's constant ($=1.38\times10^{-16}$ erg/K)

T : temperature (K),

γ : surface tension (=626 erg/cm^2)

f_b : covering ratio of lenticular bubbles over grain boundary (=0.2)

P_{ext} : external force (dyne/cm^2)

The external pressure P_{ext} is obtained using a procedure described below, taking into account the plenum pressure, contact pressure between pellet and cladding, and pellet internal thermal stress.

To calculate the pellet thermal stress, the finite element method is generally applied to determine the strict values of temperature distribution inside the pellet, as in the case of the thermal analysis part. However, in the case of the current model, a simplified method in which approximate temperature distribution and thermal stresses are obtained by the use of an analytical solution is adopted. That is, using the restriction equation of Lame, the temperature distribution inside the pellet is set as follows.

$$T - T_s = (T_c - T_s)\left\{1 - (r / R)^2\right\} \tag{2.1.144}$$

Here, T : temperature at radius r

T_s : pellet surface temperature

T_c : pellet center temperature

R : pellet outer radius

Then, the pellet internal thermal stress is expressed as

$$\sigma_r = \frac{E}{4(1-\nu)} a(T_c - T_s)\left\{\left(\frac{r}{R}\right)^2 - 1\right\} - P_i \tag{2.1.145}$$

$$\sigma_\theta = \frac{E}{4(1-\nu)} a(T_c - T_s)\left\{3\left(\frac{r}{R}\right)^2 - 2\right\} - P_i \tag{2.1.146}$$

$$\sigma_z = \frac{E}{4(1-\nu)} a(T_c - T_s)\left\{4\left(\frac{r}{R}\right)^2 - 1\right\} - P_i, \tag{2.1.147}$$

where

σ_r, σ_θ, σ_z : stress in the r, θ and z directions

E : Young's modulus of pellet

ν : Poisson's ratio of pellet

a : thermal expansion coefficient of pellet

P_i : contact pressure between pellet and cladding

P_f : pellet axial force.

Here, the contact pressure between pellet and cladding which was obtained in the thermal analysis is used as Pi, and the pellet axial force is set to be equal to the contact pressure ($P_f = P_i$), for convenience.

The average stress $\bar{\sigma}$ is set as

$$\bar{\sigma} = \frac{1}{3}(\sigma_r + \sigma_\theta + \sigma_z). \tag{2.1.148}$$

The stress calculation method is described below.

First, a method to calculate stresses in the $n+1$ time step, $\sigma_{r,n+1}$, $\sigma_{\theta,n+1}$ and $\sigma_{z,n+1}$, from the stresses obtained in the n time step, $\sigma_{r,n}$, $\sigma_{\theta,n}$ and $\sigma_{z,n}$, is considered. Here, stresses in the 0th time step (i.e. hot stand-by), $\sigma_{r,0}$, $\sigma_{\theta,0}$ and $\sigma_{z,0}$, are assumed to equal the plenum gas pressure. Using eqs.(2.1.145), (2.1.146) and (2.1.147), the thermal stress increments between time steps are obtained as

$$\begin{aligned}\Delta\sigma^{th}_{r,n+1} = {} & \frac{E_{n+1}}{4(1-\nu)} a_{n+1}(T_{c,n+1} - T_{s,n+1})\left\{\left(\frac{r}{R}\right)^2 - 1\right\} - P_{i,n+1} \\ & - \left\{\frac{E_n}{4(1-\nu)} a_n(T_{c,n} - T_{s,n})\left\{\left(\frac{r}{R}\right)^2 - 1\right\} - P_{i,n}\right\}\end{aligned} \tag{2.1.149}$$

$$\begin{aligned}\Delta\sigma^{th}_{\theta,n+1} = {} & \frac{E_{n+1}}{4(1-\nu)} a_{n+1}(T_{c,n+1} - T_{s,n+1})\left\{\left(3\frac{r}{R}\right)^2 - 2\right\} - P_{i,n+1} \\ & - \left\{\frac{E_n}{4(1-\nu)} a_n(T_{c,n} - T_{s,n})\left\{\left(3\frac{r}{R}\right)^2 - 2\right\} - P_{i,n}\right\}\end{aligned} \tag{2.1.150}$$

$$\begin{aligned}\Delta\sigma^{th}_{z,n+1} = {} & \frac{E_{n+1}}{4(1-\nu)} a_{n+1}(T_{c,n+1} - T_{s,n+1})\left\{4\left(\frac{r}{R}\right)^2 - 1\right\} - P_{i,n+1} \\ & - \left\{\frac{E_n}{4(1-\nu)} a_n(T_{c,n} - T_{s,n})\left\{4\left(\frac{r}{R}\right)^2 - 1\right\} - P_{i,n}\right\}.\end{aligned} \tag{2.1.151}$$

The 0th approximation of the stresses in the $n+1$ time step is set as

$$\sigma^0_{r,n+1} = \sigma_{r,n} + \Delta\sigma^{th}_{r,n+1} \tag{2.1.152}$$

$$\sigma^0_{\theta,n+1} = \sigma_{\theta,n} + \Delta\sigma^{th}_{\theta,n+1} \tag{2.1.153}$$

$$\sigma^0_{z,n+1} = \sigma_{z,n} + \Delta\sigma^{th}_{z,n+1}. \tag{2.1.154}$$

Substituting eqs.(2.1.152), (2.1.153) and (2.1.154) into eq. (2.1.148), the 0th approximation of the average stress $\bar{\sigma}^0_{n+1}$ is obtained as

$$\bar{\sigma}^0_{n+1} = \frac{1}{3}\left(\sigma^0_{r,n+1} + \sigma^0_{\theta,n+1} + \sigma^0_{z,n+1}\right). \tag{2.1.155}$$

Here, when $\bar{\sigma}^0_{n+1}$ is less than the plenum gas pressure P_{gas},

$$\bar{\sigma}^0_{n+1} = P_{gas,n+1} \tag{2.1.156}$$

holds. When $\bar{\sigma}^0_{n+1}$ is larger than the yielding stress σ_Y,

$$\bar{\sigma}^0_{n+1} = \sigma_{Y,n+1} \tag{2.1.157}$$

is set.

Next, calculation of thermal stress alleviation by creep is carried out in an approximate manner, by setting the equivalent stress σ_{eq} as

$$\sigma_{eq} = |\bar{\sigma}^0_{n+1}|.$$

The change of equivalent creep strain is assumed to be in proportion to the creep rate determined by a creep function f (MATPRO-09 equation[14]), and η is set as a proportion coefficient, the following holds:

$$\Delta\bar{\varepsilon}^c_{n+1} = f(T, \sigma_{eq}, G, f_d, \dot{F}) \cdot \eta \cdot \Delta t, \tag{2.1.158}$$

where

T : temperature

σ_{eq} : equivalent stress

G : grain size

f_d : pellet theoretical density ratio

$\dot{F}$: fission density

Δt : time step width.

Here, $\eta = 10^{-4}$ is adopted as an empirically obtained fitting parameter.

By substitution of the thus obtained $\Delta\bar{\varepsilon}^c_{n+1}$ into the equation

$$\bar{\sigma}^1_{n+1} = \bar{\sigma}^0_{n+1} + E\Delta\bar{\varepsilon}^c_{n+1}, \tag{2.1.159}$$

the first approximation of the average stress $\bar{\sigma}^1_{n+1}$ is obtained. However, proportion coefficient between σ and $\Delta\varepsilon$ in creep deformation is set as the pellet Young's modulus itself on the assumption that the coefficient depends linearly on the Young's modulus.

Thereafter, a convergence calculation regarding σ_{n+1} is performed using the Newton-

Raphson method, on the assumption that $-\sigma_{Y,n+1} \le \bar{\sigma}_{n+1} \le -P_{gas,n+1}$. The obtained $\bar{\sigma}_{n+1}$ is the thermal stress for grain boundary bubble gas. Therefore, $P_{ext}=\bar{\sigma}_{n+1}$ holds. Namely, this stress acts on the bubbles as an external pressure P_{ext} in eq.(2.1.142).

The stresses in the $n+1$ time step $\sigma_{r,n+1}$, $\sigma_{\theta,n+1}$ and $\sigma_{z,n+1}$ are obtained as

$$\begin{aligned}\sigma_{r,n+1} &= \sigma_{r,n} + \Delta\sigma^{th}_{r,n+1} + E\Delta\bar{\varepsilon}^{c}_{n+1}\\ \sigma_{\theta,n+1} &= \sigma_{\theta,n} + \Delta\sigma^{th}_{\theta,n+1} + E\Delta\bar{\varepsilon}^{c}_{n+1}\\ \sigma_{z,n+1} &= \sigma_{z,n} + \Delta\sigma^{th}_{z,n+1} + E\Delta\bar{\varepsilon}^{c}_{n+1}.\end{aligned} \qquad (2.1.160)$$

Here, $\sigma_{i,n+1} < 0$, namely the stress is compressive.

Selection of option IPEXT Regarding the P_{ext} evaluation method, a condition can be selected from among the following 8 conditions using IPEXT. The default value of IPEXT = 1.

IPEXT=0: P_{ext}=0, IPEXT=1: P_{ext}=plenum pressure, IPEXT=2: P_{ext}=contact pressure between pellet and cladding, IPEXT=3: P_{ext}=max (plenum pressure, contact pressure),
IPEXT=11: P_{ext}=thermal stress (taking into account the plenum pressure),
IPEXT=12: P_{ext}=thermal stress (taking into account the contact pressure between pellet and cladding),
IPEXT=13: P_{ext}=thermal stress (taking into account the plenum pressure and contact pressure),
IPEXT=14: P_{ext}=average stress obtained by stress calculation in Detailed Mechanical Analysis (I). Here, when Detailed Mechanical Analysis (II) is used, the results will be the same as those in the case of IPEXT = 13.

Fitting parameters OPORO, FBSAT, ALHOT In the mechanistic model (IGASP=0), fraction of open gas bubbles of FP at grain boundary is designated by OPORO. The default value is 0.0. FBSAT gives a multiplication factor for the saturation amount of gas at grain boundary. The default value is 1.0.

η in eq.(2.1.158) can be designated by ALHOT. The default value is 0.0001.

(2)－7 Determination of time－step width

In the mechanistic FP gas release model, the calculation is performed with an original time-step width that is determined using apparent diffusion coefficient D' and node interval in the second layer ΔR_2 as

$$\Delta t = \frac{\Delta R_2^2}{D'} \times 0.05 \times \mathrm{FMULT}. \qquad (2.1.161)$$

FMULT Fitting parameter for controlling time-step width. The default value is 1.0.

2.1.5 Gas diffusion and flow in the gap

(1) Assumptions and methods

Diffusion and flow calculation of gap gas is based on the following assumptions.

① Helium and Nitrogen (or Argon), as well as Xenon and Krypton are completely mixed instantaneously; therefore, behavior of Nitrogen (or Argon) is represented by that of Helium, and also behavior of Krypton is represented by that of Xenon. Thus, calculation is performed for a 2-component mixed gas, i.e. mixture of Helium and Xenon.

② Counter-diffusion occurs with Helium and Xenon which pass through the gap.

③ The counter-diffusion calculation is performed using an implicit solution based on Fick's first law. The diffusion is independent of flow caused by pressure difference in the fuel rod.

④ Pressure inside the fuel rod is uniform during the diffusion calculation.

⑤ Pressures at different parts inside the fuel rod are assumed to be equilibrated instantaneously. Therefore, gas flow between the axial segments induced by the pressure difference in the fuel rod also occurs instantaneously.

(2) Equation for the gap region

The following is a list of symbols used.

N : gas molar number (mol)

n : molar density (mol/cm^3)

D^{12} : counter-diffusion constant (m^2/s) ($D^{12} = D^{21}$)

T : temperature (K)

V : volume (m^3)

C : molar fraction $\left(C_1 = n_1 / \left(n_1 + n_2\right)\right)$

Subscripts are

I : kind of gas (1 = Xenon, 2 = Helium),

j : axial segment $\left(j = P_L, 1, 2, 3, \cdots, N, P_U\right)$ (P_L : lower plenum, P_U : upper plenum).

In particular, subscripts for molar density are

n_{ij} : density of gas i at axial segment j,

n_j : density of all gases at axial segment j.

Figure 2.27 shows the present model of calculation.

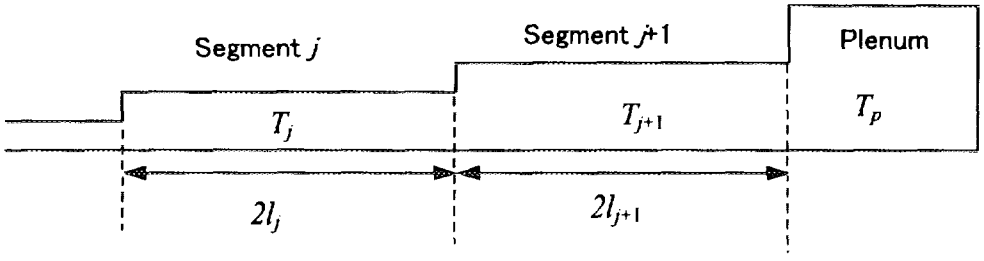

Fig. 2.27 Gas diffusion and flow model.

The total amount of gas i at axial segment j is

$$N_{i,j} = n_{i,j} V_j$$
$$= C_{i,j}\, n_j\, V_j = \frac{P}{R} C_{i,j} \frac{V_j}{T_j}. \tag{2.1.162}$$

Here, each segment has a channel cross-sectional area of S_j and length of $2l_j$; also, the boundary of segments j and $j+1$ is indicated by *.

The amount of gas 1 (Xe) $G_1(j \to j+1)$ flowing from segment j to segment $j+1$ over the boundary * is obtained on the basis of Fick's law,

$$G_1(j \to *) = S_j D_j^{12} \frac{n_{1,j} - n_{1,*}}{l_j}. \tag{2.1.163}$$

Similarly, the amount of gas 1 (Xe) flowing into segment $j+1$ over * is represented as

$$G_1(* \to j+1) = S_{j+1} D_{j+1}^{12} \frac{n_{1,*} - n_{1,j+1}}{l_{j+1}}. \tag{2.1.164}$$

From the continuous condition,

$$G_1(j \to *) = G_1(* \to j+1)$$

holds and

$$S_j D_j^{12} \frac{n_{1,j} - n_{1,*}}{l_j} = S_{j+1} D_{j+1}^{12} \frac{n_{1,*} - n_{1,j+1}}{l_{j+1}} \tag{2.1.165}$$

can be obtained. By solving this equation for $n_{1,*}$, we obtain

$$n_{1,*} = \frac{S_j D_j^{12} l_{j+1}\, n_{1,j} + S_{j+1}\, D_{j+1}^{12}\, l_j\, n_{1,j+1}}{S_{j+1}\, D_{j+1}^{12}\, l_j + S_j D_j^{12} l_{j+1}}. \tag{2.1.166}$$

Using eq. (2.1.163), we obtain the following equation.

$$G_1(j \to j+1) = G_1(j \to *) = \frac{S_j D_j^{12} S_{j+1} D_{j+1}^{12}}{S_{j+1} D_{j+1}^{12} l_j + S_j D_j^{12} l_{j+1}} \left(n_{1,j} - n_{1,j+1}\right) \tag{2.1.167}$$

Here, by setting

$$F_{j,j+1} = \frac{S_j D_j^{12} S_{j+1} D_{j+1}^{12}}{S_{j+1} D_{j+1}^{12} l_j - S_j D_j^{12} l_{j+1}}, \tag{2.1.168}$$

eq. (2.1.167) is expressed as

$$G_1(j \to j+1) = F_{j,j+1}\left(n_{1,j} - n_{1,j+1}\right). \tag{2.1.169}$$

Meanwhile, regarding gas 2 (He),

$$G_2(j \to j+1) = F_{j,j+1}\left(n_{2,j} - n_{2,j+1}\right) \tag{2.1.170}$$

is obtained.

Through addition of eqs.(2.1.169) and (2.1.170), the total amount of inflow mixed gas can be calculated as

$$G(j \to j+1) = F_{j,j+1}\left(n_j - n_{j+1}\right). \tag{2.1.171}$$

Here, the next equation

$$n_j = n_{1,j} + n_{2,j}\ ,\ n_{j+1} = n_{1,j+1} + n_{2,j+1}$$

holds.

Since in general, the gap temperatures at segments j and j+1 differ, the following equation holds in the equilibrium state.

$$n_j \neq n_{j+1} \tag{2.1.172}$$

According to eq. (2.1.171), however, even if segments j and j+1 are in equilibrium, imaginary flow from segment j to j+1 is present in the numerical calculation.

This is because Fick's first law is applied to a field with a temperature gradient. To eliminate this flow, a second term representing the effect of temperature difference must be added to both eqs. (2.1.171) and (2.1.172).

The second term to be added to eq. (2.1.171) is

$$G(j \to j+1) = F_{j,j+1}\left\{\left(n_j - n_{j+1}\right) - \left(\bar{n}_j - \bar{n}_{j+1}\right)\right\}, \tag{2.1.173}$$

where $\overline{n}_j$ and $\overline{n}_{j+1}$ are given by the ideal gas law as follows.

$$\overline{n}_j = \frac{P}{R}\frac{1}{T_j}, \overline{n}_{j+1} = \frac{P}{R}\frac{1}{T_{j+1}} \tag{2.1.174}$$

The amount of flow of each component, namely eqs.(2.1.171) and (2.1.172), is given, respectively, as follows.

$$G_1(j \to j+1) = F_{j,j+1}\left\{\left(n_{1,j} - n_{1,j+1}\right) - \left(\overline{n}_{1,j} - \overline{n}_{1,j+1}\right)\right\} \tag{2.1.175}$$

$$G_2(j \to j+1) = F_{j,j+1}\left\{\left(n_{2,j} - n_{2,j+1}\right) - \left(\overline{n}_{2,j} - \overline{n}_{2,j+1}\right)\right\} \tag{2.1.176}$$

Here,

$$\overline{n}_{1,j} = \frac{P}{R}\frac{\overline{C}_1}{T_j} \quad , \quad \overline{n}_{1,j+1} = \frac{P}{R}\frac{\overline{C}_1}{T_{j+1}} \tag{2.1.177}$$

$$\overline{C}_1 = \frac{N_{1,j} + N_{1,j+1}}{V_j + V_{j+1}} = \frac{n_{1,j}V_j + n_{1,j+1}V_{j+1}}{V_j + V_{j+1}} \tag{2.1.178}$$

$$\overline{n}_{2,j} = \frac{P}{R}\frac{\overline{C}_2}{T_j} \quad , \quad \overline{n}_{2,j+1} = \frac{P}{R}\frac{\overline{C}_2}{T_{j+1}} \tag{2.1.179}$$

$$\overline{C}_2 = \frac{N_{2,j} + N_{2,j+1}}{V_j + V_{j+1}} = \frac{n_{2,j}V_j + n_{2,j+1}V_{j+1}}{V_j + V_{j+1}} \tag{2.1.180}$$

$$\overline{C}_1 + \overline{C}_2 = 1. \tag{2.1.181}$$

(3) Implicit solution of He−Xe counter−diffusion model

The flux $J_{1,R}$ of gas 1 (Xe) that diffuses through the boundary surface R (boundary between segments j−1 and j) into segment j is given by

$$J_{1,R} = F_{j-1,j}\left\{\left(n_{1,j-1} - n_{1,j}\right) - \left(\overline{n}_{1,j-1} - \overline{n}_{1,j}\right)\right\}. \tag{2.1.182}$$

The flux $J_{1,S}$ of gas 1 (Xe) that diffuses through the boundary surface S (boundary between segments j and j+1) into segment j+1 is given by

$$J_{1,S} = F_{j+1,j}\left\{\left(n_{1,j} - n_{1,j+1}\right) - \left(\overline{n}_{1,j} - \overline{n}_{1,j+1}\right)\right\}. \tag{2.1.183}$$

Then, the change in the amount of Xenon in segment j is given by

$$V_j \frac{\partial n_{1,j}}{\partial t} = J_{1,R} - J_{1,S} . \tag{2.1.184}$$

Through differentiation of eq.(2.1.184) using eqs.(2.1.182) and (2.1.183) and the implicit method, the following equation is obtained. Here, k denotes time-step number.

$$\frac{n_{1,j}^{k+1} - n_{1,j}^{k}}{\Delta t} = \frac{1}{V_j^{\theta 1}} \left\{ F_{j-1,j}^{\theta_1} \left[\left(n_{1,j-1}^{\theta_2} - n_{1,j}^{\theta_2} \right) - \left(\bar{n}_{1,j-1}^{\theta_1} - \bar{n}_{1,j}^{\theta_1} \right) \right] - F_{j-1,j}^{\theta_1} \left[\left(n_{1,j}^{\theta_2} - n_{1,j+1}^{\theta_2} \right) - \left(\bar{n}_{1,j}^{\theta_1} - \bar{n}_{1,j+1}^{\theta_1} \right) \right] \right\} \tag{2.1.185}$$

Here,

θ_1 = interpolation with respect to temperature, volume, pressure and equilibrium molar ratio,

θ_2 = interpolation with respect to molarity.

θ_1 and θ_2 are the interpolation parameters in a converging loop in the axial direction and in the counter-diffusion calculation, respectively. θ_1 changes in the converging loop in the axial direction, but remains constant in the counter-diffusion calculation.

Fitting parameters THG1 and THG2 — θ_1 and θ_2 are designated by THG1 and THG2, respectively. Their default value is 1.0.

Therefore, an interpolation equation for θ_2,

$$n_{1,j}^{\theta 2} = (1-\theta_2) n_{1,j}^{k} + \theta_2 n_{1,j}^{k+1} , \tag{2.1.186}$$

is substituted into eq. (2.1.185), and the following equation is obtained.

$$\begin{aligned} \frac{n_{1,j}^{k+1} - n_{1,j}^{k}}{\Delta t} = {} & \frac{\theta_2 F_{j-1,j}^{\theta_1}}{V_j^{\theta_1}} n_{1,j-1}^{k+1} - \frac{\theta_2 \left\{ F_{j,j+1}^{\theta_1} + F_{j-1,j}^{\theta_1} \right\}}{V_j^{\theta_1}} n_{1,j}^{k+1} \\ & + \frac{\theta_2 F_{j-1,j}^{\theta_1}}{V_j^{\theta_1}} n_{1,j+1}^{k+1} + \frac{1}{V_j^{\theta_1}} \left\{ F_{j-1,j}^{\theta_1} \left[(1-\theta_2) \left(n_{1,j-1}^{k} - n_{1,j}^{k} \right) \right. \right. \\ & \left. \left. - \left(\bar{n}_{1,j-1}^{\theta_1} - \bar{n}_{1,j}^{\theta_1} \right) \right] - F_{j,j+1}^{\theta_1} \left[(1-\theta_2) \left(n_{1,j}^{k} - n_{1,j+1}^{k} \right) - \left(\bar{n}_{1,j}^{\theta_1} - \bar{n}_{1,j+1}^{\theta_1} \right) \right] \right\} . \end{aligned} \tag{2.1.187}$$

Through rearrangement of eq. (2.1.187),

$$A_j n_{1,j-1}^{k+1} + B_j n_{1,j}^{k+1} + C_j \cdot n_{1,j+1}^{k+1} = D_j . \tag{2.1.188}$$

Here,

$$A_j = -\frac{\theta_2 F_{j-1,j}^{\theta_1}}{V_j^{\theta_1}} \Delta t \tag{2.1.189}$$

$$B_j = 1 + -\frac{\theta_2\left\{F^{\theta_1}_{j-1,j} + F^{\theta_1}_{j,j+1}\right\}}{V^{\theta_1}_j}\Delta t \tag{2.1.190}$$

$$C_j = -\frac{\theta_2 F^{\theta_1}_{j,j+1}}{V^{\theta_1}_j}\Delta t \tag{2.1.191}$$

$$\begin{aligned} D_j = {} & \frac{1}{V^{\theta_1}_j}F^{\theta_1}_{j,j-1}(1-\theta_2)\Delta t\; n^k_{1,j-1} + \left\{1 - \frac{1}{V^{\theta_1}_j}\left(F^{\theta_1}_{j,j-1} + F^{\theta_1}_{j,j+1}\right)(1-\theta_2)\Delta t\right\} n^k_{1,j} \\ & + \frac{1}{V^{\theta_1}_j}F^{\theta_1}_{j,j+1}(1-\theta_2)\Delta t\; n^k_{1,j+1} + \frac{1}{V^{\theta_1}_j}\left\{F^{\theta_1}_{j,j+1}\left(\bar{n}^{\theta_1}_{1,j} - \bar{n}^{\theta_1}_{1,j+1}\right) - F^{\theta_1}_{j,j-1}\left(\bar{n}^{\theta_1}_{1,j-1} - \bar{n}^{\theta_1}_{1,j}\right)\right\}\Delta t. \end{aligned} \tag{2.1.192}$$

First, the upper and lower axial segments including plenum are considered.

Since there is no boundary surface R for the first segment,

$$\begin{aligned} V_1\frac{\partial n_{1,1}}{\partial t} &= -J_{1,S} \\ &= -F_{1,2}\left[\left(n_{1,1} - n_{1,2}\right) - \left(\bar{n}_{1,1} - \bar{n}_{1,2}\right)\right] \end{aligned} \tag{2.1.193}$$

holds; therefore, the following equation holds.

$$\begin{aligned} \frac{n^{k+1}_{1,1} - n^k_{1,1}}{\Delta t} = {} & -\frac{\theta_2 F^{\theta_1}_{1,2}}{V^{\theta_1}_1}n^{k+1}_{1,1} + \frac{\theta_2 F^{\theta_1}_{1,2}}{V^{\theta_1}_1}n^{k+1}_{1,2} - \frac{(1-\theta_2)F^{\theta_1}_{1,2}}{V^{\theta_1}_1}n^k_{1,1} \\ & + \frac{(1-\theta_2)F^{\theta_1}_{1,2}}{V^{\theta_1}_1}n^k_{1,2} + \frac{F^{\theta_1}_{1,2}}{V^{\theta_1}_1}\left(\bar{n}^{\theta_1}_{1,1} - \bar{n}^{\theta_1}_{1,2}\right) \end{aligned} \tag{2.1.194}$$

This equation is rearranged using

$$\begin{aligned} & B_1 = 1 + \frac{\theta_2 F^{\theta_1}_{1,2}}{V^{\theta_1}_1}\Delta t\;,\; C_1 = -\frac{\theta_2 F^{\theta_1}_{1,2}}{V^{\theta_1}_1}\Delta t \\ & D_1 = \left(1 - \frac{(1-\theta_2)F^{\theta_1}_{1,2}}{V^{\theta_1}_1}\Delta t\right)n^k_{1,1} + \frac{(1-\theta_2)F^{\theta_1}_{1,2}}{V^{\theta_1}_1}\Delta t n^k_{1,2} + \frac{F^{\theta_1}_{1,2}}{V^{\theta_1}_1}\left(\bar{n}^{\theta_1}_{1,1} - \bar{n}^{\theta_1}_{1,2}\right)\Delta t, \end{aligned} \tag{2.1.195}$$

and we obtain

$$B_1 \cdot n^{k+1}_{1,1} + C \cdot n^{k+1}_{1,2} = D_1\,. \tag{2.1.196}$$

Similarly, there is no boundary surface S for the uppermost segment n, and thus the following equation holds.

$$\begin{aligned} V_n\frac{\partial n_{1,n}}{\partial t} &= -J_{1,R} \\ &= -F_{n-1,n}\left[\left(n_{1,n-1} - n_{1,n}\right) - \left(\bar{n}_{1,n-1} - \bar{n}_{1,n}\right)\right] \end{aligned} \tag{2.1.197}$$

Therefore, by setting

$$A_n = -\frac{\theta_2 F^{\theta_1}_{n-1,n}}{V^{\theta_1}_n}\Delta t\ ,\ B_n = 1 + \frac{\theta_2 F^{\theta_1}_{n-1,n}}{V^{\theta_1}_n}\Delta t$$

$$D_n = \frac{(1-\theta_2)F^{\theta_1}_{n-1,n}}{V^{\theta_1}_n}\Delta t\ n^k_{1,n-1} + \left(1 - \frac{(1-\theta_2)F^{\theta_1}_{n-1,n}}{V^{\theta_1}_n}\Delta t\right) n^k_{1,n,n} - \frac{F^{\theta_1}_{n-1,n}}{V^{\theta_1}_n}\left(\overline{n}^{\theta_1}_{1,n-1} - \overline{n}^{\theta_1}_{1,n}\right)\Delta t \quad (2.1.198)$$

we obtain

$$A_n \cdot n^{k+1}_{1,n-1} + B_n \cdot n^{k+1}_{1,n} = D_n\ . \quad (2.1.199)$$

Combining the above, we obtain the following equation for the diffusion of gas 1.

$$\begin{bmatrix} B_1C_1 & & & & & & \\ A_2B_2C_2 & & & & & & \\ & A_3B_3C_3 & & & & & \\ & \ddots & \ddots & & & & \\ & & \ddots & \ddots & & & \\ & & & \ddots & \ddots & & \\ & & & & A_{n-2}B_{n-2}C_{n-2} & & \\ & & & & & A_{n-1}B_{n-1}C_{n-1} & \\ & & & & & A_n\ B_n & \end{bmatrix} \begin{Bmatrix} n^{k+1}_{1,1} \\ n^{k+1}_{1,2} \\ n^{k+1}_{1,3} \\ \vdots \\ n^{k+1}_{1,n-2} \\ n^{k+1}_{1,n-1} \\ n^{k+1}_{1,n} \end{Bmatrix} = \begin{Bmatrix} D_1 \\ D_2 \\ D_3 \\ \vdots \\ D_{n-2} \\ D_{n-1} \\ D_n \end{Bmatrix} \quad (2.1.200)$$

Gas concentration $n^{k+1}_{1,j}$ of each axial segment is obtained by solving eq. (2.1.200).

(4) Counter-diffusion constant

The gas counter-diffusion constant adopts Present's constant[21].

$$D^{12} = \frac{3}{8}\left(\frac{\pi kT}{2m^*}\right)^{\frac{1}{2}} \frac{1}{n\pi d^2_{12}}, \quad (2.1.201)$$

where

$$m^* = \frac{m_1 m_2}{m_1 + m_2} \quad (m:\ \text{weight of one molecule})$$

$$d_{12} = \tfrac{1}{2}(d_1 + d_2) \quad (d:\ \text{diameter of one molecule})$$

$n = n_1 + n_2$ (molar density)

k : Boltzmann's constant

T : temperature (K).

(5) Pressure adjustment calculation

Setting the total gas molar number as N_j for each axial segment at the end of time step,

$$N_j = \sum_i N_{ij} , \tag{2.1.202}$$

holds, where i represents kind of gas. For the entire volume of the fuel rod inner space, the gas molar number is given by

$$N = \sum_i N_j . \tag{2.1.203}$$

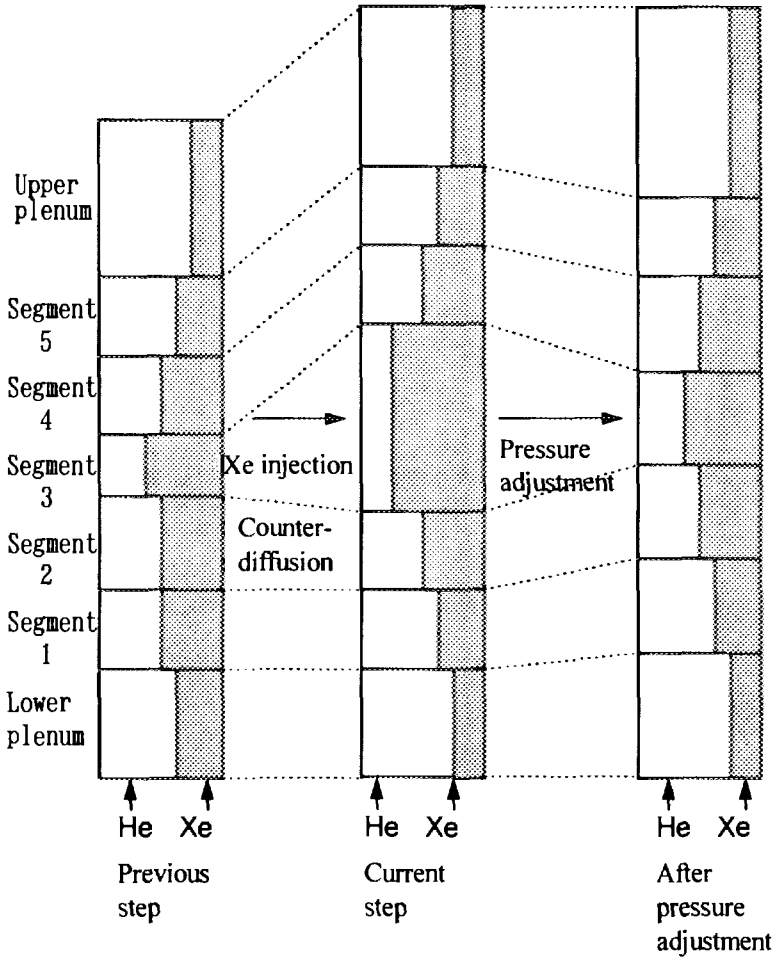

Fig. 2.28 Calculation of pressure adjustment (vertical axis: gas molar number).

Since

$$P = N \cdot R \cdot \frac{1}{\sum_j \left(\frac{V}{T}\right)_j} \tag{2.1.204}$$

holds from the ideal gas law, the total molar number of gas N_j' in segment j after the calculation of pressure adjustment is given by

$$N_j' = \frac{P}{R}\left(\frac{V}{T}\right)_j . \tag{2.1.205}$$

The discrepancy between N_j and $N_j'$is adjusted by balancing of the input and output flows between the upper and lower adjacent segments, beginning from the lowest part of pellet stack (see Fig. 2.28).

Namely, if the following are set,

$N_{i\to j}$: molar number of mixed gas transported from segment i to segment j

f_{ij} : fraction of segment i in segment j before transport,

the gas molar number i for segment j after transport is given by

$$N_{ij}' = f_{ij}\left\{N_j - \sum_k N_{j\to k}\right\} + \sum_l f_{il} N_{l\to j} . \tag{2.1.206}$$

(6) Method of space volume calculation

The void space volumes inside the fuel rod are classified into plenum volume, gap volume, pellet center hole volume and free gas volume inside the stack, as the reference temperature of each volume differs in the pressure calculation.

FEMAXI-IV assumes that no change occurs for both the pellet center hole volume and free gas volume inside the stack during irradiation.

The center hole volume is given using the initial inner radius of pellet r_{pi} and the length l_Z^j of axial segment j as

$$V_h^j = \pi r_{pi}^2 l_Z^j . \tag{2.1.207}$$

The free gas volume inside the stack includes dish volume, chamfer volume, pellet-to-pellet free space volume and void volume in cracks.

When the length of one pellet is set as l_p, dish volume per pellet as V_{dish}, chamfer volume as V_{chem}, pellet-to-pellet free space volume as V_p, and void volume in crack as V_{crack}, the equations

$$V_p = \pi r_{po}^2 \Delta l / 2 \tag{2.1.208}$$

$$V_{crack} = 2\pi r_{po} u^{rel} l_p \tag{2.1.209}$$

hold, where

r_{po} : outer radius of pellet

Δl : pellet-to-pellet aperture width

u^{rel} : radial displacement of pellet caused by relocation.

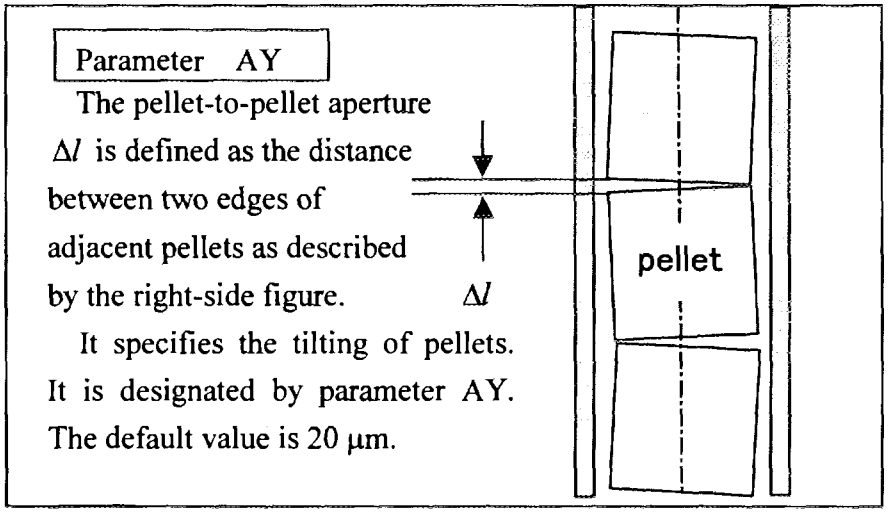

The free gas volume V_{int}^{j} in the stack in axial segment j is given by

$$V_{\text{int}}^{j} = \left(V_{dish} + V_{cham} + \pi r_{po}^{2}\Delta l / 2 + 2\pi r_{po} u^{rel} \cdot l_{p}\right)\frac{l_{Z}^{j}}{l_{p}}. \tag{2.1.210}$$

In contrast to the above, plenum volume and gas volume are assumed to change during irradiation. The plenum volume change is obtained from the change in axial segment length inside the stack. In segment j, setting the thermal expansion strain averaged by pellet volume as ε_{th}^{j}, densification strain as ε_{den}^{j}, and solid swelling strain as ε_{ss}^{j}, the segment length $\tilde{l}_{Z,p}^{j}$ including the changes by these strains is

$$\tilde{l}_{Z,p}^{j} = \left(1 + \varepsilon_{th}^{j} + \varepsilon_{den}^{j} + \varepsilon_{ss}^{j}\right)l_{Z}^{j} \tag{2.1.211}$$

In cladding, setting the thermal strain as $\Delta\varepsilon_{c,th}^{j}$ and strain by irradiation growth as $\Delta\varepsilon_{c,irr}^{j}$, the segment length $\tilde{l}_{Z,C}^{j}$ is

$$\tilde{l}_{Z,C}^{j} = \left(1 + \varepsilon_{c,th}^{j} + \varepsilon_{c,irr}^{j}\right)l_{Z}^{j}\ . \tag{2.1.212}$$

Similarly, when the plenum length $l_{Z,pl}$ is set as

$$l_{Z,pl} = \left(1 + \varepsilon_{c,th}^{pl} + \varepsilon_{c,irr}^{pl}\right)l_{Z,pl}\ , \tag{2.1.213}$$

the change in plenum volume ΔV_{pl} is given by

$$\Delta V_{pl} = \pi r_{ci}^2 \left(\sum_{j=1}^{NAXI} \left(\tilde{l}_{Z,c}^{j} - \tilde{l}_{Z,p}^{j} \right) + \tilde{l}_{Z,pl} - l_{Z,pl} \right), \tag{2.1.214}$$

where NAXI represents the number of axial segments, and r_{ci} the cladding inner radius.

Accordingly, when the initial plenum volume is set as V_{pl}, the plenum volume is

$$\tilde{V}_{pl} = V_{pl} + \Delta V_{pl} \tag{2.1.215}$$

The gap volume of axial segment j is given as follows, using the gap width δ obtained from eq. (2.1.95). Here, $\delta = 0$ is assumed when numerically $\delta < 0$.

$$\tilde{V}_{gap,j} = 2\pi r_{ci} \cdot \delta \cdot \tilde{l}_{Z,p}^{j} \tag{2.1.216}$$

(7) Gas pressure

It is assumed that the gas in the fuel rod behaves as an ideal gas and the pressure in the fuel rod is uniform. Then the gas pressure is calculated as

$$P_{gas} = \frac{n_T \cdot R}{\dfrac{V_{pl}}{T_{pl}} + \displaystyle\sum_{j=1}^{M} \left(\frac{V_{gap}^{j}}{T_{gap}^{j}} + \frac{V_{h}^{j}}{T_{pi}^{j}} + \frac{V_{\mathrm{int}}^{j}}{T_{av}^{j}} \right)}, \tag{2.1.217}$$

where

P_{gas} : gas pressure inside fuel rod (Pa)

n_T : total molar number of all gases (mol)

R : gas constant, 8.314 J/K · mol

V_{pl} : plenum volume (m^3)

T_{pl} : plenum gas temperature (K)

T_w : coolant temperature (K)

V_{gap}^{j} : gap volume in axial segment j (m^3)

V_h^j : pellet center hole volume in axial segment j (m^3)

V_{int}^{j} : free gas volume in pellet stack (m^3)

T_{gap}^{j} : gap temperature in axial segment j (K)

$= 0.5(T_{ps}^{j} + T_{ci}^{j})$

T_{pi}^{j} : pellet center temperature in axial segment j (K)

T_{pi}^{j} : volumetric average temperature of pellet in axial segment j (K).

Here, the free gas volume V_{int}^{j} includes dish volume, chamfer volume, pellet-to-pellet free

space volume, and volume between crack surfaces (= void volume in crack). V_{int}^{J} is already known by eq.(2.1.210)

Fitting parameter DTPL	The plenum gas temperature T_{pl} is given as follows using coolant temperature T_{cool}. $T_{pl} = T_{cool}$ + DTPL The default value of DTPL is 25 (K).

2.1.6 Time step control

The time-step width is automatically controlled in FEMAXI-IV. In the entire calculation, it is determined by the restriction Δt_1, while in the thermal analysis it is subdivided by Δt_2 in gas diffusion calculation. The restriction is explained as,

①Δt_1 is the minimum among the values determined by the following four conditions.

1) Changes in linear heat rate is within 10 W/cm during one time-step.

2) Changes in burnup is within 500 MWd/t during one time-step.

2) Creep strain rate is limited so that creep strain increment does not exceed elastic strain.

4) time step width is within 1.5 times the former time step width.

The values for the conditions 1) and 2) are determined in subroutine PHIST to stabilize the solution. The condition 3) is a restriction to avoid divergence in creep calculation for all elements, and Δt_1 is determined by

$$\Delta t \leq \frac{\bar{\sigma}}{E \cdot \dot{\bar{\varepsilon}}^{c}} \cdot \mathrm{EFCOEF} \qquad (2.1.218)$$

where EFCOF is a tuning parameter.

The condition 4) restricts the expansion of Δt_1 within a factor of 1.5 when rod power increases at less than 10W/cm · s during one time step.

In the entire length mechanical analysis and local mechanical analysis, subdivision of Δt_1 is performed within these analyses in accordance with the change of pellet-cladding contact state. See sections 2.2.11 and 2.3.3.

However, in the thermal analysis, a time step width Δt_2 which is smaller than Δt_1 can be used in the following manner.

② Δt_2 is used for gas diffusion time-step width, which is the subdivision of Δt_1 and determined as the shortest time among the time required to reach the equilibrium state of gas flow in each axial segment and the time determined from the maximum amount of transport of gas between segments as well as from pressure adjustment conditions, with its upper limit value set as either 100 ms or Δt_1.

The time required to reach the equilibrium state in each axial segment is derived from eq. (2.1.184) as

$$\Delta t_j^i = \frac{\left(n_{1,j} - \bar{n}_{1,j}\right)V_j}{J_{1,R} - J_{1,S}}, \tag{2.1.219}$$

where the superscript i represents axial segment number.

Next, the time determined from the maximum amount of transport of gas between segments is obtained as follows. Using the maximum molar number of the gas transported between segments N_{max} as standard, since $(J_{1,R})_j = (J_{1,S})_{j-1}$, we represent Δt_2 as follows using $(J_{1,R})_j$.

$$\Delta t_j^2 = \frac{N_{\max}}{\left(J_{1,R}\right)_j} \tag{2.1.220}$$

Then, the time determined from the pressure adjustment conditions in gas flow is obtained as follows. Due to the assumption of instantaneous equilibrium of pressure inside the fuel rod, numerical instability resulting from gas flow between segments may occur. To avoid this instability, we must impose a restriction on the amount of gas transport at each segment. Setting the gas transport rate in each segment as β (mol/s), the restriction is given by

$$\Delta t_j^3 = \frac{N_{\max}}{\beta_j}. \tag{2.1.221}$$

Thus, under the conditions

$$\Delta t_{21} = \min\left(\Delta t_1^1, \Delta t_2^1, \cdots, \Delta t_n^1\right) \cdot \eta_2 \tag{2.1.222}$$

$$\Delta t_{22} = \min\left(\Delta t_1^2, \Delta t_2^2, \cdots, \Delta t_n^2\right) \tag{2.1.223}$$

$$\Delta t_{23} = \min\left(\Delta t_1^3, \Delta t_2^3, \cdots, \Delta t_n^3\right), \tag{2.1.224}$$

Δt_2 is given by

$$\Delta t_2 = \min\left(\Delta t_{21}, \Delta t_{22}, \Delta t_{23}\right). \tag{2.1.225}$$

N_{max} in eqs. (2.1.220) and (2.1.221) and η_2 are the control parameters programmed in the code.

Fitting parameters AMLMX2, AMLX3, DTPR and FAC

N_{max} in eq. (2.1.20) is set by AMLMX2, and the default value is 10^{-6} (mol).
N_{max} in eq. (2.1.221) is set by AMLMX3, and the default value is 2×10^{-6} (mol).
η_2 in eq. (2.1.222) is set by DTPR, and the default value is 0.01.
Default value of tuning parameter EFCOEF is 1.0

2.2 Mechanical Behavior over Entire Length of Fuel Rod (Detailed Mechanical Analysis I [FEMROD] *)

(*) In Detailed Mechanical Analysis I, the analysis over the entire fuel rod is performed at the routine FEMROD. In Detailed Mechanical Analysis II described in Chapters 2 and 3, local analysis of the fuel rod deformation is performed at other routines. Anlayses I and II are exclusive with respect to each other; therefore, one of the two analyses is selected using the input parameter IFEMRD.

IFEMRD=0: local analysis, IFEMRD=1: analysis over entire length.

2.2.1 Finite element model

As shown in Fig. 2.29, the analysis model includes a 2-dimensional axisymmetrical system in which the entire length of the fuel rod is divided into axial segments, and each segment is further divided into concentric ring elements in the radial direction. In this system, the stress/strain analysis is performed using the finite element method with quadrangular elements with three degrees of freedom as shown in Fig. 2.30.

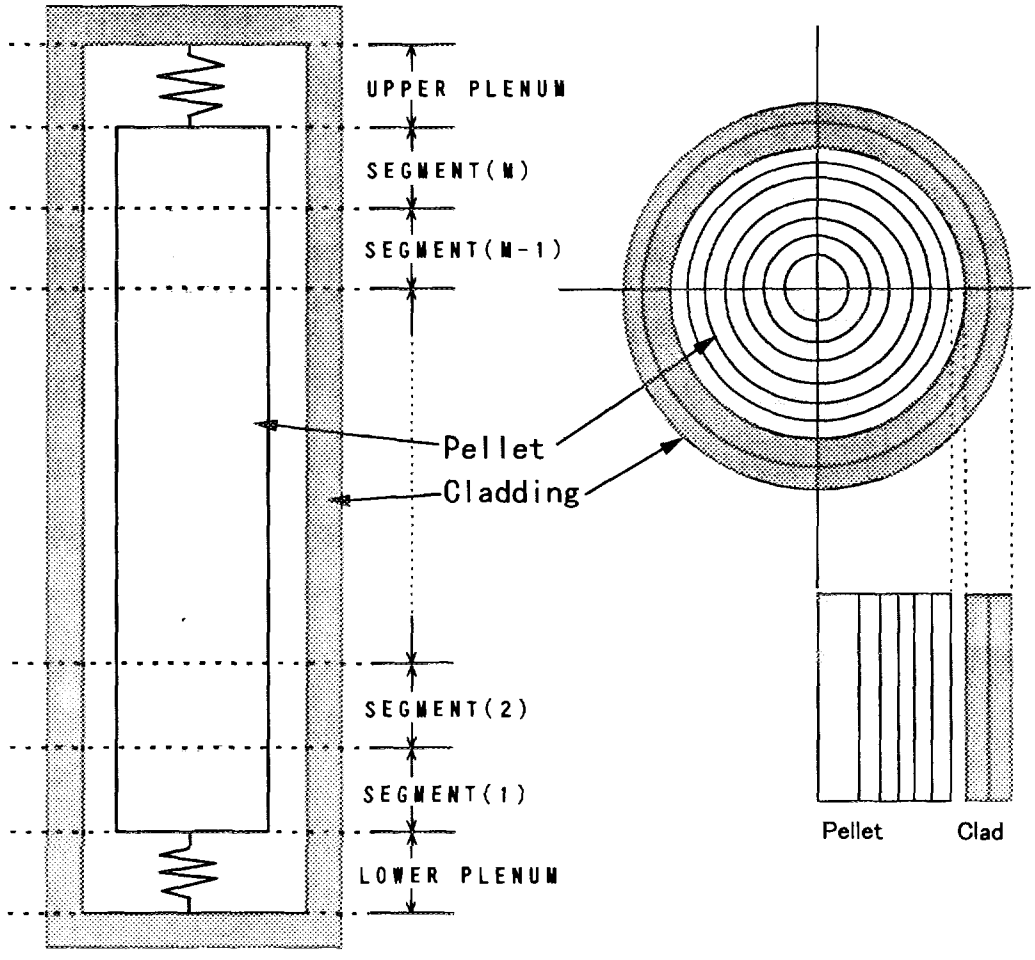

Fig. 2.29 Shape model.

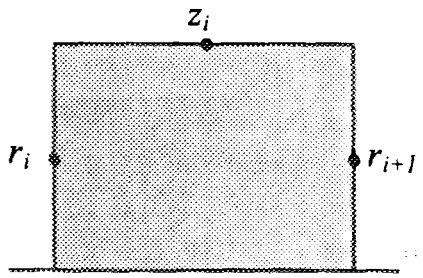

Fig. 2.30 Quadrangular model element with three degrees of freedom.

Figure 2.31 shows the relationship between mesh division and degree of freedom of each node in an axial segment.

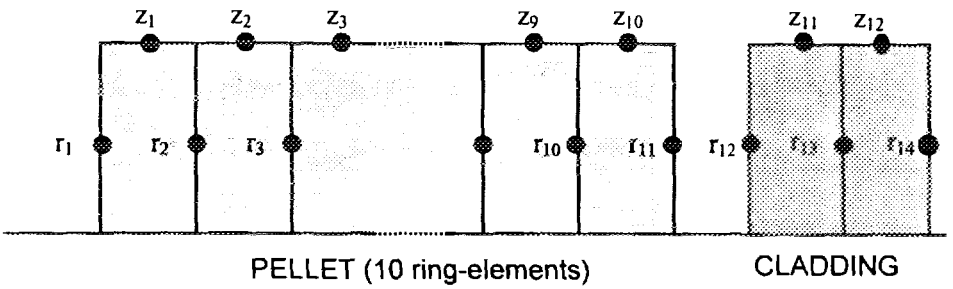

Fig. 2.31 Mesh division of the finite element method (for one segment).

As shown in Fig. 2.31, each node has only one degree of freedom, both in the axial and radial directions. On the assumption that the axial displacements of all the nodes $z_1 \sim z_{10}$ for the pellet are identical, the degree of freedom of one element is used as a representative value,

$$z_1 = z_2 = z_3 = \ldots\ldots = z_{10} \quad (= z_p) \tag{2.2.1}$$

Here, we obtain various matrices of one element which are hereafter used in the basic equation of the FEM analysis. First, we obtain strain-displacement matrix $[B]$. Setting radial displacement v and axial displacement as ω, the displacement (v,ω) at an arbitrary point in the element (r,z) shown in Fig. 2.30 is given by

$$v = \frac{r_{i+1} - r}{r_{i+1} - r_i} v_i + \frac{r - r_i}{r_{i+1} - r_i} v_{i+1} \tag{2.2.2}$$

$$\omega = \frac{z}{z_i} \omega_i . \tag{2.2.3}$$

The strain component in the axisymmetrical coordinate system is as follows.

$$\{\varepsilon\} = \begin{Bmatrix} \varepsilon_r \\ \varepsilon_\theta \\ \varepsilon_z \end{Bmatrix} = \begin{Bmatrix} \partial_v / \partial r \\ v / r \\ \partial\omega / \partial z \end{Bmatrix} \equiv [B]\{u\} \tag{2.2.4}$$

Using eqs. (2.2.2) and (2.2.3), the following equations hold.

$$\begin{aligned} \frac{\partial v}{\partial r} &= -\frac{1}{r_{i+1} - r_i} v_i + \frac{1}{r_{i+1} - r_i} v_{i+1} \\ \frac{v}{r} &= \frac{r_{i+1} - r}{r(r_{i+1} - r_i)} v_i + \frac{r - r_i}{r(r_{i+1} - r_i)} v_{i+1} \end{aligned} \tag{2.2.5}$$

Setting r as central-point coordinate of the element in the radial direction $\frac{r_i + r_{i+1}}{2}$, the following equations hold.

$$\begin{aligned} \frac{v}{r} &= \frac{r_{i+1} - \frac{r_i + r_{i+1}}{2}}{\frac{r_i + r_{i+1}}{2}(r_{i+1} - r_i)} v_i + \frac{\frac{r_i + r_{i+1}}{2} - r_i}{\frac{r_i + r_{i+1}}{2}(r_{i+1} - r_i)} v_{i+1} \\ &= \frac{1}{r_i + r_{i+1}} v_i + \frac{1}{r_i + r_{i+1}} v_{i+1} \end{aligned} \tag{2.2.6}$$

$$\frac{\partial \omega}{\partial z} = \frac{1}{z_i} \omega_i \tag{2.2.7}$$

Substituting eqs. (2.2.5), (2.2.6) and (2.2.7) into eq. (2.2.4), we obtain

$$\begin{Bmatrix} \varepsilon_{r,i} \\ \varepsilon_{\theta,i} \\ \varepsilon_{z,i} \end{Bmatrix} = \begin{bmatrix} -\frac{1}{r_{i+1} - r_i} & \frac{1}{r_{i+1} - r_i} & 0 \\ \frac{1}{r_{i+1} + r_i} & \frac{1}{r_{i+1} + r_i} & 0 \\ 0 & 0 & \frac{1}{z_i} \end{bmatrix} \begin{Bmatrix} v_i \\ v_{i+1} \\ \omega_i \end{Bmatrix}. \tag{2.2.8}$$

Accordingly, we obtain the components of matrix [B] as follows.

$$[B]=\begin{bmatrix} -\dfrac{1}{r_{i+1}-r_i} & \dfrac{1}{r_{i+1}-r_i} & 0 \\ \dfrac{1}{r_{i+1}+r_i} & \dfrac{1}{r_{i+1}+r_i} & 0 \\ 0 & 0 & \dfrac{1}{z_i} \end{bmatrix} \tag{2.2.9}$$

The volume of each element V_i is given as

$$V_i = \pi\left(r_{i+1}^2 - r_i^2\right)z_i . \tag{2.2.10}$$

Next, we obtain strain-stress matrix [C]. The stress-strain relationship is

$$\{\Delta\sigma\} = [D]\{\Delta\varepsilon^e\}, \tag{2.2.11}$$

where [D] is the stress-strain matrix that represents the stiffness of an element.

When matrix [C] is defined as an inverse matrix of [D], eq. (2.2.11) is expressed as

$$\{\Delta\varepsilon^e\} = [C]\{\Delta\sigma\}. \tag{2.2.12}$$

Accordingly, matrix [C] is given by

$$[C]=\frac{1}{E}\begin{bmatrix} 1 & -\nu & -\nu \\ -\nu & 1 & -\nu \\ -\nu & -\nu & 1 \end{bmatrix}, \tag{2.2.13}$$

where E is Young's modulus and ν is the Poisson ratio.

Here, solution of the basic equation of constitutive equations for stress-strain analysis is outlined. The external force and initial strain vector are set as $\{F\}$ and $\{\Delta\varepsilon_0\}$, respectively. When the calculation has proceeded to the (n)th time step and calculation for the next (n+1)th time step is performed, the equilibrium equation

$$\{F_{n+1}\} = \int [B]^T \{\sigma_{n+1}\} dV \tag{2.2.14}$$

is given using the principle of virtual work.

Here,

$\{F_{n+1}\}$: external force vector at (n+1)th time step

$\{\sigma_{n+1}\}$: stress vector at (n+1)th time step.

To distinguish between unknown and known values, we divide $\{\sigma_{n+1}\}$ into known stress $\{\sigma_n\}$ and unknown stress $\{\Delta\sigma_{n+1}\}$; then we obtain transformed equations of eq.(2.2.14) as

$$\{F_{n+1}\} = \int [B]^T \{\sigma_n\} dV + \int [B]^T \{\Delta\sigma_{n+1}\} dV \tag{2.2.15}$$

$$\int [B]^T \{\Delta\sigma_{n+1}\} dV = \{F_{n+1}\} - \int [B]^T \{\sigma_n\} dV . \tag{2.2.16}$$

The right side of eq. (2.2.16) consists of known values and the left side consists of unknown values. Substituting eq. (2..2.11) into eq. (2.2.16), we obtain

$$\int [B]^T [D] \{\Delta\varepsilon^e_{n+1}\} dV = \{F_{n+1}\} - \int [B]^T \{\sigma_n\} dV . \tag{2.2.17}$$

Here, the following equation holds among elestic strain increment $\{\Delta\varepsilon^e_{n+1}\}$, total strain increment $\{\Delta\varepsilon_{n+1}\}$, and the known value initial strain increment $\{\Delta\varepsilon_{0,n+1}\}$.

$$\{\Delta\varepsilon^e_{n+1}\} = \{\Delta\varepsilon_{n+1}\} - \{\Delta\varepsilon_{0,n+1}\} \tag{2.2.18}$$

Accordingly, substituting eq. (2.2.18) into eq. (2.2.17), we obtain

$$\int [B]^T [D] \{\Delta\varepsilon_{n+1} - \Delta\varepsilon_{0,n+1}\} dV = \{F_{n+1}\} - \int [B]^T \{\sigma_n\} dV . \tag{2.2.19}$$

Transposing the known value term $\int [B]^T [D] \{\Delta\varepsilon_{0,n+1}\} dV$ to the right-hand side,

$$\int [B]^T [D] \{\Delta\varepsilon_{n+1}\} dV = \{F_{n+1}\} + \int [B]^T [D] \{\Delta\varepsilon_{0,n+1}\} dV - \int [B]^T \{\sigma_n\} dV \tag{2.2.20}$$

is obtained. Substituting eq. (2.2.4) into eq. (2.2.20), we obtain

$$\begin{aligned} &\int [B]^T [D][B] dV \{\Delta u_{n+1}\} \\ &= \{F_{n+1}\} + \int [B]^T [D] \{\Delta\varepsilon_{0,n+1}\} dV - \int [B]^T \{\sigma_n\} dV, \end{aligned} \tag{2.2.21}$$

and the unknown value $\{\Delta u_{n+1}\}$ can be calculated by integration.

Namely, expressing equation (2.2.21) in a descrete form with summation of M elements,

$$\begin{aligned} &\sum_{i=1}^{M} [B_i]^T [D_i][B_i] \Delta V_i \{\Delta u_{n+1}\} \\ &= \{F_{n+1}\} + \sum_{i=1}^{M} [B_i]^T [D_i] \{\Delta\varepsilon^i_{0,n+1}\} \Delta V_i - \sum_{i=1}^{M} [B_i]^T \{\sigma^i_n\} \Delta V_i \end{aligned} \tag{2.2.22}$$

(ΔV_i represents the volume of the elelment i,
and M represents total number of elements),

The unknown displacement increment vector $\{\Delta u_{n+1}\}$ is expressed using known values.

The above is the basic calculation method. In actual calculations, a more complex solution is required due to the use of implicit solutions for creep and plasticity.

In the next section, modification of the basic equations when implicit solutions are used

will be described.

2.2.2 Basic equations

The equilibrium condition at time t_{n+1} is expressed as follows using the principle of virtual work, similar to the case of eq. (2.2.14).

$$\int_V [B]^T \{\sigma_{n+1}\} dV - \{F_{n+1}\} = 0 \tag{2.2.23}$$

The equation representing the relationship between elastic strain increment and stress increment (=eq. (2.2.12))□during time increment $\Delta t_{n+1}(= t_{n+1} - t_n)$ is expressed as follows, with consideration given to time dependence of [C].

$$\{\Delta\varepsilon^e_{n+1}\} = [C_{n+\theta}]\{\Delta\sigma_{n+1}\} \tag{2.2.24}$$

Here,

$$[C_{n+\theta}] = (1-\theta)[C_n] + \theta[C_{n+1}] \qquad \left(\theta = \frac{1}{2}\right)$$

$\{\Delta\varepsilon^e_{n+1}\}$: elastic strain increment vector

$[C_{n+\theta}]$: strain-stress matrix

$\{\Delta\sigma_{n+1}\}$: stress increment vector

θ : parameter for the implicit solution.

The elastic strain increment vector is expressed as

$$\begin{aligned}\{\Delta\varepsilon^e_{n+1}\} = \{\Delta\varepsilon_{n+1}\} - \{\Delta\varepsilon^{th}_{n+1}\} - \{\Delta\varepsilon^{rel}_{n+1}\} - \{\Delta\varepsilon^{den}_{n+1}\} - \{\Delta\varepsilon^{sw}_{n+1}\} \\ - \{\Delta\varepsilon^{HP}_{n+1}\} - \{\Delta\varepsilon^{P}_{n+1}\} - \{\Delta\varepsilon^{c}_{n+1}\}.\end{aligned} \tag{2.2.25}$$

Here,

$\{\Delta\varepsilon_{n+1}\}$: total strain increment vector

$\{\Delta\varepsilon^{th}_{n+1}\}$: thermal strain increment vector

$\{\Delta\varepsilon^{rel}_{n+1}\}$: pellet relocation strain increment vector

$\{\Delta\varepsilon^{crk}_{n+1}\}$: pellet crack strain increment vector

$\{\Delta\varepsilon^{den}_{n+1}\}$: pellet densification strain increment vector

$\{\Delta\varepsilon^{sw}_{n+1}\}$: pellet swelling strain increment vector

$\{\Delta\varepsilon^{HP}_{n+1}\}$: pellet hot-press strain increment vector

$\{\Delta\varepsilon^{P}_{n+1}\}$: plastic strain increment vector

$\{\Delta\varepsilon^{c}_{n+1}\}$: creep strain increment vector.

Of these, strain increment vectors which do not depend on stress are collectively treated as an initial strain increment vector as

$$\left\{\Delta\varepsilon_{n+1}^{o}\right\}=\left\{\Delta\varepsilon_{n+1}^{th}\right\}-\left\{\Delta\varepsilon_{n+1}^{rel}\right\}-\left\{\Delta\varepsilon_{n+1}^{den}\right\}-\left\{\Delta\varepsilon_{n+1}^{sw}\right\} \tag{2.2.26}$$

where $\left\{\Delta\varepsilon_{n+1}^{o}\right\}$: initial strain increment vector.

Furthermore, when the pellet hot-press strain increment vector is integrated into the pellet plastic and creep strain increment vectors as described in detail in section 2.2.4, eq. (2.2.25) is expressed as

$$\left\{\Delta\varepsilon_{n+1}^{e}\right\}=\left\{\Delta\varepsilon_{n+1}\right\}-\left\{\Delta\varepsilon_{n+1}^{o}\right\}-\left\{\Delta\varepsilon_{n+1}^{P}\right\}-\left\{\Delta\varepsilon_{n+1}^{c}\right\}. \tag{2.2.27}$$

Here,

$\left\{\Delta\varepsilon_{n+1}^{P}\right\}$: plastic strain increment vector including hot press strain

$\left\{\Delta\varepsilon_{n+1}^{c}\right\}$: creep strain increment vector including hot press strain.

Meanwhile, the total strain is associated with nodal displacement as

$$\left\{\Delta\varepsilon_{n+1}\right\}=[B]\left\{\Delta u_{n+1}\right\}, \tag{2.2.28}$$

where $\left\{\Delta u_{n+1}\right\}$ represents nodal displacement increment vector.

Using eqs. (2.2.25) and (2.2.27), we rewrite the stress-strain relationship equation (2.2.24) as

$$[C_{n+\theta}]\left\{\Delta\sigma_{n+1}\right\}-[B]\left\{\Delta u_{n+1}\right\}+\left\{\Delta\varepsilon_{n+1}^{o}\right\}+\left\{\Delta\varepsilon_{n+1}^{P}\right\}+\left\{\Delta\varepsilon_{n+1}^{c}\right\}=0. \tag{2.2.29}$$

In the calculation of the (n+1)th time step, iteration of the stress calculation is required for obtaining strain increment vectors $\left\{\Delta\varepsilon_{n+1}^{crk}\right\}$, $\left\{\Delta\varepsilon_{n+1}^{P}\right\}$ and $\left\{\Delta\varepsilon_{n+1}^{c}\right\}$ in eq. (2.2.25), which depend on stress. The Newton-Raphson method is used for the iteration with counter i. When the i-th iteration is completed and the (i+1)th iteration is being performed, eq. (2.2.29) is expressed as

$$\begin{aligned}&\left[C_{n+\theta}^{i}\right]\left\{d\sigma_{n+1}^{i+1}\right\}-[B]\left\{\Delta u_{n+1}^{i+1}\right\}\\&\quad+\left\{\Delta\varepsilon_{n+1}^{o}\right\}+\left\{\Delta\varepsilon_{n+1}^{P,i+1}\right\}+\left\{\Delta\varepsilon_{n+1}^{c,i+1}\right\}+\left[C_{n+\theta}^{i}\right]\left(\left\{\sigma_{n+\theta}^{i}\right\}-\left\{\sigma_{n}\right\}\right)=0,\end{aligned} \tag{2.2.30}$$

where

$$\left\{d\sigma_{n+1}^{i+1}\right\}=\left\{\sigma_{n+1}^{i+1}\right\}-\left\{\sigma_{n+1}^{i}\right\}.$$

Model parameter LMAX
The number of iterations in the Newton-Raphson method is given by LMAX. The default value of LMAX is 2.

At this time, the equilibrium condition (2.2.23) is represented as

$$\int_V [B]^T \{\sigma^i_{n+1}\} dV + \int_V [B]^T \{d\sigma^{i+1}_{n+1}\} dV = \{F_{n+1}\}. \quad (2.2.31)$$

In eqs. (2.2.30) and (2.2.31), $\{d\sigma^{i+1}_{n+1}\}$, $\{\Delta\varepsilon^{crk,i+1}_{n+1}\}$, $\{\Delta\varepsilon^{P,i+1}_{n+1}\}$, $\{\Delta\varepsilon^{c,i+1}_{n+1}\}$ and $\{\Delta u^{i+1}_{n+1}\}$ are the unknown values. Therefore, the number of unknown values exceeds the number of equations, i.e. two equations, eqs. (2.2.30) and (2.2.31), the solution cannot be obtained; thus it is necessary to reduce the number of unknown values to two.

Here, the unknown values $\{\Delta\varepsilon^{crk,i+1}_{n+1}\}, \{\Delta\varepsilon^{P,i+1}_{n+1}\}, \{\Delta\varepsilon^{c,i+1}_{n+1}\}$ which depend on $\{d\sigma^{i+1}_{n+1}\}$ can be eliminated by expression of them using $\{\Delta u^{i+1}_{n+1}\}$ and $\{d\sigma^{i+1}_{n+1}\}$. Actual methods will be introduced in the next section.

2.2.3 Pellet cracks

The behavior of a pellet with cracks was explained in section 2.1.3 (3)–(5). Here, the difference in the crack models between that in the mechanical analysis and that in the thermal analysis is described. The concept of the crack model in the mechanical analysis is explained using the schematic shown in Fig. 2.32.[2]

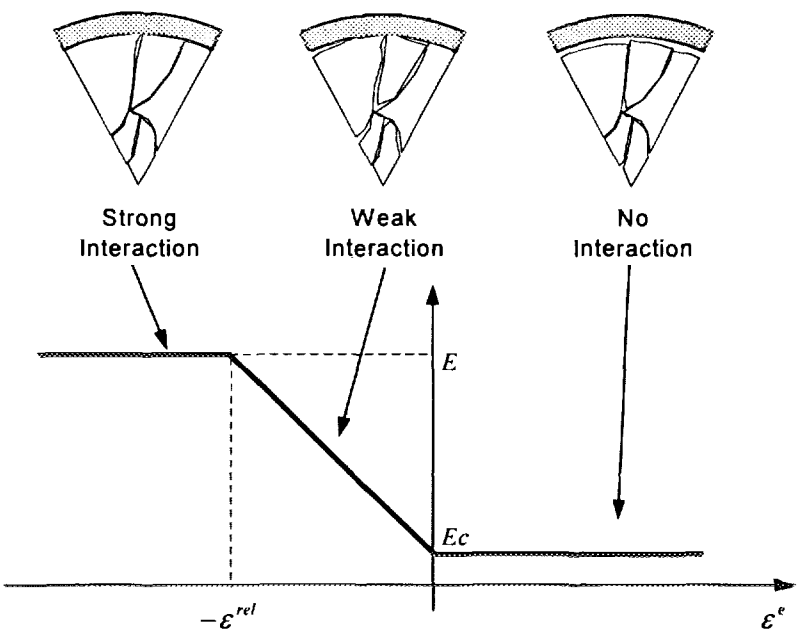

Fig. 2.32 Stiffness model of pellet with cracks.

When a pellet is in a tensile state in the i direction (axial, circumferential or radial direction), it is assumed that cracks are generated on the surface perpendicular to the i direction and the apparent Young's modulus in the i direction decreases to approximately 1/100 of the original material property value. (Since the Young's modulus occupies a diagonal position in the FEM matrix of the present detailed mechanical analysis, the value cannot be 0, while in the thermal analysis model, this modulus is set as 0 in equations.)

When a pellet is in a compressive state, it is assumed that the elasticity of the pellet partly recovers when strain is generated by relocation. That is, in the initial state, i.e. burnup=0, power=0, and $\varepsilon_i - \varepsilon_i^o = 0$, Young's modulus of the pellet E_i is a small value represented by E_c. The pellet behavior change with increasing power is described as follows.

① When the pellet is not in contact with the cladding, thermal stress in the pellet is small due to the presence of cracks; accordingly, the pellet is thermally deformed in accordance with its natural thermal expansion coefficient and the gap is narrowed.

② When the pellet is in contact with the cladding, the compressive strain inside the pellet by the restraint of the cladding increases. Since the gap generated on the cracked surface of the pellet is compressed by relocation, the stiffness of the pellet increases. This process is approximated by linear changing of Young's modulus. Namely, the process modeled here is one in which a mechanical interaction between a cracked and relocated pellet and the cladding is gradually enhanced.

③ Next, elasticity of a pellet completely recovers to that represented by the original elastic coefficient=compression stiffness when pieces of the pellet are compressed by cladding so that they fill the gap generated by relocation. Here, the strong interaction between pellet and cladding is modeled.

Fitting parameter ECRAC3	Young's modulus of a pellet with cracks is set by ECRAC3. The default value of ECRAC3 is 2×10^9 (N/m^2), which is approximately 1/100 of original Young's modulus of UO_2.

Model parameter IYNG (used only in the mechanical calculations)
The pellet stiffness model shown in Fig. 2.32 is for the case IYNG = 0. The default value of IYNG is 1. When IYNG=1, the region between $-\varepsilon^{rel}$ and 0 is described by a straight line. When IYNG=0, this region is described by a concave quadratic function.

Next, based on the above-described model, a mechanical analysis is performed as follows.

Regarding the pellet cracks, a crack strain increment $\left\{\Delta\varepsilon_{n+1}^{crk}\right\}$ which is proportional to the change in $\{\Delta\sigma\}$ is given by transformation of the [C] matrix elements in eq. (2.2.29) from eq. (2.2.13). The strain-stress matrix of the pellet $\left[\tilde{C}\right]$ is represented as

$$\left[\tilde{C}\right]=\begin{bmatrix} \frac{1}{E_r} & -\frac{\nu}{E} & -\frac{\nu}{E} \\ -\frac{\nu}{E} & \frac{1}{E_z} & -\frac{\nu}{E} \\ -\frac{\nu}{E} & -\frac{\nu}{E} & \frac{1}{E_\theta} \end{bmatrix}. \tag{2.2.32}$$

Here,

E_r : Young's modulus in the radial direction (Pa)

E_z : Young's modulus in the axial direction (Pa)

E_θ : Young's modulus in the circumferential direction (Pa)

E : Young's modulus of pellet (material property) (Pa)

ν : Poisson's ratio (–).

The apparent Young's modulus in each direction E_i (E_r, E_z, E_θ) is defined as follows.

$$E_i=\begin{cases} E_c & , \ 0 \leqq \varepsilon_i-\varepsilon_i^o \\ -\dfrac{\varepsilon_i-\varepsilon_i^o}{\varepsilon_i^{rel}}\left(E-E_c\right)+E_c & , -\varepsilon_i^{rel}<\varepsilon_i-\varepsilon_i^o<0 \\ E & , \ \varepsilon_i-\varepsilon_i^o \leqq -\varepsilon_i^{rel} \end{cases} \tag{2.2.33}$$

Here,

ε_i : strain in i direction

ε_i^o : initial strain in i direction

ε_i^{rel} : initial relocation strain in i direction (input data)

E_c : effective Young's modulus of pellet with cracks in a tensile state.

From eq. (2.2.24),

$$\left\{\Delta\varepsilon^{e}_{n+1}\right\}=\left[C_{n+\theta}\right]\left\{\Delta\sigma_{n+1}\right\}, \tag{2.2.34}$$

and setting the sum of elastic strain increment and crack strain increment as

$$\left\{\Delta\varepsilon^{e}_{n+1}+\Delta\varepsilon^{crk,i+1}_{n+1}\right\}=\left[\widetilde{C}_{n+\theta}\right]\left\{\Delta\sigma^{i+1}_{n+1}\right\}, \tag{2.2.35}$$

we obtain the crack strain increment vector using eqs. (2.2.34) and (2.2.35) as

$$\begin{aligned}\left\{\Delta\varepsilon^{crk,i+1}_{n+1}\right\}&=\left\{\left[\widetilde{C}_{n+\theta}\right]-\left[C_{n+\theta}\right]\right\}\left\{\Delta\sigma^{i+1}_{n+1}\right\}\\&=\left(\begin{bmatrix}\frac{1}{E_r}&-\frac{\nu}{E}&-\frac{\nu}{E}\\-\frac{\nu}{E}&\frac{1}{E_z}&-\frac{\nu}{E}\\-\frac{\nu}{E}&-\frac{\nu}{E}&\frac{1}{E_\theta}\end{bmatrix}-\begin{bmatrix}\frac{1}{E}&-\frac{\nu}{E}&-\frac{\nu}{E}\\-\frac{\nu}{E}&\frac{1}{E}&-\frac{\nu}{E}\\-\frac{\nu}{E}&-\frac{\nu}{E}&\frac{1}{E}\end{bmatrix}\right)\begin{Bmatrix}\Delta\sigma^{i+1}_{r,n+1}\\\Delta\sigma^{i+1}_{z,n+1}\\\Delta\sigma^{i+1}_{\theta,n+1}\end{Bmatrix}\\&=\begin{Bmatrix}\left(\frac{1}{E_r}-\frac{1}{E}\right)\Delta\sigma^{i}_{r,n+1}\\\left(\frac{1}{E_z}-\frac{1}{E}\right)\Delta\sigma^{i}_{z,n+1}\\\left(\frac{1}{E_\theta}-\frac{1}{E}\right)\Delta\sigma^{i}_{\theta,n+1}\end{Bmatrix}+\begin{Bmatrix}\left(\frac{1}{E_r}-\frac{1}{E}\right)d\sigma^{i+1}_{r,n+1}\\\left(\frac{1}{E_z}-\frac{1}{E}\right)d\sigma^{i+1}_{z,n+1}\\\left(\frac{1}{E_\theta}-\frac{1}{E}\right)d\sigma^{i+1}_{\theta,n+1}\end{Bmatrix}.\end{aligned} \tag{2.2.36}$$

Thus, the unknown value crack strain increment $\left\{\Delta\varepsilon^{crk,i+1}_{n+1}\right\}$ in eq. (2.2.30) can be eliminated.

Accordingly, eq. (2.2.30) can be transformed as follows. From the equation

$$\begin{aligned}&\left[C^{i}_{n+\theta}\right]\left\{d\sigma^{i+1}_{n+1}\right\}-\left[B\right]\left\{\Delta u^{i+1}_{n+1}\right\}+\left\{\Delta\varepsilon^{0}_{n+1}\right\}\\&+\left\{\left[\widetilde{C}^{i}_{n+\theta}\right]-\left[C^{i}_{n+\theta}\right]\right\}\left(\left\{\sigma^{i}_{n+1}\right\}+\left\{d\sigma^{i+1}_{n+1}\right\}-\left\{\sigma_n\right\}\right)+\left\{\Delta\varepsilon^{P,i+1}_{n+1}\right\}+\left\{\Delta\varepsilon^{c,i+1}_{n+1}\right\}+\left[C^{i}_{n+\theta}\right]\left(\left\{\sigma^{i}_{n+1}\right\}-\left\{\sigma_n\right\}\right)=0,\end{aligned}$$

we obtain

$$\left[\widetilde{C}^{i}_{n+\theta}\right]\left\{d\sigma^{i+1}_{n+1}\right\}-\left[B\right]\left\{\Delta u^{i+1}_{n+1}\right\}+\left\{\Delta\varepsilon^{0}_{n+1}\right\}+\left\{\Delta\varepsilon^{P,i+1}_{n+1}\right\}+\left\{\Delta\varepsilon^{c,i+1}_{n+1}\right\}+\left[\widetilde{C}^{i}_{n+\theta}\right]\left(\left\{\sigma^{i}_{n+1}\right\}-\left\{\sigma_n\right\}\right)=0. \tag{2.2.37}$$

Fitting parameters FRELOC and EPSRLZ (used only in the mechanical
Relocation strain ε^{rel} in the radial direction is given by the value which is calculated from the initial radial gap width multiplied by RELOC and divided by the pellet radius. In the axial direction, relocation strain ε^{rel} is directly set by EPSRLZ. The default values of FRELOC and EPSRLZ are 0.5 and 0.003, respectively.

Fitting parameters FACR and FACZ

$E_i = E$ holds when $\varepsilon_i - \varepsilon_i^0 = -\varepsilon_i^{rel}$; however, these values are adjusted using parameters FACR in the circumferential direction and FACZ in the axial direction as $\varepsilon_i - \varepsilon_i^0 = -\varepsilon_i^{rel} \cdot \mathrm{FACR}$ and $\varepsilon_i - \varepsilon_i^0 = -\varepsilon_i^{rel} \cdot \mathrm{FACZ}$, respectively. The default values of FACR and FACZ are both 1.

2.2.4 Creep

The creep equation of cladding and pellet is generally represented as

$$\dot{\bar{\varepsilon}}^c = f\left(\bar{\sigma}, \bar{\varepsilon}^H, T, \phi, F\right). \tag{2.2.38}$$

Here,

$\dot{\bar{\varepsilon}}^c$: equivalent creep strain rate (1/s)

$\bar{\sigma}$: equivalent stress (Pa)

$\bar{\varepsilon}^H$: creep hardening parameter (–)

T : temperature (K)

ϕ : fast neutron flux (n/m^2·s)

F : fission rate (fission/m^3·s).

If the creep hardening parameter $\bar{\varepsilon}^H$ is assumed to be equal to the equivalent creep strain $\bar{\varepsilon}^C$, the variation rate of the hardening parameter is represented as

$$\dot{\bar{\varepsilon}}^H = f\left(\bar{\sigma}, \bar{\varepsilon}^H, T, \phi, \dot{F}\right). \tag{2.2.39}$$

Equation (2.2.38) is an equation of creep under uniaxial stress. When this equation is generalized for a multi-axial stress state, the creep strain rate vector $\left\{\dot{\varepsilon}^c\right\}$ is expressed as a vector function of stress vector and creep hardening parameter. When this vector function is set as $\{\beta\}$, $\left\{\dot{\varepsilon}^c\right\}$ is represented as

$$\left\{\dot{\varepsilon}^c\right\} = \left\{\beta\left(\{\sigma\}, \bar{\varepsilon}^H\right)\right\}. \tag{2.2.40}$$

where T, ϕ and F are omitted because they are known parameters.

When a calculation at time t_n is finished and a calculation in the next time increment Δt_{n+1} is being performed, the creep strain increment vector is represented as

$$\left\{\Delta\varepsilon_{n+1}^c\right\} = \Delta t_{n+1}\left\{\dot{\varepsilon}_{n+\theta}^c\right\} = \left\{\beta\left\{\sigma_{n+\theta}\right\}, \bar{\varepsilon}_{n+\theta}^H\right\}, \tag{2.2.41}$$

where

$$\{\sigma_{n+\theta}\} = (1-\theta)\{\sigma_n\} + \theta\{\sigma_{n+1}\}$$
$$\bar{\varepsilon}^H_{n+\theta} = (1-\theta)\bar{\varepsilon}^H_n + \theta\bar{\varepsilon}^H_{n+1}$$

(here, $0 \leqq \theta \leqq 1$).

When $\theta = 0$ is assumed, the above equation represents a method to treat the creep rate which is determined by a state amount, which is a known value, at the starting point of an increment, i.e. the initial strain method. In this case, the calculation procedure is simple but the solution tends to be numerically unstable; therefore, it is known that the time increment width must be extremely small at high creep rate.

In contrast, when $\theta \neq 0$ is assumed, the calculation procedure becomes complex since the equation contains unknown values; however, as θ approaches 1, the stability of the numerical solution improves; this method of setting $\theta \neq 0$ is called an implicit solution.

In FEMAXI-IV, $\theta = 0$ is set to stress the importance of the stability.

Now, in a calculation performed from t_n to t_{n+1}, when the (i+1)th iteration by the Newton-Raphson method is being performed after completion of the (i)th iteration (see eqs. (2.2.30) and (2.2.31)), the creep rate vector can be expressed as follows.

The creep equation (2.2.40) is represented as follows, using a flow rule and eq. (2.2.38).

Since the function form of each principal direction component is identical,

$$\{\dot{\varepsilon}^c\} = \dot{\bar{\varepsilon}}^c \left\{\frac{d\bar{\sigma}}{d\sigma}\right\} = \frac{3f}{2\bar{\sigma}}\{\sigma'\} \tag{2.2.42}$$

Here, $\bar{\sigma}$ is an equipvalent stress which will be defined by eq. (2.2.54), given later.

Also, $\{\sigma'\}$ is a deviation stress vector given by

$$\{\sigma'\} = \begin{Bmatrix} \dfrac{2\sigma_r - \sigma_z - \sigma_\theta}{3} + 2\alpha(\sigma_r + \sigma_z + \sigma_\theta) \\ \dfrac{2\sigma_z - \sigma_\theta - \sigma_r}{3} + 2\alpha(\sigma_r + \sigma_z + \sigma_\theta) \\ \dfrac{2\sigma_\theta - \sigma_r - \sigma_z}{3} + 2\alpha(\sigma_r + \sigma_z + \sigma_\theta) \end{Bmatrix},$$

which represents deviations of each principal stress component from averages.

Accordingly, the following equation holds.

$$\begin{aligned}\left\{\dot{\varepsilon}^{c,i+1}_{n+\theta}\right\} &= \left\{\beta\left(\left\{\sigma^{i}_{n+\theta}\right\}+\theta\left\{d\sigma^{i+1}_{n+1}\right\},\quad \bar{\varepsilon}^{H,i}_{n+\theta}+\theta d\bar{\varepsilon}^{H,i+1}_{n+1}\right)\right\} \\ &= \frac{3f\left(\bar{\sigma}\left(\left\{\sigma^{i}_{n+\theta}\right\}+\theta\left\{d\sigma^{i+1}_{n+1}\right\}\right),\quad \bar{\varepsilon}^{H,i}_{n+\theta}+\theta d\bar{\varepsilon}^{H,i+1}_{n+1}\right)}{2\bar{\sigma}\left(\left\{\sigma^{i}_{n+\theta}\right\}+\theta\left\{d\sigma^{i+1}_{n+1}\right\}\right)} \\ &\quad\times\left\{\sigma'\left(\left\{\sigma^{i}_{n+\theta}\right\}+\theta\left\{d\sigma^{i+1}_{n+1}\right\}\right)\right\}\end{aligned} \tag{2.2.43}$$

Here, $\left\{d\sigma^{i+1}_{n+1}\right\}$ and $\left\{d\bar{\varepsilon}^{H,i+1}_{n+1}\right\}$ are the amounts of correction made by iteration calculation.

Through first-order Taylor expansion, we approximate eq. (2.2.43) as follows.

$$\begin{aligned}\left\{\dot{\varepsilon}^{c,i+1}_{n+\theta}\right\} &= \frac{3}{2\bar{\sigma}^{i}_{n+\theta}}f^{i}_{n+\theta}\left\{\sigma'^{i}_{n+\theta}\right\}-\frac{3}{2\left(\bar{\sigma}^{i}_{n+\theta}\right)^{2}}f^{i}_{n+\theta}\left\{\sigma'^{i}_{n+\theta}\right\}\left[\frac{\partial\bar{\sigma}}{\partial\sigma}\right]^{i}_{n+\theta}\theta\left\{d\sigma^{i+1}_{n+1}\right\} \\ &\quad+\frac{3}{2\bar{\sigma}^{i}_{n+\theta}}f'_{n+\theta}\left[\frac{\partial\sigma'}{\partial\sigma}\right]^{i}_{n+\theta}\theta\left\{d\sigma^{i+1}_{n+1}\right\}+\frac{3}{2\bar{\sigma}^{i}_{n+\theta}}\left\{\sigma'^{i}_{n+\theta}\right\}\left(\frac{\partial f}{\partial\bar{\sigma}}\right)^{i}_{n+\theta}\left[\frac{\partial\bar{\sigma}}{\partial\sigma}\right]^{i}_{n+\theta}\theta\left\{d\sigma^{i+1}_{n+1}\right\} \\ &\quad+\frac{3}{2\bar{\sigma}^{i}_{n+\theta}}\left\{\sigma'^{i}_{n+\theta}\right\}\left(\frac{\partial f}{\partial\bar{\varepsilon}^{H}}\right)^{i}_{n+\theta}\theta d\bar{\varepsilon}^{H,i+1}_{n+1} \\ &= \left\{\dot{\varepsilon}^{c,i}_{n+\theta}\right\}+\frac{3}{2\bar{\sigma}^{i}_{n+\theta}}\left(\left(\frac{\partial f}{\partial\bar{\sigma}}\right)^{i}_{n+\theta}-\frac{f^{i}_{n+\theta}}{\bar{\sigma}^{i}_{n+\theta}}\right)\left[\sigma'\frac{\partial\bar{\sigma}}{\partial\sigma}\right]^{i}_{n+\theta}\theta\left\{d\sigma^{i+1}_{n+\theta}\right\} \\ &\quad+\frac{3f^{i}_{n+\theta}}{2\bar{\sigma}^{i}_{n+\theta}}\left[\frac{\partial\sigma'}{\partial\sigma}\right]^{i}_{n+\theta}\theta\left\{d\sigma^{i+1}_{n+1}\right\}+\frac{3}{2\bar{\sigma}'^{i}_{n+\theta}}\left\{\sigma'^{i}_{n+\theta}\right\}\left(\frac{\partial f}{\partial\bar{\varepsilon}^{H}}\right)^{i}_{n+\theta}\theta d\bar{\varepsilon}^{H,i+1}_{n+1}\end{aligned} \tag{2.2.44}$$

The above equation is rearranged using the relationship $\left\{\frac{\partial\bar{\sigma}}{\partial\sigma}\right\}=\frac{3}{2\bar{\sigma}}\left\{\sigma'\right\}$ as

$$\begin{aligned}\left\{\dot{\varepsilon}^{c,i+1}_{n+\theta}\right\} &= \left\{\dot{\varepsilon}^{c,i}_{n+\theta}\right\} \\ &\quad+\frac{9}{4\left(\bar{\sigma}^{i}_{n+\theta}\right)^{2}}\left(\left(\frac{\partial f}{\partial\bar{\sigma}}\right)^{i}_{n+\theta}-\frac{f^{i}_{n+\theta}}{\bar{\sigma}^{i}_{n+\theta}}\right)\left[\sigma'_{i}\sigma'_{j}\right]^{i}_{n+\theta}\theta\left\{d\sigma^{i+1}_{n+1}\right\} \\ &\quad+\frac{3f^{i}_{n+\theta}}{2\bar{\sigma}^{i}_{n+\theta}}\left[\frac{\partial\sigma'}{\partial\sigma}\right]^{i}_{n+\theta}\theta\left\{d\sigma^{i+1}_{n+1}\right\}+\frac{3}{2\bar{\sigma}^{i}_{n+\theta}}\left\{\sigma'^{i}_{n+\theta}\right\}\left(\frac{\partial f}{\partial\bar{\varepsilon}^{H}}\right)^{i}_{n+\theta}\theta d\bar{\varepsilon}^{H,i+1}_{n+1}.\end{aligned} \tag{2.2.45}$$

Meanwhile, the creep hardening increment is represented as follows using eq. (2.2.39).

$$\begin{aligned}\Delta\bar{\varepsilon}^{H,i+1}_{n+\theta} &= \Delta t_{n+1}f\left(\bar{\sigma}^{i+1}_{n+\theta},\bar{\varepsilon}^{H,i+1}_{n+\theta}\right) \\ &= \Delta t_{n+1}f\left(\bar{\sigma}\left(\left\{\sigma^{i}_{n+\theta}\right\}+\theta\left\{d\sigma^{i+1}_{n+1}\right\}\right),\bar{\varepsilon}^{H,i}_{n+\theta}+\theta\, d\bar{\varepsilon}^{H,i+1}_{n+1}\right)\end{aligned}$$

This equation is approximated by carrying out the first-order Taylor expansion as

$$\Delta\bar{\varepsilon}^{H,i+1}_{n+\theta} = \Delta\bar{\varepsilon}^{H,i}_{n+\theta} + d\bar{\varepsilon}^{i+1}_{n+1}$$
$$= \Delta t_{n+1} f'_{n+\theta} + \theta\,\Delta t_{n+1}\left(\frac{\partial f}{\partial \bar{\sigma}}\right)^{i}_{n+\theta}\left[\frac{\partial \bar{\sigma}}{\partial \sigma}\right]^{i}_{n+\theta}\left\{d\sigma^{i+1}_{n+1}\right\} \tag{2.2.46}$$
$$+ \theta\,\Delta t_{n+1}\left(\frac{\partial f}{\partial \varepsilon^{H}}\right)^{i}_{n+\theta} d\bar{\varepsilon}^{H,i+1}_{n+1}.$$

Here, since $\Delta\bar{\varepsilon}^{H,i+1}_{n+\theta} = \Delta t_{n+1} f^{i}_{n+\theta}$, $d\bar{\varepsilon}^{H,i+1}_{n+1}$ is expressed as

$$d\bar{\varepsilon}^{H,i+1}_{n+1} = \frac{\theta\Delta t_{n+1}\left(\frac{\partial f}{\partial \bar{\sigma}}\right)^{i}_{n+\theta}\left[\frac{\partial \bar{\sigma}}{\partial \sigma}\right]^{i}_{n+\theta}\left\{d\sigma^{i+1}_{n+1}\right\}}{1-\theta\Delta t_{n+1}\left(\frac{\partial f}{\partial \bar{\varepsilon}^{H}}\right)^{i}_{n+\theta}}. \tag{2.2.47}$$

Substituting this equation into eq. (2.2.45) and rearranging, we obtain

$$\left\{\dot{\varepsilon}^{c,i+1}_{n+\theta}\right\} = \left\{\dot{\varepsilon}^{c,i}_{n+\theta}\right\} + F_1\theta\left[\sigma'_i\sigma'_j\right]^{i}_{n+\theta}\left\{d\sigma^{i+1}_{n+1}\right\} + F_2\theta\left[\frac{\partial\sigma'}{\partial\sigma}\right]^{i}_{n+1}\left\{d\sigma^{i+1}_{n+1}\right\}, \tag{2.2.48}$$

where

$$F_1 = \frac{9}{4\left(\bar{\sigma}^{i}_{n+\theta}\right)^2}\left(\left(\frac{\partial f}{\partial \bar{\sigma}}\right)^{i}_{n+\theta} - \frac{f^{i}_{n+\theta}}{\bar{\sigma}^{i}_{n+\theta}} + \frac{\left(\frac{\partial f}{\partial \bar{\varepsilon}^{H}}\right)^{i}_{n+\theta}\theta\Delta t_{n+1}\left(\frac{\partial f}{\partial \bar{\sigma}}\right)^{i}_{n+\theta}}{1-\theta\Delta t_{n+1}\left(\frac{\partial f}{\partial \bar{\varepsilon}^{H}}\right)^{i}_{n+\theta}}\right) \tag{2.2.49}$$

$$F_2 = \frac{3f'_{n+\theta}}{2\bar{\sigma}^{i}_{n+\theta}}. \tag{2.2.50}$$

The creep strain increment is given as

$$\left\{\Delta\varepsilon^{c,i+1}_{n+1}\right\} = \Delta t_{n+1}\left\{\dot{\varepsilon}^{c,i+1}_{n+\theta}\right\}$$
$$= \left\{\Delta\varepsilon^{c,i}_{n+1}\right\} + \left[C^{c,i}_{n+\theta}\right]\left\{d\sigma^{i+1}_{n+1}\right\}. \tag{2.2.51}$$

where

$$\left[C^{c,i}_{n+\theta}\right] = \theta\Delta t_{n+1}\left(F_1\left[\sigma'_i\sigma_j\right]^{i}_{n+\theta} + F_2\left[\frac{\partial\sigma'^{\,i}}{\partial\sigma}_{n+\theta}\right]\right).$$

Thus, $\left\{\Delta\varepsilon^{c,i+1}_{n+1}\right\}$ in eq. (2.2.37) was eliminated. Substituting eq. (2.2.51) into eq. (2.2.37) and rearranging, we obtain

$$\begin{aligned}\left\{d\sigma_{n+1}^{i+1}\right\} = \left[\hat{D}_{n+\theta}^{i}\right]\left(\left[B\right]\left\{\Delta u_{n+1}^{i+1}\right\} - \left[C_{n+\theta}^{i}\right]\left(\left\{\sigma_{n+1}^{i}\right\} - \left\{\sigma_{n}\right\}\right)\right. \\ \left. - \left\{\Delta\varepsilon_{n+1}^{0}\right\} - \left\{\Delta\varepsilon_{n+1}^{C,i}\right\} - \left\{\Delta\varepsilon_{n+1}^{P,i+1}\right\}\right),\end{aligned} \tag{2.2.52}$$

where

$$\left[\hat{D}_{n+1}^{i}\right] = \left(\left[C_{n+1}^{i}\right] + \left[C_{n+1}^{C,i}\right]\right)^{-1}$$
$$\left\{\Delta u_{n+1}^{i+1}\right\} = \left\{u_{n+1}^{i}\right\} + \left\{du_{n+1}^{i+1}\right\} - \left\{u_{n}\right\},$$

and ^ means the apparent stiffness.

2.2.5 Plasticity

The yield condition of pellet and cladding is given by

$$h(\{\sigma\}) = K(\bar{\varepsilon}^P, T), \tag{2.2.53}$$

where

$\bar{\varepsilon}^P$: equivalent plastic strain

T : temperature

K : yield surface area

h : yield function.

The yield function h is given as follows, with consideration of the cladding anisotropy and the pellet compressibility (hot-press). However, the shear component is not taken into account in this model.

$$h = \frac{3}{2(F+G+H)}\left[\left\{H(\sigma_r - \sigma_\theta)^2 + F(\sigma_\theta - \sigma_z)^2 + G(\sigma_z - \sigma_r)^2\right\} + 3\alpha(\sigma_r + \sigma_z + \sigma_\theta)^2\right]^{\frac{1}{2}} \equiv \bar{\sigma} \tag{2.2.54}$$

Here,

H, F, G : anisotropic coefficients (H = 1, F = 1 and G = 1 are set for the pellet based on the assumption of isotropy of the pellet)

α : pellet hot-press parameter (α = 0 for cladding)[22].

Fitting parameters H0(2), F0(2) and G0(2) Anisotropic coefficients of cladding H, F and G are designated by H0(2), F0(2) and G0(2). The default values for these are 1.0.

Fitting parameter IHOT When IHOT=1, pellet hot-press parameter α is defined as a function of porosity p as $\alpha = \text{BETAX}\frac{p}{1-D_0}$.

Here, p: porosity inside a pellet

D_0: initial theoretical density ratio

BETAX: initial value of hot-press parameter.

Fitting parameter BETAX

Pellet hot-press parameter α is designated by BETAX. The default value is 0.002.

The plastic strain increment vector from time t_n to t_{n+1} is represented by the flow rule as

$$\left\{\Delta\varepsilon_{n+1}^{P}\right\} = \Delta\bar{\varepsilon}_{n+1}^{P}\left\{\frac{\partial h}{\partial\sigma}\right\}_{n+\theta} . \tag{2.2.55}$$

During the (i+1)th iteration that follows the (i)th iteration, the yield condition and flow rule are expressed as

$$h\left(\left\{\sigma_n\right\}+\left\{\Delta\sigma_{n+1}^{i+1}\right\}\right) = K\left(\bar{\varepsilon}_n^{P}+\Delta\bar{\varepsilon}_{n+1}^{P,i+1}\,,\,T_n+\Delta T_{n+1}\right) \tag{2.2.56}$$

$$\left\{\Delta\varepsilon_{n+1}^{P,i+1}\right\} = \Delta\bar{\varepsilon}_{n+1}^{P,i+1}\left\{\frac{\partial h}{\partial\sigma}\right\}_{n+\theta}^{i} . \tag{2.2.57}$$

Performing the first-order Taylor expansion for eq. (2.2.56) with respect to $\left\{\Delta\sigma_{n+1}^{i+1}\right\}$, $\Delta\bar{\varepsilon}_{n+1}^{P,i+1}$ and ΔT_{n+1}, we obtain the following approximation.

$$h\left\{\sigma_n\right\}+\left\lfloor\frac{\partial h}{\partial\sigma}\right\rfloor_{n+\theta}^{i}\left\{\Delta\sigma_{n+1}^{i+1}\right\} = K\left(\bar{\varepsilon}_n^{P}\;T_n\right)+\left(\frac{\partial K}{\partial\bar{\varepsilon}^{P}}\right)_{n+\theta}^{i}\Delta\bar{\varepsilon}_{n+1}^{P,i+1}+\left(\frac{\partial K}{\partial T}\right)_{n+\theta}\Delta T_{n+1} \tag{2.2.58}$$

By substituting

$$\left\{\Delta\sigma_{n+1}^{i+1}\right\} = \left\{\Delta\sigma_{n+1}^{i}\right\}+\left\{d\sigma_{n+1}^{i+1}\right\}-\left\{\sigma_n\right\} \tag{2.2.59}$$

into eq. (2.2.58) and rearranging the equation, we obtain

$$\begin{aligned}\Delta\bar{\varepsilon}_{n+1}^{P,i+1} = \frac{1}{H_{n+\theta}^{\prime i}}\Bigg(&\left\lfloor\frac{\partial h}{\partial\sigma}\right\rfloor_{n+\theta}^{i}\left(\left\{\sigma_{n+1}^{i}\right\}-\left\{\sigma_n\right\}\right)+h\left(\left\{\sigma_n\right\}\right)-K\left(\bar{\varepsilon}_n^{P},T_n\right)\\&-\left(\frac{\partial K}{\partial T}\right)_{n+\theta}\Delta T_{n+1}+\left\lfloor\frac{\partial h}{\partial\sigma}\right\rfloor_{n+\theta}^{i}\left\{d\sigma_{n+1}^{i+1}\right\}\Bigg),\end{aligned} \tag{2.2.60}$$

where

$$H_{n+\theta}^{\prime i} = \left(\frac{\partial K}{\partial\bar{\varepsilon}_P}\right)_{n+\theta}^{i} . \tag{2.2.61}$$

Substituting eq. (2.2.52) into eq. (2.2.60), we obtain

$$\begin{aligned}&H_{n+1}^{\prime i}\;\Delta\bar{\varepsilon}_{n+1}^{P,i+1}+\left(\frac{\partial K}{\partial T}\right)_{n+\theta}\Delta T_{n+1}-h\left(\left\{\sigma_n\right\}\right)+K\left(\bar{\varepsilon}_n^{P},T_n\right)\\&=\left\lfloor\frac{\partial\sigma}{\partial\sigma}\right\rfloor_{n+\theta}^{i}\left(\left\{\sigma_{n+1}^{i}\right\}-\left\{\sigma_n\right\}\right)\\&\quad+\left\lfloor\frac{\partial h}{\partial\sigma}\right\rfloor_{n+\theta}^{i}\left[\hat{D}_{n+\theta}^{i}\right]\left(\left[B\right]\left\{\Delta u_{n+1}^{i+1}\right\}-\left[C_{n+\theta}^{i}\right]\left(\left\{\sigma_{n+1}^{i}\right\}-\left\{\sigma_n\right\}\right)-\left\{\Delta\varepsilon_{n+1}^{o}\right\}-\Delta\bar{\varepsilon}_{n+1}^{P,i+1}\left[\frac{\partial h}{\partial\sigma}\right]_{n+\theta}^{i}\right).\end{aligned} \tag{2.2.62}$$

Rearranging eq. (2.2.54) with respect to $\Delta\bar{\varepsilon}^{P,i+1}_{n+1}$, we obtain

$$\Delta\bar{\varepsilon}^{P,i+1}_{n+1}=\frac{\left\lfloor\frac{\partial h}{\partial\sigma}\right\rfloor^{i}_{n+\theta}\left[\hat{D}^{i}_{n+\theta}\right]\left([B]\left\{\Delta u^{i+1}_{n+1}\right\}-\left[C^{i}_{n+\theta}\right]\left(\left\{\sigma^{i}_{n+1}\right\}-\left\{\sigma_n\right\}\right)-\left\{\Delta\varepsilon^{o}_{n+1}\right\}-\left\{\Delta\varepsilon^{c,i}_{n+1}\right\}\right)}{H'^{i}_{n+\theta}+\left\lfloor\frac{\partial h}{\partial\sigma}\right\rfloor^{i}_{n+\theta}\left[\hat{D}^{i}_{n+\theta}\right]\left\{\frac{\partial h}{\partial\sigma}\right\}^{i}_{n+\theta}}$$
$$+\frac{\left\lfloor\frac{\partial h}{\partial\sigma}\right\rfloor^{i}_{n+\theta}\left(\left\{\sigma^{i}_{n+1}\right\}-\left\{\sigma_n\right\}\right)-\left(\frac{\partial K}{\partial T}\right)_{n+\theta}\Delta T_{n+1}-h\left(\left\{\sigma_n\right\}\right)+K\left(\bar{\varepsilon}^{P}_{n},T_n\right)}{H'^{i}_{n+\theta}+\left\lfloor\frac{\partial h}{\partial\sigma}\right\rfloor^{i}_{n+\theta}\left[\hat{D}^{i}_{n+\theta}\right]\left\{\frac{\partial h}{\partial\sigma}\right\}^{i}_{n+\theta}}. \tag{2.2.63}$$

Using eq. (2.2.57) and substituting the above equation into eq. (2.2.52), we obtain

$$\left\{d\sigma^{i+1}_{n+1}\right\}=\left[\hat{D}^{i}_{n+\theta}\right]\left([B]\left\{\Delta u^{i+1}_{n+1}\right\}-\left[C^{i}_{n+\theta}\right]\left(\left\{\sigma^{i}_{n+1}\right\}-\left\{\sigma_n\right\}\right)-\left\{\Delta\varepsilon^{o}_{n+1}\right\}-\left\{\Delta\varepsilon^{c,i}_{n+1}\right\}\right)$$
$$-\frac{\left[\hat{D}^{i}_{n+\theta}\right]\left\{\frac{\partial h}{\partial\sigma}\right\}^{i}_{n+\theta}\left\lfloor\frac{\partial h}{\partial\sigma}\right\rfloor^{i}_{n+\theta}\left[\hat{D}^{i}_{n+\theta}\right]}{H'^{i}_{n+\theta}+\left\lfloor\frac{\partial h}{\partial\sigma}\right\rfloor^{i}_{n+\theta}\left[\hat{D}^{i}_{n+\theta}\right]\left\{\frac{\partial h}{\partial\sigma}\right\}^{i}_{n+\theta}}$$
$$\times\left([B]\left\{\Delta u^{i+1}_{n+1}\right\}-\left[C^{i}_{n+\theta}\right]\left(\left\{\sigma^{i}_{n+1}\right\}-\left\{\sigma_n\right\}\right)-\left\{\Delta\varepsilon^{o}_{n+1}\right\}-\left\{\Delta\varepsilon^{c,i}_{n+1}\right\}\right) \tag{2.2.64}$$
$$-\frac{\left[\hat{D}^{i}_{n+\theta}\right]\left\{\frac{\partial h}{\partial\sigma}\right\}^{i}_{n+\theta}\left(\left\lfloor\frac{\partial h}{\partial\sigma}\right\rfloor^{i}_{n+\theta}\left(\left\{\sigma^{i}_{n+1}\right\}-\left\{\sigma_n\right\}\right)-\left(\frac{\partial K}{\partial T}\right)_{n+\theta}\Delta T_{n+1}-h\left(\left\{\sigma_n\right\}\right)+K\left(\bar{\varepsilon}^{P}_{n},T_n\right)\right)}{H'^{i}_{n+\theta}+\left\lfloor\frac{\partial h}{\partial\sigma}\right\rfloor^{i}_{n+\theta}\left[\hat{D}^{i}_{n+\theta}\right]\left\{\frac{\partial h}{\partial\sigma}\right\}^{i}_{n+\theta}}.$$

This equation is rearranged as follows.

$$\left\{d\sigma^{i+1}_{n+1}\right\}=\left[\hat{D}^{P,i}_{n+\theta}\right]\left([B]\left\{\Delta u^{i+1}_{n+1}\right\}-\left[C^{i}_{n+\theta}\right]\left(\left\{\sigma^{i}_{n+1}\right\}-\left\{\sigma_n\right\}\right)-\left\{\Delta\varepsilon^{o}_{n+1}\right\}-\left\{\Delta\varepsilon^{c,i}_{n+1}\right\}\right)$$
$$+\left\{S^{i}_{n+\theta}\right\}\Delta T_{n+1}-\left\{Z_1\right\}-\left\{Z_2\right\} \tag{2.2.65}$$

Here, the following equations hold.

$$\left[\hat{D}^{P,i}_{n+\theta}\right]=\left[\hat{D}^{i}_{n+\theta}\right]-\frac{\left[\hat{D}^{i}_{n+\theta}\right]\left[\frac{\partial h}{\partial\sigma}\right]^{i}_{n+\theta}\left\lfloor\frac{\partial h}{\partial\sigma}\right\rfloor^{i}_{n+\theta}\left[\hat{D}^{i}_{n+\theta}\right]}{H'^{i}_{n+\theta}+\left\lfloor\frac{\partial h}{\partial\sigma}\right\rfloor^{i}_{n+\theta}\left[\hat{D}^{i}_{n+\theta}\right]\left\{\frac{\partial h}{\partial\sigma}\right\}^{i}_{n+\theta}} \tag{2.2.66}$$

$$\left\{S^{i}_{n+\theta}\right\}=\frac{\left[\hat{D}^{i}_{n+\theta}\right]\left\{\frac{\partial h}{\partial\sigma}\right\}^{i}_{n+\theta}\left(\frac{\partial K}{\partial T}\right)_{n+\theta}}{H'^{i}_{n+\theta}+\left\lfloor\frac{\partial h}{\partial\sigma}\right\rfloor^{i}_{n+\theta}\left[\hat{D}^{i}_{n+\theta}\right]\left\{\frac{\partial h}{\partial\sigma}\right\}^{i}_{n+\theta}} \tag{2.2.67}$$

$$\{Z_1\} = \frac{\left[\hat{D}^i_{n+\theta}\right]\left\{\frac{\partial h}{\partial \sigma}\right\}^i_{n+\theta}\left|\frac{\partial h}{\partial \sigma}\right|^i_{n+\theta}\left(\{\sigma^i_{n+1}\} - \{\sigma_n\}\right)}{H'^i_{n+\theta} + \left|\frac{\partial h}{\partial \sigma}\right|^i_{n+\theta}\left[\hat{D}^i_{n+\theta}\right]\left\{\frac{\partial h}{\partial \sigma}\right\}^i_{n+\theta}} \tag{2.2.68}$$

$$\{Z_{21}\} = \frac{\left[\hat{D}^i_{n+\theta}\right]\left\{\frac{\partial h}{\partial \sigma}\right\}^i_{n+\theta}\left[\frac{\partial h}{\partial \sigma}\right]^i_{n+\theta}\left(h(\{\sigma_n\}) - K(\bar{\varepsilon}^p_n, T_n)\right)}{H'^i_{n+\theta} + \left|\frac{\partial h}{\partial \sigma}\right|^i_{n+\theta}\left[\hat{D}^i_{n+\theta}\right]\left\{\frac{\partial h}{\partial \sigma}\right\}^i_{n+\theta}} \tag{2.2.69}$$

Thus, the unknown value $\left\{\Delta\varepsilon^{p,i+1}_{n+1}\right\}$ in eq. (2.2.30) was eliminated.

Accordingly, eq. (2.2.65) is a constitutive equation in which all the unknown values regarding pellet cracks, as well as creep and plasticity of pellet and cladding are eliminated.

In the above calculation, for the yield stress and creep rate of pellet and cladding, the same material properties values as those used in section 2.1.3 (contact force evaluation model) are used.

2.2.6 Derivation of stiffness equation

The constitutive equation (2.2.65) in which pellet cracks, creep and plasticity are expressed with known values is rewritten as

$$\begin{aligned}\left\{d\sigma^{i+1}_{n+1}\right\} = \left[\hat{D}^{P,i}_{n+\theta}\right]\left(\left[B\right]\left\{\Delta u^{i+1}_{n+1}\right\} - \left[C^i_{n+\theta}\right]\left(\left\{\sigma^i_{n+1}\right\} - \left\{\sigma_n\right\}\right) - \left\{\Delta\varepsilon^o_{n+1}\right\} - \left\{\Delta\varepsilon^{C,i}_{n+1}\right\}\right) \\ + \left\{S^i_{n+\theta}\right\}\ \Delta T_{n+1} - \left\{Z_1\right\} - \left\{Z_2\right\}.\end{aligned} \tag{2.2.65}$$

Substituting eq. (2.2.65) into the equilibrium condition equation (2.2.31) and rearranging the equation, we obtain the following stiffness equation.

$$\left[K^i_{n+\theta}\right]\left\{\Delta u^{i+1}_{n+1}\right\} = \left\{\Delta\hat{F}^i_{n+1}\right\} \tag{2.2.70}$$

For applying stiffness equation (2.2.70) to each element, each term of the equation is determined by integral with element volume, as shown in the following equations.

$$\left[K^i_{n+\theta}\right] = 2\pi\int\int\left[B\right]^T\left[\hat{D}^{P,i}_{n+\theta}\right]\left[B\right]\ \ rdrdz \tag{2.2.71}$$

$$\begin{aligned}\left\{\Delta\hat{F}^{i}_{n+1}\right\} &= 2\pi\int\int[B]^{T}\left[\hat{D}^{P,i}_{n+\theta}\right]\left\{\left[C^{i}_{n+\theta}\right]\left(\left\{\sigma'_{n+1}\right\}-\left\{\sigma_{n}\right\}\right)\right.\\ &\quad\left.+\left\{\Delta\varepsilon^{o}_{n+1}\right\}+\left\{\Delta\varepsilon^{c,i}_{n+1}\right\}\right\}\quad rdrdz\\ &\quad-2\pi\int\int[B]^{T}\left(\left\{S'_{n+\theta}\right\}\Delta T_{n+1}-\left\{Z_{1}\right\}-\left\{Z_{2}\right\}\right)\quad rdrdz\\ &\quad+\left\{F_{n+1}\right\}-2\pi\int\int[B]^{T}\left(\sigma^{i}_{n+\theta}\right)\quad rdrdz\end{aligned}\tag{2.2.72}$$

Here, the right-hand side of the stiffness equation of elements is expressed with $\left\{\Delta\hat{F}^{i}_{n+1}\right\}$ because this value represents the load increment vector, since the solution obtained from stiffness equation (2.2.70) is a displacement increment, $\left\{\Delta u^{i+1}_{n+1}\right\}$. The symbol ^ in $\Delta\hat{F}^{i}_{n+1}$ means that this term is a tentative value of ΔF_{n+1} during the iteration calculation.

Next, treatment method for spring elements in the upper and lower plenums will be explained. Regarding the spring elements in the upper and lower plenums, a degree of freedom is considered only in the axial direction, and only initial elastic strain (thermal strain) is allowed. Therefore, when

$$\left\{\Delta\varepsilon^{p}_{n+1}\right\}=0,\quad\left\{\Delta\varepsilon^{c}_{n+\theta}\right\}=0$$

are assumed in eq. (2.2.29), we obtain

$$\left[C_{n+\theta}\right]\left\{\Delta\sigma_{n+1}\right\}-\left[B\right]\left\{\Delta u_{n+1}\right\}+\left\{\Delta\varepsilon^{o}_{n+\theta}\right\}=0.\tag{2.2.73}$$

Equation (2.2.73) can also be expressed as

$$\left[C_{n+\theta}\right]\left(\left\{\sigma_{n+1}\right\}+\left\{d\sigma^{i+1}_{n+\theta}\right\}-\left\{\sigma_{n}\right\}\right)-\left[B\right]\left\{\Delta u^{i+1}_{n+\theta}\right\}+\left\{\Delta\varepsilon^{o}_{n+\theta}\right\}=0.$$

Here, if we permute $\left[D_{n+\theta}\right]=\left[C_{n+\theta}\right]^{-1}$, the following equation holds.

$$\left\{d\sigma^{i+1}_{n+\theta}\right\}=\left[D_{n+\theta}\right]\left(\left[B\right]\left\{\Delta u^{i+1}_{n+\theta}\right\}-\left\{\Delta\varepsilon^{o}_{n+1}\right\}-\left[C_{n+\theta}\right]\left\{\sigma^{i}_{n+1}\right\}-\left\{\sigma_{n}\right\}\right)\tag{2.2.74}$$

Substituting this equation into eq. (2.2.31), we obtain

$$\begin{aligned}&\int_{v}[B]^{T}\left[D_{n+\theta}\right]\left(\left[B\right]\left\{\Delta u^{i+1}_{n+1}\right\}-\left\{\Delta\varepsilon^{o}_{n+1}\right\}-\left[C_{n+\theta}\right]\left(\left\{\sigma'_{n+1}\right\}-\left\{\sigma_{n}\right\}\right)\right)dV\\ &+\int_{v}[B]^{T}\left\{\sigma^{i}_{n+1}\right\}dV=\left\{F_{n+1}\right\}.\end{aligned}\tag{2.2.75}$$

Moving the unknown values to the left-hand side of this equation, we obtain

$$\begin{aligned}&\int_{v}[B]^{T}\left[D_{n+\theta}\right]\left[B\right]\left\{\Delta u^{i+1}_{n+1}\right\}dV\\ &=\left\{F_{n+1}\right\}+\int_{v}[B]^{T}\left[D_{n+\theta}\right]\left\{\Delta\varepsilon^{o}_{n+1}\right\}dV+\int_{v}[B]^{T}\left(\left\{\sigma^{i}_{n+1}\right\}-\left\{\sigma_{n}\right\}\right)dV\\ &\quad-\int_{v}[B]^{T}\left\{\sigma^{i}_{n+1}\right\}dV,\end{aligned}\tag{2.2.76}$$

and the following equation holds.

$$\int_v [B]^T [D_{n+\theta}][B]\{\Delta u_{n+1}^{i+1}\} = \{F_{n+1}\} + \int_v [B]^T [D_{n+\theta}]\{\Delta \varepsilon_{n+1}^{o}\} dV - \int_v [B]^T \{\sigma_n\} dV \tag{2.2.77}$$

Equation (2.2.77) can be expressed as

$$\begin{aligned} &[K_{n+\theta}^i]\{\Delta u_{n+1}^{i+1}\} = \{\Delta \hat{F}_{n+1}^i\} \\ &[K_{n+\theta}^i] = \int [B]^T [\hat{D}_{n+\theta}^{P,i}][B] dV \\ &\{\Delta \hat{F}_{n+1}^i\} = \{F_{n+1}\} - \int [B]^T [D_{n+\theta}]\{\Delta \varepsilon_{n+1}^0\} dV - \int [B]^T \{\sigma_n\} dV \end{aligned} \tag{2.2.78}$$

Therefore, eq.(2.2.78) is the constitutive equation in which the unknown variables are eliminated. This equation is expressed using vectors, but a degree of freedom is allowed only in the axial direction.

The external force is given as

$$F_{n+1} = \pi r_{ci}^2 P_{gas,n+1} - \pi r_{co}^2 P_{water,n+1}. \tag{2.2.79}$$

Here,

r_{co} : cladding outer radius (m)

r_{ci} : cladding inner radius (m)

$P_{water,n+1}$: coolant pressure in (n+1)th stage (Pa)

$P_{gas,n+1}$: plenum pressure in (n+1)th stage (Pa).

The third term on the right-hand side of eq. (2.2.77) is given by

$$\int [B]^T \{\sigma_n\} dV = k\left(v_{pl,n} - v_{u,n}\right), \tag{2.2.80}$$

where

k : spring constant (N/m)

$v_{pl,n}$: upper part displacement of plenum in nth stage (m)

$v_{u,n}$: upper part displacement of pellet (or cladding) in (n)th stage (m).

A similar calculation is applied to the lower plenum.

2.2.7 External force and contact force acting on pellet and cladding

Forces acting on pellet and cladding are shown in Fig. 2.33.

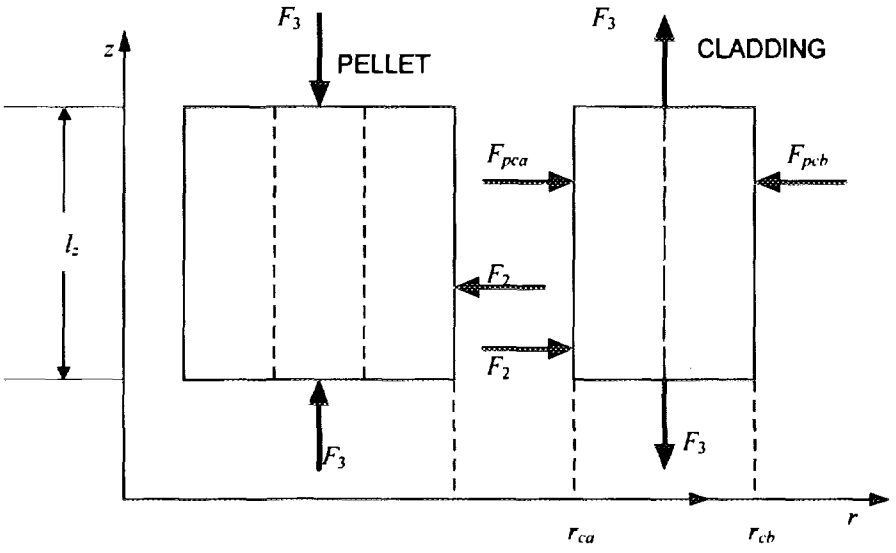

Fig. 2.33 Forces acting on pellet and cladding.

Here,

F_2 : contact force between pellet and cladding

F_3 : axial force

F_{pca} : plenum gas pressure

F_{pcb} : coolant pressure.

The contact force between pellet and cladding is calculated independently of the calculation described in section 2.1.3.

Since gas is introduced inside the pellet by plenum gas pressure through the cracks, pellet compressive deformation caused by the plenum gas pressure are ignored in the calculation.

2.2.8 Boundary conditions

The boundary conditions are explained using the case of a three-layer pellet and two-layer cladding as an example, as shown in Fig. 2.34, and formulation for the total matrix is performed.

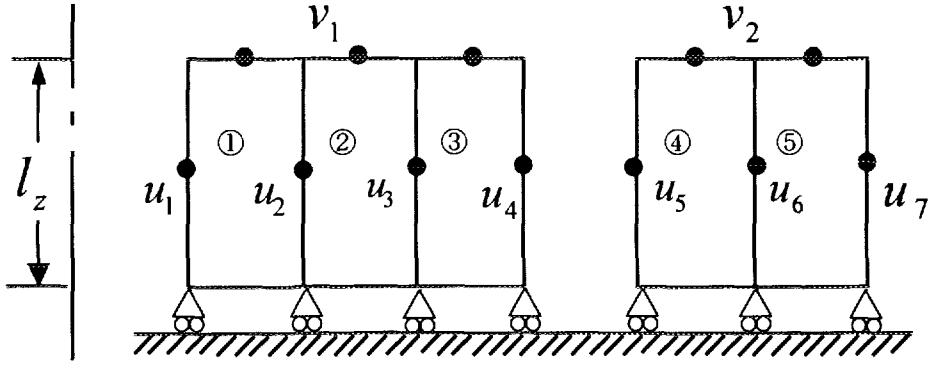

Fig. 2.34 Example of analysis model.

In Fig. 2.34, u is the radial displacement, and v is the axial displacement.

The stiffness equations for each element (2.2.70) and (2.2.72) and the stiffness equation (2.2.78) for upper and lower plenums are shown below.

$$\left[K^{i}_{n+\theta}\right]\left\{\Delta u^{i+1}_{n+1}\right\} = \left\{\Delta \hat{F}^{i}_{n+1}\right\} \tag{2.2.70}$$

$$\begin{aligned}\left\{\Delta \hat{F}^{i}_{n+1}\right\} = {} & 2\pi \int\int [B]^{T}\left[\hat{D}^{P,i}_{n+\theta}\right]\left\{\left[\tilde{C}^{i}_{n+\theta}\right]\left(\left\{\sigma^{i}_{n+1}\right\} - \left\{\sigma_{n}\right\}\right)\right. \\ & \left. + \left\{\Delta\varepsilon^{o}_{n+1}\right\} + \left\{\Delta\varepsilon^{c,i}_{n+1}\right\}\right\} r\,dr\,dz \\ & - 2\pi \int\int [B]^{T}\left(\left\{S^{i}_{n+\theta}\right\}\Delta T_{n+1} - \left\{Z_1\right\} - \left\{Z_2\right\}\right) r\,dr\,dz \\ & + \left\{F_{n+1}\right\} - 2\pi \int\int [B]^{T}\left(\sigma^{i}_{n+1}\right) r\,dr\,dz\end{aligned} \tag{2.2.72}$$

$$\begin{aligned}&\left[K^{i}_{n+\theta}\right]\left\{\Delta u^{i+1}_{n+1}\right\} = \left\{\Delta \hat{F}^{i}_{n+1}\right\} \\ &\left[K^{i}_{n+\theta}\right] = \int_{V} [B]^{T}\left[\hat{D}^{P,i}_{n+\theta}\right][B]\,dV \\ &\left\{\Delta \hat{F}^{i}_{n+1}\right\} = \left\{F_{n+1}\right\} - \int_{V} [B]^{T}\left[D_{n+\theta}\right]\left\{\Delta\varepsilon^{0}_{n+1}\right\} dV - \int_{V} [B]^{T}\left\{\sigma_{n}\right\} dV\end{aligned} \tag{2.2.78}$$

When the Newton-Raphson iteration is completed, these equations can be expressed as follows with omission of subscripts for iteration i.

$$\left[K_{n+\theta}\right]\left\{\Delta u_{n+1}\right\} = \left\{\Delta F_{n+1}\right\} \tag{2.2.81}$$

Equation (2.2.81) can be expressed as follows for convenience in the following discussion.

$$\left[B_{ee}\right]\left\{\Delta u_{n+1}\right\} = \left\{F_{n+1}\right\} + \left\{B_{et,n+1}\right\} \tag{2.2.82}$$

Here,

$$\begin{aligned}&\left[B_{ee}\right] = \left[K_{n+\theta}\right] \\ &\left\{B_{et,n+1}\right\} = \left\{\Delta F_{n+1}\right\} - \left\{F_{n+1}\right\}.\end{aligned}$$

Thus, the element matrices have been formulated; the formulation of the total matrix is explained next.

The total matrix for the segments is represented as follows, using the model shown in Fig. 2.34 as an example.

$$
\begin{bmatrix}
B_{11}^1 & B_{12}^1 & 0 & 0 & 0 & 0 & 0 & B_{13}^1 & 0 \\
B_{21}^1 & B_{22}^1 + B_{11}^2 & B_{12}^1 & 0 & 0 & 0 & 0 & B_{23}^1 + B_{13}^2 & 0 \\
0 & B_{21}^2 & B_{22}^1 + B_{11}^3 & B_{12}^3 & 0 & 0 & 0 & B_{23}^2 + B_{13}^2 & 0 \\
0 & 0 & B_{21}^3 & B_{22}^3 & 0 & 0 & 0 & B_{23}^3 & 0 \\
0 & 0 & 0 & 0 & B_{11}^4 & B_{12}^4 & 0 & 0 & B_{13}^4 \\
0 & 0 & 0 & 0 & B_{21}^4 & B_{22}^4 + B_{12}^5 & B_{12}^5 & 0 & B_{23}^4 + B_{13}^5 \\
0 & 0 & 0 & 0 & 0 & B_{21}^5 & B_{22}^5 & 0 & B_{23}^5 \\
B_{31}^1 & B_{32}^1 + B_{31}^2 & B_{32}^2 + B_{31}^3 & B_{21}^3 & 0 & 0 & 0 & B_{33}^1 + B_{33}^2 + B_{33}^3 & 0 \\
0 & 0 & 0 & 0 & B_{31}^4 & B_{32}^4 + B_{31}^5 & B_{32}^5 & 0 & B_{33}^4 + B_{33}^5
\end{bmatrix}
\begin{Bmatrix}
\Delta u_1 \\ \Delta u_2 \\ \Delta u_3 \\ \Delta u_4 \\ \Delta u_5 \\ \Delta u_6 \\ \Delta u_7 \\ \Delta v_1 \\ \Delta v_2
\end{Bmatrix}
$$

$$
= \begin{Bmatrix} 0 \\ 0 \\ 0 \\ 0 \\ F_{pca} \\ 0 \\ -F_{pcb} \\ 0 \\ 0 \end{Bmatrix} + \begin{Bmatrix} B_{et,1}^1 \\ B_{et,2}^1 + B_{et,1}^2 \\ B_{et,2}^2 + B_{et,1}^3 \\ B_{et,2}^3 \\ B_{et,1}^4 \\ B_{et,2}^4 + B_{et,1}^5 \\ B_{et,2}^5 \\ B_{et,3}^1 + B_{et,3}^2 + B_{et,3}^3 \\ B_{et,3}^4 + B_{et,3}^5 \end{Bmatrix} \tag{2.2.83}
$$

In this equation, the suffix number $*$ of B^* represents the number of elements in Fig. 2.34, and only F_{pca} and F_{pcb} in Fig. 2.33 are considered as external force vectors $\{F_{n+1}\}$. Therefore, as a boundary condition for the total matrix of the segment, that corresponding to the contact state between pellet and cladding must be incorporated. Below, a case in which the pellet is in contact with the cladding is analyzed.

(1) Clogged gap state case

In the case of a clogged gap state, the displacement of the outermost layer of the pellet Δu_4 and the displacement of the innermost layer of the cladding Δu_5 are positioned in the same place of the displacement vector matrix. Therefore, eq. (2.2.82) is given by

$$
\left[\begin{array}{ccc:c}
 & B_{8\times 8} & & \begin{matrix}0\\ \vdots \\ \vdots \\ 0 \\ 1 \\ -1\end{matrix} \\
\hdashline
0 \cdots & \cdots & \cdots 0\ 1\ -1 & 0
\end{array}\right]
\left\{\begin{array}{c}
\vdots \\ \vdots \\ \Delta u_4 = \Delta u_5 \\ \vdots \\ \Delta v_1 \\ \Delta v_2 \\ \hdashline F_3
\end{array}\right\}
= \left\{\begin{array}{c} F_{n+1} \\ \hdashline 0 \end{array}\right\} + \left\{\begin{array}{c} B_{et} \\ \hdashline \end{array}\right\}. \tag{2.2.84}
$$

F_3 is obtained by solving eq. (2.2.84).

Then, eq. (2.3.83) is rearranged as follows and incorporated into the total matrix.

$$\left[\begin{array}{cc|cccccc|cc}
B_{33}^{1+2+3} & 0 & -B_{31}^{1} & -B_{32}^{1} & -B_{32}^{2}-B_{31}^{3} & -B_{32}^{3} & 0 & 0 & -B_{33}^{1+2+3} & 0 \\
0 & B_{33}^{4+5} & 0 & 0 & 0 & -B_{31}^{4} & -B_{32}^{4} & -B_{31}^{5} & 0 & -B_{33}^{4+5} \\
\hline
-B_{31}^{1} & 0 & & & & & & & B_{31}^{1} & 0 \\
-B_{32}^{1}-B_{31}^{2} & 0 & & & & & & & B_{32}^{1}+B_{31}^{2} & 0 \\
-B_{32}^{2}-B_{31}^{3} & 0 & & & & B_{6\times 6} & & & B_{32}^{2}+B_{31}^{3} & 0 \\
-B_{32}^{3} & -B_{31}^{4} & & & & & & & -B_{32}^{3} & B_{31}^{4} \\
0 & -B_{31}^{4}-B_{31}^{5} & & & & & & & 0 & B_{32}^{4}+B_{31}^{3} \\
0 & -B_{32}^{5} & & & & & & & 0 & B_{32}^{3} \\
\hline
-B_{33}^{1+2+3} & 0 & B_{31}^{1} & B_{32}^{1}+B_{31}^{2} & B_{32}^{2}+B_{31}^{3} & B_{32}^{3} & 0 & 0 & B_{33}^{1+2+3} & 0 \\
0 & -B_{33}^{4+5} & 0 & 0 & 0 & B_{31}^{4} & B_{32}^{4}+B_{31}^{5} & B_{32}^{5} & 0 & B_{33}^{4+5}
\end{array}\right] \times$$

$$\left\{\begin{array}{c}
\Delta u_{1,l}^{L} \\ \Delta u_{2,l}^{L} \\ \Delta u_{1,l} \\ \Delta u_{2,l} \\ \Delta u_{3,l} \\ \Delta u_{4,l}=\Delta u_{5,l} \\ \Delta u_{6,l} \\ \Delta u_{7,l} \\ \Delta u_{1,l}^{U} \\ \Delta u_{2,l}^{U}
\end{array}\right\}=\left\{\begin{array}{c}
F_{3,l} \\ -F_{3,l} \\ 0 \\ 0 \\ 0 \\ -F_{2,l}+F_{2,l}+F_{pca} \\ 0 \\ -F_{pcb} \\ -F_{3,l} \\ F_{3,l}
\end{array}\right\}+\left\{\begin{array}{c}
\\ \\ \\ \\ \\ B_{el,l} \\ \\ \\ \\ \\
\end{array}\right\}. \qquad (2.2.85)$$

l in eq. (2.2.85) is a segment number. Also, $B_{33}^{1+2+3}=B_{33}^{1}+B_{33}^{2}+B_{33}^{3}$ is used. This matrix is symmetric.

(2) Sliding state case

In the case of sliding, the equation below is given in place of eq. (2.2.84).

$$\left[\begin{array}{ccccccccc|c}
 & & & & B_{9\times 9} & & & & & 0 \\
 & & & & & & & & & \vdots \\
 & & & & & & & & & 0 \\
 & & & & & & & & & 1 \\
 & & & & & & & & & -1 \\
 & & & & & & & & & 0 \\
 & & & & & & & & & 0 \\
 & & & & & & & & & \mu \\
 & & & & & & & & & -\mu \\
\hline
0 & \cdots & 0 & 1 & -1 & 0 & \cdots & 0 & 0 & 0
\end{array}\right]\left\{\begin{array}{c}
\vdots \\ \vdots \\ \Delta u_4 \\ \Delta u_5 \\ \vdots \\ \vdots \\ \Delta v_1 \\ \Delta v_2 \\ \hline F_2
\end{array}\right\}=\left\{\begin{array}{c}
 \\ \\ F_{n+1} \\ \\ \\ \\ \\ \\ \hline 0
\end{array}\right\}+\left\{\begin{array}{c}
 \\ \\ B_{el} \\ \\ \\ \\ \\ \\ \hline 0
\end{array}\right\} \qquad (2.2.86)$$

where μ : friction coefficient.

F_2 is obtained by solving eq. (2.2.86). Then, using

$$F_3 = \mu F_2, \tag{2.2.87}$$

we incorporate eq. (2.2.85) into the total matrix.

The friction coefficient μ must be corrected with respect to the different frictional areas, because F_2 is affected by the area of the pellet side $2\pi r_o l_z$, and F_3 is affected by the area of the pellet cross section $\pi(r_o^2 - r_i^2)$. Namely, the following conversion is performed.

$$\mu = \frac{r_o^2 - r_i^2}{2 r_o l_z} \cdot \mu^* \tag{2.2.88}$$

Here,

r_i : pellet inner diameter

r_o : pellet outer diameter

l_z : length of the pellet in the axial direction

μ^* : friction coefficient (measured value)

Fitting parameter AMU
Friction coefficient μ is designated by AMU.
The default value of AMU is 0.4.

(3) Open gap state case

When gaps are open, no contact force is generated; therefore, contact forces in the radial and axial directions F_2 and F_3 in eq. (2.2.81) are set to be 0 and incorporated into the total matrix.

2.2.9 Creation of total matrix

When the number of axial segments of the pellet stack is assumed to be 3, the total matrix regarding the pellet stack is given by

$$\begin{bmatrix} B_{ee}^{1} & & \\ & B_{ee}^{2} & \\ & & B_{ee}^{3} \end{bmatrix} \begin{Bmatrix} \Delta u_{1,1}^{L} \\ \Delta u_{2,1}^{L} \\ \Delta u_{1} \\ \vdots \\ \Delta u_{1,1}^{U} + \Delta u_{1,2}^{L} \\ \Delta u_{2,1}^{L} + \Delta u_{1,2}^{L} \\ \Delta u_{2} \\ \vdots \\ \Delta u_{1,2}^{U} + \Delta u_{1,3}^{L} \\ \Delta u_{2,2}^{U} + \Delta u_{2,3}^{L} \\ \Delta u_{3} \\ \vdots \\ \Delta u_{1,3}^{U} \\ \Delta u_{2,3}^{U} \end{Bmatrix} = \begin{Bmatrix} F_{n+1} \end{Bmatrix} + \begin{Bmatrix} B_{ef,n+1} \end{Bmatrix}. \tag{2.2.89}$$

In order to avoid complexity in the later discussion, we express eq. (2.2.89) as follows through rearrangement of this equation, similar to the case of eqs. (2.2.81) and (2.2.82).

$$\left[B_{ee}^{T}\right] \{\Delta u\} = \{\Delta F\} \ . \tag{2.2.90}$$

2.2.10 Boundary conditions for upper plenum and lower plenum

The presence of the upper and the lower plenums gives a boundary condition for the mechanical analysis. Described below are how this boundary condition is reflected in the total matrix.

(1) Upper plenum

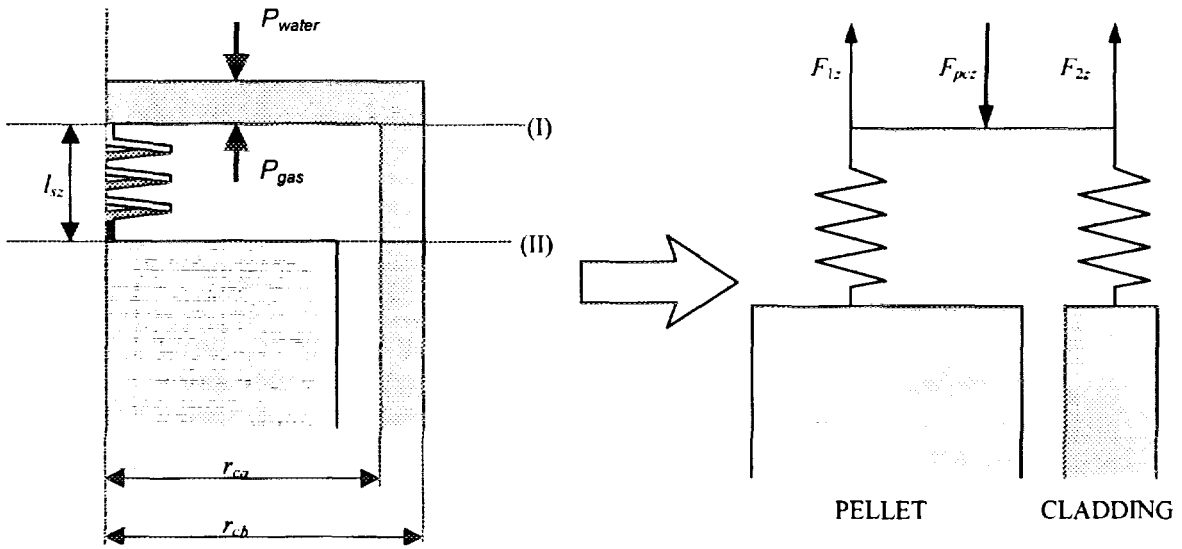

Fig. 2.35 Boundary conditions for upper plenum

When plenum pressure is represented as P_{gas}, coolant pressure as P_{water}, inner radius of cladding as N_{ca}, and outer radius of cladding as r_{cb}, the external force F_{pcz} on boundary plane (I) is given as

$$F_{pcz} = \pi r_{ca}^2 P_{gas} - \pi r_{cb}^2 P_{water} . \tag{2.2.91}$$

F_{pcz} on boundary plane (I) is equal to the sum of force F_{1z} given by the plenum spring and reaction force F_{2z} which is produced in the axial direction by the elasticity of the cladding surrounding the plenum. F_{pcz} is given by

$$F_{pcz} = -\left(F_{1z} + F_{2z}\right) . \tag{2.2.92}$$

Here, with the plenum spring constant assigned as k_s and the apparent spring constant of the cladding for the plenum part as k_c, F_{1z} and F_{2z} are given by

$$\left.\begin{aligned} F_{1z} &= -k_s\left(v_{sz} - v_{1,3}^u\right) + k_s\alpha_s l_{sz}^u\left(T_{n+1} - T_o\right) \\ F_{2z} &= -k_c\left(v_{sz} - v_{23}^u\right) + k_s\alpha_c l_{sz}^u\left(T_{n+1} - T_o\right) \end{aligned}\right\}, \tag{2.2.93}$$

where

v_{sz} : axial displacement at boundary plane (I)

$v^{u}_{1,3}$: axial displacement of pellet at boundary plane (II)

$v^{u}_{2,3}$: axial displacement of cladding at boundary plane (II)

α_s : thermal expansion coefficient of plenum spring

α_c : thermal expansion coefficient of cladding for the plenum part

l^{u}_{sz} : upper plenum length

T_{n+1} : plenum temperature at current time step ((n+1)th step)

T_0 : initial plenum temperature.

Fitting parameters XKSU, XKSL, AKSU and AKSL

Spring constant of upper plenum XKSU, spring constant of lower plenum XKSL, thermal expansion coefficient of upper plenum spring AKSU, and thermal expansion coefficient of lower plenum spring AKSL are designated by input values.

Default values are: XKSU=1500 (N/m), XKSL=2500 (N/m), and AKSU=AKSL=1.5 × 10^{-5} (1/K).

Next, eq. (2.2.93) is rearranged to express the increments as follows.

$$\left.\begin{aligned}\Delta F_{1z} &= -k_s\left(\Delta v_{sz} - \Delta v^{U}_{1,3}\right) + k_s\alpha_s l^{U}_{sz}\left(T_{n+1} - T_n\right)\\ \Delta F_{2z} &= -k_c\left(\Delta v_{sz} - \Delta v^{U}_{2,3}\right) + k_c\alpha_s l^{U}_{sz}\left(T_{n+1} - T_n\right)\end{aligned}\right\} \tag{2.2.94}$$

Then eq. (2.2.94) is rewritten as

$$\left.\begin{aligned}\begin{Bmatrix}-\Delta F_{1z}\\ \Delta F_{1z}\end{Bmatrix} &= \begin{Bmatrix}-k_s\alpha_s l^{U}_{sz}\left(T_{n+1} - T_n\right)\\ k_s\alpha_s l^{U}_{sz}\left(T_{n+1} - T_n\right)\end{Bmatrix} + \begin{bmatrix}k_s & -k_s\\ -k_s & k_s\end{bmatrix}\begin{Bmatrix}\Delta v_{sz}\\ \Delta v^{U}_{1,3}\end{Bmatrix}\\ \begin{Bmatrix}-\Delta F_{2z}\\ \Delta F_{2z}\end{Bmatrix} &= \begin{Bmatrix}-k_c\alpha_c l^{U}_{sz}\left(T_{n+1} - T_n\right)\\ k_c\alpha_c l^{U}_{sz}\left(T_{n+1} - T_n\right)\end{Bmatrix} + \begin{bmatrix}k_c & -k_c\\ -k_c & k_c\end{bmatrix}\begin{Bmatrix}\Delta v_{sz}\\ \Delta v^{U}_{2,3}\end{Bmatrix}\end{aligned}\right\}. \tag{2.2.95}$$

Rearranging eq. (2.2.95), we obtain

$$\begin{Bmatrix}\Delta F_{fcz}\\ \Delta F_{1z}\\ \Delta F_{2z}\end{Bmatrix} = \begin{Bmatrix}-\Delta F_{1z} - \Delta F_{2z}\\ \Delta F_{1z}\\ \Delta F_{2z}\end{Bmatrix} = \begin{Bmatrix}-\left(k_s\alpha_s + k_c\alpha_c\right)l^{U}_{sz}\left(T_{n+1} - T_n\right)\\ k_s\alpha_s l^{U}_{sz}\left(T_{n+1} - T_n\right)\\ k_c\alpha_c l^{U}_{sz}\left(T_{n+1} - T_n\right)\end{Bmatrix} + \begin{bmatrix}k_s & +k_c & -k_s & -k_c\\ & -k_s & k_s & 0\\ & -k_c & k_c & k_c\end{bmatrix}\begin{Bmatrix}\Delta v_{sz}\\ \Delta v^{U}_{1,3}\\ \Delta v^{U}_{2,3}\end{Bmatrix} \tag{2.2.96}$$

Equation (2.2.96) is substituted into eq. (2.2.90). Here, it is not necessary to consider ΔF_{1z} and $\Delta F_{2,z}$, since these can be given as reaction forces from the lower segment when the total matrix is solved. Therefore, eq. (2.2.90) is the total matrix to be solved and can be expressed as

$$\left[\begin{array}{cccc|c} & & & & 0 \\ & B_{ce}^{T} & & & \vdots \\ & & & & 0 \\ \hline & & B_{ce}+k_s & B_{ce}-k_s & \\ & & B_{ce} & B_{ce}+k_c-k_c & \\ \hline 0 \cdots \cdots 0 & & -k_s & -k_c \quad k_s+k_c & \end{array}\right]\left\{\begin{array}{c} \vdots \\ \Delta U \\ \vdots \\ \hline \Delta v_{1,3}^{U} \\ \Delta v_{2,3}^{U} \\ \Delta v_{3z} \end{array}\right\}=\left\{\begin{array}{c} \vdots \\ \Delta F \\ \vdots \\ \hline \Delta F_{1z}-k_s\alpha_s l_{3z}\left(T_{n+1}-T_n\right) \\ \Delta F_{2z}-k_c\alpha_c l_{3z}\left(T_{n+1}-T_n\right) \\ \Delta F_{pz}+\left(k_s\alpha_s+k_c\alpha_c\right) l_{3z}\left(T_{n+1}-T_n\right) \end{array}\right\}. \tag{2.2.97}$$

(2) Lower plenum

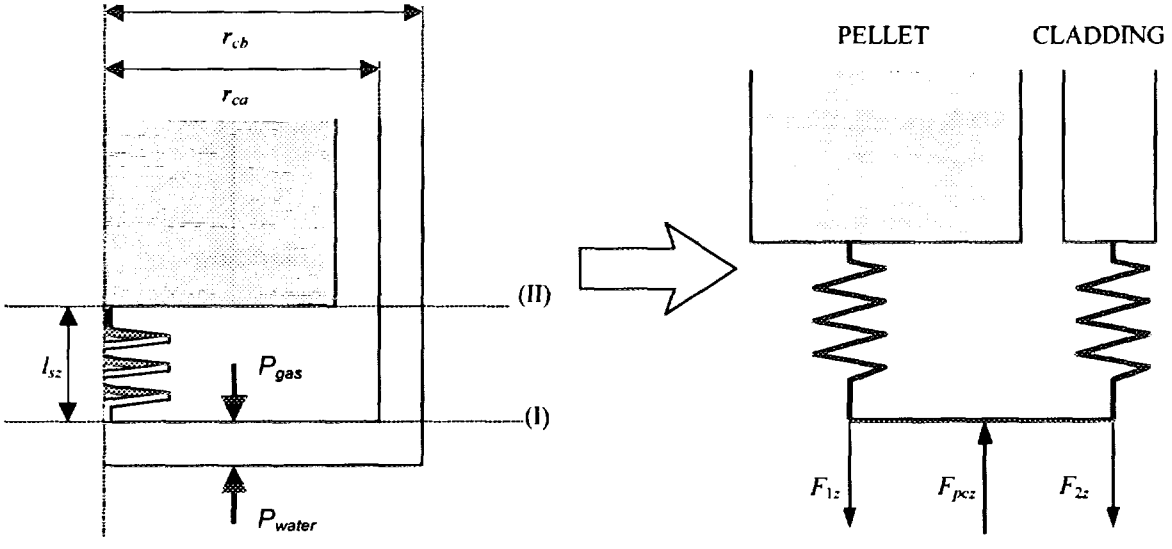

Fig. 2.36 Boundary conditions for lower plenum.

When no lower plenum exists, boundary conditions are satisfied if the degree of freedom and rows and columns in the matrix which correspond to the lower plenum are omitted, because $\Delta v_{1,1}^{L}=\Delta v_{2,1}^{L}=0$ holds in eq. (2.2.89).

When a lower plenum exists, since $\Delta v_{1,1}^{L}\neq 0$, and $\Delta v_{2,1}^{L}\neq 0$,

$$\left.\begin{aligned} \Delta F_{1z} &= -k_s v_{1,1}^{L}+k_s\alpha_s l_{sz}^{L}\left(T_{n+1}-T_n\right) \\ \Delta F_{2z} &= -k_c v_{2,1}^{L}+k_c\alpha_c l_{sz}^{L}\left(T_{n+1}-T_n\right) \end{aligned}\right\}. \tag{2.2.98}$$

Here,

l_{sz}^{L} : lower plenum length.

When eq. (2.2.98) is expressed in incremental form, we obtain

$$\left.\begin{aligned}\Delta F_{1z} &= -k_s \Delta v_{1,1}^{L} + k_s \alpha_s l_{sz}^{L}\left(T_{n+1} - T_n\right) \\ \Delta F_{2z} &= -k_c \Delta v_{2,1}^{L} + k_c \alpha_c l_{sz}^{L}\left(T_{n+1} - T_n\right)\end{aligned}\right\}. \tag{2.2.99}$$

Substituting eq. (2.2.99) into eq. (2.2.97), we obtain

$$\left[\begin{array}{cc|ccc|ccc}
B_{ee}+k_s & B_{ee} & 0 & \cdots & 0 & 0 & \cdots & 0 \\
B_{ee} & B_{ee}+k_c & 0 & \cdots & 0 & \vdots & & \vdots \\
\hline
0 & 0 & & & & \vdots & & \vdots \\
\vdots & \vdots & & B_{ee} & & \vdots & & \vdots \\
\vdots & \vdots & & & & 0 & \cdots & 0 \\
\hline
\vdots & \vdots & 0 & \cdots & 0 & B_{ee}+k_s & B_{ee} & -k_s \\
\vdots & \vdots & \vdots & & \vdots & B_{ee} & B_{ee}+k_c & -k_c \\
0 & 0 & 0 & \cdots & 0 & -k_s & -k_c & k_s+k_c
\end{array}\right]
\left\{\begin{array}{c}
\Delta v_{1,1}^{L} \\ \Delta v_{2,1}^{L} \\ \vdots \\ \Delta u \\ \vdots \\ \Delta v_{1,3}^{U} \\ \Delta v_{2,3}^{U} \\ \Delta v_{sz}
\end{array}\right\}
=
\left\{\begin{array}{c}
-\Delta F_{1z} + k_s \alpha_s l_{sz}^{L}\left(T_{n+1} - T_n\right) \\
-\Delta F_{2z} + k_c \alpha_c l_{sz}^{L}\left(T_{n+1} - T_n\right) \\
\hline
\vdots \\
\Delta F \\
\vdots \\
\hline
\Delta F_{1z} - k_s \alpha_s l_{sz}\left(T_{n+1} - T_n\right) \\
\Delta F_{2z} - k_c \alpha_c l_{sz}\left(T_{n+1} - T_n\right) \\
\Delta F_{pz} + \left(k_s \alpha_s + k_c \alpha_c\right) l_{sz}\left(T_{n+1} - T_n\right)
\end{array}\right\}. \tag{2.2.100}$$

Here, $-\Delta F_{1z}$ and $-\Delta F_{2,z}$ are given as reaction forces of segment 1.

Equation (2.2.100) is the total matrix (symmetrical matrix) to be solved.

2.2.11 Judgment conditions of contact between pellet and cladding

As judgment conditions of contact between pellet and cladding, three states, namely open gap, clogged gap and sliding states, are considered. The transition among the three states is shown in Fig. 2.37 and Table 2.1

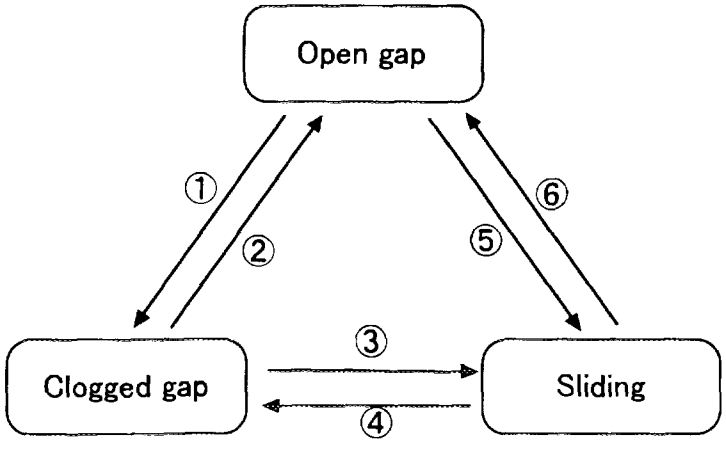

Fig. 2.37 Change in contact states. (Refer to Table 2.1 for numbers 1–6.)

Table 2.1 Changes and conditions of contact states.

Number	State change	Condition of state change and treatment
①	Open gap→ Clogged gap	When gap width changes from positive to negative, time-step control is performed and a state is judged to be a clogged gap state when the condition $\|F_3\| < \mu \|F_2\|$ is satisfied.
②	Clogged gap → Open gap	When contact force F_2 changes from negative to positive, a state is judged to be an open gap state. Time-step control is performed.
③	Clogged gap → Sliding	When a contact state changes under the condition $\|F_3\| \geq \mu \|F_2\|$, it is judged to be a sliding state. Time-step control is not performed.
④	Sliding → Clogged gap	When a contact state changes under the condition $\|F_3\| < \mu \|F_2\|$, it is judged to be a clogged gap state. Time-step control is not performed.
⑤	Sliding → Open gap	Same as in case ②.
⑥	Open gap → Sliding	When gap width changes from positive to negative, time-step control is performed, and when the condition $\|F_3\| \geq \mu \|F_2\|$ is satisfied, a state is judged to be a sliding state.

Here, F_2 : contact force between pellet and cladding in the radial direction
F_3 : contact force between pellet and cladding in the axial direction
μ : coefficient of friction between pellet and cladding.

(1) Judgment of clogged gap state/sliding state

① Clogged gap state condition

A state is judged to be a clogged gap state when the following conditions are satisfied: the displacement increment of the pellet is identical to that of the cladding and the axial force is smaller than the maximum static friction force determined from the contact force; namely,

$$\left.\begin{aligned} \Delta v_p &= \Delta v_c \\ |F_3| &< \mu |F_2| \end{aligned}\right\} \tag{2.2.101}$$

holds, where Δv_p is the axial displacement increment of pellet, Δv_c is the axial displacement increment of cladding, and μ is the friction coefficient corrected in terms of cross-sectional area, as described in section 2.2.8.

When a clogged gap state is assumed, $\Delta v_p = \Delta v_c$ is given as a boundary condition for judgment. Therefore, when $|F_3| < \mu |F_2|$ is not satisfied, the contact state is changed from the clogged gap state to the sliding state.

② Sliding state condition

In a sliding state, since the boundary condition

$$|F_3| = \mu |F_2| \qquad (2.2.102)$$

is given, the equation below cannot be used as a contact-state judgment condition from a sliding state to a clogged gap state.

$$F_3 < \mu F_2$$

Therefore, when a calculation shows a contradictory result in the direction of axial force and displacement increment even if an axial force exists, namely,

when $F_3 \times F_2 > 0$ (since $F_2 < 0$, $F_3 < 0$), $\Delta v_p < \Delta v_c$,

or

when $F_3 \times F_2 < 0$ (since $F_2 < 0$, $F_3 > 0$), $\Delta v_p > \Delta v_c$,

the contact state is changed from a sliding state to a clogged gap state.

Also, when

$$F_2 \times F_3 = 0,$$

the contact state is a clogged gap state. This is because $F_2 < 0$, and thus $F_3 = 0$.

(2) Force acting on a boundary surface

As shown in Fig. 2.38, the force which acts on a boundary surface $S_{i,j+1}$ is given by

$$\begin{aligned} S_{i,j+1} &= F_{3,U} + \left(F_{3,5} - F_{3,U}\right) + \left(F_{3,4} - F_{3,5}\right) \\ &\quad + \cdots + \left(F_{3,i} - F_{3,j+1}\right) \\ &= F_{3,i}. \end{aligned} \qquad (2.2.103)$$

This force is not affected by forces from another segment, $F_{3,j}(j \neq i)$. Therefore, judgment of clogged gap/sliding states in all axial segments can be performed simultaneously according to the judgment conditions described above.

This fact indicates that the axial force which acts on a segment always balances the contact force between pellet and cladding in the axial direction (=friction force), and that the magnitude of this axial force determines whether a sliding or clogged gap state exists under the contact condition.

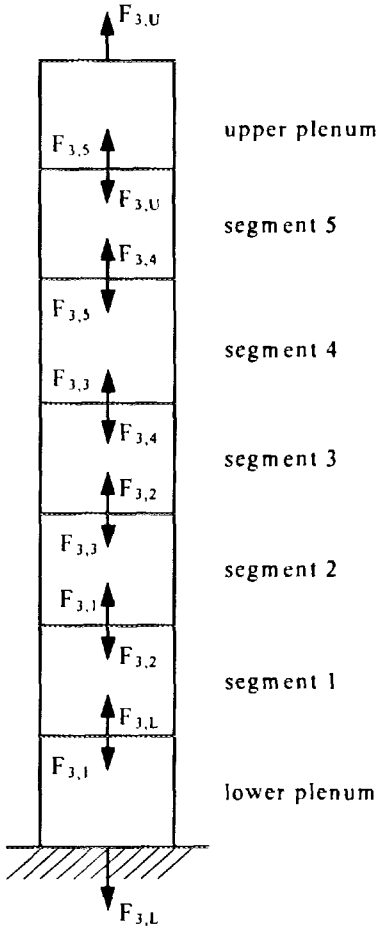

Fig. 2.38 Axial force acting on pellet.

Therefore, unless strong PCMI (pellet-clad mechanical interaction) is generated, axial force does not become large, because axial force is significantly mitigated by sliding when PCMI is weak.

(3) Time-step control

After the iteration calculation for assumption and judgment of clogged gap/sliding states described above is converged for all segments, if a contact state is changed (non-contact $\rightleftarrows$ contact), time-step control is performed and a state is changed at the time described below.

- Non-contact → contact: the time point when gap width becomes zero.
- Contact → non-contact: the time point when contact pressure becomes zero.

In these cases, all time-dependent variables are corrected to the values at the time of state change, by means of linear interpolation in terms of time. Then, the time-step width Δt_l (defined in Table 2.1) is changed, i.e., further divided, and the mechanical analysis calculations are performed under the new contact condition.

Namely, in the thermal analysis part, time step Δt_l is divided using the method described in section 2.1.6, and in the mechanical analysis part, time step Δt_l is divided by this time-step control. The time-step control is also applied in the local mechanical analysis.

Model parameter LCMAX

The maximum number of judgments on the state change within one time step is designated by LCMAX. The default value of LCMAX is 3.

2.3 Local Mechanical Behavior [Detailed Mechanical Analysis II]

In local mechanical analysis, axis-symmetric FEM is applied to half a pellet length. We call this part an **objective segment**. Figures 2.39(a) and (b) show a mesh division of the present FEM model. As an element, a rectangular 8-node iso-parametric element is used, and displacement in the element is approximated by a quadratic function of displacement of nodes.

Figure 2.39(a) illustrates half a pellet length of the objective segment which is divided into coaxial ring elements to be analyzed in axi-symmetrical coordinate.

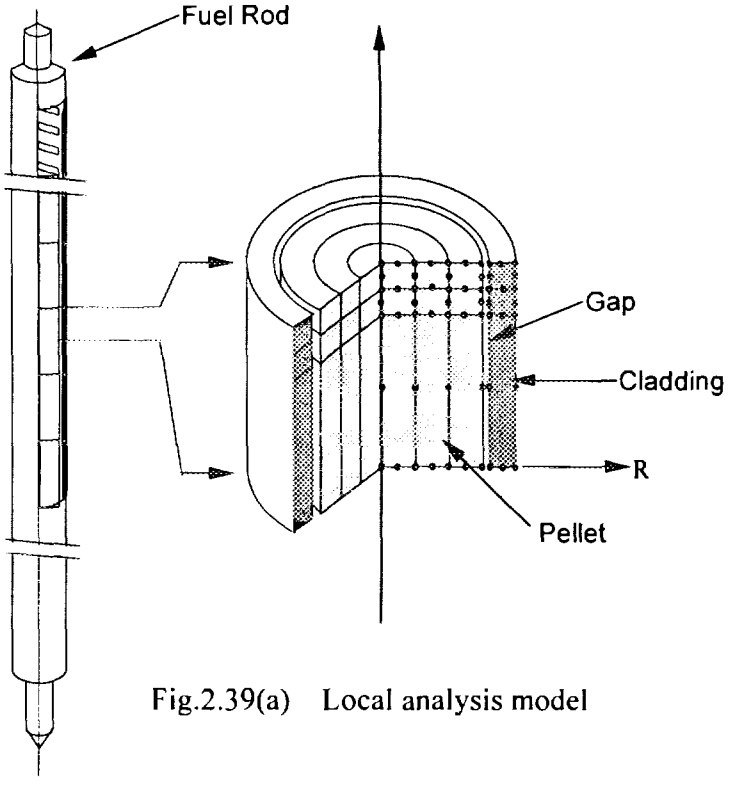

Fig.2.39(a) Local analysis model

Figure 2.39(b) shows in an accurate manner the elements and nodes of the objective segment. A pellet is divided to 5 radial rings, while cladding is dealt with as one element. Half a pellet length is divided to the axial parts with lengths of 1:3:6 ratio. Each element has 8 nodes. Nodes of pellet and cladding across the gap form a node-couple, which is explained later in section 2.3.3(2).

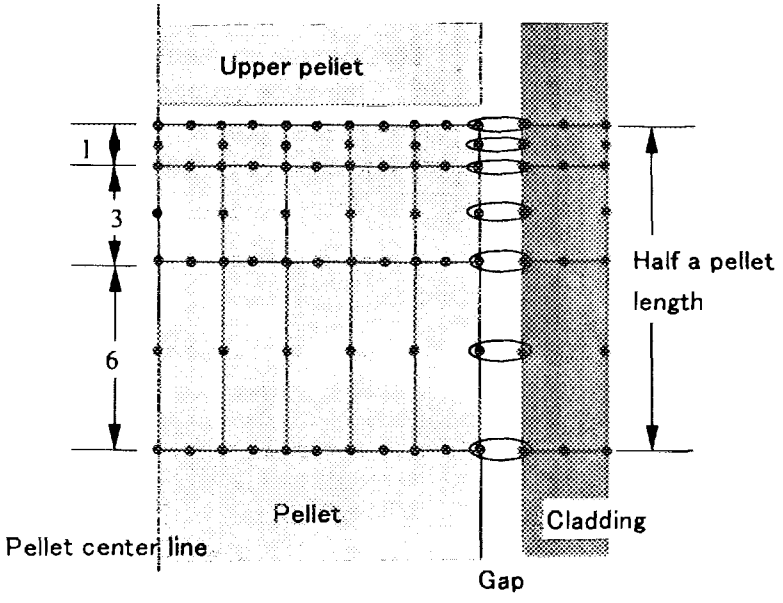

Fig.2.39 (b) Elements and node for half a pellet length

In this section, the strain component within an element is defined as

$$\{\varepsilon\} = \begin{Bmatrix} \varepsilon_r \\ \varepsilon_z \\ \varepsilon_\theta \\ \gamma_{rz} \end{Bmatrix} = \begin{Bmatrix} \dfrac{du}{dr} \\ \dfrac{dv}{dz} \\ \dfrac{u}{r} \\ \left(\dfrac{\partial v}{\partial r}\right) + \left(\dfrac{\partial u}{\partial z}\right) \end{Bmatrix}, \tag{2.3.1}$$

where ε_r, ε_z, ε_θ and γ_{rz} are strains in the radial, axial, circumferential and shearing (r, z) directions, respectively. The shearing component was not considered in the previous section; however, since one of the objectives here is stress evaluation at a ridge part of a pellet under bending deformation, the shearing component is taken into account in this section.

2.3.1 Basic equations

The equilibrium condition at time t_{n+1} is represented, based on the principle of virtual work, as

$$\int [B]^T \{\sigma_{n+1}\} dV - \{F_{n+1}\} = 0 . \tag{2.3.1}$$

Here,

$[B]^T$: transposed matrix of a strain-displacement matrix $[B]$

$\{\sigma_{n+1}\}$: stress vector at time t_{n+1}

$\{F_{n+1}\}$: node point loading vector at time t_{n+1}.

The strain-displacement matrix $[B]$ is assumed to be determined from a dimension prior to deformation. $[B]$ matrix is given by eq. (2.3.19), presented later.

The constitutive equation (stress-strain relationship equation) is given by

$$\{\sigma_{n+1}\} = [\overline{D}]\{\Delta\varepsilon^e_{n+1}\}, \tag{2.3.2}$$

where

$\{\Delta\sigma_{n+1}\}$: stress increment vector from time t_n to t_{n+1}

$\{\Delta\varepsilon^e_{n+1}\}$: elastic increment vector from time t_n to t_{n+1}

$$[D_{n+\theta}] = (1-\theta)[D_n] + \theta[D_{n+1}] \quad \left(\theta = \frac{1}{2}\right)$$

$[D_n]$: stress-strain matrix (stiffness) at time t_n.

If matrix [C] is defined as an inverse matrix of this D matrix, eq. (2.3.2) is transformed as

$$\{\Delta\varepsilon^e_{n+1}\} = [C_{n+\theta}]\{\Delta\sigma_{n+1}\}. \tag{2.3.3}$$

Matrix [C] in eq. (2.3.3) is given as

$$[C] = \frac{1}{E}\begin{bmatrix} 1 & -\nu & -\nu & 0 \\ -\nu & 1 & -\nu & 0 \\ -\nu & -\nu & 1 & 0 \\ 0 & 0 & 0 & 2(1+\nu) \end{bmatrix}, \tag{2.3.4}$$

where E is Young's modulus and ν is Poisson's ratio.

The elastic strain increment vector can be expressed as

$$\{\Delta\varepsilon^e_{n+1}\} = \{\Delta\varepsilon_{n+1}\} - \{\Delta\varepsilon^0_{n+1}\} - \{\Delta\varepsilon^p_{n+1}\} - \{\Delta\varepsilon^c_{n+1}\}, \tag{2.3.5}$$

where

$\{\Delta\varepsilon_{n+1}\}$: total strain increment vector
$\{\Delta\varepsilon^0_{n+1}\}$: initial strain increment vector
$\{\Delta\varepsilon^p_{n+1}\}$: plastic strain increment vector
$\{\Delta\varepsilon^c_{n+1}\}$: creep strain increment vector.

Strains by thermal expansion, densification, swelling and relocation are treated as initial strains. The strain-displacement relationship is expressed as

$$\{\Delta\varepsilon_{n+1}\} = [B](\{u_{n+1}\} - \{u_n\}), \tag{2.3.6}$$

where

$\{u_n\}$: node point displacement vector at time t_{n+1}.

The following equation is obtained from eqs. (2.3.2)～(2.3.6.).

$$[\overline{C}_{n+\theta}](\{\sigma_{n+1}\} - \{\sigma_n\}) - [B](\{u_{n+1}\} - \{u_n\}) + \{\Delta\varepsilon^0_{n+1}\} + \{\Delta\varepsilon^p_{n+1}\} + \{\Delta\varepsilon^c_{n+1}\} = 0 \tag{2.3.7}$$

Here,

$$[\overline{C}_{n+\theta}] = ([C_{n+1}] + [C_n])/2 \ :$$

$$[C_n] : [D_n]^{-1}.$$

Equations (2.3.1) and (2.3.7) are the basic equations for obtaining unknown values $\{\sigma_{n+1}\}$ and $\{u_{n+1}\}$.

Equation (2.3.7) can be solved by iteration using the Newton-Raphson method, since $\{\Delta\varepsilon^p_{n+1}\}$ and $\{\Delta\varepsilon^c_{n+1}\}$ are functions of unknown value $\{\sigma_{n+1}\}$ (refer to sections 2.2.4 and 2.2.5 for details). Pellet cracks, creep and plasticity are treated similarly to the case of entire length mechanical analysis.

At the (n+1)th stage (time-step) calculation, when the ith iteration is completed and the (i+1)th iteration is being performed, eq. (2.3.7) is expressed as

$$[\overline{C}_{n+\theta}]\left(\{\sigma^i_{n+1}\}+\{d\sigma^{i+1}_{n+1}\}-\{\sigma_n\}\right)-[B]\left(\{u^i_{n+1}\}+\{du^{i+1}_{n+1}\}-\{u_n\}\right)+\{\Delta\varepsilon^0_{n+1}\}+\{\Delta\varepsilon^p_{n+1}\}+\{\Delta\varepsilon^c_{n+1}\}=0. \tag{2.3.8}$$

Here,

$$\{d\sigma^{i+1}_{n+1}\}=\{\sigma^{i+1}_{n+1}\}-\{\sigma^i_{n+1}\} \tag{2.3.9}$$

$$\{du^{i+1}_{n+1}\}=\{u^{i+1}_{n+1}\}-\{u^i_{n+1}\}. \tag{2.3.10}$$

The equilibrium condition of eq. (2.3.1) is given by substituting eq.(2.3.9) into eq.(2.3.1) as

$$\int[B]^T\{\sigma^i_{n+1}\}dV+\int[B]^T\{d\sigma^{i+1}_{n+1}\}dV=\{F_{n+1}\}. \tag{2.3.11}$$

2.3.2 Stiffness equation

The formulation method of the stiffness equation is the same for the local mechanical analysis and the mechanical analysis over the entire-length of the fuel rod. Therefore, by substituting eq. (2.2.60) which was obtained in the entire-length mechanical analysis part into the equilibrium condition equation (2.3.7), we obtain the equilibrium condition at the (i+1)th iteration.

Note: Equation (2.2.65) is to be substituted into eq. (2.3.11). In formulation of eqs. (2.2.66) to (2.2.69) which should be incorporated in eq. (2.2.65), strain components are taken into account. Therefore, the yielding function h (=equivalent stress $\bar{\sigma}$) shown by eq. (2.2.54) is modified as follows to be expressed in its original form.

$$h=\bar{\sigma}=\left[\frac{3}{2(F+G+H)}\left\{H(\sigma_r-\sigma_z)^2+F(\sigma_z-\sigma_\theta)^2+G(\sigma_\theta-\sigma_r)^2+2N\tau^2_{rz}\right\}+3\alpha(\sigma_r+\sigma_z+\sigma_\theta)^2\right]^{\frac{1}{2}}$$

That is,

$$\begin{aligned}
&\int[B]^T\left\{\sigma^i_{n+1}\right\}dV + \int[B]^T\left[\hat{D}^{P,i}_{n+\theta}\right][B]\left\{du^{i+1}_{n+1}\right\}dV \\
&\quad - \int[B]^T\left[\hat{D}^{P,i}_{n+\theta}\right]\left[\overline{C}^i_{i+\theta}\right]\left(\left\{\sigma^i_{n+1}\right\} - \left\{\sigma_n\right\}\right)dV \\
&\quad - \int[B]^T\left[\hat{D}^{P,i}_{n+\theta}\right]\left(\left\{\Delta\varepsilon^{0i}_{n+1}\right\} - \left\{\Delta\varepsilon^{c,i}_{n+1}\right\}\right)dV \\
&\quad + \int[B]^T\left(\left\{S^i_{n+1}\right\}\Delta T_{n+1} - \left\{Z_1\right\} - \left\{Z_2\right\}\right)dV = \left\{F_{n+1}\right\}
\end{aligned} \tag{2.3.12}$$

is obtained, where

$$\left[\tilde{C}\right] = \begin{bmatrix} \frac{1}{E_r} & -\frac{\nu}{E} & -\frac{1}{E} & 0 \\ -\frac{\nu}{E} & \frac{1}{E_z} & -\frac{\nu}{E} & 0 \\ -\frac{\nu}{E} & -\frac{\nu}{E} & \frac{1}{E_\theta} & 0 \\ 0 & 0 & 0 & \frac{4(1+\nu)}{E_r + E_z} \end{bmatrix}. \tag{2.3.13}$$

Equation (2.3.13) is rearranged as follows.

$$\left[K^i_{n+\theta}\right]\left\{\Delta u^{i+1}_{n+1}\right\} = \left\{\Delta\hat{F}^i_{n+1}\right\} \tag{2.3.14}$$

This is the stiffness equation for elements.

Here,

$$\left[K^i_{n+\theta}\right] = \int[B]^T\left[\hat{D}^{P,i}_{n+\theta}\right][B]dV \tag{2.3.15}$$

$$\begin{aligned}
\left\{\Delta\hat{F}^i_{n+1}\right\} &= \left\{F_{n+1}\right\} - \int[B]^T\left\{\sigma^i_{n+1}\right\}dV \\
&\quad - \int[B]^T\left[\hat{D}^{P,i}_{n+\theta}\right]\left\{\left[\overline{C}^i_{i+\theta}\right]\left(\left\{\sigma^i_{n+1}\right\} - \left\{\sigma_n\right\}\right) + \left\{\Delta\varepsilon^{0i}_{n+1}\right\} - \left\{\Delta\varepsilon^{c,i}_{n+1}\right\}\right\}dV \\
&\quad - \int[B]^T\left(\left\{S^i_{n+1}\right\}\Delta T_{n+1} - \left\{Z_1\right\} - \left\{Z_2\right\}\right)dV
\end{aligned} \tag{2.3.16}$$

hold and represent stiffness matrix and loading vector, respectively.

Assuming axis-symmetry in deformation and performing the integration of θ coordinates in the circumferential direction in eqs. (2.3.15) and (2.3.16), we obtain

$$\left[K^i_{n+\theta}\right] = 2\pi\iint[B]^T\left[\hat{D}^{P,i}_{n+\theta}\right][B]rdrdz \tag{2.3.17}$$

$$\begin{aligned}\left\{\Delta\hat{F}^{i}_{n+1}\right\} &= \left\{F_{n+1}\right\} - 2\pi\iint[B]^{T}\left\{\sigma^{i}_{n+1}\right\}rdrdz \\ &- 2\pi\iint[B]^{T}\left[\hat{D}^{P,i}_{n+\theta}\right]\left\{\left[\overline{C}^{i}_{i+\theta}\right]\left(\left\{\sigma^{i}_{n+1}\right\} - \left\{\sigma_{n}\right\}\right) + \left\{\Delta\varepsilon^{0i}_{n+1}\right\} - \left\{\Delta\varepsilon^{c,i}_{n+1}\right\}\right\}rdrdz \\ &- 2\pi\iint[B]^{T}\left(\left\{S^{i}_{n+1}\right\}\Delta T_{n+1} - \left\{Z_{1}\right\} - \left\{Z_{2}\right\}\right)rdrdz.\end{aligned} \tag{2.3.18}$$

On the right-hand side of eq. (2.3.18), the first term is the non-equilibrium residue, the second term is an apparent load due to stress and initial strain, and the third term is a compensation term for yield stress change.

The stiffness equation for one element is shown below.

Displacement of an arbitrary point of an element in the axial and circumferential directions {u,v} and displacement at 8 nodes $\{u^1,v^1,u^2,v^2...,u^8,v^8\}$ are related as follows.

$$\begin{Bmatrix} u \\ v \end{Bmatrix} = [N]\begin{Bmatrix} u^1 \\ v^1 \\ u^2 \\ v^2 \\ \vdots \\ u^8 \\ v^8 \end{Bmatrix} \tag{2.3.19}$$

Here, [N] is called a form function, which is a matrix with the following shape.

$$[N] = [N_1 I, N_2 I, N_3 I, \cdots, N_8 I] \tag{2.3.20}$$

Using a local coordinate system shown in Fig. 2.40 (given later), N_i is expressed as

$$\left.\begin{aligned} N_1 &= (1-\xi)(1-\eta)(-\xi-\eta-1)/4 \\ N_2 &= (1+\xi)(1-\eta)(+\xi-\eta-1)/4 \\ N_3 &= (1+\xi)(1-\eta)(+\xi-\eta-1)/4 \\ N_4 &= (1-\xi)(1+\eta)(-\xi+\eta-1)/4 \\ N_5 &= (1+\xi)(1-\xi)(1-\eta)/2 \\ N_6 &= (1+\xi)(1+\eta)(1-\eta)/2 \\ N_7 &= (1-\xi)(1+\eta)(1-\eta)/2 \\ N_8 &= (1-\xi)(1+\eta)(1-\eta)/2 \end{aligned}\right\}. \tag{2.3.21}$$

Strain in the element of the axis-symmetrical problem is given by the following equation, which includes shearing components, different from the equation in the Detailed Mechanical Analysis I.

$$\{\varepsilon\} = \begin{Bmatrix} \varepsilon_r \\ \varepsilon_z \\ \varepsilon_\theta \\ \varepsilon_{rz} \end{Bmatrix} = \begin{Bmatrix} \partial V/\partial r \\ \partial W/\partial z \\ v/r \\ \partial V/\partial z + \partial W/\partial r \end{Bmatrix} = [B]\{u\}. \tag{2.3.22}$$

Therefore, matrix [B] is given by

$$[B] = [\mathbf{B}_1, \mathbf{B}_2, \mathbf{B}_3, \cdots, \mathbf{B}_8]. \tag{2.3.23}$$

Here, submatrix $\mathbf{B}_i$ is given by

$$\mathbf{B}_i = \begin{pmatrix} \dfrac{\partial N_i}{\partial r} & 0 \\ 0 & \dfrac{\partial N_i}{\partial z} \\ \dfrac{N_i}{r} & 0 \\ \dfrac{\partial N_i}{\partial z} & \dfrac{\partial N_i}{\partial r} \end{pmatrix}. \tag{2.3.24}$$

In eq. (2.3.21), N_i is defined using a local coordinate system. For representation of matrix [B] in eq. (2.3.22) in concrete form, the following coordinate transformation is performed.

The relationship between a local coordinate system and a cylindrical coordinate system r,z is given by

$$\begin{Bmatrix} \dfrac{\partial N_i}{\partial \xi} \\ \dfrac{\partial N_i}{\partial \eta} \end{Bmatrix} = \begin{pmatrix} \dfrac{\partial r}{\partial \xi} & \dfrac{\partial z}{\partial \xi} \\ \dfrac{\partial r}{\partial \eta} & \dfrac{\partial z}{\partial \eta} \end{pmatrix} \begin{Bmatrix} \dfrac{\partial N_i}{\partial r} \\ \dfrac{\partial N_i}{\partial z} \end{Bmatrix} = [\mathbf{J}] \begin{Bmatrix} \dfrac{\partial N_i}{\partial r} \\ \dfrac{\partial N_i}{\partial z} \end{Bmatrix} \tag{2.3.25}$$

or

$$\begin{Bmatrix} \dfrac{\partial N_i}{\partial r} \\ \dfrac{\partial N_i}{\partial z} \end{Bmatrix} = [\mathbf{J}]^{-1} \begin{Bmatrix} \dfrac{\partial N_i}{\partial \xi} \\ \dfrac{\partial N_i}{\partial \eta} \end{Bmatrix}. \tag{2.3.26}$$

Here, [J] is a Jacobian matrix. The location in an element (r,z) is represented using a nodal coordinate system (r_i, z_i, i=1～8) as

$$\left.\begin{aligned} r &= \sum_{i=1}^{8} N_i r_i \\ z &= \sum_{i=1}^{8} N_i z_i \end{aligned}\right\}.$$

Using this relationship, the Jacobian matrix [**J**] is expressed as

$$[\mathbf{J}] = \begin{pmatrix} \sum_{i=1}^{8} \frac{\partial N_i}{\partial \xi} r_i & \sum_{i=1}^{8} \frac{\partial N_i}{\partial \xi} z_i \\ \sum_{i=1}^{8} \frac{\partial N_i}{\partial \eta} r_i & \sum_{i=1}^{8} \frac{\partial N_i}{\partial \eta} z_i \end{pmatrix}. \tag{2.3.27}$$

Therefore, $[\mathbf{J}]^{-1}$ is given by

$$[\mathbf{J}]^{-1} = \frac{1}{\det[\mathbf{J}]} \begin{pmatrix} \sum_{i=1}^{8} \frac{\partial N_i}{\partial \eta} z_i & -\sum_{i=1}^{8} \frac{\partial N_i}{\partial \xi} z_i \\ -\sum_{i=1}^{8} \frac{\partial N_i}{\partial \eta} r_i & \sum_{i=1}^{8} \frac{\partial N_i}{\partial \xi} r_i \end{pmatrix}. \tag{2.3.28}$$

Here,

$$\det[\mathbf{J}] = \left(\sum_{i=1}^{8} \frac{\partial N_i}{\partial \xi} r_i\right)\left(\sum_{i=1}^{8} \frac{\partial N_i}{\partial \eta} z_i\right) - \left(\sum_{i=1}^{8} \frac{\partial N_i}{\partial \eta} r_i\right)\left(\sum_{i=1}^{8} \frac{\partial N_i}{\partial \xi} z_i\right). \tag{2.3.29}$$

Components in eq. (2.3.24) are transformed into a local coordinate system using the above relationships, and we obtain

$$\left.\begin{aligned} \frac{\partial N_i}{\partial r} &= \frac{1}{\det[\mathbf{J}]}\left(\left(\sum_{j=1}^{8} \frac{\partial N_j}{\partial \eta} z_j\right)\frac{\partial N_i}{\partial \xi} - \left(\sum_{j=1}^{8} \frac{\partial N_j}{\partial \xi} z_j\right)\frac{\partial N_i}{\partial \eta}\right) \\ \frac{\partial N_i}{\partial z} &= \frac{1}{\det[\mathbf{J}]}\left(\left(\sum_{j=1}^{8} \frac{\partial N_j}{\partial \xi} r_j\right)\frac{\partial N_i}{\partial \eta} - \left(\sum_{j=1}^{8} \frac{\partial N_j}{\partial \eta} r_j\right)\frac{\partial N_i}{\partial \xi}\right) \\ \frac{N_i}{r} &= \frac{N_i}{\sum_{j=1}^{8} N_i r_i} \end{aligned}\right\}. \tag{2.3.30}$$

drdz is transformed by the equation

$$drdz = \det[\mathbf{J}] d\xi d\eta. \tag{2.3.31}$$

Using the above transformation equation, we express eqs. (2.3.17) and (2.3.18) using a local coordinate system as follows.

$$\left[K^{i}_{n+\theta}\right] = 2\pi \int_{-1}^{1}\int_{-1}^{1}[B]^{T}\left[\hat{D}^{P,i}_{n+\theta}\right][B]\left(\sum_{j=1}^{8} N_j r_j\right)\det[\mathbf{J}]d\xi d\eta \tag{2.3.32}$$

$$\begin{aligned}\left\{\Delta\hat{F}^{i}_{n+1}\right\} &= \left\{F_{n+1}\right\} - 2\pi\int_{-1}^{1}\int_{-1}^{1}[B]^{T}\left\{\sigma^{i}_{n+1}\right\}d\xi d\eta \\ &- 2\pi\int_{-1}^{1}\int_{-1}^{1}[B]^{T}\left[\hat{D}^{P,i}_{n+\theta}\right]\left\{\left[\overline{C}^{i}_{i+\theta}\right]\left(\left\{\sigma^{i}_{n+1}\right\} - \left\{\sigma_{n}\right\}\right) + \left\{\Delta\varepsilon^{0i}_{n+1}\right\} - \left\{\Delta\varepsilon^{c,i}_{n+1}\right\}\right\}d\xi d\eta \\ &- 2\pi\int_{-1}^{1}\int_{-1}^{1}[B]^{T}\left(\left\{S^{i}_{n+1}\right\}\Delta T_{n+1} - \left\{Z_1\right\} - \left\{Z_2\right\}\right)d\xi d\eta\end{aligned} \tag{2.3.33}$$

In FEMAXI-IV, this integration is approximated by a Gaussian integration as

$$\int_{-1}^{1}\int_{-1}^{1} f(\xi,\eta)d\xi d\eta = \sum_{i=1}^{n}\sum_{j=1}^{m} H_i H_j f(\xi_i,\eta_j). \tag{2.3.34}$$

In the case of rectangular 8-node elements, the number of integration points is known to be sufficient with $n = m = 2$. In this case, since $H_i = H_j = 1$, the following equation is used.

$$\int_{-1}^{1}\int_{-1}^{1} f(\xi,\eta)d\xi d\eta = \sum_{i=1}^{2}\sum_{j=1}^{2} f(\xi_i,\eta_j) \tag{2.3.35}$$

Here,

n : number of integration points in the ξ direction
m : number of integration points in the η direction
ξ_I : coordinates of integration point in the ξ direction
η_j : coordinates of integration point in the η direction
H_i, H_j : weighted coefficients.

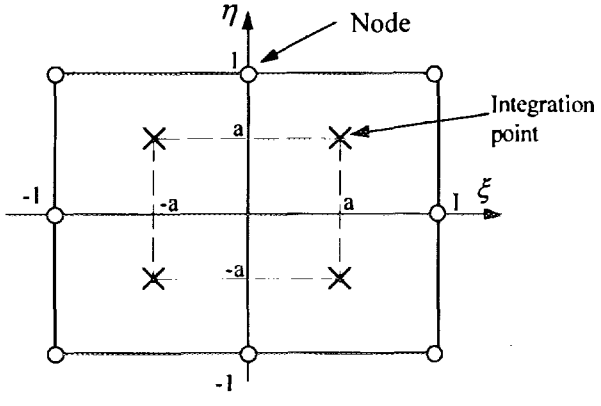

Fig. 2.40 Integration points for rectangular 8-node element.

The number of integration points is 4, the coordinates of each point are (a,a), (a,−a), (−a,a) and (−a,−a) as shown in Fig. 2.40, and a=0.5773502691*. (*Note: the Gauss's integral

formula for 2-point approximation $= \int_{-1}^{1} f(x)dx \cong \left(f(a) + f(-a)\right)$

By calculation of the stress vector, strain vector and compensation term for each of the 4 integration points, the integral terms in eqs. (2.3.32) and (2.3.33) can be obtained.

2.3.3 Boundary conditions

(1) Geometric modeling and boundary conditions

The finite element model (geometric model) for mechanical analysis is applied to half the pellet length, as shown in Fig. 2.41. This model has a total of 8 boundaries: 4 on the pellet side ((1) – (4)) and 4 on the cladding side ((5) – (8)). Boundary conditions are determined from symmetry of deformation, coolant pressure, gas pressure and contact state.

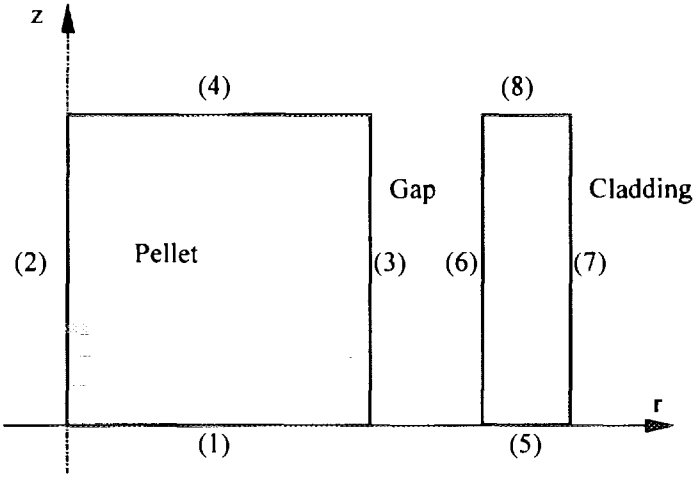

Fig. 2.41 Boundaries of the geometric model

The loading vector in eq. (2.3.1) is expressed as the total load which acts on nodes located on the 8 boundaries, as follows.

$$\left\{F_{n+1}\right\} = \left\{F_{n+1}^{(1)}\right\} + \left\{F_{n+1}^{(2)}\right\} + \left\{F_{n+1}^{(3)}\right\} + \left\{F_{n+1}^{(4)}\right\} + \left\{F_{n+1}^{(5)}\right\} + \left\{F_{n+1}^{(6)}\right\} + \left\{F_{n+1}^{(7)}\right\} + \left\{F_{n+1}^{(8)}\right\} \qquad (2.3.36)$$

Here, $\left\{F_{n+1}^{(i)}\right\}$ is the vector of loading which acts on the node at boundary (i).

Plane symmetry is assumed on boundaries (1) and (5), and nodes on these boundaries do not deform in the axial direction; that is,

$$\left\{\Delta v^{(1)}\right\} = 0 \qquad (2.3.37)$$

$$\left\{\Delta v^{(5)}\right\} = 0 \qquad (2.3.38)$$

is assumed. Here, $\left\{\Delta v^{(1)}\right\}$ and $\left\{\Delta v^{(5)}\right\}$ are the deformation increment vectors of nodes on

boundaries (1) and (5), in the axial direction, respectively. The constraint force generated at boundary (1) due to the constraint condition of eq. (2.3.37) is $\left\{F_{n+1}^{(1)}\right\}$, and the constraint force generated at boundary (5) due to the condition of eq. (2.3.38) is $\left\{F_{n+1}^{(5)}\right\}$.

At boundary (2), in the case of a solid pellet, nodes located on the boundary are not displaced in the radial direction since axis-symmetry is assumed for deformation. That is,

$$\left\{\Delta u^{(2)}\right\} = 0 \tag{2.3.39}$$

is assumed. Here, $\left\{\Delta u^{(2)}\right\}$ is the radial displacement increment vector for the node located on boundary (2).

The constraint force generated at boundary (2) (rotationally symmetric axis) by the condition of eq. (2.3.39) is $\left\{F_{n+1}^{(2)}\right\}$. Here, in the case of a hollow pellet, $\left\{F_{n+1}^{(2)}\right\} = 0$ holds since radial displacement is not restricted.

The surface force given by coolant pressure acts on boundary (7). $\left\{F_{n+1}^{(7)}\right\}$ represents the vector of equivalent node point loading due to this action.

At boundary (3), contact force exists due to the interaction (PCI) of boundaries (3) and (6). Gas pressure inside the fuel rod also acts on boundary (3); however, this is not taken into consideration since it is canceled by gas pressure present in a crack gap inside the pellet. $\left\{F_{n+1}^{(3)}\right\}$ is a vector of contact force generated by the interaction of boundary (3) with the pellet (boundary (6)).

At boundary (6), actions of contact force produced by PCI and gas pressure are considered. $\left\{F_{n+1}^{(6)}\right\}$ represents the sum of the contact force vector and the vector of equivalent node point loading by gas pressure.

At boundary (8), the number of degrees of freedom in the axial direction of a node group on the boundary is set as 1 based on the assumption of symmetry of deformation.

$$\left\{\Delta v^{(8)}\right\} = \Delta\bar{v}^{(8)} \tag{2.3.40}$$

Here, $\Delta\bar{v}^{(8)}$ is the axial displacement increment of nodes on boundary (8). At boundary (8), in addition to the restraint force generated from the condition of eq. (2.3.71), such loads as axial tensile load produced by the PCI in an upper region of a fuel rod, and axial loads given by gas pressure and coolant pressure are considered . The axial tensile load due to PCI in the upper region of the fuel rod which acts on boundary (8) is determined in an empirical manner.

This will be explained later.

At boundary (4), the above-described loads in the axial direction which is determined empirically acts as a compressive force. The contact force distribution which can be obtained by solving the pellet/pellet contact problem on the assumption of plane symmetry under this axial load is the load acting on the boundary.

As described above, the kinds of load which act on the 8 boundaries are of the following 6 types: reaction due to constraint of displacement, equivalent nodal force due to coolant pressure, equivalent nodal force due to gas pressure, pellet/cladding contact force, axial tensile load, and pellet/pellet contact force balanced with the axial tensile load.

For clarity of expression, these forces are represented by subscripts R, W, G, PC, AX, and PP, respectively, and eq. (2.3.36) is expressed as

$$\begin{aligned}\left\{F_{n+1}\right\} = &\left\{F_{n+1}^{(1),R}\right\} + \left\{F_{n+1}^{(2),R}\right\} + \left\{F_{n+1}^{(3),PC}\right\} + \left\{F_{n+1}^{(4),PP}\right\} + \left\{F_{n+1}^{(5),R}\right\} + \left\{F_{n+1}^{(6),PC}\right\} \\ &+ \left\{F_{n+1}^{(6),G}\right\} + \left\{F_{n+1}^{(7),W}\right\} + \left\{F_{n+1}^{(8),R}\right\} + \left\{F_{n+1}^{(8),AX}\right\} + \left\{F_{n+1}^{(8),W}\right\} + \left\{F_{n+1}^{(8),G}\right\}.\end{aligned} \tag{2.3.41}$$

These forces are classified into three types according to the method of treatment of forces as

$$\left\{F_{n+1}\right\} = \left\{F'_{n+1}\right\} + \left\{F''_{n+1}\right\} + \left\{F'''_{n+1}\right\}, \tag{2.3.42}$$

where

$$\left\{F'_{n+1}\right\} = \left\{F_{n+1}^{(6),G}\right\} + \left\{F_{n+1}^{(7),W}\right\} + \left\{F_{n+1}^{(8),W}\right\} + \left\{F_{n+1}^{(8),G}\right\} \tag{2.3.43}$$

$$\left\{F''_{n+1}\right\} = \left\{F_{n+1}^{(1),R}\right\} + \left\{F_{n+1}^{(2),R}\right\} + \left\{F_{n+1}^{(5),R}\right\} + \left\{F_{n+1}^{(8),R}\right\} \tag{2.3.44}$$

$$\left\{F'''_{n+1}\right\} = \left\{F_{n+1}^{(3),PC}\right\} + \left\{F_{n+1}^{(4),PP}\right\} + \left\{F_{n+1}^{(6),PC}\right\} + \left\{F_{n+1}^{(8),AX}\right\}. \tag{2.3.45}$$

$\left\{F'_{n+1}\right\}$ is treated as those in which values are known at time t_{n+1}, and $\left\{F''_{n+1}\right\}$ is the constraint force due to the known boundary condition (designated displacement). $\left\{F'''_{n+1}\right\}$ is determined by boundary conditions which depend on unknown values; for obtaining $\left\{F'''_{n+1}\right\}$, the interaction between pellet andcladding, as well as pellet and pellet must be solved.

(2) Interaction between pellet and cladding

The solution to obtain $\left\{F'''_{n+1}\right\}$ in eq. (2.3.45) is given below. When iteration of the

Newton-Raphson method is completed, eqs. (2.3.14), (2.3.15) and (2.3.16) are expressed as follows with omission of subscript i for iteration. Here, ^ indicates that the value is a tentative one during the iteration calculation.

$$\left[K_{n+\theta}\right]\left\{\Delta u_{n+1}\right\} = \left\{\Delta \hat{F}_{n+1}\right\} \tag{2.3.46}$$

$$\left[K_{n+\theta}\right] = \int [B]^T \left[\hat{D}''_{n+\theta}\right][B]dV \tag{2.3.47}$$

$$\begin{aligned}\left\{\Delta \hat{F}_{n+1}\right\} = &\left\{F_{n+1}\right\} - \int [B]^T \left\{\sigma_{n+1}\right\}dV \\ &- \int [B]^T \left[\hat{D}^P_{n+\theta}\right]\left\{\left[\overline{C}_{i+\theta}\right]\left(\left\{\sigma'_{n+1}\right\} - \left\{\sigma_n\right\}\right) + \left\{\Delta\varepsilon^0_{n+1}\right\} - \left\{\Delta\varepsilon^c_{n+1}\right\}\right\}dV \\ &- \int [B]^T \left(\left\{S_{n+1}\right\}\Delta T_{n+1} - \left\{Z_1\right\} - \left\{Z_2\right\}\right)dV\end{aligned} \tag{2.3.48}$$

Here, with substitution of eq. (2.3.42) into the right-hand side of eq. (2.3.48), the load term can be given by

$$\begin{aligned}\left\{\Delta \hat{F}_{n+1}\right\} = &\left\{F'_{n+1}\right\} + \left\{F''_{n+1}\right\} + \left\{F'''_{n+1}\right\} - \int [B]^T \left\{\sigma_{n+1}\right\}dV \\ &- \int [B]^T \left[\hat{D}^P_{n+\theta}\right]\left\{\left[\overline{C}_{i+\theta}\right]\left(\left\{\sigma'_{n+1}\right\} - \left\{\sigma_n\right\}\right) + \left\{\Delta\varepsilon^0_{n+1}\right\} - \left\{\Delta\varepsilon^c_{n+1}\right\}\right\}dV \\ &- \int [B]^T \left(\left\{S_{n+1}\right\}\Delta T_{n+1} - \left\{Z_1\right\} - \left\{Z_2\right\}\right)dV \\ = &\left\{\Delta \hat{F}'_{n+1}\right\} + \left\{F'''_{n+1}\right\},\end{aligned} \tag{2.3.49}$$

where

$$\begin{aligned}\left\{\Delta \hat{F}'_{n+1}\right\} = &\left\{F'_{n+1}\right\} + \left\{F''_{n+1}\right\} - \int [B]^T \left\{\sigma_{n+1}\right\}dV \\ &- \int [B]^T \left[\hat{D}^P_{n+\theta}\right]\left\{\left[\overline{C}_{i+\theta}\right]\left(\left\{\sigma'_{n+1}\right\} - \left\{\sigma_n\right\}\right) + \left\{\Delta\varepsilon^0_{n+1}\right\} - \left\{\Delta\varepsilon^c_{n+1}\right\}\right\}dV \\ &- \int [B]^T \left(\left\{S_{n+1}\right\}\Delta T_{n+1} - \left\{Z_1\right\} - \left\{Z_2\right\}\right)dV.\end{aligned} \tag{2.3.50}$$

Here, $\left\{\Delta \hat{F}'_{n+1}\right\}$ is the node point loading increment vector under the condition $\left\{F''_{n+1}\right\}$ (non-contact condition).

Substituting eq. (2.3.49) into eq. (2.3.46), we obtain

$$\left[K_{n+\theta}\right]\left\{\Delta u_{n+1}\right\} = \left\{\Delta \hat{F}'_{n+1}\right\} + \left\{F'''_{n+1}\right\}. \tag{2.3.51}$$

As shown in Fig. 2.42, the two planes contacting each other are expressed by several contact node couples. As contact conditions, three states are considered: non-contact state, clogged gap state and sliding state.

In FEMAXI-IV, this pellet/cladding contact problem is solved in the following procedure.

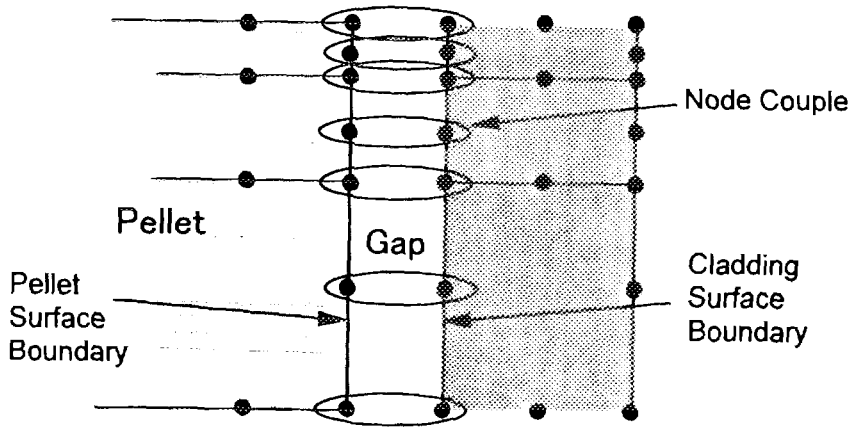

Fig. 2.42 Pellet-cladding contact node couple.

① A contact state (either contact or non-contact) is assumed for each couple of nodes which are possibly in contact with each other. Initially, this assumption is made based on the results for the previous time step.

② The stiffness equation is solved using boundary conditions corresponding to the assumed contact state (contact or non-contact).

③ Based on the solutions of nodal displacement and contact force obtained in ②, judgment is made on whether or not the assumption made in ① for each node couple is correct. If one of the assumptions is contradictory to the solution obtained by calculation at one node couple, the procedure is returned to ①, the assumption is corrected for the node couple, and procedures ② and ③ are performed again.

④ Thus, the calculation procedures from ①to ③are repeated until no discrepancy is observed between the assumption and calculated results. When a change in state of non-contact or contact (clogged gap state or sliding state) occurs, interpolation is

carried out for the calculated results into the time when the change in state occurred,

the assumption is corrected after that time and the procedure is returned to ① for continuous calculation.

When a pellet is not in contact with the cladding, $\left\{F_{n+1}^{(3),PC}\right\}$ and $\left\{F_{n+1}^{(6),PC}\right\}$ in eq. (2.3.41) are zero. As described later, $\left\{F_{n+1}^{(4),PP}\right\}$ and $\left\{F_{n+1}^{(8),AX}\right\}$ are also set as zero, and accordingly $\left\{F_{n+1}^{\prime\prime\prime}\right\}=0$.

Therefore, from eq. (2.3.51) we obtain

$$\left[K_{n+\theta}\right]\left\{\Delta u_{n+1}\right\}=\left\{\Delta\hat{F}_{n+1}^{\prime}\right\}. \tag{2.3.52}$$

When one contact node couple is in a sliding state and the remaining contact node couples

are in a non-contact state, then $\left\{F_{n+1}^{(3),PC}\right\}$ and $\left\{F_{n+1}^{(6),PC}\right\}$ are represented as

$$\left\{F_{n+1}^{(3),PC}\right\}=\begin{Bmatrix}0\\ \vdots\\ 0\\ U_{n+1}\\ V_{n+1}\\ 0\\ \vdots\\ 0\end{Bmatrix} \tag{2.3.53}$$

$$\left\{F_{n+1}^{(6),PC}\right\}=\begin{Bmatrix}0\\ \vdots\\ 0\\ -U_{n+1}\\ -V_{n+1}\\ 0\\ \vdots\\ 0\end{Bmatrix}, \tag{2.3.54}$$

where

$$V_{n+1}=\pm\mu U_{n+1} \tag{2.3.55}$$

V_{n+1} : contact force in the radial direction at time step t_{n-1}

U_{n+1} : contact force in the axial direction at time step t_{n-1}

μ : pellet/cladding friction coefficient.

Therefore, eq. (2.3.52) is represented as

$$\begin{array}{c} \\ i\\ j\\ k\\ l\\ \\ \\ m\end{array}\begin{pmatrix} & & & & 0\\ & & & & \vdots\\ & & & & 0\\ & & & & -1\\ & & K_{n+\theta} & & \pm\mu\\ & & & & 1\\ & & & & \pm\mu\\ & & & & 0\\ & & & & \vdots\\ & & & & 0\\ 0 & \cdots & 0 & -1\ 0\ 1\ 0\ 0 & \cdots & 0 & 0\end{pmatrix}\begin{Bmatrix}\\ \Delta u_{p,n+1}\\ \Delta v_{p,n+1}\\ \Delta u_{c,n+1}\\ \Delta v_{c,n+1}\\ \\ \\ \\ U_{n+1}\end{Bmatrix}=\begin{Bmatrix}\\ \\ \\ \\ \Delta\hat{F}'_{n+1}\\ \\ \\ \\ 0\end{Bmatrix}. \tag{2.3.56}$$

Here,

$\Delta u_{p,n+1}$: radial displacement increment of the node on the pellet side of a sliding-state contact node couple at time t_{n+1}

$\Delta v_{p,n+1}$: axial displacement increment of the node on the pellet side of a sliding-state contact node couple at time t_{n+1}

$\Delta u_{c,n+1}$: radial displacement increment of the node on the cladding side of a sliding-state contact node couple at time t_{n+1}

$\Delta v_{c,n+1}$: axial displacement increment of the node on the cladding side of a sliding-state contact node couple at time t_{n+1}.

Equations expressing degrees of freedom of contact nodes i, j, k and l in the above equation are

$$K_{n+\theta}^{(i)}\{\Delta u_{n+1}\} = \Delta\hat{F}_{n+1}^{\prime(i)} + U_{n+1} \tag{2.3.57}$$

$$K_{n+\theta}^{(j)}\{\Delta u_{n+1}\} = \Delta\hat{F}_{n+1}^{\prime(j)} \pm \mu U_{n+1} \tag{2.3.58}$$

$$K_{n+\theta}^{(k)}\{\Delta u_{n+1}\} = \Delta\hat{F}_{n+1}^{\prime(k)} - U_{n+1} \tag{2.3.59}$$

$$K_{n+\theta}^{(l)}\{\Delta u_{n+1}\} = \Delta\hat{F}_{n+1}^{\prime(k)} \pm \mu U_{n+1}. \tag{2.3.60}$$

Also,

$$-\Delta u_{p,n+1} + \Delta u_{c,n+1} = 0. \tag{2.3.61}$$

The stiffness equation when one contact node couple is in a clogged gap state and all the other couples are in a non-contact state is represented as

$$\begin{array}{c} \\ i \\ j \\ k \\ l \\ \\ m \end{array}\!\!\left(\begin{array}{cccccccccc|cc} & & & & & & & & & & 0 & 0 \\ & & & & & & & & & & \vdots & \vdots \\ & & & & & & & & & & 0 & 0 \\ & & & & & & & & & & -1 & 0 \\ & & & & & K_{n+\theta} & & & & & 0 & -1 \\ & & & & & & & & & & 1 & 0 \\ & & & & & & & & & & 0 & 1 \\ & & & & & & & & & & 0 & 0 \\ & & & & & & & & & & \vdots & \vdots \\ & & & & & & & & & & 0 & 0 \\ \hline 0 & \cdots & 0 & -1 & 0 & 1 & 0 & 0 & \cdots & 0 & 0 & 0 \\ 0 & \cdots & 0 & 0 & -1 & 0 & 1 & 0 & \cdots & 0 & 0 & 0 \end{array}\right)\left\{\begin{array}{c} \\ \\ \\ \\ \Delta u_{p,n+1} \\ \Delta v_{p,n+1} \\ \Delta u_{c,n+1} \\ \Delta v_{c,n+1} \\ \\ \\ \\ \hline U_{n+1} \\ V_{n+1} \end{array}\right\} = \left\{\begin{array}{c} \\ \\ \\ \\ \Delta\hat{F}_{n+1}^{\prime} \\ \\ \\ \\ \\ \\ \\ \hline 0 \\ 0 \end{array}\right\}. \tag{2.3.62}$$

Here,

$\Delta u_{p,n+1}$: radial displacement increment of the node on the pellet side of a clogged-gap-state contact node couple at time t_{n+1}

$\Delta v_{p,n+1}$: axial displacement increment of the node on the pellet side of a clogged-gap-state contact node couple at time t_{n+1}

$\Delta u_{c,n+1}$: radial displacement increment of the node on the cladding side of a clogged-gap-state contact node couple at time t_{n+1}

$\Delta v_{c,n+1}$: axial displacement increment of the node on the cladding side of a clogged-gap-state contact node couple at time t_{n+1}.

Stiffness equations expressing degrees of freedom of contact nodes i, j, k and l in the above equation are

$$K_{n+\theta}^{(i)}\{\Delta u_{n+1}\} = \Delta \hat{F}_{n+1}^{\prime(1)} + U_{n+1} \tag{2.3.63}$$

$$K_{n+\theta}^{(j)}\{\Delta u_{n+1}\} = \Delta \hat{F}_{n+1}^{\prime(j)} + V_{n+1} \tag{2.3.64}$$

$$K_{n+\theta}^{(k)}\{\Delta u_{n+1}\} = \Delta \hat{F}_{n+1}^{\prime(k)} - U_{n+1} \tag{2.3.65}$$

$$K_{n+\theta}^{(l)}\{\Delta u_{n+1}\} = \Delta \hat{F}_{n+1}^{\prime(k)} - V_{n+1}. \tag{2.3.66}$$

Also,

$$-\Delta u_{p,n+1} + \Delta u_{c,n+1} = 0. \tag{2.3.67}$$

$$-\Delta v_{p,n+1} + \Delta v_{c,n+1} = 0. \tag{2.3.68}$$

At judgment of the contact state and after this judgment, the following processes are carried out.

①In cases of a non-contact state at the previous time step

Presence of overlap of displacement is checked for. Namely,

$$g_{n+1} = g_n - \Delta u_{p,n+1} + \Delta u_{c,n+1}, \tag{2.3.69}$$

where

g_{n+1} : gap width at time step t_{n+1}.

When $g_{n+1} > 0$, eq. (2.3.69) is judged as being converged; when $g_{n+1} \leq 0$, the time step is returned to $t_{n+\alpha}$ using the equation

$$t_{n+\alpha} = \frac{t_{n+1} - t_n}{g_n - g_{n+1}} g_n + t_n. \tag{2.3.70}$$

Then, the calculation from time $t_{n+\alpha}$ to t_{n+1} is performed again after changing of the contact

state to a clogged gap state.

②In cases of a clogged gap state at the previous time step

The state change is judged in terms of a contact force vector. Namely, when

$$U_{p,n+1} < 0 \text{ and } \left|V_{p,n+1}\right| < \mu\left|U_{p,n+1}\right| \tag{2.3.71}$$

are satisfied, the contact state is judged as being converged;

when

$$U_{p,n+1} < 0 \text{ and } \left|V_{p,n+1}\right| \geq \mu\left|U_{p,n+1}\right| \tag{2.3.72}$$

are satisfied, the assumed contact state is changed to a sliding state and the calculation is performed again. Also, when

$$U_{p,n+1} \geq 0, \tag{2.3.73}$$

the contact state is changed from a clogged gap state to a non-contact state; therefore, the time step is returned to $t_{n+\alpha}$ using

$$t_{n+\alpha} = \frac{t_{n+1} - t_n}{U_{p,n} - U_{p,n+1}} U_{p,n} + t_n, \tag{2.3.74}$$

and the calculation from time $t_{n+\alpha}$ to t_{n+1} is performed again after changing of the contact state to a non-contact state.

③In cases of a sliding state at the previous time step

The state change is judged in terms of a contact force vector. Namely, when

$$U_{p,n+1} < 0 \text{ and } \left|V_{p,n+1}\right| \geq \mu\left|U_{p,n+1}\right| \tag{2.3.75}$$

are satisfied, the contact state is judged as being converged. However, when

$$U_{p,n+1} < 0 \text{ and } \left|V_{p,n+1}\right| < \mu\left|U_{p,n+1}\right| \tag{2.3.76}$$

hold, the contact state is changed to a clogged gap state.

Also, when

$$U_{p,n+1} < 0 \text{ and } \left|v^*_{p,n+1}\right| \leq \left|v^*_{c,n+1}\right| \tag{2.3.77}$$

are satisfied, the assumed contact state is changed from a sliding state to a clogged gap state.

Here,

$v^{*}_{p,n+1}$: axial displacement of a node on the pellet side after the start of contact

$v^{*}_{c,n+1}$: axial displacement of a node on the cladding side after the start of contact.

In contrast, when

$$U_{p,n+1} \geq 0 \tag{2.3.78}$$

is satisfied, the contact state is judged as being changed from a sliding state to a non-contact state; the time step is returned to $t_{n+\alpha}$ using eq. (2.3.74) and the variable values are interpolated for the time step $t_{n+\alpha}$; then the calculation from time $t_{n+\alpha}$ to t_{n+1} is performed again after changing of the contact state to a non-contact state.

In a system having several contact node couples as shown in Fig. 2.42, if we try to converge the contact state for each node couple independently, a large number of iterations are required for convergence of the entire system. Therefore, the following conditions are added in order to reduce the number of the iterations.

① For node couples in the contact state, all of the states are initially assumed to be clogged gap states.

② Among them, if some node couples satisfy the condition $|V_{p,n+1}| \geq \mu |U_{p,n+1}|$, the assumed contact state for such node couples and contact states of node couples located above them are changed to sliding states.

③ At this time, directions of sliding are aligned. That is, friction force is exerted downward on the pellet surface, and upward on the inner surface of cladding. However, if all axial components of the contact force of the node couples which were judged to be in a sliding state when they were assumed to be in a clogged gap state are in the reverse directions, the direction of sliding should be reversed.

With the above method, convergence of the entire system can be achieved within less than 3 iterations in general cases.

(3) Axial loads －Interaction between pellet/pellet－

When the gap width between a pellet and cladding which is located above the objective segment is less than a predetermined value, it is assumed that the pellet and cladding above the objective segment are in a clogged gap state, which restricts the axial displacement of the objective pellet; that is, locking is generated.

For modeling of the locking condition, among nodes which are distributed on the upper surface of the objective segment, a displacement increment of node i with the maximum coordinate value in the axial direction is set to be equal to the displacement increment of the boundary surface of the pellet, i.e., boundary (8) shown in Fig. 2.41. By this setting, axial load is generated for the pellet and cladding. This condition is called a locking condition.

Fitting parameter GAPLK	The radial gap width with which the locking condition is given is adjusted by GAPLK. The default value of GAPLK is 3 (μm).

The procedures for the judgment of contact condition between a pellet in the objective segment and a pellet located above it, as well as the process following the judgment are as follows.

When the axial coordinate of another node j on the upper surface of the pellet in the objective segment exceeds that of node i, the axial displacement increment of node j is also set to be equal to the axial displacement increment of the boundary surface (8), as in the case of the node i. That is, the locking condition is set on node j, also. At this time, the time is returned to the state change point $t_{n+\alpha}$ using the equation

$$t_{n+\alpha} = \frac{\overline{Z}_{i,n} - Z_{j,n}}{Z_{j,n+1} - Z_{j,n} - \left(\overline{Z}_{i,n+1} - \overline{Z}_{i,n}\right)}\left(t_{n+1} - t_n\right) + t_n . \qquad (2.3.79)$$

Here,

$\overline{Z}_{i,n}$, $\overline{Z}_{n+1}$: axial coordinates of node i in the locking condition at time t_n and t_{n+1}

$Z_{j,n}$, $Z_{j,n+1}$: axial coordinates of node j at time t_n and t_{n+1}.

From time $t_{n+\alpha}$ to t_{n+1}, the degree of freedom in the axial direction of node j is set as the same degree of freedom in the axial direction of nodes i, which is also the same degree of freedom in the axial direction of the upper edge surface of the cladding (boundary (8)), namely the common degree of freedom; then the calculation is performed again.

By this method, the locking condition is generally realized by setting of a boundary condition in which axial displacement increments of a pellet-node group which supports the axial load on boundary (4) and those of a cladding-node group on boundary (8) are set to be equal. In this procedure, the number of degrees of freedom of the pellet-node group in the axial direction is assumed to be one, and those of the cladding-node group is also assumed to be one. That is, they are assumed to have common degrees of freedom. (see Fig. 2.41)

The contact force in the axial direction at an arbitrary time of an arbitrary node in the contact state is given by eq. (2.3.1). That is, in

$$\{F_{n+1}\} = \int [B]^T \{\sigma_{n+1}\} dV , \tag{2.3.1}$$

since the only load which acts on boundary (4) is the contact force in the axial direction $\{F_{n+1}^{(4),PP}\}$,

$$\{F_{n+1}^{(4),PP}\} = \{F_{n+1}\} = \int [B]^T \{\sigma_{n+1}\} dV \tag{2.3.80}$$

holds.

The contact force in the axial direction of a node obtained from eq. (2.3.80) is represented by V_{n+1}. When $V_{n+1} < 0$, the locking condition is maintained on this node. When $V_{n+1} \geq 0$, the locking condition is judged to be disengaged, and the time is returned to $t_{n+\alpha}$ using the equation

$$t_{n+\alpha} = \frac{V_n}{V_n - V_{n+1}} (t_{n+1} - t_n) + t_n . \tag{2.3.81}$$

From time $t_{n+\alpha}$ to t_{n+1}, the degree of freedom in the axial direction of this node is set to be different from the common degree of freedom.

Here, when the sign of V is positive at all nodes on the edge surface of the pellet, the locking condition is disengaged.

A locking condition is set for the second time or later when a node on the edge surface of the pellet reaches the axial coordinates at the time when the previous locking condition was disengaged. Here, the load $\{F^{(8)}\}$ which acts on the upper edge surface of the cladding (boundary (8)) at the time of the locking condition setting is expressed as

$$\{F^{(8)}\} = \{F^{(8),R}\} + \{F^{(8),AX}\} + \{F^{(8),W}\} + \{F^{(8),G}\}, \tag{2.3.82}$$

where

$\{F^{(8)}\}$: axial load which acts on boundary (8)

$\{F^{(8),R}\}$: nodal force generated by setting of the number of degrees of freedom in the axial direction as 1 at boundary (8)

$\{F^{(8),AX}\}$: axial tensile load due to the locking condition at boundary (8)

$\{F^{(8),W}\}$: axial load due to coolant pressure

$\{F^{(8),G}\}$: axial load due to plenum gas pressure.

2.4 Material Properties

The following tables show the material properties and equations installed in the present FEMAXI-IV(Ver.2). An asterisk * in the right column indicates that reference source is unknown.

2.4.1 Material properties of pellet

(1) Pellet thermal conductivity

UO_2 thermal conductivity (1) MATPRO-Version 09	Condition	Ref.
for a temperature range of 0–1,650°C: $K = \left\{\frac{1-\beta(1-D)}{1-0.05\beta}\right\} \cdot \left\{\frac{40.4}{464+T} + 1.216\times10^{-4}\exp\left(1.867\times10^{-3}T\right)\right\}$ for a temperature range of 1,650–2,840°C $K = \left\{\frac{1-\beta(1-D)}{1-0.05\beta}\right\} \cdot \left\{0.0191 + 1.216\times10^{-4}\exp\left(1.867\times10^{-3}T\right)\right\}$ K : thermal conductivity of UO_2 pellet (W/cm・K) D : UO_2 theoretical density ratio T : temperature (°C) β : porosity coefficient: $\beta = 2.58 - 0.58\times10^{-3}T$	Default value: IPTHCN=1	14
UO_2 thermal conductivity (2) Washington $K = F \cdot \left\{(0.040 + 2.57\times10^{-4}\cdot T_K)^{-1} + 72.6\times10^{-12}\cdot T_K^{\,3}\right\}$ (W/mK) $F = 1.0 - 2.5\cdot P$ P: porosity=1.0 - (actual UO_2 density/theoretical density) T_K : temperature (K)	IPTHCN=2	23
UO_2 thermal conductivity (3) Hirai $K = K_{95\%TD}\cdot(1-\beta p)/(1-0.05\cdot\beta)$ (W/mK) $K_{95\%TD} = (2.35\times10^{-2} + 2.55\times10^{-4}\cdot T_K)^{-1} + 3.57\times10^{-12}\cdot T_K^{\,3}$ $\beta = 2.58 - 0.58\times10^{-3}T$ →Ref.(14) P: porosity T_K : temperature (K)	IPTHCN=3	24
UO_2 thermal conductivity (4) Halden $K = F/\left\{0.1148 + 0.0035\cdot B + (2.475\times10^{-4} - 8\times10^{-7}\cdot B)T\right\} + F\cdot0.0132\exp(0.00188\cdot T)$ (W/mK) $F = (1-\beta p)/(1-0.05\cdot\beta)$ $\beta = 2.58 - 0.58\times10^{-3}T$ →Ref.(14) P: porosity B : burnup (MWd/kgUO_2) T : temperature (℃)	IPTHCN=4	25

UO_2 thermal conductivity (5) Modified Hirai		
$K = K_{95\%TD} \cdot (1 - \beta p) / (1 - 0.05 \cdot \beta) \quad (W / mK)$ $K_{95\%TD} = \left\{(2.35 \times 10^{-2} + 4.8 \times 10^{-3} \cdot B) + (2.55 \times 10^{-4} - 16.0 \times 10^{-7} \cdot B) \cdot T_K\right\}^{-1}$ $+ 3.57 \times 10^{-12} \cdot T_K^{\,3}$ $\beta = 2.58 - 0.58 \times 10^{-3} T$ →Ref.(14) P: porosity T_K : temperature (K) B : burnup (MWd/kg-U)	IPTHCN=5	24
UO_2 thermal conductivity (6) Forsberg		
$K = F\left\{0.047 + 1.73 \times 10^{-3} \cdot B + (2.5 \times 10^{-4} - 5.41 \times 10^{-8} \cdot B) T_K\right\}^{-1}$ (W / mK) $F = 1.0 - \beta \cdot p$ $\beta = 2.58 - 0.58 \times 10^{-3} T$ →Ref.(14) P: porosity T_K : temperature (K) B : burnup (MWd/kg-U)	IPTHCN=6	26
UO_2 thermal conductivity (7) Kjaer-Pedersen		
$K = 93 / (0.0224 \cdot T_K + 1.1 + 56 \cdot P + 3 \cdot G(B)) + 2.5 \cdot 10^{-14} \cdot T_K^{\,4}$ $B \le 10 \quad G = (B / 10)^2$ $B \ge 10 \quad G = ((B - 7.5) / 10)^{0.5}$ P: porosity T_K : temperature (K) B : burnup (MWd/kg-U)	IPTHCN=7	27
MOX pellet thermal conductivity Martin	Condition	Ref.
1) In the case of 12%≤PuO_2≤30% $K = \left(0.037 + 3.33y + 2.37 \times 10^{-4} T_K\right)^{-1} + 78.9 \times 10^{-12} T_K^{\,3}$ 2) In the case of 0%≦PuO_2≦12% $K = (f) = Ku(1 - f / 0.12) + K(Mox) x\ f / 0.12$ Here, K : thermal conductivity (W/m ・ K) T_K : temperature (K) y : MO_{2-y} K_u : UO_2 thermal conductivity (W/m ・ K) $K_u = \left[\left(0.035 + 2.25 \cdot 10^{-4} \cdot T_K\right)^{-1} + 83.0 \cdot 10^{-12} \cdot T_K^{\,3}\right] \cdot (1 + z)$ $(z : UO_{2-z}, \quad 0 \le z \le 0.05)$	MOX=1	28

When MOX=1, the following values are designated by input.

Variable name	Content	Default value
PU	PuO_2 weight ratio (converted to molar fraction by the code)	0.0
Y	Value of y for MO_{2-y} (this value is also used for z)	0.0

Thermal conductivity of pellet containing Gadolinium Fukushima	Condition	Ref.
$K = \frac{1}{aT + b}$ Here, K : thermal conductivity (W/m ・ K) T : temperature (°C) a, b : function of Gd_2O_3 concentration (see table below) Gd_2O_3 (−) a b 0.0 2.32733×10^{-4} 1.180229×10^{-1} 0.03 2.131412×10^{-4} 1.732423×10^{-1} 0.057 1.996481×10^{-4} 2.069985×10^{-1} 0.085 1.961735×10^{-4} 2.342200×10^{-1} In order to interpolate a, b for other Gd_2O_3 concentrations, two values of a and b in the above table whose Gd_2O_3 concentrations sandwich the current Gd_2O_3 concentration are substituted into $K = rA^{Gd}$ to obtain r and A, so that the two values of K coincide.	IGD=1	29

In the case of IGD=1, the following value is input.

Variable name	Content	Default value
GD	Gd_2O_3 concentration (Weight fraction)	0.0

(2) Pellet thermal expansion

Equations representing pellet thermal expansion are selected from among the following.

UO_2 thermal expansion (1) MATPRO-Version 09	Condition	Ref.
$\frac{\Delta L}{L} = -4.972\times10^{-4} + 7.107\times10^{-6}T + 2.581\times10^{-9}T^2 + 1.140\times10^{-13}T^3$ $\frac{\Delta L}{L}$: linear thermal expansion T : temperature (°C)	IPTHEX=0 (default value) IPTHEX=1	14
UO_2 thermal expansion (2) Burdick and Parker $\frac{\Delta L}{L} = -3.0289\times10^{-4} + 8.4217\times10^{-6}T + 2.1481\times10^{-9}T^2$ T : temperature (°C) temperature range: 27–1260°C $\Delta L / L$: linear thermal expansion normalized by the length at 27°C.	IPTHEX=2	*
UO_2 thermal expansion (3) Halden $\frac{\Delta L}{L} = 6.0\times10^{-6}T + 2.0\times10^{-9}T^2 + 1.7\times10^{-12}T^3$ T : temperature (°C) temperature range: 900–2,800°C (melting point)	IPTHEX=3	*
UO_2 thermal expansion (4) Conway and Fincel $\frac{\Delta L}{L} = -1.723\times10^{-4} + 6.797\times10^{-6}T + 2.896\times10^{-9}T^2$ T : temperature (°C) temperature range: 1,000–2,250°C	IPTHEX=4	*

(3) UO_2 theoretical density

UO_2 density MATPRO-Version 09	Condition	Ref.
$\rho = 10.96$, ρ : UO_2 theoretical density (g/cm^3)	No restrictions	14

(4) UO_2 Young's modulus

UO_2 Young's modulus MATPRO-Version 09	Condition	Ref.
$E = 2.26\times10^{11}\left(1-1.131\times10^{-4}T\right)\left[1-2.62(1-D)\right]$ E : Young's modulus (Pa) T : temperature (°C) D : theoretical density ratio	No restrictions	14

(5) UO_2 Poisson's ratio

Poisson's ratio of UO_2 MATPRO-Version 09	Condition	Ref.
$\nu = 0.316$	No restrictions	14

(6) UO_2 creep

Creep of UO_2 MATPRO-Version 09	Condition	Ref.
$\varepsilon = \frac{(A_1 + A_2\dot{F})\sigma \exp(-Q_1 / RT)}{(A_3 + D)G^2} + \frac{A_4\sigma^{4.5}\exp(-Q_2 / RT)}{(A_5 + D)} + A_6\sigma\dot{F}\exp(-Q_3 / RT)$ ε : steady-state creep rate (1/h) $A_1 = 9.728 \times 10^6$ $A_2 = 3.24 \times 10^{-12}$ $A_3 = -87.7$ $A_4 = 1.376 \times 10^{-4}$ $A_5 = -90.5$ $A_6 = 9.24 \times 10^{-28}$ $Q_1 = 90{,}000$ (cal / mol) $Q_2 = 132{,}000$ (cal / mol) $Q_3 = 5{,}200$ (cal / mol) F : fission rate $8.4 \times 10^{17} \sim 1.18 \times 10^{20}$ (fiss./m^3 · sec) σ : stress 1,000-16,000 (psi) T : temperature 713-2,073 (K) D : density 92-98 (%TD) G : grain size 4-35 (μm) R : gas constant 1.987 (cal/mol · K)	No restrictions	14

The following fitting parameters can be used for the UO_2 creep rate equation.

Variable name	Content	Default value
FCRFAC	Magnification factor for the creep rate equation (deformation model)	10.0
TCS	Cut-off value at the reference temperature in the creep calculation (deformation model) (K)	2073.15
TCRMX	Cut-off value at the reference temperature in the creep calculation (thermal model) (K)	1773.15

(7) UO_2 swelling

Shown below are the equations representing UO_2 swelling. There are two types of UO_2 swelling: solid FP swelling and gas-bubble swelling.

Using the options, one of the following two cases can be selected: a case in which the solid FP swelling and gas-bubble swelling are treated independently, and a case in which both types of swelling are given by a single material property equation.

UO_2 swelling (1) Chubb	Condition	Ref.
(gas-bubble swelling) $\left(\frac{\Delta V}{V}\right)^{gs} = 4.396 \times 10^{2} \exp\left(-\frac{1.645 \times 10^{4}}{T_S}\right)$ $T_S = T - 100$ $\left(\frac{\Delta V}{V}\right)^{gs}$: volume of gas-bubble swelling per 10^{20} fissions/cm^3 T : temperature (K)	IFSWEL=0 (default value)	30
UO_2 swelling (1a) FEMAXI-III		
(Solid FP swelling) $\left(\frac{\Delta V}{V}\right)^{ss} = 0.0025$ $\left(\frac{\Delta V}{V}\right)^{ss}$: volume of FP swelling per 10^{20} fissions/cm^3		2

In the case of ISWEL = 0, the following fitting parameters can be used.

Variable name	Content	Default value
STFCP	Suppress generation of gas-bubble swelling average contact pressure (Pa) (used in the deformation model)	-3×10^{7}
SPCON	Suppress generation of gas-bubble swelling average contact pressure (Pa) (used in the thermal model)	-10^{6}

UO_2 swelling (2) Speight	Condition	Ref.
(Gas-bubble swelling) Intragranular gas-bubble swelling $\left(\frac{\Delta V}{V}\right)^{gs1} = \frac{4}{3}\pi a^3 N$ a : intragranular gas-bubble radius (cm) N : number of gas bubbles per unit volume ($1/cm^3$) Grain-boundary gas-bubble swelling $\left(\frac{\Delta V}{V}\right)^{gs2} = Bg\frac{3\pi}{2R}h\bar{a}^3\left\{1+\frac{h^2}{3}\right\}$ Bg : number of gas bubbles per unit area ($1/cm^3$) R : grain radius (cm) $\bar{a}$: grain-boundary gas-bubble radius (cm) h : constant (=1) $\left(\frac{\Delta V}{V}\right)^{gs} = \left(\frac{\Delta V}{V}\right)^{gs1} + \left(\frac{\Delta V}{V}\right)^{gs2}$ $\left(\frac{\Delta V}{V}\right)^{gs}$: volumetric gas bubble swelling $\left(\frac{\Delta V}{V}\right)^{gs1}$: volumetric intragranular gas-bubble swelling $\left(\frac{\Delta V}{V}\right)^{gs2}$: volumetric grain-boundary gas-bubble swelling	IFSWEL=1	16
UO_2 swelling (1a) FEMAXI-III		
(Solid FP swelling) $\left(\frac{\Delta V}{V}\right)^{ss} = 0.0025$ $\left(\frac{\Delta V}{V}\right)^{gs1}$: volumetric solid FP swelling per 10^{20} fissions/cm^3		2

In the case of IFSWEL=1, the following fitting parameters can be used.

Variable name	Content	Default value
FACP	The bubble radius at grain boundary $\bar{a}$ is obtained by the following equation. $P_{in} = \frac{m}{\upsilon} RT = \frac{2r}{\bar{a}} + P_{out}$ Here, P_{in} : pressure at grain-boundary gas bubble m : gas molar number within 1 bubble v : gas-bubble volume $\left(= \pi h \bar{a}^3 \left(1 + \frac{h^2}{3} \right) \right)$ R : gas constant T : temperature r : surface tension $\bar{a}$: gas-bubble radius at grain boundary P_{out} : pressure outside grain-boundary gas bubble. P_{out} is given as $P_{out} = P_{gas} + P_{fc} \cdot \mathrm{FACP}$. Here, P_{gas} : plenum pressure P_{fc} : pellet-cladding average contact pressure. Therefore, FACP is a parameter for adjusting pressure external to the grain-boundary gas bubbles. (common to deformation and thermal models)	1.0

UO_2 swelling (3) MATPRO-Version 09		Condition	Ref.
Temperature at pellet center (°C)	Swelling ratio (%/10^{20}fiss./cm^3)	IFSWEL=2	14
$T \leq 1{,}400$	0.28		
$1{,}400 \leq T \leq 1{,}800$	$0.28[1 + 0.00575(T - 1{,}400)]$		
$1{,}800 \leq T \leq 2{,}200$	$0.28[3.3 - 0.004(T - 1{,}800)]$		
$2{,}200 < T$	0.476		

UO_2 swelling (4) Halden	Condition	Ref.
Volumetric swelling ratio: $\left(\frac{\Delta V}{V} \right) = 0.5\% / (10\, MWd / kgUO_2)$	IFSWEL=3	44

(8) Hot pressing of UO_2

The flow rule of the yield function is given as follows, including the (r, z) plane shearing force term used in Section 2.3.

$$\bar{\sigma} = \left[\frac{3}{2(F+G+H)} \left\{ H(\sigma_r - \sigma_z)^2 + F(\sigma_z - \sigma_\theta)^2 + G(\sigma_\theta - \sigma_r)^2 \right\} + 3\alpha(\sigma_r + \sigma_z + \sigma_\theta)^2 + 2N\tau_{rz}^2 \right]^{\frac{1}{2}} \tag{2.4.1}$$

$$\left\{ \Delta\varepsilon_{n+1}^P \right\} = \Delta\bar{\varepsilon}_{n+1}^P \left\{ \frac{\partial\bar{\sigma}}{\partial\sigma} \right\}_{n+\theta} \tag{2.4.2}$$

Here, α is the hot-press parameter of pellet.

When isotropy of pellet materials $(H = F = G = 1)$ is assumed, the following equation holds from eq. (2.4.1).

$$\frac{\partial\bar{\sigma}}{\partial\sigma_r} = \frac{3}{2\bar{\sigma}} \left\{ \frac{2\sigma_r - \sigma_z - \sigma_\theta}{3} + 2\alpha(\sigma_r + \sigma_z + \sigma_\theta) \right\} \tag{2.4.3}$$

Therefore,

$$\left\{ \frac{\partial\bar{\sigma}}{\partial\sigma} \right\}_{n+\theta} = \frac{1}{\bar{\sigma}_{n+\theta}} \begin{bmatrix} 1+3\alpha & -0.5+3\alpha & -0.5+3\alpha & 0 \\ & 1-3\alpha & -0.5+3\alpha & 0 \\ & Sym. & 1+3\alpha & 0 \\ & & & \frac{2}{3} \end{bmatrix} \left\{ \sigma_{n+\theta} \right\}. \tag{2.4.4}$$

Substituting eq. (2.4.4) into eq. (2.4.2) and rearranging, we obtain

$$\left\{ \Delta\varepsilon_{n+\theta}^P \right\} = \frac{(1+3\alpha)\Delta\bar{\varepsilon}_{n+1}^P}{\bar{\sigma}_{n+\theta}} \begin{bmatrix} 1 & -v^P & -v^P & 0 \\ & 1 & -v^P & 0 \\ & & 1 & 0 \\ & Sym. & & \frac{2}{3} \end{bmatrix} \left\{ \sigma_{n+\theta} \right\}. \tag{2.4.5}$$

Here, $v^P = \dfrac{0.5-3\alpha}{1+3\alpha}$.

The volume strain increment $\Delta\varepsilon_{h,n+1}^P$ due to plasticity is given by

$$\begin{aligned}\Delta\varepsilon_{h,n+1}^{P} &= \Delta\varepsilon_{n+1}^{P,r} + \Delta\varepsilon_{n+1}^{P,z} + \Delta\varepsilon_{n+1}^{P,\theta} \\ &= \frac{(1+3\alpha)\Delta\bar{\varepsilon}_{n+1}^{P}}{\bar{\sigma}}(1-2\nu^{P})(\sigma_r+\sigma_z+\sigma_\theta) \\ &= \frac{9\alpha\Delta\bar{\varepsilon}_{n+1}^{P}}{\bar{\sigma}}(\sigma_r+\sigma_z+\sigma_\theta).\end{aligned} \tag{2.4.6}$$

Since eq. (2.4.6) is also applied in the case of pellet creep, the volume strain increment $\Delta\varepsilon_{h,n+1}^{c}$ by creep is given by

$$\Delta\varepsilon_{h,n+1}^{c} = \frac{9\alpha\Delta\bar{\varepsilon}_{n+1}^{P}}{\bar{\sigma}}(\sigma_r+\sigma_z+\sigma_\theta). \tag{2.4.7}$$

Accordingly, the change in pellet volume strain accompanied by plasticity and creep flow (=hot press), $\Delta\varepsilon_{h,n+1}$, is expressed as follows.

$$\begin{aligned}\Delta\varepsilon_{h,n+1} &= \Delta\varepsilon_{h,n+1}^{P} + \Delta\varepsilon_{h,n+1}^{c} \\ &= \frac{9\alpha}{\bar{\sigma}}(\Delta\bar{\varepsilon}_{n+1}^{P} + \Delta\bar{\varepsilon}_{n+1}^{c})(\sigma_r+\sigma_z+\sigma_\theta)\end{aligned} \tag{2.4.8}$$

Here, porosity p_{n+1} at (n+1) time step is expresses as

$$p_{n+1} = p_1 + \sum_{i=1}^{n+1}\Delta\varepsilon_{h,i} + \sum_{i=1}^{n+1}\Delta\varepsilon_{swel} + \sum_{i=1}^{n+1}\Delta\varepsilon_{dens} \tag{2.4.9}$$

where p_1: initial porosity,

$\Delta\varepsilon_{swel}$: swelling strain increment,

$\Delta\varepsilon_{dens}$:densification strain increment.

Hot press of UO_2 has the fitting parameter α.

Variable name	Content	Default value
BETAX $=\alpha$, hot press parameter of UO_2	When IHOT=0, BETAX=α is fixed at the initial value. When IHOT=1, α is determined as a function of porosity as follows: $\alpha = \text{BETAX}\cdot\frac{p_{n+1}}{1-D_0}$ where p_{n+1}: porosity in pellet D_0: initial theoretical density ratio. In this case, α is diminishing to 0 with the decrease in porosity when hot press and densification proceed, though it never becomes 0.	0.002 (initial value)

(9) Densification of UO_2

The following options can be selected for the equation representing UO_2 densification.

UO_2 densification (1) FEMAXI-III	Condition	Ref.
$\frac{\Delta V}{V} = \frac{\Delta V^{max}}{V}\left(1 - e^{-c \cdot Bu}\right)$ $\frac{\Delta V}{V}$: volume contraction due to densification $\frac{\Delta V^{max}}{V}$: maximum volume contraction due to densification Bu : burnup (MWd/t-UO_2)	IDENSF=0 (default value)	2

The following fitting parameters are used in the case of IDENSF=0.

Variable name	Content	Default value
DMAX	Maximum volume contraction due to densification $\frac{\Delta V^{max}}{V}$ (%)	1.0
SBU	Burnup of 90% completion of densification, given by $C = \frac{2.3025}{SBU}$, (MWd/t-UO_2), where exp (−2.3025) =0.1.	2500.0

UO_2 densification (2) Rolstad	Condition	Ref.
The upper limit of the dimension change in the axial direction due to densification is given by $\frac{\Delta L}{L} = 22.2 \times \frac{(100 - TD)}{(TS - 1180)}$ TD : theoretical density ratio of UO_2 (%TD) TS : sintering temperature (°C). Burnup dependence: $\frac{\Delta L}{L} = -3.0 + 0.93e^{-BU} + 2.07e^{-35BU}$ BU : burnup (GWd/t-U)	IDENSF=1	31

Here, the following fitting parameter is used for IDENSF.

Variable name	Content	Default value
TDNSF	Sintering temperature (K)	2000.0

UO_2 densification (3) NRC	Condition	Ref.
Density increment due to densification $\Delta\rho$ (g/cm^3): $\begin{cases} \Delta\rho = 0 & (BU \le BU_1) \\ \Delta\rho = m\log(BU) + b & (BU_1 < BU < BU_2) \\ \Delta\rho = \Delta\rho_{sn} & (BU \ge BU_2) \end{cases}$ $\Delta\rho_{sn}$: density increment (g/cm^3) due to out-of-pile heat treatment (1,700°C×24h) BU : burnup (MWd/t) BU_1, BU_2 : constants for determining the burnup range; dependent on $\Delta\rho_{sn}$ m, b : constants for connecting the three equations for each burnup range	IDENSF=2	32

The following fitting parameter is used in the case of ISENSF=2.

Variable name	Content	Default value
DMAX	Relative density increase (%) due to out-of-pile heat treatment (1,700°C×24h).	1.0

UO_2 densification (4) Halden	Condition	ref.
Volumetric decrease by densification is: $\frac{\Delta V}{V} = -\left[\begin{array}{l} 0.01420(1-\exp(-6.7943\cdot BU)) \\ \quad + 0.00793(1-\exp(-1.1434\cdot BU)) \end{array}\right]\cdot ADST$ Here, BU: Burnup(MWd/kgUO_2) $ADST$: adjusting factor(=0.6)	IDENSF=4	44

UO_2 densification (5) Marlowe	Condition	Ref.
$\Delta\rho = \frac{M}{A}\ln\left(1+\frac{AD^0_{irr}\dot{F}t_{irr}}{{G_0}^3}\right)$	IDENSF=3	33
$\Delta\rho$: amount of in-pile densification (%TD)		
M : densification rate constant (%TD-cm)		
A : grain growth rate constant (cm)		
D^0_{irr} : irradiation diffusion constant=1.27×10^{-29} (m^3/fiss.)		
$\dot{F}$: fission rate (fiss./$cm^3\cdot s$)		
t_{irr} : irradiation time (s)		
$\dot{F}t_{irr}$: burnup (fiss./cm^3)		
G_0 : initial crystal grain size (cm)		
The constants M and A are calculated from the following equation using the results of the out-of-pile heat treatment test, in which a fuel produced in the same batch as the fuel for irradiation is used.		
$A=\frac{G^3-{G_0}^3}{Dt}$,		
$M=\frac{A\Delta\rho_{th}}{In\left(1+\frac{ADt}{{G_0}^3}\right)}$		
$D=D_0\cdot\exp(-Q/RT)$		
G : crystal grain size after heat treatment (cm)		
t : heat treatment time (s)		
$\Delta\rho_{th}$: density change due to heat treatment (%TD)		
D_0 : thermal diffusion constant 2.32×10^{-6} (cm^2/s)		
Q : 82,000 cal/mol		
R : gas constant 1.987 (cal/mol)		
T : treatment temperature (K)		

The following fitting parameters are used in the case of IDENSF=3.

Variable name	Content	Default value
DMAX	degree of in-pile densification (%TD)	1.0
GG	crystal grain size after heat treatment (m)	10^{-5}
GGO	initial crystal grain size (m)	8×10^{-6}
SITIM	heat treatment time (h)	24.0

(10) Pellet relocation

The parts of a pellet that is cracked at start-up scatter in the radial direction and consequently the gap is narrowed. This phenomenon is called relocation. In FEMAXI-IV, the initial relocation is assumed to be proportional to the gap width at hot stand-by where burnup is 0 and linear heat rate is 0, as

$$REL = \alpha \cdot \left(r_{ci}^{c} - r_{pi}^{c} \right), \tag{2.4.10}$$

where r_{ci}^{c} and r_{pi}^{c} are the cladding inner radius and pellet radius (cm) at hot stand-by, respectively. α is an empirical parameter which is determined by comparison with experimental data, and is called a relocation parameter.

The fitting parameters for relocation are as follows.

Variable name	Content	Default value
XRELOC	Relocation parameter α for the thermal model	0.2
FRELOC	Relocation parameter α for the mechanical model	0.5
EPSRLZ	Axial relocation strain for the mechanical model	0.003

(11) UO_2 plasticity

Equations representing yield stress and the strain hardening parameter (tangent stiffness) are selected from among the following.

UO_2 plasticity (1) Tachibana	Condition	Ref.
$\sigma_Y = \begin{cases} 66.9 - 0.0397 \cdot T + (520.0 - 0.386 \cdot T) \cdot \bar{\varepsilon}_p & (T \le 1200\,℃) \\ 36.6 - 0.0144 \cdot T + (139.5 - 0.06875 \cdot T) \cdot \bar{\varepsilon}_p & (T > 1200\,℃) \end{cases}$ $H' = \begin{cases} 520.0 - 0.386 \cdot T & (T \le 1200\,℃) \\ 139.5 - 0.06875 \cdot T & (T > 1200\,℃) \end{cases}$ σ_Y : yield stress (kg/mm^2) H' : tangent stiffness (kg/mm^2) T : temperature (°C)	IFY=1 (default value)	34
UO_2 plasticity (2) Rodford		
$\sigma_Y = 1176.1 - 1.688 \cdot T + 8.179 \times 10^{-4} \cdot T^2 - 1.293 \times 10^{-7} \cdot T^3$ H'=0.0 : tangential stiffness σ_Y : yield stress (MPa) T : temperature (°C)	IFY=0	*

(12) UO_2 Specific heat

UO_2 specific heat MATPRO-Version 09	Condition	Ref.
$C_P = 15.496\left[\frac{K_1\theta^2 \exp(\theta/T)}{T_2[\exp(\theta/T)-1]^2} + 2K_2T + \frac{K_3E_D}{RT^2}\exp(-E_D/RT)\right]$ C_P : UO_2 specific heat (J/kg ・ K) K_1=19.145 (cal/mol ・ K) $K_2=7.8473\times10^{-4}$ (cal/mol ・ K^2) $K_3=5.6437\times10^6$ (cal/mol) θ=535.285 (K), E_D=37,694.6 (cal/mol) T : temperature (K), R=1.987 (cal/mol ・ K)	no restrictions	14

(13) UO_2 grain growth

Equations representing UO_2 grain growth are selected from among the following.

UO_2 grain growth Itoh (modified Ainscough)	Condition	Ref.
$\frac{dD}{dt} = K\left(\frac{1}{D} - \frac{1+E\cdot N_f / N_f^{max}}{D_m}\right)$ D : grain size at time t (μm) K : rate constant (μm^2/h) $K = 5.24\times10^7 \exp(-2.67\times10^5/RT)$ R=8.314 (J/mol ・ K), T : temperature (K) D_m : limit grain size (μm) $D_m=2.23\times10^3$ exp (−7620/T) E : fitting parameter N_f : FP gas atom density at grain boundary (atoms/cm^2) N_f^{max} : saturated value of FP gas atom density at grain boundary (atoms/cm^2)	IGRAIN = 0 (default value)	20

The fitting parameters in the case of IGRAIN=0 are as follows.

Variable name	Content	Default value
AG	Fitting parameter E	1.0
GRWF	The grain growth rate is multiplied by GRWF.	1.5

UO_2 grain growth (2) Ainscough	Condition	Ref.
$\frac{dD}{dt} = k\left(\frac{1}{D} - \frac{1+0.002B}{D_m}\right)$ D : grain size at time t (μm) t : time (h) k : rate constant (μm^2/h) $k = 5.24 \times 10^{7} \exp(-2.67 \times 10^{5} / RT)$ R=8.314 (J/mol · K) T : temperature (K) temperature range : 1,300–1,500°C B : burnup (MWd/tU)	IGRAIN=1	35
UO_2 grain growth (3) MacEwan		
$D^2 - D_0^2 = k_0 t^{0.8} \exp(-87{,}000 / RT)$ D : grain size at time t (μm) D_0 : initial grain size (μm) k_0 : constant of proportionality (k_o=3.9×10^{10}) t : time (h) R : gas constant 1.987 (cal/mol · K) T : temperature (K) temperature range : 1,555–2,440°C	IGRAIN=2	36
UO_2 grain growth (4) Lyons		
$D^3 - D_0^3 = k_0 e^{-Q/RT} \cdot t$ D : grain size at time t (μm) D_0 : initial grain size (μm) k_0 : rate constant (μm^3/h) Q : activation energy required for grain growth (cal/mol) R =1.987 (cal/mol · K) T : temperature (K) t : time (h) $K_0 = \exp(5.096 + 2.476 \times 10^{-4} \cdot Q)$ For the experimental data obtained by MacEwan, Q=119,000(cal/mol)	IGRAIN=3	37
UO_2 grain growth (5) MATPRO-Version 09		
$D^4 - D_0^4 = 6.18 \times 10^{13} e^{-92{,}400/RT} \cdot t$ D : grain size at time t (μm) D_0 : initial grain size (μm) R =1.987 (cal/mol · K) T : temperature (K) t : time (h)	IGRAIN=4	14

(14) FP gas release rate

The FP gas release rates and models are selected from among the following.

FP gas release rate (1)　mechanistic model

Refer to section 2.1.4 (2).
Fitting parameters are also explained in section 2.1.4 (2).

Condition: IGRASP=0 (default value)

Ref.:

FP gas release rate (2)　temperature-dependent model

$$f = \frac{1}{V}\sum_i a_i V_i$$

V_i : UO_2 pellet cross section is concentrically divided into regions on the basis of temperature gradient, and V_i is volume per unit length in each region.

$V = \sum_i V_i$

a_i : release rate in region i

Proposer	Data		
	i	Range	a_i
R. C. Nelson	$i=1$	>1,900°C	100%
	$=2$	1,650–1,900°C	20%
	$=3$	<1,650°C	0%
Morishima	$i=1$	>1,900°C	100%
	$=2$	1,650–1,900°C	20%
	$=3$	<1,650°C	0.5%
W. B. Lewis	$i=1$	>1,600°C	95%
	$=2$	1,300–1,600°C	60%
	$=3$	1,000–1,300°C	10%
	$=4$	<1,000°C	0.5%
G. Karsten	$i=1$	>1,700°C	95%
	$=2$	1,300–1,700°C	50%
	$=3$	<1,300°C	10%

Condition: IGASP=1 (common to all models)

(Nelson model) IGAS=1

(Morishima model) IGAS=2

(Lewis model) IGAS=3

(Karsten model) IGAS=4

Ref.: *

(15) Pellet melting point

Pellet melting point　MATPRO-Version 11

$$T_m = T_u - 5.414P + 0.007468P^2 - 0.0032Bu$$

T_m : pellet melting point (°C)
T_u : melting point of unirradiated UO_2 material (=2,800°C)
P : molar fraction of PuO_2 (%)
Bu : burnup (MWd/t)

Condition: No restrictions

Ref.: 38

2.4.2 Material properties of cladding

(1) Cladding thermal conductivity

Zircaloy thermal conductivity MATPRO-Version 09	Condition	Ref.
From room temp. to melting point $k = 7.51 + 2.09 \times 10^{-2} T - 1.45 \times 10^{-5} T^2 + 7.67 \times 10^{-9} T^3$ k : thermal conductivity (W/m ・ K) T : temperature (K)	No restrictions	14
ZrO_2 (oxide layer) thermal conductivity MATPRO-A	Condition	Ref.
$k = 0.835 + 1.81 \times 10^{-4} \cdot T$ k : ZrO_2 thermal conductivity (W/m ・ K)	No restrictions	39

(2) Zircaloy thermal expansion

Regarding thermal expansion of zircaloy, only the axial expansion value is selected from among the following options.

Zircaloy thermal expansion (1) MATPRO-Version 09	Condition	Ref.
For 27–800°C, thermal expansion in the axial direction (Subcode CATHEX): $\Delta L / L_0 = -2.506 \times 10^{-5} + 4.441 \times 10^{-6} T$. Therefore, thermal expansion coefficient is $\alpha = 4.441 \times 10^{-6}$. thermal expansion in the radial direction (Subcode CDTHEX): $\Delta D / D_0 = -2.373 \times 10^{-4} + 6.721 \times 10^{-6} T$. therefore, $\alpha = 6.721 \times 10^{-6}$. T : temperature (°C)	ICATHX=0 (default value)	14
Zircaloy thermal expansion (2) Scott		
For 21–429°C, thermal expansion in the axial direction $\Delta L / L_o = 42.53230 + 3.96753T$. (in / in) $\times 10^{-6}$ T : temperature (°C)	ICATHX=1	14

(3) Young's modulus of cladding

Young's modulus of Zircaloy Fisher	Condition	Ref.
$E = \left[9.900 \times 10^5 - 566.9 \times (T - 273.15)\right] \times 9.8067 \times 10^4$ E : Young's modulus (Pa) T : temperature (K)	No restrictions	40

(4) Poisson's ratio of cladding

Poisson's ratio of Zircaloy	Fisher	Condition	Ref.
$v = 0.3303 + 8.376 \times 10^{-5}(T - 273.15)$,	T : temperature (K)	No restrictions	40

(5) Creep of Zircaloy

Zircaloy creep (1) MATPRO-Version 09	Condition	Ref.
In-pile creep equation $\dot{\varepsilon} = K\phi(\sigma + Be^{C\sigma})\exp(-10{,}000 / RT)t^{-\frac{1}{2}}$ $\dot{\varepsilon}$: biaxial creep strain rate (m/m ・ s) $K = 5.129 \times 10^{-29}$, $B = 7.252 \times 10^{2}$ $C = 4.967 \times 10^{-8}$, $R = 1.987$ (cal/mol ・ K) T : temperature (K), t : time (s) ϕ : fast neutron flux (n/m^2 ・ s) E >1.0 MeV σ : circumferential stress (N/m^2)	CRPEQ=0	14
Zircaloy creep (2) NENANSEN	CRPEQ=1	15
In-pile creep equation for Zircaloy-4 : $\dot{\varepsilon}^c = \dot{\varepsilon}^c_{th} + \dot{\varepsilon}^c_{irr}$ (1/hr) 1) thermal creep rate: setting thermal creep strain as $\varepsilon^c_{th} = K \cdot t^m$, we have the creep rate as: $\dot{\varepsilon}^c_{th} = mK^{\frac{1}{m}} \varepsilon_H^{(1-\frac{1}{m})}$ where $\varepsilon_H (= \varepsilon^c_{th}) = \sum_{k=1}^{n} \dot{\varepsilon}^c_{th,k} \cdot \Delta t_k$: thermal creep strain by the previous time step(n-1) $K = \exp\{-13.3 + (-0.416 + 8.22 \times 10^{-4} T)\sigma_{eq} + 6.59 \times 10^{-3} T\}$ $m = -1.07 + (-0.00343 + 7.27 \times 10^{-5} T)\sigma_{eq} + 1.95 \times 10^{-3} T$ σ_{eq} :equivalent stress (kgf/mm^2) T :temperature (K) 2) irradiation creep rate : (ref. source is unknown) $\dot{\varepsilon}^c_{irr} = 6.64 \times 10^{-25} \phi^{1.23} \sigma_{eq}^{1.34}$ ϕ :fast neutron flux (n/cm^{2}s)		

The following fitting parameters are used for the zircaloy creep equation.

Variable name	Content	Default value
CRFAC	For SR material, the creep strain rate is multiplied by CRFAC.	1.3
IPUGH	PUGH=0: inversion of *Pugh* is not taken into account PUGH=1: inversion of *Pugh* is taken into account	0

Here, *Pugh's* method of cladding creep inversion caused by stress reversal is explained.

When the direction of stress is reversed during creep, the primary creep occurs again. Pugh proposed a simplified method to simulate this phenomenon[41]. An outline of Pugh's method is given as follows.

1) The creep hardening is represented by $\bar{\varepsilon}^H$, and

$$\{\dot{\varepsilon}_c\} = \left\{\frac{\partial\bar{\sigma}}{\partial\sigma}\right\} f\left(\bar{\sigma}, \bar{\varepsilon}^H, T\right). \tag{2.4.11}$$

2) At the time of the first stress inversion, $\bar{\varepsilon}^H > \hat{\varepsilon}$ and

$$\hat{\varepsilon} = \varepsilon_H, \quad \bar{\varepsilon}^H = 0 \tag{2.4.12}$$

is set.

3) At the time of the second or later inversions,
when $\bar{\varepsilon}^H \geq \hat{\varepsilon}$, then $\hat{\varepsilon} = \bar{\varepsilon}^H = 0$, $\bar{\varepsilon}^H = 0$ is set, and

when $\bar{\varepsilon}^H < \hat{\varepsilon}$, then $\bar{\varepsilon}^H = \hat{\varepsilon} - \bar{\varepsilon}^H$ is set.

Figure 2.36 shows the above states.

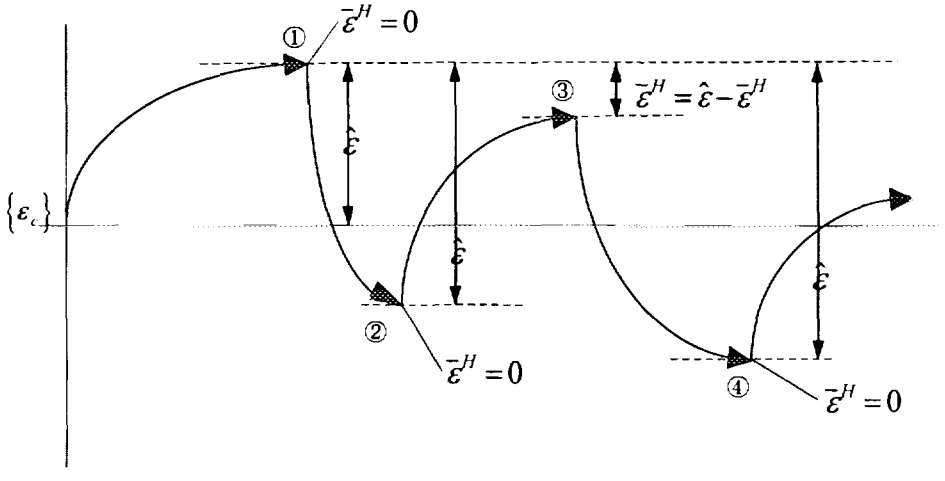

Fig. 2.43 Inversion of creep strain due to stress inversion.

Here, the stress inversion is judged as follows. Since the equation for the creep is

$$\{\dot{\varepsilon}_c\} = \left\{\frac{\partial\bar{\sigma}}{\partial\sigma}\right\} f\left(\bar{\sigma}, \bar{\varepsilon}^H, T\right), \; f \geq 0, \tag{2.4.13}$$

whether or not the sign of $\{\dot{\varepsilon}_c\}$ is reversed between the previous time step and the current time step is used for the judgment. In a multi-axial state, the judgment of sign reversal is performed using a scalar product of the component of $\{\dot{\varepsilon}_c\}$.

(6) Zircaloy plasticity

Zircaloy strain-hardening curve FEMAXI=III	Condition	Ref.
$\sigma = K\varepsilon^n$ σ : true stress (kg/mm^2), ε : true strain n : strain-hardening exponent $K = K_{0.2\%}(\frac{\sigma_y}{E} + 0.002)^{-n}$ $K_{0.2\%} = \sigma_y + 33.44(1 - \exp(-B\phi t))^{\frac{1}{2}}$ (kg/mm^2) $B = 2.92 \times 10^{-21} \exp(1 - 1.6 \times 10^{-14}\phi)$ ϕ : fast neutron flux (n/cm^2 ・ s) E >1 MeV σ_y =yield stress (kg/mm^2) =21.60–0.0213 ・ T (recrystallized material) =31.32–0.0213 ・ T (stress-relieved material) n=0.0504+0.0001435 ・ T T : temperature (°C) $220 \le T \le 450$ °C	No restrictions	2

The following parameter is used for the Zircaloy strain-hardening curve.

Variable name	Content	Default value
ISTR	In the case of ISTR $\neq 0$, $K = \sigma_y + 33.44$ is set.	0

(7) Zircaloy irradiation growth

The equation representing Zircaloy irradiation growth is selected from among the following.

Zircaloy irradiation growth (1) MATPRO-Version 09	Condition	Ref.
$\frac{\Delta L}{L} = A[\exp(240.8/T)][\phi t]^{1/2}[1 - 3f_Z][1 + 2.0CW]$ $\frac{\Delta L}{L}$: irradiation growth (–) $A = 1.407 \times 10^{-16}$ (n/m^2)$^{-1/2}$ T : temperature (K) ϕt : fast neutron fluence (n/m^2) (E >1 MeV) f_z : factor in the axial direction CW : cold work	ICAGRW=1	14

The following parameters are used in the case of ICAGRW=1.

Variable name	Content	Default value
CATEXF	Factor in the axial direction f_z	0.05
COLDW	Cold work CW	0.81

Zircaloy irradiation growth (2) Manzel	Condition	Ref.
$\frac{\Delta L}{L_0} = 0.1\left(\phi \cdot t / 10^{21}\right)^n$ $\frac{\Delta L}{L_0}$: irradiation growth (%) $\phi \cdot t$: fast neutron fluence (n/cm^2) n : constant between 0.65–0.67 (0.66 is used)	ICAGRW=2	*
Zircaloy irradiation growth (3) Hanerz		
$\left(\frac{\Delta L}{L_o}\right)\perp c = 6 \times 10^{-12}\left(\phi t\right)^{0.4}$ $\left(\frac{\Delta L}{L_o}\right)\perp c$: growth of single crystal in the direction perpendicular to the C axis. (–) $\phi \cdot t$: fast neutron fluence (n/cm^2)	ICAGRW=3	*
Zircaloy irradiation growth (4) Hesketh	Condition	Ref.
$\frac{\Delta L}{L_o} = A \cdot \sqrt{\phi \cdot t}$ $\frac{\Delta L}{L_o}$: irradiation growth (–) $\phi \cdot t$: fast neutron fluence (n/cm^2) A : fitting constant $\left(= 5 \times 10^{-14}\right)$	ICAGRW=4	42

(8) Zircaloy specific heat

Zircaloy specific heat MATPRO-Version 09	Condition	Ref.
$Cp = 245.11 + 0.15558T - 3.3414 \times 10^{-5} T^2$ Cp : specific heat (J/kg・K) T : temperature (K) (300-1090K)	No restrictions	14

(9) Zircaloy density

Zircaloy density MATPRO-Version 09	Condition	Ref.
$\rho = 6.55$ (g/cm^3)	No restrictions	14

(10) Zircaloy cladding corrosion

Cladding corrosion rate　　EPRI	Condition	Ref.
Pre-transition corrosion rate : $dS/dt = \left(A/S^2\right)\exp\left(-Q_1/RT\right)$ Post-transition corrosion rate : $dS/dt = C\exp\left(-Q_2/RT\right)$, $C = C0 + U\left(M\phi\right)^P$ Oxide layer thickness at transition : $D\exp\left(-Q_3/RT - ET\right)$ dS/dt : corrosion rate (μm/day) S : oxide layer thickness (μm) T : temperature at oxide-metal interface (K) ϕ : fast neutron flux (n/cm^{2}s) R : gas constant (1.987 cal/mol・K) $A = 6.3\times10^9$ (μm^3/day)　$Q_1 = 32289$ (cal/mol) $C_0 = 8.04\times10^7$ (μm/day)　$U = 2.59\times10^8$ (μm/day) $M = 7.46\times10^{-15}$ (cm^{2}s/n)　P = 0.24 $Q_2 = 27354$ (cal/mol)　$D = 2.14\times10^7$ (μm) $Q_3 = 10763$ (cal/mol)　$E = 1.17\times10^{-2}$ (K^{-1})	ICOPRO=1	43

2.4.3 Other material properties

(1) Gap thermal conduction

The gap conductance model is selected from among the following.

Gap conductance (1) Ross and Stoute	Condition	Ref.
Refer to section 2.1.2. Here, thermal conductivities of helium, nitrogen, krypton and xenon are as follows:(MAPRO-Version 09) $K_{He} = 3.366 \times 10^{-3} T^{0.668}$ $K_{N_2} = 2.091 \times 10^{-3} T^{0.846}$ $K_{Kr} = 4.726 \times 10^{-5} T^{0.923}$ $K_{Xe} = 3.366 \times 10^{-5} T^{0.872}$ K : thermal conductivity (W/m ・ K) T : temperature (K)	IGAPCN=0 (default value)	13
Gap conductance (2) MATPRO-Version 09		
$h_{gap} = (1 - F)h_0 + Fh_c$ h_{gap} : gap conductance (W/m^2 ・ K) h_0 : non-contact gap conductance (W/m^2 ・ K) h_c : contact gap conductance (W/m^2 ・ K) F : circumference ratio of pellet-cladding contact part $h_0 = \frac{K_{mix}}{\Delta r + \delta}$ K_{mix} : thermal conductivity of mixed gas (W/m ・ K) →auxiliary material property 1 δ : rms surface roughness of pellet and cladding (m) $\delta = 4.4 \times 10^{-6}$ Δr : hot gap width (m) $h_c = 5 \times 10^{-4} \cdot P^n + \frac{K_{mix}}{\delta}$ P : contact pressure between pellet and cladding (N/m^2) when F<1, P=0 when 0<P<1,000 psi, n=1 when P>1,000 psi, n=0.5 $F = \frac{1}{a_1\left(\frac{\Delta r \cdot 100}{R_F}\right)^{a_2} + 1.429} + 0.3$ R_F : pellet hot diameter (m) a_1, a_2 : constant depending on burnup (x)	IGAPCN=1	14

when x>600MWd/t-U,

$$a_1 = 100 - 98F'$$

$$a_2 = 4 - 0.5F'$$

$$F' = 1 - \frac{1}{\left(\frac{x-600}{1000}\right)^4 + 1}$$

when $x \le 600$ MWd/t-U,

$$a_1 = 100$$

$$a_2 = 4$$

Gap conductance (3) Ross and Stoute

$$h_{gap} = h_g + h_s$$

h_{gap} : gap conductance (W/cm ・ °C)

h_g : non-contact gap conductance (W/cm^2 ・ °C)

h_s : contact gap conductance (W/cm^2 ・ °C)

$$h_g = \frac{K_g}{C(R_1 + R_2) + (g_1 + g_2) + \Delta r}$$

IGAPCN=2 13

K_g : gap gas thermal conductivity (W/cm^2 ・ °C)

He : 0.0021, Ar : 0.00029, Kr : 0.0001

C : constant for contact pressure

$C = 2.5$ for 100 kgf/cm^2

$C = 1.5$ for 500 kgf/cm^2

R_1 and R_2 : surface roughness of pellet and cladding (cm)

g_1 and g_2 : temperature jump distance (cm)

He : 10×10^{-4}, Ar : 5×10^{-4}, Kr : 1×10^{-4}

Xe : $< 1 \times 10^{-4}$ (value of $g_1 + g_2$)

Δr : hot gap width (cm)

$$h_s = \frac{K_m \cdot P}{a \cdot H}$$

$$K_m = \frac{2K_1 \cdot K_2}{K_1 + K_2}$$

$$P = \frac{2t \cdot Ys}{ID}$$

$$a = a_0 \sqrt{R}$$

$$R = \sqrt{\frac{1}{2}\left(R_1^2 + R_2^2\right)}$$

K_1 and K_2 : thermal conductivities of pellet and cladding (W/cm ・ °C)

$$\left.\begin{array}{l} K_1 = 0.038 \\ K_2 = 0.14 \end{array}\right\} K_m = 0.05977$$

P : contact pressure (kgf/cm^2) t : cladding thickness (cm) ID : cladding inner diameter (cm) Ys : cladding yield stress (Ys = 1,980 kgf/cm^2) a : average radius of contact part (cm) $a_0 = 0.5$ cm$^{1/2}$ H : Meyer's hardness of soft side (kg/cm^2), H=3 ・ Ys		
Gap conductance (4) Dean $h_{gap} = h_s + h_g$ h_{gap} : gap conductance (Btu/h ・ ft^2 ・ °F) h_g : non-contact gap conductance (Btu/h ・ ft^2 ・ °F) h_s : contact gap conductance (Btu/h ・ ft^2 ・ °F) $h_s = 280 \cdot \frac{P}{M_2} \cdot \frac{K_1 \cdot K_2}{K_1 + K_2} \cdot \left(\frac{1}{\lambda_1 \cdot \lambda_2}\right)^{1/2}$ P : contact pressure (psi) P=267–675psi (18.6–45.7 kgf/cm^2) M_2 : Meyer's hardness of zircaloy (psi) M_2=120,000psi (84.4kg/cm^2) K_1 and K_2 : thermal conductivities of pellet and cladding K_1 = 2.20 Btu/h ・ ft^2 ・ °F (0.038 W/cm^2 ・ °C) K_2 = 8.09 Btu/h ・ ft^2 ・ °F (0.14 W/cm^2 ・ °C) λ_1 and λ_2 : wavelengths of surface profile of pellet and cladding (inch) $\lambda_1 \cdot \lambda_2 \sim RUO_2$ R_{Zr} (roughness) $= 50^{+10}_{-5} \times 10^{-6} rms(in)$ $h_g = \frac{K_g}{0.52 \cdot \delta}$ K_g : gap gas thermal conductivity (Btu/h ・ ft^2 ・ °F) Ar : 0.0168, He : 0.139, FP : 0.0088 δ : gap between pellet and cladding (ft) $\delta \sim Ruo_2$ modified Dean's equation: $h_s = 0.6P$, $h_g = \frac{K_g}{\delta + 14.4 \times 10^{-6}}$	IGAPCN=3	*

The following fitting parameter is used in the case of IGAPCN=0 or 2.

Variable name	Contents	Default value
R1	Pellet surface roughness (μm)	1.0

(2) Cladding surface heat transfer

Cladding surface heat transfer (1) Jens-Lottes	Condition	Ref.
Used for the two-phase state. $h_W = 0.1263 \cdot \exp\left(\frac{P_W}{6.201 \times 10^6}\right) q_s^{0.75}$ h_W : surface heat transfer coefficient (W/cm^2 ・ K) P_W : coolant pressure (N/m^2) q_s : heat flux of cladding outer surface (W/cm^2)	No restrictions	11
Cladding surface heat transfer (2) Dittus-Boelter		
Used for the subcool state: $h_W = 0.023 \frac{k}{De}\left(\frac{DeV\rho}{\mu}\right)^{0.2} \cdot (p_r)^{0.4}$ h_W : surface heat transfer coefficient (W/m^2 ・ K) k : coolant thermal conductivity (W/m^2 ・ K) De : equivalent diameter (m) V : coolant velocity (m/s) ρ : coolant density (kg/m^3) μ : coolant viscosity (kg/m ・ s) p_r : Prandtl number	No restrictions	10

The following fitting parameter is used for cladding surface heat transfer.

Variable name	Content	Default value
AKFAC	Cladding surface heat transfer coefficient is multiplied by AKFAC.	1.0

(3) FP gas diffusion constant

FP gas diffusion constant　　Turnbull	Condition	Ref.
$D = 7.6 \times 10^{-10} \exp\left(-7 \times 10^4 / RT\right) + S^2 j\upsilon V \div 2 \times 10^{-40} F$ (m²/s) R : gas constant =1.987 (cal/mol/K) T : temperature (K) S : atom jump distance $= \Omega^{\frac{2}{3}}$ Ω : atom volume $= 4.09 \times 10^{-29}$ (m³) $j\upsilon = 10^{13} \exp\left(-5.52 \times 10^4 / RT\right)$ $V = \frac{\left(\partial_s S^2 + ZV_o\right)}{2Z}\left[\left(1 + \frac{4K'Z}{j\upsilon\left(\partial_s S^2 + ZV_o\right)^2}\right)^{\frac{1}{2}} - 1\right]$ $\partial_s = 10^{15}$ (m⁻², sink intensity) $Z = 2$ (number of lost points) $K' = 10^4$ (loss ratio per atom) $V_0 = \exp\left(-5.52 \times 10^4 / RT\right)$ $F = 10^{19}$ (fissions/m³ ・ s, fission rate)	IGASP=0	19

(4) He-Xe gas counter diffusion constant

He-Xe gas counter diffusion constant　　Present	Condition	Ref.
$D^{12} = \frac{3}{8}\left(\frac{\pi kT}{2m^*}\right)^{\frac{1}{2}} \frac{1}{n\pi d_{12}^2}$ (m²/s) $m^* = \frac{m_1 m_2}{m_1 + m_2}$ (m : weight of 1 molecule) $d_{12} = \frac{1}{2}\left(d_1 + d_2\right)$ (d : diameter of molecule) $= 3.45 \times 10^{-10}$ (m) $n = n_1 + n_2$ (molecular density) k : Boltzmann's constant $\left(= 1.380 \times 10^{-16} \text{erg} / \text{K}\right)$ T : temperature (K)	No restrictions	21

References

(1) Nakajima T., FEMAXI-IV:A Computer Code for the Analysis of Fuel Rod Behavior under Transient Conditions, Nucl. Eng. Design 88, p.69-84 (1985)

(2) Nakajima T., Ichikawa M., et al., FEMAXI-III : A Computer Code for the Analysis of Thermal and Mechanical Behavior of Fuel Rods, JAERI 1298 (1985)

(3) Nakajima T. and Saito H., A Comparison between Fission Gas Release Data and FEMAXI-IV Code Calculations , Nucl. Eng. Design 101, p.267-279 (1987)

(4) Nakajima T., Saito H. and Osaka T., Analysis of Fission Gas Release from UO2 Fuel during Power Transients by FEMAXI-IV Code, IWGFPT-27.259, p.140-162 (1987)

(5) Nakajima T. and Ki-Seob Sim, Analysis of Fuel Behavior in Power-Ramp Tests by FEMAXI-IV Code, Res Mechanica 25, p.101-128 (1988)

(6) Uchida M., Benchmarking of FEMAXI-IV Code with Fuel Irradiation Data in Power Reactors, JAERI-M 90-002 (1990)

(7) Nakajima T., Saito H., and Osaka T., FEMAXI-IV:A Computer Code for the Analysis of Thermal and Mechanical Behavior of Light Water Reactor Fuel Rods, Trans.11th Int. Conf. on SMIRT (Tokyo, Japan), 6297 PV.C-D, p.1-6 (1991)

(8) Nakajima T., Saito H., and Osaka T., FEMAXI-IV:A Computer Code for the Analysis of Thermal and Mechanical Behavior of Light Water Reactor Fuel Rods, Nucl. Eng. Design 148, p.41-52 (1994)

(9) High Burnup Effects Data Review Committee, Summary of Battelle High Burnup Effects Program Task 3, Central Research Institute of Electric Power Inc., T90802 (1990)

(10) Dittus F.W. and Boelter L.M.K., Univ. Calif. Pubs. Eng.2, 443 (1930)

(11) Jens W.H. and Lottes P.A., Analysis of Heat Transfer, Burnout, Pressure Drop and Density Data for High Pressure Water, ANL-4627 (1951)

(12) Robertson J.A.L., $\int k d\theta$ in Fuel Irradiation, CRFD-835 (1959)

(13) Ross A.M. and Stoute R.L., Heat Transfer Coefficient between UO_2 and Zircaloy-2, CRFD-1075 (1962)

(14) MATPRO-09, A Handbook of Materials Properties for Use in the Analysis of Light Water Reactor Fuel Rod Behavior, USNRC TREE NUREG-1005 (1976)

(15) NENANSEN committee, Study on the Non-Elastic Properties of Zircaloy Cladding, Nuclear Safety Research Association Inc. Foundation (1986)

(16) Speight M.V., A Calculation on the Migration of Fission Gas in Material Exhibiting Precipitation and Re-solution of Gas Atoms under Irradiation, Nucl. Sci. Eng. 37, 180 (1969)

(17) White R.J. and Tucker M.O., A New Fission Gas Release Model, J. Nucl. Mater., 118 (1983) 1-38

(18) Ham F.S., J. Phys. Chem. Solids 6, 335 (1958)

(19) Turnbull J.A., Friskney C.A., et al., The Diffusion Coefficients of Gaseous and Volatile Species during the Irradiation of Uranium Dioxide, J. Nucl. Mater., 107 (1982) 168-184

(20) Itoh K., Iwasaki R. and Iwano Y., Finite Element Model for Analysis of Fission Gas Release from UO_2 Fuel, J.Nucl.Sci.Technol., 22, pp.129-138 (1985)

(21) Present R.D., Kinetic Theory of Gases, Mc-Graw Hill, N.Y. p.55 (1958)

(22) Rashid Y.R.,Tang H.R. and Johansson E.B., Mathematical Treatment of Hot Pressing of Reactor Fuel, Nucl. Eng. Des. 29, pp.1-6 (1974)

(23) Washington A.B.G., Preferred Values for the Thermal Conductivity of Sintered Ceramic Fuel for Fast Reactor Use, UKAEA TRG 2236(D) (1973)

(24) Ishimoto S., Hirai M., Ito K., Korey Y., J. Nucl. Sci. Technol., 31, 796-802 (1994)

(25) Wiesenack W., et al., HWR-469 (1996)

(26) Forsberg K., Lindstrom F. and Massih A.R., Modelling of Some High Burnup Phenomena in Nuclear Fuel, IAEA Technical Committee Meeting, England, Sept.1994

(27) Kjaer-Pedersen N., Rim Effect Observations from the Third Riso Fission Gas Project, Fission Release and Fuel Rod Chemistry Related to Extended Burnup, IAEA -TECDOC-697 (1993)

(28) Martin D.G., A Re-Appraisal of the Thermal Conductivity of UO_2 and Mixed(U,Pu) Oxide Fuels, J. Nucl. Mater., 110, pp.73-94 (1982)

(29) Fukushima S., Ohmichi T., Maeda A., and Watanabe H., The Effect of Gadolinium Content on the Thermal Conductivity of Near-Stoichiometric $(U,Gd)O_2$ Solid Solutions, ibid. 105, pp.201-210 (1982)

(30) Chubb W., Storhok V.W. and Keller D.L., Factors Affecting the Swelling of Nuclear Fuel at High Temperatures, Nucl. Technol. 18, pp.231-255 (1973)

(31) Rolstad E. et al., Enlarged HPG Meeting, No.1/5/HPR-188 (1074)

(32) USNRC, WASH-1236 (1972).

(33) Marlowe M.O., Predicting In-Reactor Densification Behavior of UO_2, Trans. ANS 17, 166 (1974)

(34) Tachibana T., Furuya H. and Koizumi M., Dependence on Strain Rate and Temperature Shown by Yield Stress of Uranium Dioxide, J. Nucl. Sci. Technol., 13, pp.497-502 (1976)

(35) Ainscough J.B., Oldfield B.W., and Ware J.O., Isothermal Grain Growth Kinetics in Sintered UO2 Pellets, ibid.49, 117-128 (1973/74)

(36) MacEwan J.R., Grain Growth in Sintered Uranium Dioxide:I, Equiaxed Grain Growth, J. Am. Cer. Soc. 45, 37 (1962)

(37) Lyons M.F., Boyle R.F., Davis J.H., Hazel V.E., and Rowland T.C., Nucl. Eng. Design 21, 167 (1972)

(38) Hagrman D.L. and Reyman G.A., MATPRO-Version11, NUREG/CR-0497 (1979)

(39) SCDAP/RELAP5/MOD2 Code Manual, Vol.4: MATPRO-A, A Library of Materials Properties for Light-Water-Reactor Accident Analysis, NUREG/CR-5273 (1990)

(40) Fisher E.F. and Renken C.J., Single-Crystal Elastic Moduli and the hcp-bcc Transformation in Ti, Zr, and Hf, Phys. Rev. pp.A482-A494 (1954)

(41) Pugh, Current Recommended Constitution Equations for Inelastic Analysis of FFTF Components, ORNL-TM-3602 (1972)

(42) Hesketh R.V., Non-linear Growth in Zircaloy-4, J. Nucl. Mater. 30 (1969) 217-222

(43) Gazarolli F., Garde A.M. et al., Waterside Corrosion of Zircaloy Fuel Rods, EPRI-NP 2789 (1982)

(44) Kosaka Y., Thermal Conductivity Degradation Analysis of the Ultra High Burnup Experiment (IFA-562), HWR-341 (1993)

Appendices

A1 Input Manual

A2 Input Manual for Plotter

A3 (1) Subroutine List

(2) Subroutine Tree

A4 Sample Input/Output List

A1 Input Manual

Card No.	SYMBOL (FORMAT)	
1	MTITL(I), I = 1,20 (20A4)	Free title
2	¥INPUT ¥END (2～80 columns)	Free parameter
	Calculation parameter is designated by "Name List".	
3	NAX, IFEM1, IPLANT (3I10)	Fuel rod specifications
	NAX = number of axial segments (1≤NAX≤12) IFEM = the objective segment number (1 ≤ IFEM1 ≤ NAX) IPLANT = 1 ····· in the case of Halden reactor (BWR) = 2 ····· in the case of other BWR = 3 ····· in the case of PWR	
4	MRASA, CDIN, CDOUT (I10, 2F10.0)	Cladding specifications
	MRASA = 0 ····· RA material = 1 ····· SR material CDIN = cladding inner diameter (cm) CDOUT = cladding outer diameter (cm)	
5	The number of NAX required (I = 1, NAX) IDISH(I), ICHAM(I), PDIN(I), PDIA(I), PLENG(I), ENR(I), FDENI(I), DZ(I) (2I10,6F10.0)	Pellet specifications
	Number of radial ring elements of a pellet is fixed at 5 in local mechanical analysis, and at 10 in entire rod length mechanical analysis. IDISH(I) = 0 ····· pellet without dish = 1 ····· pellet with dish on only one side = 2 ····· pellet with one dish each side ICHAM(I) = 0 ····· pellet without chamfer = 1 ····· pellet with chamfer PDIN (I) = pellet center hole diameter (cm) PDIA (I) = pellet diameter (cm) PLENG(I) = length of one pellet (cm) ENR (I) = U-235 enrichment (–) FDENI(I) = pellet theoretical density ratio (–) DZ (I) = axial segment length (cm)	
6	Input only when IDISH = 1 or 2 DISH, DEPTH, DISHB (3F10.0)	Dish specifications
	DISH = dish diameter (cm) DEPTH = dish depth (cm) DISHB = dish bottom diameter (cm)	
7	Input only when ICHAM = 1 CHAMR, CHAMZ (2F10.0)	Chamfer specifications
	CHAMR = chamfer width (cm) CHAMZ = chamfer depth (cm)	
8	PLENUM(2), GPIN, (GMIXO(I), I=1,4), PWEIT, PLENUM(1) (8F10.0)	Plenum specifications
	PLENUM(2) = upper plenum volume (cm^3) GPIN = initial gas pressure (MPa) GMIXO(I) = initial gas composition (–) i = 1 ··· He, i = 2 ··· N_2, i = 3 ··· Kr, i = 4 ··· Xe PWEIT = pellet total weight (g) PLENUM(1) = lower plenum volume (cm^3)	

Card No.	SYMBOL (FORMAT)	
9	NHIST (I10)	History point number
	Input NHIST > 1 NIST sets consisting of cards 10 and 11 are input.	
10	A1, B1, A2, A5, A3, A4, IT, IP, IS, A6 (6F10, 3I5, F5.0)	History point data
	A1 = time (Hour) B1 = burnup (MWd/tUO_2) (IBUNP = 0) MWd/tU (IBUNP = 1) GJ/kgU (IBUNP = 2) A2 = linear heat rate (W/cm) A5 = fast neutron flux (n/cm^2-s) A3 = coolant temperature (K) A4 = coolant pressure (MPa) IT = 0: time (or burnup) represents the increment from the time step set at IT=−100 (when IT= −100 is not set, it represents the time (or burnup) elapsed from the initial time). = −100 time increment from the previous time step (or burnup increment) = 100 cancellation of the IT= −100 setting (time or burnup represents the time (or burnup) that elapsed from the initial time). IP = 0 history point without output, = 1 history point with output IS = 0 no gas flow calculation: instantaneous mixing, = 1 gas flow calculation; gives Δt_2 restriction (see 2.1.6) A6 = coolant velocity (m/s) (ICLMAS=0), coolant mass flow rate (kg/cm^2s) (ICLMAS=1). Here, either A1 (time) or B1 (burnup) is designated. If both are designated, B1 is neglected. Also, input of IS is not necessary, since it is automatically set in the program when IAUTO = 1.	
11	(RH(I), I = 1, 12), II (12F5.0, 15)	Relative power profile in the axial direction
	RH(I) = relative power of axial segment j (−) (number of data: NAX) II = number of history points at which similar relative power is input. When II is designated as 2 or higher, card 11 is omitted for the input of later time step II-1.	
12	BU, (RRH(I), I=1, 10) (F10.0, 10F5.0)	Relative power profile in the radial direction
	Input only when IFLX>0 BU = burnup (unit is similar to that in card 10) RRH(I) = relative power profile of concentric ring element I (−) The input number is designated by IFLX in NAMELIST.	
13	IEND (A4)	End-of-input card
	Input "STOP".	

Variables set by NAMELIST I

Variable name	Content	Default value
	Input option	
IBUNP	Designation of unit of burnup (= 0: MWd/tUO$_2$, = 1: MWd/tU, = 2: GJ/kgU)	0
IDAY	Designation of unit of time (= 0: hr, = 1: day)	0
IFLX	Number of power history points to designate the radial power profile (= 0: Robertson model)	0
IRH	Interpolation option of axial power profile (= 0: the profile at omitted input points is the same as that in the previous stage, = 1: linear interpolation in terms of burnup is performed for omitted input points)	0
PWCHG	Input heat generation rate is multiplied by (1+PWCHG).	0.0
FAIW	Fast neutron flux per unit W/cm (n/cm^2-s/W/cm) (Fast neutron flux data can be omitted if power history data is input)	0.0
BSBUNP	Initial burnup at the start of calculation (MWd/tUO$_2$)	0.0
ICLMAS	Coolant unit option: (=0: flow rate is input in velocity (m/s), =1: flow rate is input in mass flow rate (kg/cm^{2}s))	0
	Calculation option	
IFEMRD	Calculation option (= 0: local mechanical analysis (II), = 1: entire-length fuel rod mechanical analysis (I))	
INPCK	Input check option (= 0: normal calculation, = 1: input check only)	0
ICK1	Temperature calculation option (= 0: normal calculation, = 1: temperature calculation only)	0
ICHI	Elasticity calculation (= 0: normal calculation, = 1: elasticity calculation only)	0
MPP	FP release calculation option (= 0: normal calculation, = 1: no calculation at points at which axial power profile does not change)	0
TLIM	Truncation control of CPU time (When the execution time reaches TLIM (s), the calculation is terminated.)	20000.0
	Time step control	
IAUTO	Automatic time step control option IAUTO=0: designation of IS input is effective for each input history point. IAUTO=1: 'IS=1' is automatically designated for all input history points.	1
DPXX	Power increment width per unit time step (W/cm)	10.0
DPBU	Burnup increment width per unit time step (MWd/tUO$_2$)	500
IPH	When DPXX and DPBU control is performed at the objective segment (IFEM), IPH = 0; when it is at the segment with max. power, IPH = 1.	0
EFCOEF	Time step width determination factor due to creep $\Delta t = \frac{\bar{\sigma}}{E \cdot \dot{\bar{\varepsilon}}_c} \cdot \mathrm{EFCOEF}$, where $\bar{\sigma}$ is equivalent stress, E is Young's modulus and $\dot{\bar{\varepsilon}}_c$ is equivalent creep strain rate.	1.0
LCMAX	Maximum number of judgments of clogged or sliding state of the contact between pellet and cladding.	3
LMAX	Number of iterations in the Newton-Raphson method for deformation calculation	2
ITIMY	Time step control option for elasicity/plasticity judgment (= −1: without time step control, = 0: time step control is performed only upon the removal of load, = 1: with time step control)	−1

Variables set by NAMELIST 2

Variable name	Content	Default value
	Calculation condition	
AY	Tilting of the pellet upper surface; in the case of dished pellet, AY=0 (cm)	0.002
TROOM	Room temperature, or fuel rod initial temperature (K)	291.15
ITIME	Option to change the plenum gas pressure (input the history point number)	3*0
GASPRN	Plenum gas pressure at history point of ITIME (MPa)	3*0.0
PLENM	Plenum volume at history point of ITIME (cm^3)	3*0.0
GMIXN	Gas composition at history point of ITIME (–) (1:He, 2:N_2, 3:Kr, 4:Xe)	12*0.0
GAPLK	Minimum gap width at which axial force is generated (μm)	3.0
XKSU	Upper plenum spring constant (N/m)	1500.0
ALSU	Upper plenum spring thermal expansion coefficient (1/K)	1.5×10^{-5}
XKSL	Lower plenum spring constant (N/m)	2500.0
ALSL	Lower plenum spring thermal expansion coefficient (1/K)	1.5×10^{-5}
AMU	Friction coefficient between pellet and cladding	0.4
DE	Equivalent diameter of coolant channel (cm)	0.0
FAREA	Cross sectional area of coolant channel (cm^2)	0.0
PITCH	Pitch between fuel rods (cm)	1.3
	Thermal conductivity option	
IPTHCN	Option for equation of pellet thermal conductivity (=1: MATPRO-09, =2: Washington, =3: Hirai, =4: Halden, =5: Modified Hirai(EXBURN), =6: Forsberg, =7: Kjaer-Pedersen)	0
MOX	When MOX=1 is set, Martin's thermal conductivity equation for MOX fuel is used.	0
PU	PuO_2 weight ratio (–)	0.0
Y	Value of y in MO_{2-y}	0.0
IGD	When IGD = 1 is set, Fukushima's thermal conductivity equation that includes the effect of gadolinia is used.	0
GD	Gd_2O_3 concentration (wt. frac.)	0.0
	Thermal expansion option	
IPTHEX	Option for equation representing material properties of pellet thermal expansion. = 0 or = 1: MATPRO-09, = 2: Burdick, = 3: Halden, = 4: Conway	0
ICATHX	Option for equation representing material properties of cladding thermal expansion. = 0: MATPRO-09, = 1: Scott	0
DTPL	Temperature difference between plenum and coolant temperature (K)	25.0
	Creep option	
FCRFAC	Magnification factor for pellet creep equation (deformation model)	10.0
TCS	Cut-off value of temperature in pellet creep calculation (deformation model) (K)	2073.15
TCRMX	Cut-off value of temperature in pellet creep calculation (thermal model) (K)	1773.15
CRFAC	Magnification factor for cladding creep rate (deformation model)	1.0 (RA material) 1.3 (SR material)
TCCRC	Magnification factor for cladding creep rate (thermal model)	1.0
FAIMAX	Upper limit value of fast neutron flux for calculation of cladding creep rate (n/cm^2s)	10^{14}
CRPEQ	Option for creep equation of cladding; =0:MATPRO-09, =1: NENANSEN equation for Zircaloy-4.	0

Variables set by NAMELIST 3

Variable name	Content	Default value
IPUGH	IPUGH=1 is set when Pugh's method is adopted in the cladding creep calculation	0
	Pellet crack and relocation option	
XRELOC	Relocation parameter (thermal model)	0.2
FRELOC	Relocation parameter (deformation model)	0.5
EPSRLZ	Relocation strain in the axial direction (deformation model)	0.003
FACR	When the gap is filled by the amount of relocation strain multiplied by FACR in the radial direction, stiffness of pellet is recovered (deformation model)	1.0
FACZ	When the gap is filled by the amount of relocation strain multiplied by FACR in the axial direction, stiffness of pellet is recovered (deformation model)	1.0
BUMIN	Burnup at which transfer of pellet relocation strain from the circumferential direction to the radial direction begins (MWd/tU) (thermal model)	0.0
BUMAX	Burnup at which transfer of pellet relocation strain from the circumferential direction to the radial direction is completed (MWd/tU) (thermal model)	0.0
IURS	Option for pellet stiffness recovery model in thermal model. IURS = 0: ε_R = relocation strain, IURS =1: ε_R = relocation strain + gas bubble swelling strain + creep strain	0
IYNG	Pellet crack model option (= 0: stiffness recovery follows a quadratic function, = 1: stiffness recovery follows a linear function) (deformation model)	1
ECRAC3	Pellet stiffness when completely cracked (Pa) (deformation model)	2×10^9
EFAC	Magnification factor for pellet Young's modulus	1.0
	Pellet densification option	
IDENSF	Option for equation of pellet densification = 0: FEMAXI-III, = 1: Rolstad, = 2: NRC, = 3: Marlowe, =4:Halden	0
DMAX	(Used when IDENSF = 0, 2 or 3) Maximum rate of volume shrinkage due to densification (%)	1.0
SBU	(Used when IDENSF = 0) Burnup at which 90% of densification is completed (MWd/tUO_2)	2500
TDNSF	(Used when IDENSF = 1 or 3) Sintering temperature (K)	2000
GG	(Used when IDENSF = 3) Crystal grain size after heat treatment (m)	10^{-5}
GG0	(Used when IDENSF = 3) Initial crystal grain size (m)	8×10^{-6}
SITIM	(Used when IDENSF = 3) Heat treatment time (hr)	24.0
	Pellet swelling option	
IFSWEL	Option for equation of pellet swelling = 0: Chubb, = 1: Speight, = 2: MATPRO-09, =3:Halden	0
STFCP	(Used when IFSWEL = 0) Contact pressure at which gas bubble swelling does not occur (Pa) (deformation model)	-3×10^7
SPCON	(Used when IFSWEL = 0) Contact pressure at which gas bubble swelling does not occur (Pa) (thermal model)	-10^6
FACP	(Used when IFSWEL = 1) Magnification factor for contact pressure in the external pressures on the bubble	1.0
BG	(Used when IFSWEL = 1) Number of FP gas atoms per 1 bubble at garin boundary	5×10^{-8}

Variables set by NAMELIST 4

Variable name	Content	Default value
	Pellet hot press parameter option	
BETAX	Pellet hot press parameter α	0.002
IHOT	=0: hot press parameter α is fixed at BETAX value designated by input. =1: α changes as a function of porosity.	1
	Plasticity model option	
IFY	Pellet plasticity model option, = 0: Rodford, = 1: Tachibana	1
ISTR	When ISTR≠0, K = magnitude of yield surface area of Zircaloy is set as $K = \sigma y + 33.44$ (kg/mm^2).	0
	Irradiation growth option	
ICAGRW	Cladding irradiation growth equation option: = 0: not applied, =1: MATPRO-09, = 2: Manzel = 3: Hannerz, = 4: Hesketh	1
CATEXF	(Used when ICAGRW = 1) Factor in the axial direction f_Z	0.05
COLDW	(Used when ICAGRW = 1) Cold work C_W	0.81
	FP gas release model option	
IGASP	FP gas release rate model: = 0: mechanistic model, = 1: temperature region model	0
IGAS	(Used when IGASP = 1) temperature region model option = 1: Nelson, = 2: Morishima, = 3: Lewis = 4: Karsten	0
APORE	(Used when IGASP = 0) Initial radius of in-grain bubble (cm)	0.0
BFCT	(Used when IGASP = 0) Redissolution rate of in-grain bubbles into matrix is multiplied by BFCT.	1.0
FACD	(Used when IGASP = 0) Effective diffusion coefficient in grain is multiplied by FACD.	1.0
ADDF	(Used when IGASP = 0) Redissolution rate of grain boundary bubbles into grain matrix is multiplied Jby ADDF.	9.0
FBSAT	(Used when IGASP = 0) Amount of gas saturation at grain boundary is multiplied by FPSAT.	1.0
PSAT	(Used when IGASP = 0) Limiting pressure acting on grain boundary bubbles (Pa)	10^8
IPEXT	(Used when IGASP = 0) Option for the external pressure Pext acting on grain boundary bubbles. IPEXT=0: P_{ext} =0, IPEXT=1: P_{ext}=plenum pressure, IPEXT=2: P_{ext}=contact pressure between pellet and cladding, IPEXT=3: P_{ext}= max (plenum pressure, contact pressure), IPEXT=11: P_{ext}= thermal stress (including the plenum pressure), IPEXT=12: P_{ext}=thermal stress (including the contact pressure between pellet and cladding), IPEXT=13: P_{ext}= thermal stress (including the plenum pressure and the contact pressure), IPEXT=14: P_{ext}= average stress obtained by stress calculation in the entire length mechanical analysis.	1
OPORO	(Used when IGASP = 0) ratio of open bubbles at grain boundary	0.0
ALHOT	(Used when IPEXT=10,11,12, and 13) Hot press parameter for the average stress acting on the grain boundary bubbles	0.0001
APEXT	(Used when IPEXT=14) Pext, average stress obtained in the Detailed Mechanical Analysis, is multiplied by APEXT .	1.0
FGG	(Used when IGASP = 0) Rate of grain growth sweeping of FP gas atom is multiplied by FGG.	1.0

Variables set by NAMELIST 5

Variable name	Content	Default value
	FP gas release model (Continued)	
FRMIN	(Used when IGASP = 0) Minimum FP gas release rate (%)	0.5
THEATF	(Used when IGASP = 0) Interpolation parameter used in in-grain diffusion equation θ	1.0
FMULT	(Used when IGASP = 0) Fitting factor of time step width for FP gas release model	1.0
NODEG	(Used when IGASP = 0) Number of in-grain meshes for FP gas release model (5 or less)	3
RREL	(Used when IGASP = 0) Dividing ratio of in-grain mesh for FP gas release model (to be set for each NODEG-1)	10, 1
RB	(Used when IGASP = 0) Grain boundary layer thickness (mesh for re-dissolution) (cm)	2×10^{-6}
	UO_2 grain growth option	
IGRAIN	Option for equation representing UO_2 grain growth: = 0: Itoh (modified Ainscough), = 1: Ainscough, = 2: MacEwan, = 3: Lyons, = 4: MATPRO-09	0
GR	Initial pellet grain size (μm)	10.0
GRWF	(Used when IGRAIN = 0) Grain growth rate is multiplied by GRWF	1.5
AG	(Used when IGRAIN = 0) Fitting parameter (grain growth suppression factor)	1.0

Variables set by NAMELIST 6

Variable name	Content	Default value
	Helium release option	
NTVHE	Number of time points set by TVHE	0
TVHE (13, 50)	TVHE(1, n) : number of nth time points (hr) TVHE(i+1, n) : amount of He generated in axial segment I at nth time point (mole)	650*0.
	Gas flow model option	
IST	Gas flow option: =0 : instantaneous complete mixing model =1 : gas diffusion model in the axial direction	1
GMIN	Minimum gap width used in the gap gas flow model (cm)	0.001
THG1	Interpolation parameter for temperature, volume, etc., used in FP gas flow model in the axial direction θ_1	1.0
THG2	Interpolation parameter used in diffusion calculation of FP gas flow model in the axial direction θ_2	1.0
AMLMX2	Upper limit amount of gas transported between axial segments per unit time step (mol)	10^{-6}
AMLMX3	Upper limit amount of FP gas released in each axial segment per unit time step (mol)	2×10^{-6}
DTPR	Allowable ratio of amount of FP gas release to amount of plenum gas per unit time step	0.01
ETA	Control parameter (used for determination of time step width)	0.05
	Cladding corrosion option	
ICORRO	Cladding outer surface corrosion model option =0 : not applied, =1 : Halden	0
	Gap conductance option	
IGAPCN	Gap conductance model option = 0: Modified Loss & Stoute, = 1: MATPRO-09, = 2: Loss & Stoute, = 3: modified Dean	0
R1	(Used when IGAPCN = 0 or 2) pellet surface roughness (μm)	1.0
R2	(Used when IGAPCN = 0 or 2) cladding surface roughness (μm)	1.0

Variables set by NAMELIST 7

Variable name	Content	Default value
	Plotter output option	
IPRINT	Output option (=0: no output, =1: output)	
(1)	Input data list	1
(2)	Fuel design data	1
(3)	Mesh coordinates data	1
(4)	List of parameters	1
(5)	History data	1
(6)	Results of thermal analysis of each time step	1
(7)	Results of mechanical analysis of each time step	1
(8)	Summary of thermal analysis results for each segment (thermal model)	1
(9)	Summary of mechanical analysis results for each segment (thermal model)	1
(10)	Summary of FP gas release calculation results for each segment (thermal model)	1
(11)	Summary of FP gas release calculation results for entire fuel rod (thermal model)	1
(12)	Summary of deformation behavior of pellet/cladding of each segment (mechanical model)	1
(13)	Summary of pellet stress and strain of each segment (mechanical model)	1
(14)	Summary of cladding stress and strain of each segment (mechanical model)	1
(15)	Summary of major results (final information)	1
(16)	Plotter output of thermal behavior of each segment (ON-LINE) (Unit 14)	1
(17)	Plotter output of FP gas behavior of each segment (ON-LINE) (Unit 14)	1
(18)	Plotter output of mechanical behavior (ON-LINE) (Unit 14)	1
(19)	Summary of entire-fuel-rod strain and corrosion of the objective segment	0
(20)	Not in use	0
IWNOD	Segment output option (= 0: no output, = 1: output) For IPRINT(8), IPRINT(9), IPRINT(10), IPRINT(16), IPRINT(17), output (including plotter output) is performed for segment I where IWNOD(I) = I, and output is not performed for segment I where IWNOD(I) = 0. However, if all IWNOD is 0, IWNOD(IFEM) = 1 is set only at segment IFEM.	12*0
IWTHE	Thermal analysis output option (= 0: no output, = 1: output), (Option when IPRINT(6) = 1)	
(1)	Fuel temperature	0
(2)	Gap gas	0
(3)	Grain radius	0
(4)	In-grain gas bubble radius	0
(5)	In-grain gas bubble density	0
(6)	In-grain gas diffusion coefficient	0
(7)	In-grain gas effective diffusion coefficient	0
(8)	Number of gas atoms in grain	0
(9)	Number of gas atoms at grain boundary	0
(10)	Number of gas atoms released	0
(11)	Number of gas atoms in grain and at grain boundary	0
(12)	Number of gas atoms released, in grain, and at grain boundary	0
(13)	Number of gas atoms generated	0
(14)	FP gas release rate	0
(15)	Gas density at grain boundary	0
(16)	Saturated gas density at grain boundary	0
(17)	Average stress at grain boundary	0
(18)	Conditions for thermal calculation	0
(19)	Conventional output for thermal calculation	0

Variables set by NAMELIST 8

Variable name	Content	Default value
IWFEM	**Output option for the Local Mechanical Analysis II** (effective only when IFEMRD = 0), (= 0: no output, = 1: output) (option used when IPRINT(7) = 1)	
(1)	Stress in the radial direction	0
(2)	Stress in the axial direction	1
(3)	Stress in the circumferential direction	1
(4)	Shear stress	0
(5)	Equivalent stress	1
(6)	Yield stress	0
(7)	Total strain in the radial direction	0
(8)	Total strain in the axial direction	0
(9)	Total strain in the circumferential direction	0
(10)	Total shear strain	0
(11)	Equivalent plastic strain	1
(12)	Creep strain in the radial direction	0
(13)	Creep strain in the axial direction	0
(14)	Creep strain in the circumferential direction	1
(15)	Shear creep strain	0
(16)	Equivalent creep strain	0
(17)	Elastic strain in the radial direction	0
(18)	Elastic strain in the axial direction	0
(19)	Elastic strain in the circumferential direction	0
(20)	Shear elastic strain	0
(21)	Thermal strain in the radial direction	0
(22)	Thermal strain in the axial direction	0
(23)	Densification strain	0
(24)	Swelling strain	0
(25)	Stiffness in the radial direction	0
(26)	Stiffness in the axial direction	0
(27)	Stiffness in the circumferential direction	0
(28)	Creep rate in the radial direction	0
(29)	Creep rate in the axial direction	0
(30)	Creep rate in the circumferential direction	0
(31)	Creep rate in the shear direction	0
(32)	Equivalent creep rate	0
(33)	Total strain rate in the radial direction	0
(34)	Total strain rate in the axial direction	0
(35)	Total strain rate in the circumferential direction	0
(36)	Total strain rate in the shear direction	0
(37)	Equivalent total strain rate	0
(38)	Strain energy	0
(39)	Temperature distribution in the radial direction	1
(40)	Mechanical interaction between pellet/cladding	1
(41)	Mechanical interaction between pellet/pellet	1
(42)	Displacement of node	1
(43)	Plot of "Pellet-Clad Mechanical Interaction"	1
(44)	Crack yielding map	1
(45)	Mechanical calculation conditions	1

Variables set by NAMELIST 9

Variable name	Content	Default value
IWROD	Output option for the Entire-Rod-Length Mechanical Analysis I (effective only when IFEMRD = 1), (= 0: no output, = 1: output) (Option is used when IPRINT(7) = 1)	
(1)	Stress in the radial direction	0
(2)	Stress in the axial direction	0
(3)	Stress in the circumferential direction	0
(4)	Equivalent stress	0
(5)	Yield stress	0
(6)	Creep strain in the radial direction	0
(7)	Creep strain in the axial direction	0
(8)	Creep strain in the circumferential direction	0
(9)	Creep hardening strain	0
(10)	Equivalent plastic strain	0
(11)	Swelling strain	0
(12)	Total strain in the radial direction	0
(13)	Total strain in the axial direction	0
(14)	Total strain in the circumferential direction	0
(15)	Thermal strain	0
(16)	Temperature of element	0
(17)	Pressure in the radial and axial directions	0
(18)	Displacement in the radial and axial directions	0
IPLT	Production of FEMAXI-IV plotter tape (mechanical model) (Unit 1)	0
IPLOPT	= 0: Output data at the time steps designated by input = 1: Output data at all time steps calculated = −n: Output data at every n time step (Here, data are also output at the time steps designated by input) <Off-line plotter>	0

Input method for history data

Here, the method of production of history data (card numbers 10-11) of the input file is explained.

Power history data

The following items must be input for the power history data: A1 = time (hr), B1=burnup, A2 = linear heat rate (W/cm), A5 = fast neutron flux (n/cm^2·s), A3 = coolant temperature (K), A4 = coolant pressure (MPa), IT = input generator, IP = output option, IS = temperature calculation option, A6 = coolant velocity (m/s). However, since B1 (burnup) is determined by input of A1 (time) and vice versa, either A1 or B1 should be input. The unit of B1 is designated by IBUNP of the NAMELIST: when IBUNP = 0, B1 is MWd/t-UO_2; when IBUNP = 1, B1 is MWd/t-U; and when IBUNP = 2, B1 is GJ/kg-U.

Using IT (input generator), input by incremental form is possible. IT is selected from among 0, 100, and −100; when IT = 0 is set, A1 (or B1) is recognized as a time increment from the previous history point (or burnup increment); when IT = 100, A1 (or B1) is recognized as the time increment from the first history point (or burnup increment). IP is an output option; IP ≥ 1 designates history points for detailed output, and IP = 0 designates history points for simplified output only. IS is a switching flag between steady/unsteady status in temperature calculation; since this switching is automatically performed in the code, input of IP is usually unnecessary.

－FORMAT (6F 10.0, 2I5)

F10.0	F10.0	F10.0	F10.0	F10.0	F10.0	I5	I5	I5	F5.0
A1	B2	A2	A5	A3	A4	IT	IP	IS	A6

Relative power profile

Here, the input method for relative power profile is explained. RH is the relative power profile and designates the power ratio for A2 (linear heat rate, which was given by the history data) at the central position of an axial segment. Therefore, the number of RH data to be input is NAX (number of axial segments), whose maximum is 12. When an identical power profile is input at history points, the input can be omitted using II (history point option).

－FORMAT (12F5.0, I5)

12F 5.0	I 5
(RH(I), I=1, 12)	I I

where NAX (number of segments) sets of data should be set for RH.

Input method

For input of power history, the power-history-point number pairs of data (combination of power history data and relative power profile) must be input.

Example of input (1)

An example of input for a case with one axial segment, where the power is increased to 500 W/cm during a period of 10 hr, is shown below. Here, the following values were used: fast neutron flux=2.5×10^{13} (n/cm^2·s) when 500 W/cm is reached; coolant temperature= 513.15 (K);

coolant pressure= 3.4 (MPa) and coolant velocity= 3.0 (m/s).

Example of input (1)

```
....5....0....5....0....5....0....5....0....5....0....5....0....5....0....5....0....5....0
    2
                                        513.15      3.4         1       3.0
1.0                                                         2
   10.0              500.0   2.5E13                         1
....5....0....5....0....5....0....5....0....5....0....5....0....5....0....5....0....5....0
```

In the first line, NHIST = 2 is shown; the number of history points is 2.

In the second line, a hot stand-by state is set in the initial history data. Input for the hot stand-by state is not necessary since the following values are set: time (A1), 10^{-5} (hr); linear heat rate (A2), 10^{-3} (W/cm); fast neutron flux (A5), 2×10^{1} (n/cm^2·s).

In the third line, RH(1) = 1.0 is set, since this case deals with a calculation of 1 axial segment for the input of relative power profile. The history point option is set as II = 2, which means that the same relative power profile is used for the two history points.

The fourth line shows input of A1 = 10 (hr), A2 = 500 (W/cm) and A5 = 2.5×10^{13} (n/cm^2·s) for the history data of the second history point. Therefore, the time step is automatically divided, and at each division point, values of time-dependent variables are obtained by linear interpolation. Input of coolant temperature and coolant pressure is omitted; this means that the same values as those for the first history point are used; that is, A3=513.14 and A4 = 3.4 are input.

For the output option, IP = 1 is set in the second and third lines; therefore, detailed output is performed both in the hot stand-by state and when 500 W/cm is reached.

Example of output (2)

An example with 12 axial segments is shown in which base irradiation is first performed at 200 W/cm up to 20GWd/tUO_2. The power is decreased thereafter, and then increased to 250 W/cm. After conditioning for 72 hr, the power is increased to 500 W/cm, maintained for 24 hr, and finally the power is decreased. Here, the power increase rate is 200 W/cm·hr in every period.

The following values are set: fast neutron flux=10^{14} (n/cm^2·s) when 500 W/cm is reached; coolant temperature = 513.15 (K); coolant pressure = 3.4 (MPa); and coolant velocity is

constant at 3.0 (m/s). The relative power profile is given for base irradiation and for ramp irradiation. During the base irradiation, output of calculation results is performed at 5GWd/t-UO_2, 10GWd/t-UO_2, 15GWd/t-UO_2 and at 20GWd/t-UO_2; and during the ramp irradiation, the output of calculation is also performed at every 50 W/cm power increment above 250 W/cm. When the power is maintained at 500 W/cm, the output of calculation is obtained after 1, 3, 6, 12 and 24 hr.

Example of output (2)

```
....5....0....5....0....5....0....5....0....5....0....5....0....5....0....5....0....5....0
        21
       0.0                    0.001     2.0E09     513.15        3.4          2        3.0
 0.77 0.85 0.90 0.92 0.94 0.96 0.98 1.00 1.02 1.05 1.10 1.15     7
       1.0                    200.0     4.0E13                                1
                 5000.0
                10000.0
                15000.0
                20000.0       200.0     4.0E13                                1
       1.0                    0.001     2.0E09                      -100      1
       1.0                    0.001     2.0E09                      -100
 0.93 0.94 0.95 0.96 0.97 0.98 0.99 1.00 1.01 1.02 1.04 1.06    14
      1.25                    250.0     5.0E13                      -100
      72.0                    250.0     5.0E13                      -100      1
      0.25                                                          -100
       0.5
      0.75
       1.0
      1.25                    500.0     1.0E14                                1
       1.0                                                          -100
       3.0
       6.0
      12.0
      24.0                    500.0     1.0E14                                1
       2.5                    0.001     2.0E09                      -100      1
STOP
....5....0....5....0....5....0....5....0....5....0....5....0....5....0....5....0....5....0
```

The simplified output is obtained for the 21 history points shown above. Among these history points, IP ≥ 1 is designated only at points where detailed output is required; here IP = 2 is input and detailed output information is obtained at history points after this designation. The unit of burnup should be MWd/t-UO_2; therefore, IBUNP = 0.

The first line shows the number of history points, NHIST = 21.

The second line shows the history data of the hot stand-by state.

Data in the third line show that the same relative power profile is used from the first history point to the 7th history point.

The fourth line shows the second history point data of A1 = 1(hr), A2 = 200(W/cm) and A5 = 4×10^{13} (n/cm^2·s). Coolant temperature and pressure are the same as those in the hot stand-by state.

The 5th to 8th lines show input to extend burnup up to 20 GWd/tUO$_2$ at 200 (W/cm), and simplified output is obtained at 5 GWd/tUO$_2$ and at 15 GWd/tUO$_2$. A2 (linear heat rate) and A5 (fast neutron flux) are obtained by interpolation. During this stage, A2 = 200 (W/cm) and A5 = 4×10^{13} (n/cm^2·s) are used.

The 9th line shows setting of IT = −100. This means that the power was decreased to 0.001 (W/cm) within 1 hr from the burnup of 20 GWd/tUO$_2$ shown in line 8.

The 10th line shows that the relative power profile was changed after the power levelled off at 0.001 (W/cm) for 1 hr.

The 11th line shows that the relative power profile given in the 11th line is applied from the 8th history point up to the last (21st) history point. Here, since a power of 0 is not allowed, a value of around 10^{-3} (W/cm) must be set.

The 12th line shows that the power was increased to 250 (W/cm) within 12.5 hr, and the 13th line shows that the power was maintained at 250 (W/cm) for 72 hr.

The 14th to 18th lines show that the power was increased by 50 W/cm within 0.25 hr (200 W/cm·hr) after being maintained at 250 (W/cm) for 72 hr. Namely, elapsed time at the previous history point where IT = −100 was designated (shown in the 13th line) is given by A1. Since the linear heat rate is given by the linear interpolation, setting of A2 = 300, 350, 400 and 450 in lines 14-17 gives the same results. Similarly, the fast neutron flux used here gives the same results by setting A5 = 6×10^{13}, 7×10^{13}, 8×10^{13} and 9×10^{13}.

The 19th-23rd lines show history data which were set to obtain simplified output when the power is maintained at 500 (W/cm) and at 1, 3, 6 and 12 hr from the starting time. The detailed output is obtained 24 hr after the starting time.

The 24th line shows that the power was decreased within a 2.5-hr period starting from 24 hr from the starting time. Here, since the coolant temperature and pressure were set as constant, input for them at the second and later history points was omitted. Also, since linear heat rate and fast neutron flux are obtained by linear interpolation, input error occurs if no power is generated at the last history point. (Both values should not be zero.)

A2 Input Manual for Plotter

Card No.	SYMBOL (FORMAT)	
1	Comments	
2	ISET (*)	Total number of figures

Input ISET-sets consisting of the following cards

3	IRNUM, ITOPT, ISYM (*)	Function setting
	IRNUM: number of lines drawn in one figure (maximum of 5 lines) ITOPT: designation of graph type ITOPT = 0 X axis represents time, burnup or linear heat rate ITOPT = 1 X axis represents coordinates in the radial or axial direction ITOPT = 2 Construct a diagram for comparison of calculated values with measured values (in this case, maximum value of IRM becomes 4 since one line is used for the measured values) ISYM: Center symbol option = 0 center symbol is not plotted = 1 center symbol is plotted	
4	IXOPT, IXOPT2, IYOPT2, IYNUM, (IYOPT(I), I=1, IYNUM) (*)	Axis setting
	IXOPT: setting of the contents of X axis (set when ITOPT = 0 or 2) = 1: time = 2: coordinates in the radial direction (–) (set when ITOPT = 1) = 3: coordinates in the axial direction (–) = 4: burnup (at the objective segment) = 5: linear heat rate (at the objective segment, W/cm) = 6: burnup (average on all axial segments) =7: linear heat rate (average on all axial segments, W/cm) IXOPT2: setting of units for time and burnup Setting of units when X axis represents time (IXOPT = 1) IXOPT2 = 0: hour IXOPT2 = 1: day Setting of units when X axis represents burnup (IXOPT = 4 or 6) IXOPT2 = 0: MWd/tUO$_2$ IXOPT2 = 1: GWd/tUO$_2$ IXOPT2 = 2: MWd/tU IXOPT2 = 3: GWd/tU IYOPT2; setting of units for time and burnup Setting of units when Y axis represents time (IYOPT(I)=1 or 12) IYOPT2 =0 MWd / tUO$_2$ IYOPT2 =1 GWd / tUO$_2$ IYOPT2 =2 MWd / tU IYOPT2 =3 GWd / tU IYNUM: number of Y axes. When more than 2 physical properties are set for Y axis (IYNUM ≧2), IYNUM = IRNUM must be set since one graph is drawn for one Y axis. (IYOPT(I), I = 1, IYNUM): select contents of Y axis from Tables 1 to 3 and input the physical quantity number.	
5	(IR(I), I = 1, IRNUM) (*)	Radial mesh number
	(IR(I), I = 1, IRNUM): radial mesh number is set for each figure. When setting is not necessary, input 1.	

Card No.	SYMBOL (FORMAT)	
6	(IZ(I), I = 1, IRNUM) (*)	Axial segment number
	(IZ(I), I = 1, IRNUM) Set the segment number in the axial direction for each figure. Input I when setting is not necessary.	
7	(ITIM(I), I = 1,2) or (ITIM(I), I = I, RNUM) (*)	Time step number
	(When ITOPT = 0 or 2, input (ITIM(I), I = 1,2)) ITIM(1) = set a time step number for starting point of the figure ITIM(2) = set a time step number for end point of the figure (When ITOPT = 1, input (ITIM(I), I = 1, RNUM)) set a time step number for each figure	
8	X0, XM, XNUM, IXN, IFLAG(6) (*)	Setting of X-axis scale
	This card is a DUMMY when IXOPT=2 or 3. X0: minimum value of X-axis scale XM: maximum value of X-axis scale XNUM: increment of X-axis scale IXN: number of digits after decimal point on X axis (example) IXN = −1 for 10 IXN = 1 for 10.0 IXN = 2 for 10.00 IFLAG(6): setting of X-axis scale =3: automatic scaling is applied to X axis ≠3: X axis is drawn with designated scaling by input	
9	IYNUM cards are required (I = 1, IYNUM) Y0(I), YM(I), YNUM(I), IYN(I), IFLAG(I) (*)	Setting of Y-axis scale
	Y0(I): minimum value of Y-axis scale YM(I): maximum value of Y-axis scale YNUM(I): increment of Y-axis scale IYN(I): number of digits after decimal point on Y axis (input in the same manner as for IXN) IFLAG(I): option for Y-axis scale = 0: scale is expressed with real numbers (decimal number expression) = 1: scale is expressed with floating format = 2: logarithmic scaling is used for Y axis = 3: automatic scaling is applied to Y axis When IFLAG(I) = 3, Y0～IYN are DUMMY, since automatic scaling is selected.	

(Note 1) When ITOPT = 2, measured values are input from unit 2. Therefore, data row for (X, Y) must be prepared in unit 2.

(Note 2) Data specified by asterisk (*) are input with free format.

Table (1): Physical Quantities of Y axis (1) (**):designated by IYOPT2

Group	No.	Item	Unit
A Data regarding time and burnup	1	Rod average burnup	(**)
	2	FP gas release rate	(%)
	3	Rod internal pressure	(MPa)
	4	Plenum volume	(cc)
	5	Pellet elongation (when IFEMRD=1, pellet elongation at the ojective segment designated by IFEM)	(%)
	6	Entire rod elongation (in the case of IFEMRD=1)	(%) (μm)
	7	Maximum change of cladding outer radius	(W/cm)
	8	Average linear heat rate in the axial direction	(g/cm^2)
	9	Average iodine concentration	(g/cm^2)
	10	Maximum iodine concentration	(g/cm^2)
	67	Average change in cladding outer radius	(μm)

Table (2): Physical Quantities of Y axis (2) (**):designated by IYOPT2

Group	No	Item	Unit
B Data regarding time, burnup and axial coordinate	11	Linear heat rate (thermal analysis=TA)	(W/cm)
	12	Burnup (TA)	(MWd/tUO_2)
	13	Diametral gap width (mechanical analysis; when IFEMRD=0, gap at each axial segment, and when IFEMRD=1, gap at each node couple is output sequentially)	(μm)
	14	PCMI pressure (radial direction)	(MPa)
	15	FP gas release rate (TA)	(%)
	16	Frictional force between pellet and cladding in the axial direction (mechanical analysis)	(MPa)
	17	Pellet elongation	(%)
	18	Cladding elongation (Items 17 and 18 are output from mechanical analysis. When IFEMRD=0, elongation at each axial segment is obtained; when IFEMRD=1, the same values in the axial direction are output)	(%)
	19	Gap conductance (TA)	(W/cm^2C)
	20	Coolant temperature (TA)	(°C)
	21	Cladding inner surface temperature (TA)	(°C)
	22	Cladding outer surface temperature (TA)	(°C)
	23	Pellet center temperature (TA)	(°C)
	24	Pellet outer surface temperature (TA)	(°C)
	25	Cladding outer radius change(the same as 13)	(μm)
	26	Composition of Xe + Kr (TA)	(%)
	68	Pellet density (TA)	(T·D)

Table (3): Physical Quantities of Y axis (3)

Group	No.	Item	Unit
C Data regarding time, burnup, coordinates in the axial and radial directions	27	Pellet equivalent stress	(MPa)
	28	Pellet average stress	(MPa)
	29	Pellet stress in the radial direction	(MPa)
	30	Pellet stress in the circumferential direction	(MPa)
	31	Pellet stress in the axial direction	(MPa)
	32	Pellet elastic strain in the radial direction	(0.01%)
	33	Pellet elastic strain in the circumferential direction	(0.01%)
	34	Pellet elastic strain in the axial direction	(0.01%)
	35	Pellet equivalent creep strain	(0.01%)
	36	Pellet creep strain in the radial direction	(0.01%)
	37	Pellet creep strain in the circumferential direction	(0.01%)
	38	Pellet creep strain in the axial direction	(0.01%)
	39	Pellet equivalent elastic strain	(0.01%)
	40	Pellet strain in the radial direction	(0.01%)
	41	Pellet strain in the circumferential direction	(0.01%)
	42	Pellet strain in the axial direction	(0.01%)
	43	Pellet thermal expansion strain in the radial direction	(0.01%)
	44	Pellet thermal expansion strain in the axial direction	(0.01%)
	45	Pellet swelling strain (⊿L/L)	(0.01%)
	46	Pellet element temperature	(℃)
	47	Pellet FP gas release rate	(%)
	48	Cladding equivalent stress	(MPa)
	49	Cladding average stress	(MPa)
	50	Cladding stress in the radial direction	(MPa)
	51	Cladding stress in the circumferential direction	(MPa)
	52	Cladding stress in the axial direction	(MPa)
	53	Cladding elastic strain in the radial direction	(0.01%)
	54	Cladding elastic strain in the circumferential direction	(0.01%) (0.01%)
	55	Cladding elastic strain in the axial direction	(0.01%)
	56	Cladding equivalent creep strain	(0.01%)
	57	Cladding creep strain in the radial direction	(0.01%)
	58	Cladding creep strain in the circumferential direction	(0.01%)
	59	Cladding creep strain in the axial direction	(0.01%)
	60	Cladding equivalent elastic strain	(0.01%)
	61	Cladding strain in the radial direction	(0.01%)
	62	Cladding strain in the circumferential direction	(0.01%)
	63	Cladding strain in the axial direction	(0.01%)
	64	Cladding thermal strain in the radial direction	(0.01%)
	65	Cladding thermal strain in the axial direction	(0.01%)
	66	Cladding swelling strain	

[Comment on the C-group of Physical Quantities in Plotter Figure]

In the following explanation, thermal analysis is identical irrespective of IFEMRD value designated by input. Also, FP gas release rate (No.47) is an exception of the explanation, because it is always output at each axial segment.

(1) Physical quantities No.27～46 for pellet

① In the case of IFEMRD=0, or local mechanical analysis, stress, strain, and temperature are evaluated at points indicated by × marks, which are the Gauss's integral points. See Fig.2.39(b). Displacement is evaluated at node point.

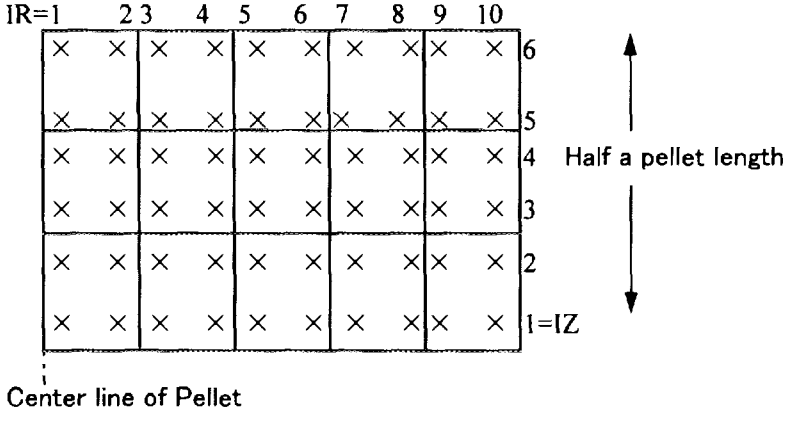

② In the case of IFEMRD=1, or entire length mechanical analysis, stress, strain, and temperature are evaluated at points indicated by × marks, which are the Gauss's integral points. See Fig.2.29.

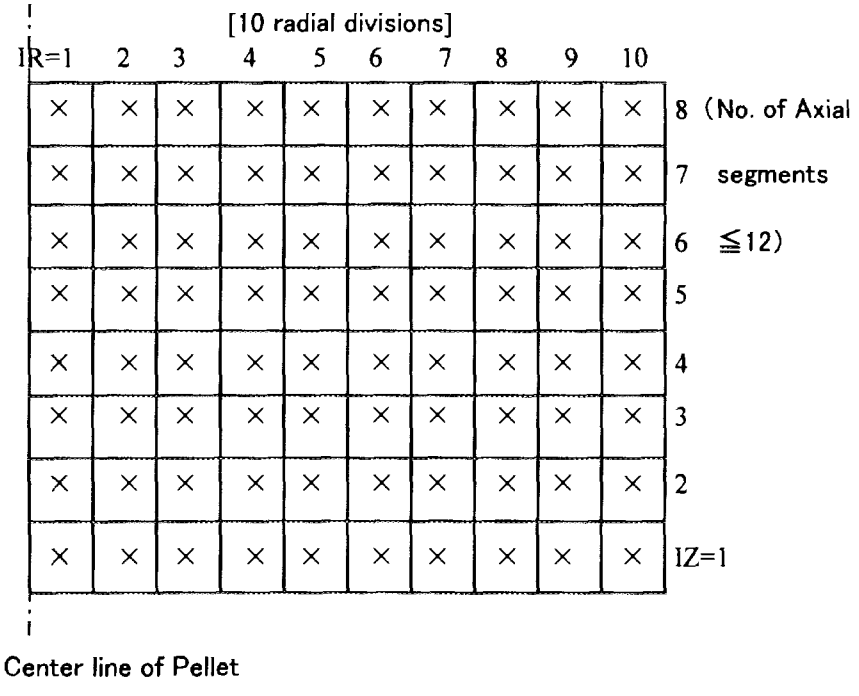

(1) Physical quantities No.48～66 for cladding

Stress, strain, and temperature are evaluated at points indicated by × marks, or the Gauss's integral points.

① In the case of IFEMRD=0, or local mechanical analysis:
See Fig.2.39(b). Displacement is evaluated at node.

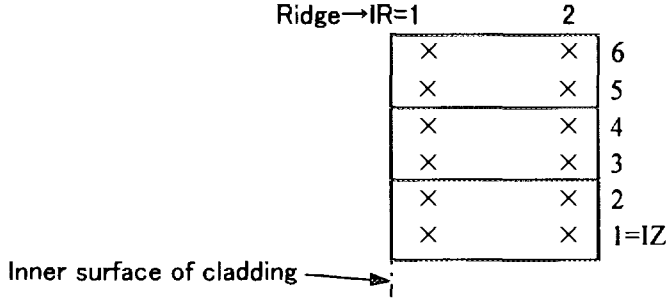

②In the case of IFEMRD=1, or entire length mechanical analysis, stress, strain, and temperature are evaluated at points indicated by × marks, which are the Gauss's integral points. See Fig.2.29.

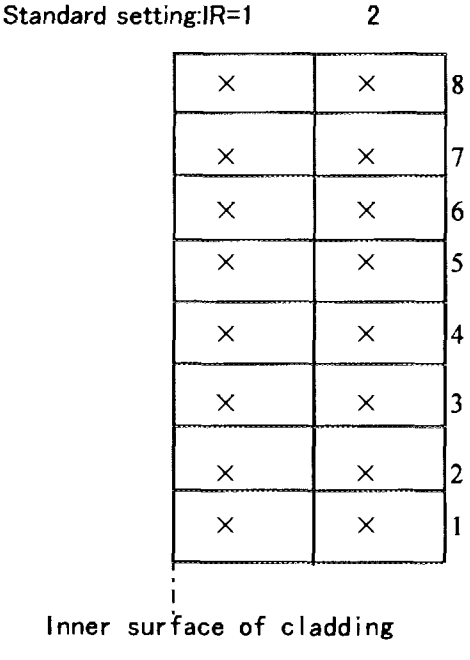

A3 (1) Subroutine List

Table A1 lists the FEMAXI-IV subroutines which are classified in terms of their analytical functions. The abbreviations in the table are as follows:

P : Program controlling routines, plotter routines, and other auxiliary function subroutines which are not included in the analytical models.

T : Subroutines used in the thermal analysis models.

M1: Subroutines used in the entire rod length mechanical analysis model.

M2 : Subroutines used in the local mechanical analysis model.

Table A1 FEMAXI-IV Subroutine and functions

Name	Function	P	T	M1	M2
AAZERO	Zero setting of common areas	○			
ADBU	Calc. of burnup increment from time history increment	○			
ADRESS	Calc. of address in matrix			○	
ADTM	Calc. of time history increment from burnup increment	○			
ADVANC	Updating of grain size and FP gas atom density in FP release model		○		
AXIVAL	Y-axis setting for ON-LINE plotter	○			
BBL	Calc. of in-grain bubble radius		○		
BBLDEN	Calc. of in-grain bubble density		○		
BDMAT	Formation of $[B]^T[D]$ matrix				○
BLOCKDATA	Block data list	○			
BMAT	Formation of [B] matrix				○
BOUNDF	Calc. of nodal force on the upper surface of pellet in the axial direction				○
BURNUP	Calc. of burnup	○			
CAGROW	Calc. of irradiation growth strain of cladding in the axial direction			○	○
CANDM	FP release model routine		○		
CATHEX	Calc. of thermal expansion of cladding in the axial direction			○	○
CCREEP	Calc. of cladding creep strain		○		
CDTHEX	Calc. of thermal expansion of cladding in the radial direction		○	○	○
CELMOD	Calc. of cladding Young's modulus		○	○	○
CFRFZ	Calc. of cladding axial force				○
CHCAP	Calc. of cladding volumetric specific heat		○		
CHSOFT	Calc. of stress-differential term of cladding yield function			○	○
CLBDF	Calc. of contact force on the upper surface of pellet				○
CLEAR	Zero setting of real number areas	○			

Table A1 (continued)

Name	Function	P	T	M1	M2
CMAT	Calc. of effective Young's moduli of pellet and cladding, and Poisson's ratio				○
CMAT1	Formation of pellet [C] matrix			○	
CMAT2	Formation of cladding [C] matrix			○	
CNSTR	Setting of displacement increment			○	
COLECT	Calc. of total stiffness matrix and loading vector				○
COORDI	Setting of shape coordinates for FEM in the local mechanical analysis				○
CPOIR	Calc. of Poisson's ratio of cladding		○	○	○
CPUGH	Control routine of PUGH's reversal method				○
CRACK	Setting of pellet crack status				○
CREEP1	Formation of $[C^c]$ matrix and creep strain vector $\{\Delta \varepsilon^c\}$				○
CREEP2	Formation of creep strain increment $\{\Delta \varepsilon^c\}$ of cladding				○
CRPEP2	Formation of cladding creep strain rate $1/\varepsilon^c$ (MATPRO-9)				○
CRPEP3	Formation of cladding creep strain rate $1/\varepsilon^c$ (NENANSEN)				○
CRPEQ2	Formation of $\frac{1}{\varepsilon^c}(=f), \frac{\partial f}{\partial \sigma}, \frac{\partial f}{\partial \varepsilon^H}$ in cladding creep (MATPRO-9)				○
CRPEQ3	Formation of $\frac{1}{\varepsilon^c}(=f), \frac{\partial f}{\partial \sigma}, \frac{\partial f}{\partial \varepsilon^H}$ in cladding creep (NENANSEN)				○
CRPHD2	Formation of $\frac{1}{\varepsilon^H}(=g), \frac{\partial g}{\partial \sigma}, \frac{\partial g}{\partial \varepsilon^c}$ in cladding creep (MATPRO-9)				○
CRPHD3	Formation of $\frac{1}{\varepsilon^H}(=g), \frac{\partial g}{\partial \sigma}, \frac{\partial g}{\partial \varepsilon^c}$ in cladding creep (NENANSEN)				○
CRPM11	Formation of $[C^c]$ matrix and pellet creep vector $\{\Delta \varepsilon^c\}$				○
CRPM12	Formation of creep strain increment $\{\Delta \varepsilon^c\}$ of pellet				○
CTHCON	Calc. of cladding thermal conductivity		○		
CTSOFT	Calc. of temperature differential term in cladding yield function			○	○
CUBIC	Calc. of largest real number solution of cubic equation (bubble radius)		○		
CYIE	Calc. of Zircaloy yield stress (0.2% proof stress)			○	○
CYIE2	Calc. of Zircaloy yield stress (size of yiels surface at $\bar{\varepsilon}^p$)			○	○
CYLD	Calc. of Zircaloy yield stress (0.2% proof stress)		○		

Table A1 (continued)

Name	Function	P	T	M1	M2
DELTAN	FEM mesh element data in the local mechanical analysis				○
DENSF	Pellet densification model		○		○
DEVSIG	Deviation stress				○
DFCLAD	Formation of loading vector of cladding			○	
DFPLT	Formation of loading vector of pellet			○	
DFX	Determines the size of cladding yield surface			○	○
DIFC	Diffusion coefficient of FP atom in pellet grains		○		
DIFCON	Xe-He mutual diffusion coefficient		○		
DOT	Routine for Pugh's reversal method in cladding creep			○	○
DPMAT	Formation of $[D^P]$ matrix				○
DPST	Calc. of $\Delta\bar{\varepsilon}^p$				○
ELMLP1	Control of formation of element stiffness matrix and loading vector				○
ELMLP2	Control of calculation of stress-strain of elements				○
EQIEPS	Calc. of equivalent strain				○
EQISIG	Calc. of equivalent stress				○
EQSCAL	Convergence calculation of size of yield surface at $\bar{\varepsilon}^p$			○	○
ESMAT	Formation of element stiffness matrix				○
FCREEP	Calc. of pellet creep strain (MATPRO-09)		○		
FDIST	Calc. of flux depression in pellet in the radial direction		○		
FDISTF	Calc. of flux depression in pellet in the radial direction		○		
FELMOD	Calc. of pellet Young's modulus		○	○	○
FEMAX4	Control of entire program	○			
FEMRD1	Connecting routine of thermal analysis and rod entire length mechanical analysis			○	
FFG	Calc. of sweeping ratio of FP atoms by grain growth		○		
FGPRO	Calc. of FP gas generation		○		
FGRELN	Calc. of FP gas release rate at each element of pellet		○		

Table A1 (continued)

Name	Function	P	T	M1	M2
FHSOFT	Calc. of stress-differential term of pellet yield function σ_y				○
FISGAS	Reference table to determine FP gas release rate at each temperature range		○		
FISRAT	Calc. of nuclear fission density	○			
FLMCON	Calc. of cladding surface heat transfer coefficient by Jens-Lottes equation		○		
FLOAD	Calc. of element loading vector				○
FLXDEP	Calc. of flux depression in pellet in the radial direction		○		
FORCE	Calc. of total external force vector				○
FPOIR	Poisson's ratio of pellet			○	○
FPRES2	Calc. of effective width of surface nodes				○
FTSOFT	Calc. of temperature-differential term of pellet yield function σ_Y				○
FX	Routine to determine the size of cladding yield surface			○	○
FYIE	Pellet yield stress (0.2% proof stress)			○	○
GAPCON	Calc. of gap conductance		○		
GAPELN	Contact judgment of pellet/clad and pellet/pellet				○
GAPMOD	Convergence calculation of gap conductance		○		
GAPS	Calc. of gap width			○	
GAULP1	Formation of stiffness matrix and loading vectors at gauss point in element				○
GAULP2	Calc. of stress-strain at gauss point in element				○
GDTHCN	Thermal conductivity of Gadolinia		○		
GPSSET	Setting of boundary conditions				○
GRAIN	Calc. of pellet grain growth		○		
GRAPH1	Control routine for ON-LINE plotter (thermal analysis)	○			
GRAPH2	Control routine for ON-LINE plotter (FP gas release analysis)	○			
GRAPH3	Control routine for ON-LINE plotter (stress-strain analysis)	○			
GRID	Setting of grid point for ON-LINE plotter	○			

Table A1 (continued)

Name	Function	P	T	M1	M2
GTHCON	Thermal conductivity of gases		○		
HEAD2	Title of the rod entire length mechanical analysis	○			
HEADER	Title of the local mechanical analysis	○			
HEATG	Thermal conductivity of Zirconia		○		
HOTVOL	Auxiliary routine to calculate plenum volume		○		
HTX	Cladding surface heat transfer coefficient by Jens-Lottes eq.		○		
ICLEAR	Zero setting of integer areas	○			
INIGAS	Calc. of plenum pressure and volume at hot stand-by		○		
INIMAT	Calc. of [C] matrix				○
INISTR	Calc. of initial strain				○
INPGER	Generator of historical input data	○			
INPHIS	Input routine of power history	○			
INPIMG	Print-out of input data image	○			
INPR	Radial meshing in the local mechanical analysis				○
INPUT1	Input routine for thermal analysis	○			
INPZ	Axial meshing in the local mechanical analysis				○
INTG	Calc. of the coefficient matrices [A] and [E] for FP gas release		○		
INTGH	Calc. of the coefficient matrix [H] for FP gas release		○		
INTGX	Volumetric integral of residual FP in pellet grains		○		
INTPLT	Routine of quadratic interpolation	○			
INV3	Inverse matrix of 3×3 symmetrical matrix			○	
INVERS	Inverse matrix of 4×4 symmetrical matrix				○
JACK2	Jacobian of quadratic elements				○
LENGT	Calc. of character length for ON-LINE plotter	○			
LINER	Pattern of lines in plotter output figure	○			
LINSET	Setting of node array at outer surface in the local mechanical analysis				○

Table A1 (continued)

Name	Function	P	T	M1	M2
LOCALI	Storage and extract of information at gauss point				○
LSYM	Printing of symbols for ON-LINE plotter	○			
MAIN	Main routine	○			
MATDAT	Setting of materials properties for heat conduction calc.		○		
MDEPS0	Calc. of initial strain in rod entire length analysis			○	
MDSIG	Calc. of stress in the rod entire length analysis			○	
MODIFY	Setting of contact boundary conditions in local mechanical analysis				○
MODSET	Calc. of total matrix area in local mechanical analysis				○
MOVE	Storage of total matrix (entire length analysis)			○	
MTDF	Formation of total loading vector (entire length analysis)			○	
NCOUPL	Initial setting of contact pair in local mechanical analysis				○
ONPLOT	Control routine for ON-LINE plotter	○			
OPTSO2	Solution of asymmetrical matrix			○	○
OPTSOL	Solution of symmetrical matrix			○	
OURELM	Output of stress and strain at element gauss point				○
OUREM	Auxiliary routine for OURELM				○
OUTND	Auxiliary routine for output of nodal displacement				○
OUTND	Output of nodal displacement				○
OUTP	Output of time-dependent variables in the entire length analysis			○	
OUTP1	Output of time-dependent variables in the local mechanical analysis				○
OUTPT0	Final summary output 0			○	
OUTPT1	Final summary output 1		○	○	
OUTPT2	Final summary output 2		○	○	
P2	Shape function of quadratic element				○
PAPLOT	Map of crack and yield of pellet				○
PDENS	Densification strain of pellet		○	○	

Table A1 (continued)

Name	Function	P	T	M1	M2
PFRFZ	Calc. of pellet axial force			○	
PHCAP	Specific volumetric heat of pellet		○		
PHIST	Time step control	○			
PJUMP	Initial relocation		○		○
PLOTLN	Mapping of gap contact state				○
POWDIS	Calc. of power distribution		○		
PPLOT	Auxiliary routine for PLOTLN				○
PRHIS2	Output routine for power history	○			
PRINT0	Output of input data of thermal calculation		○		
PRINT1	Output of time-dependent variables in thermal analysis		○		
PRINT2	Output of time-dependent variables in gap gas state		○		
PRINT3	Output of time-dependent temperature distribution		○		
PRINT5	Detailed output of time-dependent variables in thermal analysis		○		
PRIOPT	Option output in local mechanical analysis	○			
PROPT2	Option output for entire length analysis	○			
PROBD1	Setting of pellet axial force condition				○
PROBDF	Judgment of pellet/pellet contact state				○
PROBTY	Judgment of yield/unloading state				○
PROFIL	Address calculation by profile method				○
PSWEL	Pellet swelling strain				○
PSWELT	Pellet swelling strain by solid FP atoms		○	○	○
PTHCON	UO_2 pellet thermal conductivity		○		
PTHEX	Pellet thermal expansion		○	○	○
PUGH	Calc. of cladding creep by PUGH's reversal method				○
PUTHCN	MOX pellet thermal conductivity		○		

Table A1 (continued)

Name	Function	P	T	M1	M2
PX2	$\frac{\partial N}{\partial \xi}$ of quadratic element of FEM				○
PY2	$\frac{\partial N}{\partial \eta}$ of quadratic element of FEM				○
RDGAS1	Setting of time step width for gas transfer calculation in the axial direction		○		
RDGAS2	Diffusion and flow transfer of gas in the axial direction		○		
RDTEMP	Control of entire thermal analysis		○		
REDSTR	Re-distribution of FP density after grain growth of pellet		○		
REPLG	Updating of stress and strain at gauss point				○
REPLN	Updating of displacement and nodal force at each node point				○
SBES0	0-th Bessel function		○		
SBES1	Primary Bessel function		○		
SECOND	Calculation time (s)			○	
SETPL1	Mapping of cracked, elastic and plastic regions				○
SETPL2	Mapping of cracked, elastic and plastic regions				○
SETPL3	Mapping of cracked, elastic and plastic regions				○
SETPLT	Mapping of cracked, elastic and plastic regions				○
SETR	Re-meshing of pellet grains after grain growth		○		
SETR0	Initial setting of in-grain coordinate of pellet		○		
SHAPE2	Quadratic shape function				○
SOLVE	Solver for FP gas release calculation of 3 elements		○		
SOLVE2	Solver for FP gas release calculation		○		
SOLVF2	Setting of sliding state between pellet and cladding			○	
SOLVF3	Setting of clogged state between pellet and cladding			○	

Table A1 (continued)

Name	Function	P	T	M1	M2
SSMAT	Formation of total matrix for each segment			○	
STRESS	Stress strain calculation				○
SUFCN	Control of cladding surface heat transfer coefficient		○		
SWELL	Pellet swelling model related to FP gas release model		○	○	○
TEMP1D	One dimensional heat conduction calculation		○		
TERP	Calc. routine for ON-LINE PLOTTER plotter		○		
THERFD	Calc. of gap closure by FP gas swelling of pellet		○		
THGAPN	Deformation calculation in thermal analysis		○		
TIC	Auxiliary routine for ON-LINE plotter	○			
TIMEB	Time step control by pellet/pellet contact in the axial direction				○
TIMEG	Time step control by pellet/clad contact in the radial direction				○
TIMER	Main routine for time step control				○
TIMEY	Time step control by plasticity/unloading				○
TMELT	Calc. of pellet melting point		○		
TMSTP	Determination of time step in entire length analysis			○	
TYPE1	ON-LINE plotter type 1	○			
TYPE2	ON-LINE plotter type 2	○			
URSWEL	Chubb'sBMI model of pellet swelling strain		○	○	○
USMESH	Meshing for heat conduction calculation		○		
USTEMP	Main routine for heat conduction calculation		○		
VLUMES	Calc. of plenum volume		○		
XBDMAT	$[B]^T[D]$ matrix			○	
XBMAT	[B] matrix			○	
XCPEP2	Calc. of cladding creep strain rate $\dot{\varepsilon}^{\theta}$			○	

Table A1 (continued)

Name	Function	P	T	M1	M2
XCPEQ2	Calc. of $\dot{\bar{\varepsilon}}^c(=f)$ and $\frac{\partial f}{\partial \bar{\sigma}}, \frac{\partial f}{\partial \bar{\varepsilon}^c}$ in cladding creep			○	
XCPHD2	Calc. of $\dot{\bar{\varepsilon}}^H(=g)$ and $\frac{\partial g}{\partial \bar{\sigma}}, \frac{\partial g}{\partial \bar{\varepsilon}^H}$ in cladding creep			○	
XCPM11	Formation of $[C^c]$ matrix and $\{\Delta \varepsilon^c\}$ vector in pellet creep			○	
XCPM12	Formation of strain increment $\{\Delta \varepsilon^c\}$ of pellet creep			○	
XCREP1	Formation of $[C^c]$ matrix and $\{\Delta \varepsilon^c\}$ vector in cladding creep			○	
XCREP2	Formation of strain increment $\{\Delta \varepsilon^c\}$ of cladding			○	
XDPMAT	$[D^p]$ matrix			○	
XDPST	Calc. of equivalent plastic strain increment			○	
XDVSIG	Deviation stress			○	
XELML1	Formation of element matrix and loading vector			○	
XELML2	Calc. of stress and strain in element			○	
XEQEPS	Equivalent strain			○	
XEQSIG	Equivalent stress			○	
XESMAT	Element stiffness matrix			○	
XFHSFT	Stress-differential term in pellet yield function			○	
XFLOAD	Element loading vector			○	
XFTSFT	Temperature-differential term of pellet yield function			○	
XIODD	Calc. of iodine concentration			○	
XPCM	Main routine for the entire length analysis			○	
XPJUMP	Initial relocation			○	
XPRBTY	Judgment of plasticity/unloading			○	
XPSWEL	Pellet swelling strain			○	
XPUGH	Pugh's reversal method for cladding creep			○	

A3-(2) Subroutine Tree

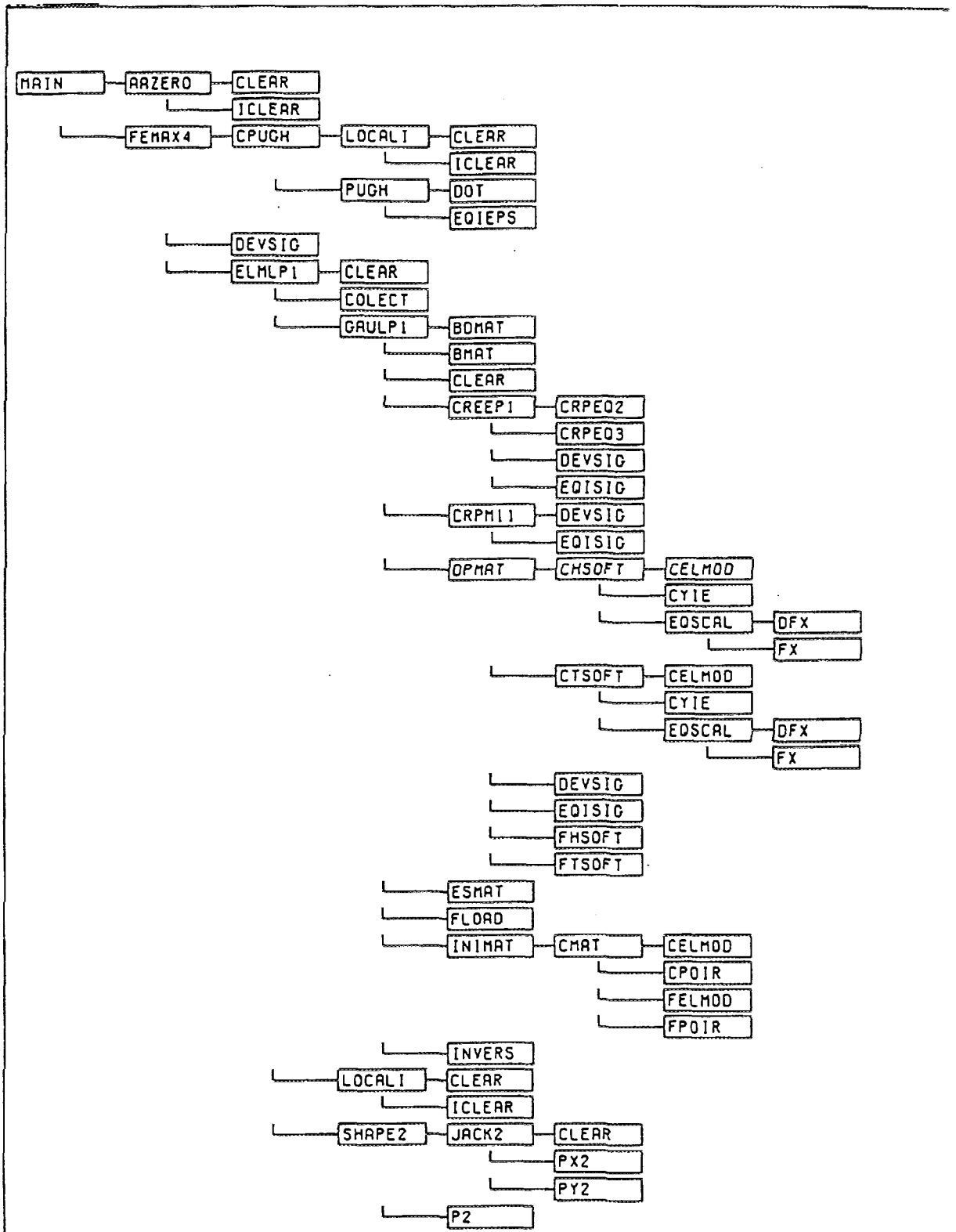
MAIN
AAZERO
CLEAR
ICLEAR
FEMAX4
CPUGH
LOCALI
CLEAR
ICLEAR
PUGH
DOT
EQIEPS
DEVSIG
ELMLP1
CLEAR
COLECT
GAULP1
BDMAT
BMAT
CLEAR
CREEP1
CRPEQ2
CRPEQ3
DEVSIG
EQISIG
CRPM11
DEVSIG
EQISIG
DPMAT
CHSOFT
CELMOD
CYIE
EQSCAL
DFX
FX
CTSOFT
CELMOD
CYIE
EQSCAL
DFX
FX
DEVSIG
EQISIG
FHSOFT
FTSOFT
ESMAT
FLOAD
INIMAT
CMAT
CELMOD
CPOIR
FELMOD
FPOIR
INVERS
LOCALI
CLEAR
ICLEAR
SHAPE2
JACK2
CLEAR
PX2
PY2
P2

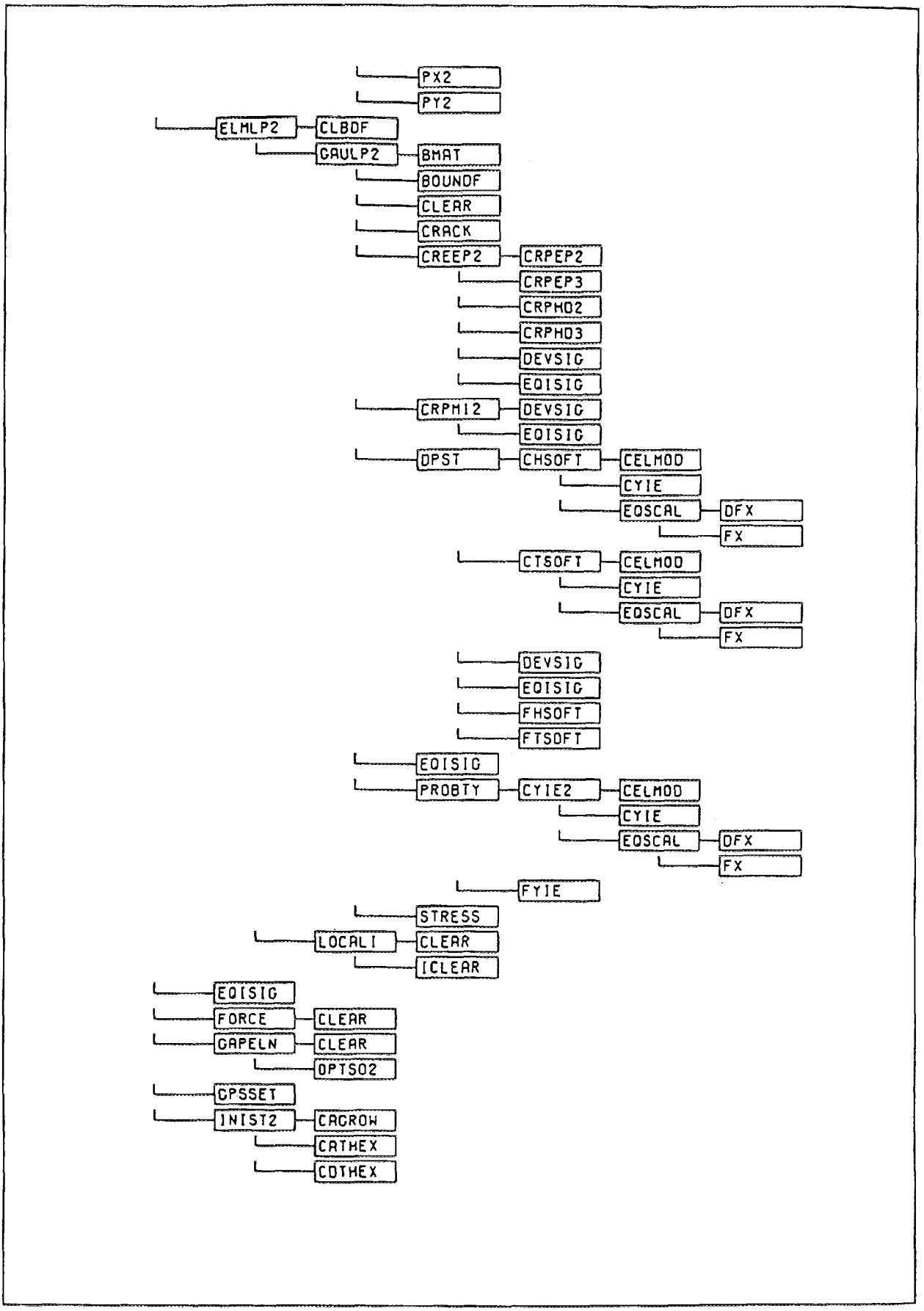
PX2
PY2
ELMLP2
CLBDF
GAULP2
BMAT
BOUNDF
CLEAR
CRACK
CREEP2
CRPEP2
CRPEP3
CRPHD2
CRPHD3
DEVSIG
EQISIG
CRPMI2
DEVSIG
EQISIG
DPST
CHSOFT
CELMOD
CYIE
EQSCAL
DFX
FX
CTSOFT
CELMOD
CYIE
EQSCAL
DFX
FX
DEVSIG
EQISIG
FHSOFT
FTSOFT
EQISIG
PROBTY
CYIE2
CELMOD
CYIE
EQSCAL
DFX
FX
FYIE
STRESS
LOCALI
CLEAR
ICLEAR
EQISIG
FORCE
CLEAR
GAPELN
CLEAR
OPTSO2
GPSSET
INIST2
CAGROW
CATHEX
COTHEX

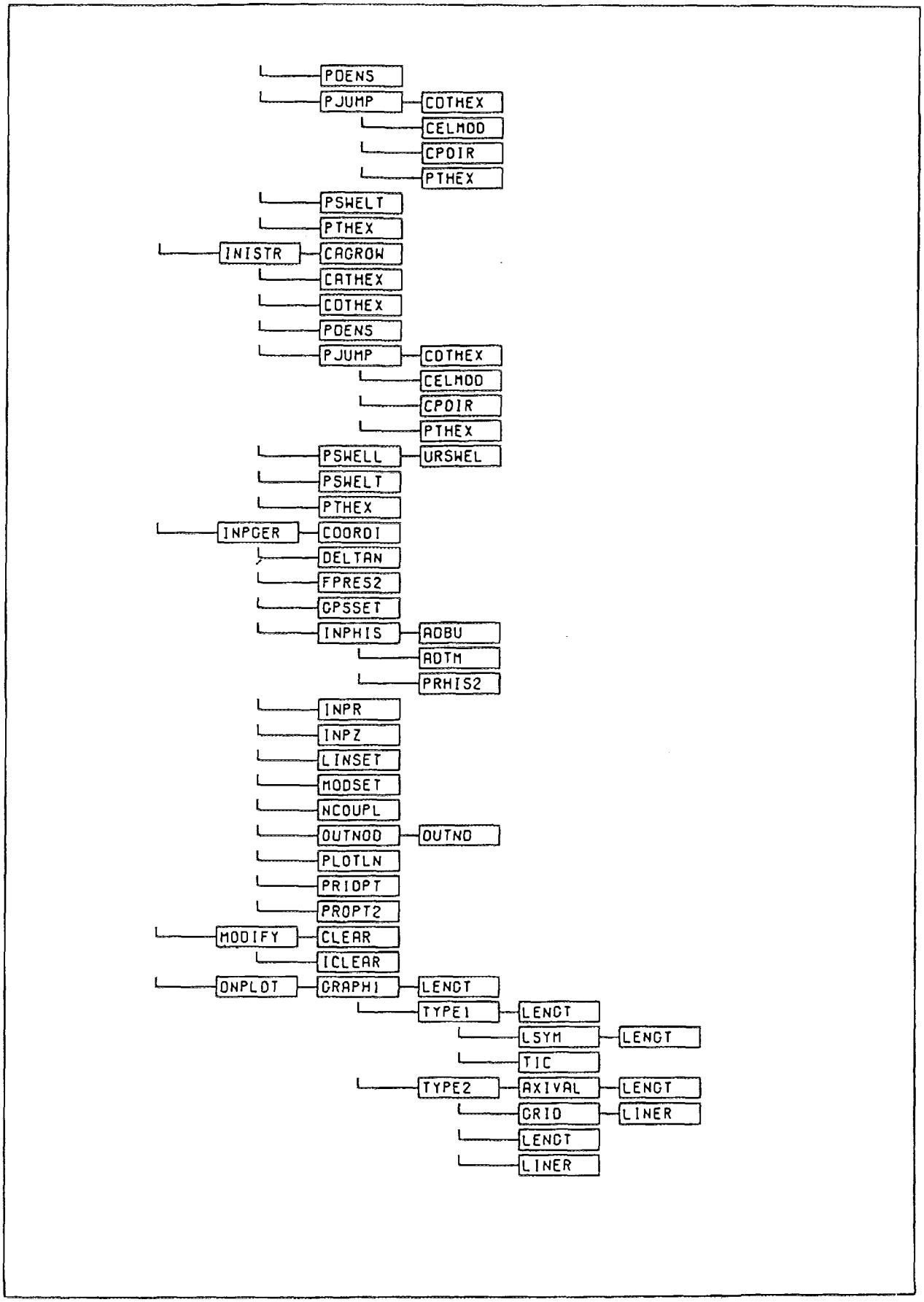
PDENS
PJUMP
COTHEX
CELMOD
CPOIR
PTHEX
PSWELT
PTHEX
INISTR
CAGROW
CATHEX
COTHEX
PDENS
PJUMP
COTHEX
CELMOD
CPOIR
PTHEX
PSWELL
URSWEL
PSWELT
PTHEX
INPGER
COORDI
DELTAN
FPRES2
GPSSET
INPHIS
AOBU
AOTM
PRHIS2
INPR
INPZ
LINSET
MODSET
NCOUPL
OUTNOD
OUTNO
PLOTLN
PRIOPT
PROPT2
MODIFY
CLEAR
ICLEAR
ONPLOT
GRAPH1
LENGT
TYPE1
LENGT
LSYM
LENGT
TIC
TYPE2
AXIVAL
LENGT
GRID
LINER
LENGT
LINER

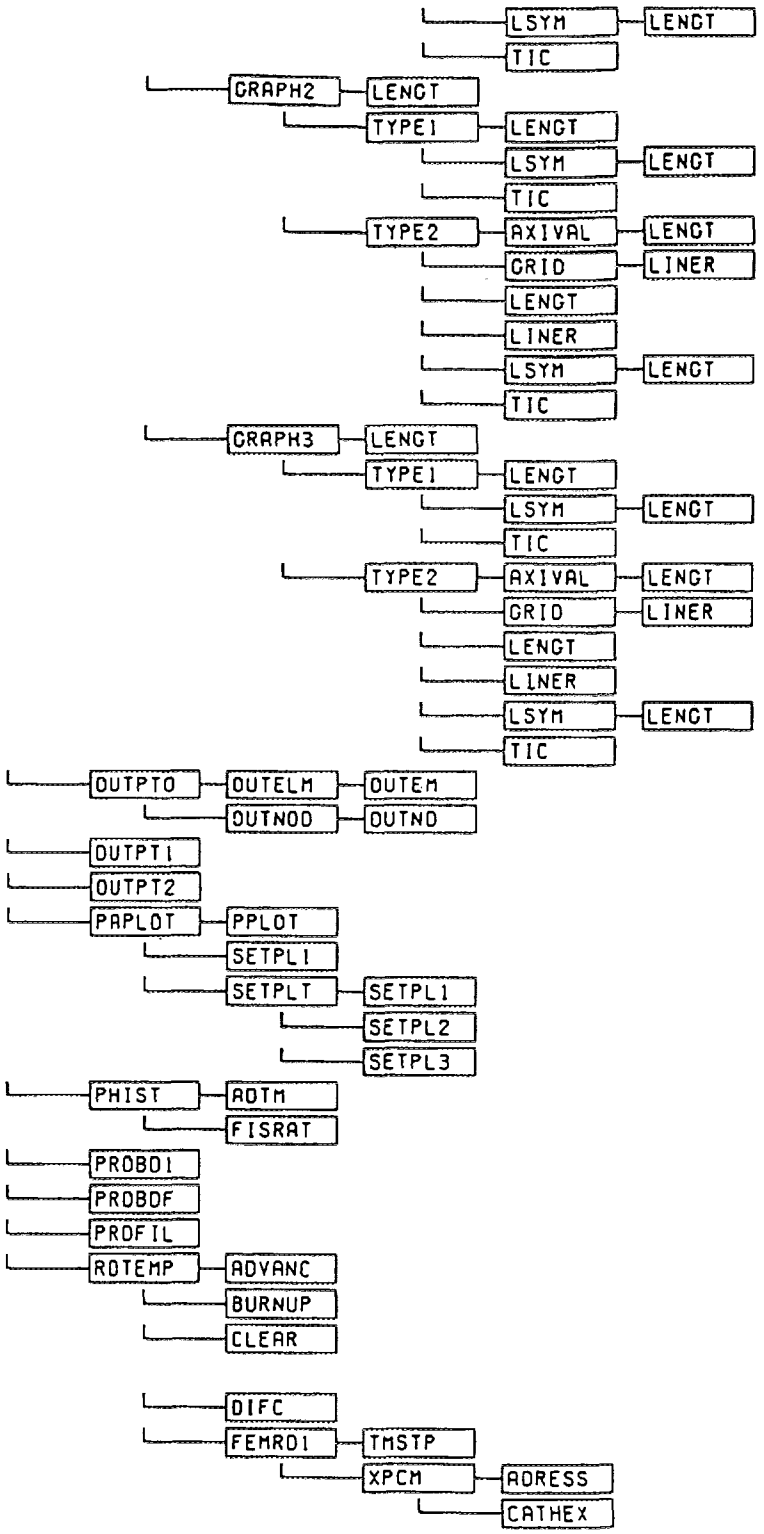
LSYM
LENGT
TIC
GRAPH2
LENGT
TYPE1
LENGT
LSYM
LENGT
TIC
TYPE2
AXIVAL
LENGT
GRID
LINER
LENGT
LINER
LSYM
LENGT
TIC
GRAPH3
LENGT
TYPE1
LENGT
LSYM
LENGT
TIC
TYPE2
AXIVAL
LENGT
GRID
LINER
LENGT
LINER
LSYM
LENGT
TIC
OUTPTO
OUTELM
OUTEM
OUTNOD
OUTND
OUTPT1
OUTPT2
PAPLOT
PPLOT
SETPL1
SETPLT
SETPL1
SETPL2
SETPL3
PHIST
ADTM
FISRAT
PROBD1
PROBDF
PROFIL
ROTEMP
ADVANC
BURNUP
CLEAR
DIFC
FEMRD1
TMSTP
XPCM
ADRESS
CATHEX

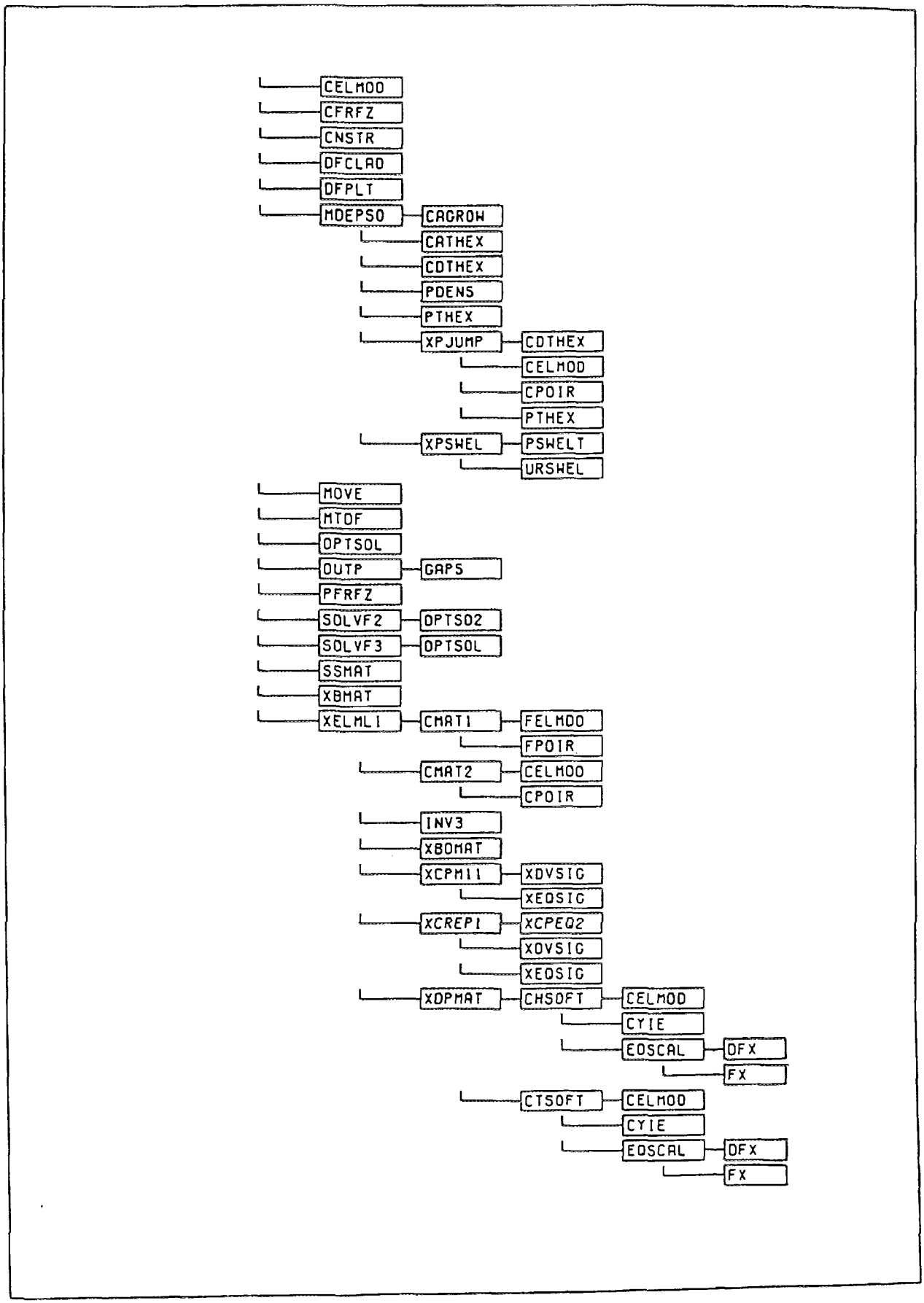
CELMOD
CFRFZ
CNSTR
DFCLAD
DFPLT
MDEPSO
CAGROW
CATHEX
CDTHEX
PDENS
PTHEX
XPJUMP
CDTHEX
CELMOD
CPOIR
PTHEX
XPSWEL
PSWELT
URSWEL
MOVE
MTOF
OPTSOL
OUTP
GAPS
PFRFZ
SOLVF2
OPTSO2
SOLVF3
OPTSOL
SSMAT
XBMAT
XELMLI
CMAT1
FELMOD
FPOIR
CMAT2
CELMOD
CPOIR
INV3
XBOMAT
XCPM11
XDVSIG
XEOSIG
XCREP1
XCPEQ2
XDVSIG
XEOSIG
XDPMAT
CHSOFT
CELMOD
CYIE
EOSCAL
DFX
FX
CTSOFT
CELMOD
CYIE
EOSCAL
DFX
FX

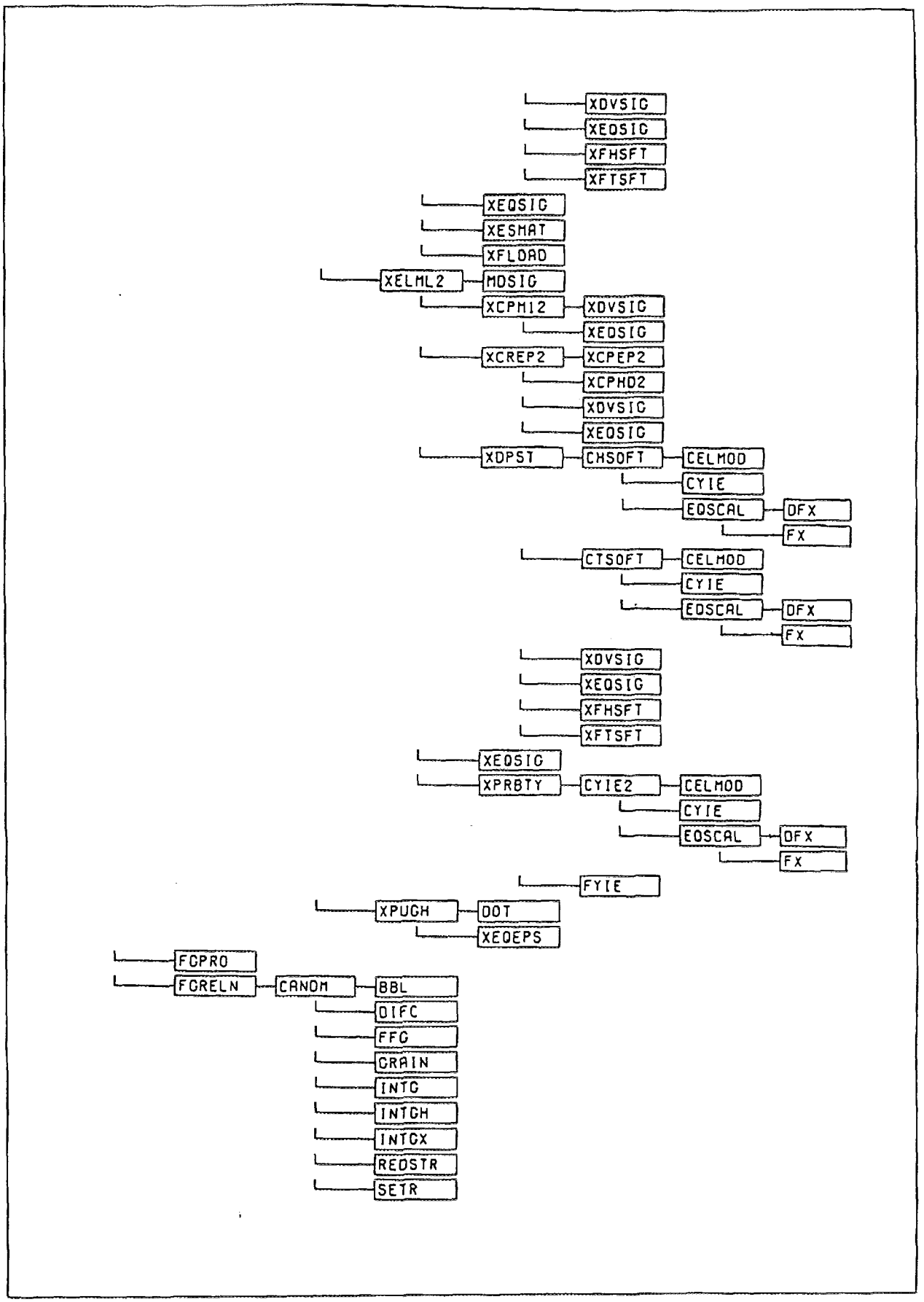
XDVSIG
XEQSIG
XFHSFT
XFTSFT
XEQSIG
XESMAT
XFLOAD
XELML2
MDSIG
XCPM12
XDVSIG
XEQSIG
XCREP2
XCPEP2
XCPHD2
XDVSIG
XEQSIG
XDPST
CHSOFT
CELMOD
CYIE
EQSCAL
DFX
FX
CTSOFT
CELMOD
CYIE
EQSCAL
DFX
FX
XDVSIG
XEQSIG
XFHSFT
XFTSFT
XEQSIG
XPRBTY
CYIE2
CELMOD
CYIE
EQSCAL
DFX
FX
FYIE
XPUCH
DOT
XEQEPS
FCPRO
FCRELN
CANOM
BBL
DIFC
FFG
GRAIN
INTG
INTGH
INTGX
REDSTR
SETR

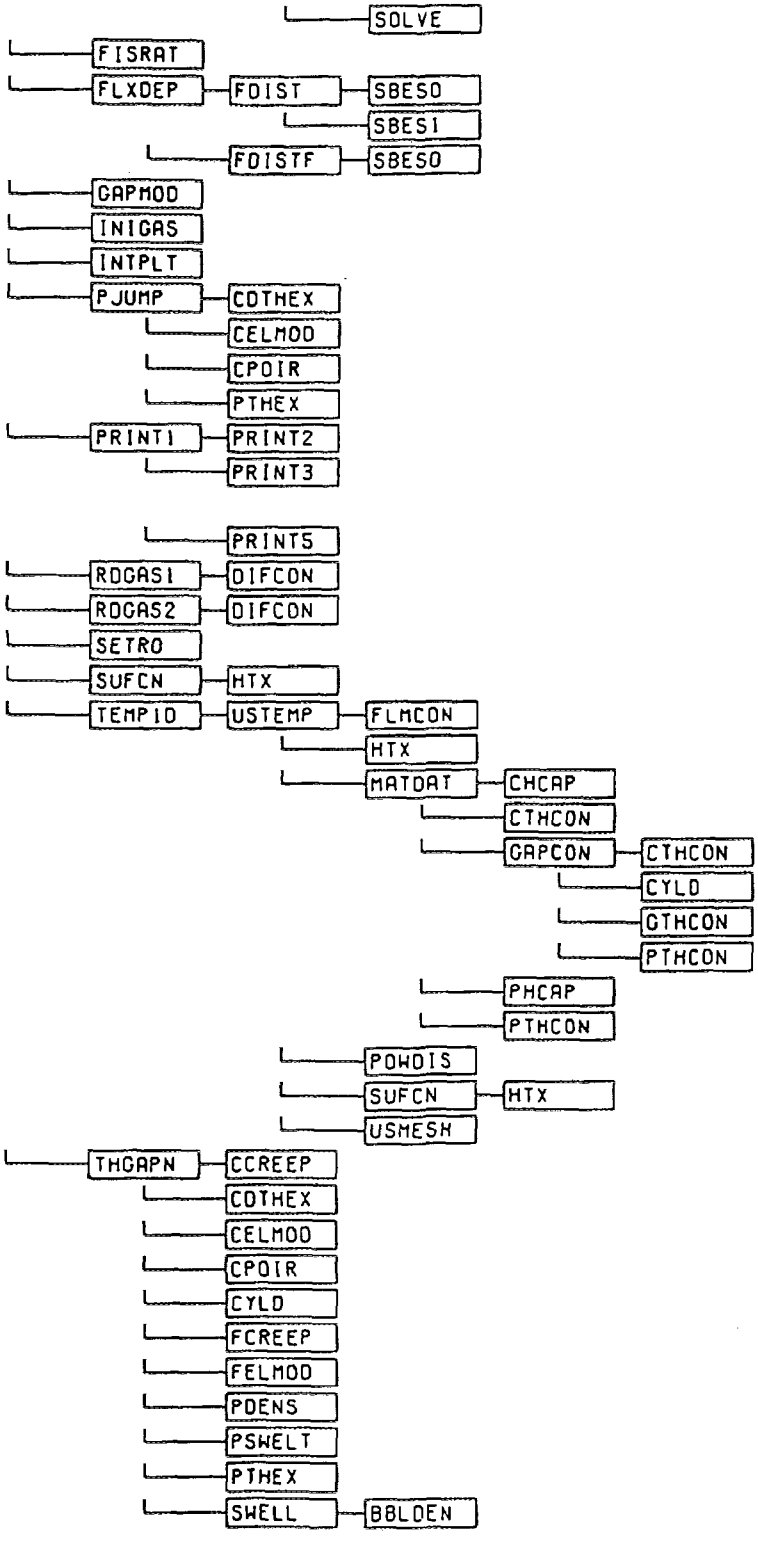
SOLVE
FISRAT
FLXDEP
FDIST
SBES0
SBES1
FDISTF
SBES0
GAPMOD
INIGAS
INTPLT
PJUMP
CDTHEX
CELMOD
CPOIR
PTHEX
PRINT1
PRINT2
PRINT3
PRINT5
RDGAS1
DIFCON
RDGAS2
DIFCON
SETRO
SUFCN
HTX
TEMPID
USTEMP
FLMCON
HTX
MATDAT
CHCAP
CTHCON
GAPCON
CTHCON
CYLD
GTHCON
PTHCON
PHCAP
PTHCON
POWDIS
SUFCN
HTX
USMESH
THGAPN
CCREEP
CDTHEX
CELMOD
CPOIR
CYLD
FCREEP
FELMOD
PDENS
PSWELT
PTHEX
SWELL
BBLDEN

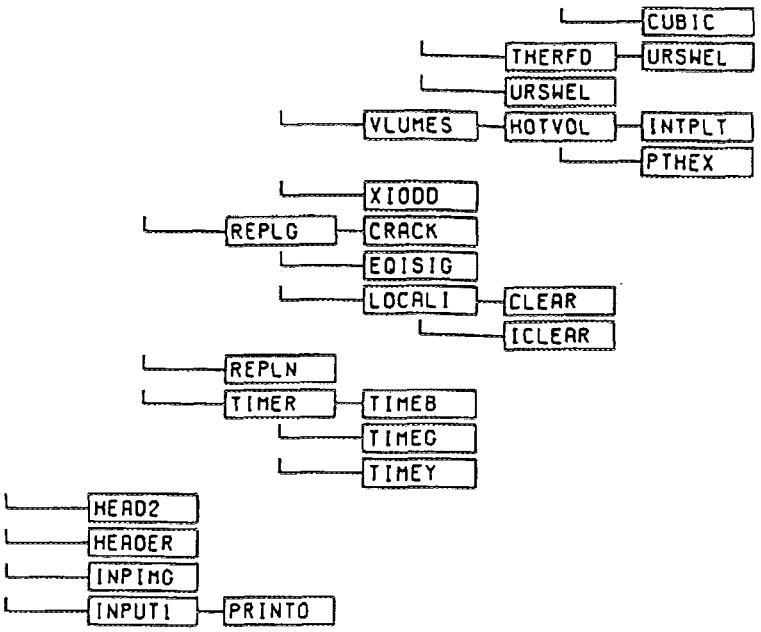
CUBIC
THERFD
URSWEL
URSWEL
VLUMES
HOTVOL
INTPLT
PTHEX
XIODD
REPLG
CRACK
EQISIG
LOCALI
CLEAR
ICLEAR
REPLN
TIMER
TIMEB
TIMEG
TIMEY
HEAD2
HEADER
INPIMG
INPUTI
PRINTO

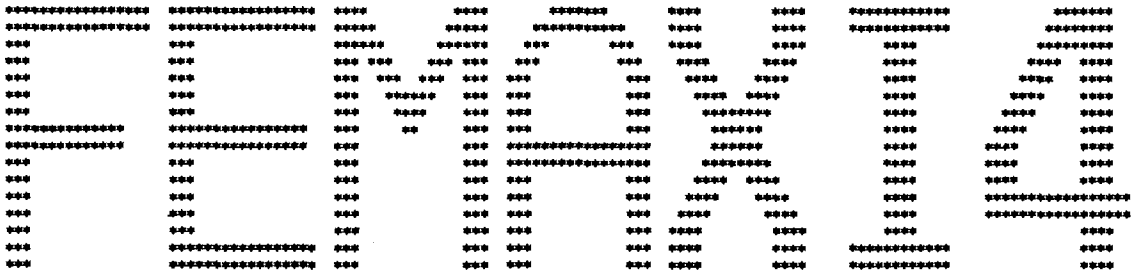

FUEL ELEMENT MODELING BY AXI SYMMETRIC FINITE ELEMENT METHOD

VERSION 4.0

RUN DATE 97/Jun/30

ZORITA-1 GROUP A < Z001P > NOMINAL

A4 Sample Input/Output

Title
(To be output at any time)

The title which was in card 1 of the input file is shown here.

INPUT DATA LIST

```
                   1         2         3         4         5         6         7         8
CARD NO.  ....5....0....5....0....5....0....5....0....5....0....5....0....5....0....5....0
      1.  ZORITA-1 GROUP A  < Z001P > NOMINAL
      2.   $INPUT IBUNP=1,ICK1=0,GR=10.,IPLT=1,BETAX=0.002,IFEMRO=0,
      3.         R1=1.,EPSRLZ=5.D-3,IPLOPT=-5,DMAX=2.,GRWF=1.,SBU=1.D4,FCRFAC=1.,
      4.         IWTHE=18*1,IPTHCN=1,BUMIN=5000.0,BUMAX=20000.0,IURS=0,
      5.         ICORRO=1,EFCOEF=1.,INPCK=0,
      6.   $END
      7.           8         4         3
      8.           1    0.9486     1.072
      9.           2         0       0.0     0.932     1.520     0.060     0.940   27.0875
     10.           2         0       0.0     0.932     1.520     0.060     0.940   27.0875
     11.           2         0       0.0     0.932     1.520     0.060     0.940   27.0875
     12.           2         0       0.0     0.932     1.520     0.060     0.940   27.0875
     13.           2         0       0.0     0.932     1.520     0.060     0.940   27.0875
     14.           2         0       0.0     0.932     1.520     0.060     0.940   27.0875
     15.           2         0       0.0     0.932     1.520     0.060     0.940   27.0875
     16.           2         0       0.0     0.932     1.520     0.060     0.940   27.0875
     17.      0.7456     0.034
     18.     30.9493      3.45       1.0       0.0       0.0       0.0
     19.          21
     20.                           0.001    5.3013    555.15     13.79         0      6.50
     21.  0.8001.0501.1401.2001.1601.1501.000.500                         21
     22.     5.00                  260.0    5.3013                                 0
     23.      -         5000.0     260.0                                           0
     24.               10000.0     260.0                                           0
     25.               15000.0     260.0                                           0
     26.               20000.0     260.0                                           0
     27.               25000.0     260.0                                           0
     28.               30600.0     260.0                                           0
     29.     5.00                  304.0    5.3013                            -100    0
     30.               33000.0     304.0                                       100    0
     31.               36000.0     304.0                                       100    0
     32.               39000.0     304.0                                       100    0
     33.               42500.0     304.0                                       100    0
     34.     5.00                  269.0    5.3013                            -100    0
     35.               45000.0     269.0                                       100    0
     36.               48000.0     269.0                                       100    0
     37.               51000.0     269.0                                       100    0
     38.               54000.0     269.0                                       100    0
     39.               57500.0     269.0                                       100    1
     40.     5.00                  269.0    5.3013    555.15     13.79 -100    0      6.50
     41.     5.00                  0.001    1.0009    291.15       0.1 -100    2      6.50
     42.  STOP
          ....5....0....5....0....5....0....5....0....5....0....5....0....5....0....5....0
```

Input data list
(Output in the case of IPRINT(1)=1)

Image of the input file

Column gage for confirmation of data

ZORITA-1 GROUP A < ZOO1P > NOMINAL

P.W.R. FUEL ROD.

*INPUT DATA

(1) PELLET SPECIFICATIONS ——

NODE	DIAMETER (CM) INSIDE	DIAMETER (CM) OUTSIDE	SHAPE CHAMF	SHAPE DISH	U-235 ENRICH.	FRACTIONAL DENSITY	ONE PELLET LENGTH (CM)	NODE LENGTH (CM)
1	0.000	0.932		**	0.060	0.940	1.520	27.087
2	0.000	0.932		**	0.060	0.940	1.520	27.087
3	0.000	0.932		**	0.060	0.940	1.520	27.087
* 4	0.000	0.932		**	0.060	0.940	1.520	27.087
5	0.000	0.932		**	0.060	0.940	1.520	27.087
6	0.000	0.932		**	0.060	0.940	1.520	27.087
7	0.000	0.932		**	0.060	0.940	1.520	27.087
8	0.000	0.932		**	0.060	0.940	1.520	27.087

DISH DIAMETER (CM) = 0.748 DISH DEPTH (CM) = 0.034 DISH BOTTOM (CM) = 0.000
PELLET TOTAL WEIGHT (GRAM) = 1501.202
GRAIN SIZE (MICRON) = 10.000
MAXIMUM FRACTIONAL DENSITY = 0.960
SATURATE BURNUP (MWD/TUO2) = 10000.000

(2) OTHERS

CLAD. MATERIAL IS STRESS RELIEVED ZIRCALOY
CLAD. INSIDE DIAMETER (CM) = 0.949
CLAD. OUTSIDE DIAMETER (CM) = 1.072

THERMAL RELOCATION (-) = 0.200
UPPER PLENUM VOLUME (CM**3) = 30.949
LOWER PLENUM VOLUME (CM**3) = 0.000
INITIAL GAS PRESSURE (MPA) = 3.450

INITIAL GAS COMPOSITION (PERCENT)
HELIUM = 100.0
NITROGEN= 0.0
KRYPTON = 0.0
XENON = 0.0
PELLET SURFACE ROUGHNESS (CM) = 0.0001
CLADDING SURFACE ROUGHNESS (CM) = 0.0001
ROOM TEMPERATURE (DEG.K) = 291.15

Fuel design data
(Output in the case of IPRINT(2)=1)

(1) Pellet

Inner diameter, outer diameter, shape, U-235, enrichment, density ratio, height, axial segment length

A single asterisk is used to mark the objective segment

In the case of dish pellet or chamfer pellet, form, pellet total weight, grain size, final density due to densification, and completion burn-up are output

(2) Others

Cladding material, inner diameter, outer diameter, ratio of thermal relocation, upper and lower plenum volumes, initial gas pressure, plasticity, pellet/cladding surface roughness, room temperature

```
*******************************************************************************************************
*                                                                                                     *
*   ZORITA-1 GROUP A  < Z001P > NOMINAL                             — FEMAXI-IV ( VER-00 ) —          *
*                                                                                                     *
*******************************************************************************************************

                     NODAL POINT AND ELEMENT CONNECTION MAP

                     *** PELLET ***                      GAP     *** CLADDING ***

        7+ 11+ 18+ 22+ 29+ 33+ 40+ 44+ 51+ 55+ 62         I  69+ 73+ 80
       +       +       +       +       +       +             +       +
        6   3  17   6  28   9  39  12  50  15  61         I  68  18  79
       +       +       +       +       +       +             +       +
        5+ 10+ 16+ 21+ 27+ 32+ 38+ 43+ 49+ 54+ 60         I  67+ 72+ 78
       +       +       +       +       +       +             +       +
        4   2  15   5  26   8  37  11  48  14  59         I  66  17  77
       +       +       +       +       +       +             +       +
        3+  9+ 14+ 20+ 25+ 31+ 36+ 42+ 47+ 53+ 58         I  65+ 71+ 76
       +       +       +       +       +       +             +       +
        2   1  13   4  24   7  35  10  46  13  57         I  64  16  75
       +       +       +       +       +       +             +       +
        1+  8+ 12+ 19+ 23+ 30+ 34+ 41+ 45+ 52+ 56         I  63+ 70+ 74


                                          ***** NODAL COORDINATE (MICRON) *****

 (R-DIRECTION)                                                                   GAP
   0.0  466.0  932.0 1398.0 1864.0 2330.0 2796.0 3262.0 3728.0 4194.0 4660.0I 4743.0 5051.5 5360.0
   0.0         932.0        1864.0        2796.0        3728.0        4660.0I 4743.0        5360.0
   0.0  466.0  932.0 1398.0 1864.0 2330.0 2796.0 3262.0 3728.0 4194.0 4660.0I 4743.0 5051.5 5360.0
   0.0         932.0        1864.0        2796.0        3728.0        4660.0I 4743.0        5360.0
   0.0  466.0  932.0 1398.0 1864.0 2330.0 2796.0 3262.0 3728.0 4194.0 4660.0I 4743.0 5051.5 5360.0
   0.0         932.0        1864.0        2796.0        3728.0        4660.0I 4743.0        5360.0
   0.0  466.0  932.0 1398.0 1864.0 2330.0 2796.0 3262.0 3728.0 4194.0 4660.0I 4743.0 5051.5 5360.0

 (Z-DIRECTION)                                                                   GAP
7260.0 7265.3 7281.1 7307.5 7344.5 7392.1 7450.6 7519.8 7600.0 7600.0 7600.0I 7600.0 7600.0 7600.0
6050.0        6067.6        6120.4        6208.8        6333.3        6333.3I 6333.3        6333.3
4840.0 4843.5 4854.1 4871.6 4896.3 4928.1 4967.0 5013.2 5066.7 5066.7 5066.7I 5066.7 5066.7 5066.7
3630.0        3640.5        3672.2        3725.3        3800.0        3800.0I 3800.0        3800.0
2420.0 2421.8 2427.0 2435.8 2448.2 2464.0 2483.5 2506.6 2533.3 2533.3 2533.3I 2533.3 2533.3 2533.3
1210.0        1213.5        1224.1        1241.8        1266.7        1266.7I 1266.7        1266.7
   0.0    0.0    0.0    0.0    0.0    0.0    0.0    0.0    0.0    0.0    0.0I    0.0    0.0    0.0
```

FEM node information

(Output in the case of IPRINT(3)=1)

Element number and node number for mesh division applied to half-length pellet

```
5+ 10+ 16+
+       +
4   2  15
+       +
```

Coordinates in the radial and axial directions of each node

NAMELIST PARAMETERS(1)

INPUT OPTION

PARAMETER	DESCRIPTION	DIMENSION	VALUE
(1) OPTION FOR INPUT			
IBUNP	OPTION FOR BURNUP UNIT (=0;MWD/TUO2 ,=1;MWD/TU, =2;GJ/KGU)	-	1
IDAY	OPTION FOR TIME UNIT (=0;HR,=1;DAY)	-	0
IFLX	OPTION TO GIVE RADIAL FLUX DEPRESSION PROFILE	-	0
IRH	POWER INCREMENT WIDTH FOR ATTENDED SEGMENT	-	0
PWCHG	MAGNIFICATION ON LHR BY MULTIPLYING THE FACTOR (1+PWCHG)	-	0.00
FAIW	FAST NEUTRON FLUX PER 1W/CM	N/CM2-SEC/W/CM	0.000E+00
ICLMAS	OPTION FOR COOLANT FLOW (=0:VELOCITY(M/S),=1:FLUX(KG/CM2-S))	-	0
(2) OPTION FOR CALCULATION			
INPCK	INPUT DATA CHECK OPTION (=0;CALCULATION ,=1;INPUT DATA CHECK)	-	0
ICK1	FEM MECHANICAL CALCULATION OPTION (=0;CALCULATE ,=1;NOT CALCULATE)	-	0
ICH1	ELASTIC CALCULATION OPTION (LOCAL MODEL) (=0;NORMAL ,=1;ELASTIC)	-	0
IELAST	ELASTIC CALCULATION OPTION (WHOLE ROD MODEL) (=0;NORMAL ,=1;ELASTIC)	-	0
MPP	THERMAL CALCULATION OPTION (=0;STANDARD ,=1;SIMPLE)	-	0
IFEMRD	FEM MECHANICAL CALCULATION OPTION(=0;LOCAL MODEL,=1;WHOLE ROD MODEL)	-	0
TLIM	LIMITING TIME FOR CPU	SEC	20000.00
IST	OPTION FOR GAP GAS MODEL (=0;INPUT ,=1:GAS FLOW MODEL)	-	1
ZR	ZIRCONIUM LINER THICKNESS	CM	0.000E+00
(3) CONDITION FOR CALCULATION			
ITIME	NUMBER OF HISTORY POINTS CHANGING PLENUM GAS PRESSURE	-	0 0 0
GASPRN	PLENUM GAS PRESSURE AT THE HISTORY POINT	PA	0.000 0.000 0.000
PLENM	PLENUM GAS VOLUME AT THE HISTORY POINT	CM**3	0.000 0.000 0.000
GMIXN	PLENUM GAS COMPOSITION AT THE HISTORY POINT (HE, N2, KR, XE)	-	0.000 0.000 0.000 0.000 0.000 0.000 0.000 0.000 0.000 0.000 0.000 0.000
IOPT1	BOTTOM PLENUM OPTION (=0;NO BOTTOM ,=1;BOTTOM PLENUM IS PRESENT)	-	0
XKSU	ELASTIC CONSTANT OF UPPER PLENUM	N/M	1500.00
ALSU	THERMAL EXPANSION RATIO OF UPPER PLENUM SPRING	1/K	1.500E-05
XKSL	ELASTIC CONSTANT OF LOWER PLENUM	N/M	2500.00
ALSL	THERMAL EXPANSION RATIO OF LOWER PLENUM SPRING	1/K	1.500E-05
AMU	FRICTION COEFFICIENT BETWEEN PELLET AND CLADDING	-	0.40
DE	EQUIVALENT HYDRAULIC DIAMETER	CM	0.94
FAREA	FLOW AREA OF COOLANT	CM**2	0.79
PITCH	FUEL ROD PITCH	CM	1.30
DTPL	DIFFERENCE BETWEEN PLENUM TEMPERATURE AND COOLANT TEMP.	-	25.00
TROOM	ROOM TEMPERATURE	K	291.15

NAMELIST PARAMETERS(2)

INPUT OPTION

PARAMETER	DESCRIPTION	DIMENSION	VALUE
(1) CONTROLE OF TIME STEP			
IAUTO	OPTION FOR AUTOMATIC CONTROL OF TIME STEP	-	1
DPXX	UPPER LIMIT OF POWER DEPENDENT TIME STEP	W/CM	10.000
DPBU	UPPER LIMIT OF BURNUP DEPENDENT TIME STEP	MWD/TUO2	500.000

Parameter list
(Output in the case of IPRINT(4)=1)

IPH	POWER INCREMENT WIDTH FOR ATTENDED SEGMENT (=0, IFEM SEGMENT , =1 : MAXIMUM POWER SEGMENT)	-	0
EFCOEF	CREEP DEPENDENT TIME STEP CONTROL PARAMETER	-	10.000
LCMAX	MAXIMUM NUMBER OF JUDGEMENTS OF PELLET-CLAD CONTACT STATE	-	3
LMAX	NUMBER OF ITERATION OF NEWTON-LAPHSON METHOD	-	2
ITIMY	TIME STEP CONTROLE OPTION FOR ELASTO-PLASTIC ANALYSIS	-	-1
FAC	TIME STEP CONTROLE FACTOR	-	1.000E+04

(2) OPTION FOR THERMAL CONDUCTANCE

IPTHCN	OPTION FOR PELLET THERMAL CONDUCTIVITY (=0, 1 : MATPRO-09, =1 : LYOS)	-	1
MOX	MOX=1 ADOPTS MARTIN-S THERMAL CONDUCTIVITY FORMULA	-	0
PU	WEIGHT FRACTION WHEN MOX=1	-	0.000
Y	VALUE OF Y FOR MO2-Y	-	0.000
IGD	IGD ADOPTS THERMAL CONDUCTIVITY FORMULA BY FUKUSHIMA	-	0
GD	DENSITY OF GD203 (WEIGHT FRACTION)	-	0.000

(3) OPTION FOR THERMAL EXPANSION

IPTHEX	OPTION FOR FORMULA OF PELLET THERMAL EXPANSION	-	0
ICATHX	OPTION FOR FORMULA OF CLAD THERMAL EXPANSION	-	0

(4) OPTION FOR CREEP

FCRFAC	MAGNIFICATION ON PELLET CREEP FORMULA (MECHANICAL MODEL)	-	1.000
TCS	CUT OFF VALUE OF TEMP. WITHIN PELLET CREEP CAL. (MECHANICAL MODEL)	K	2073.150
TFCRFC	MAGNIFICATION ON PELLET CREEP FORMULA (THERMAL MODEL)	-	1.000
TCRMX	CUT OFF VALUE OF TEMP. WITHIN PELLET CREEP CAL. (THERMAL MODEL)	K	1773.150
CRFAC	MAGNIFICATION ON CLAD CREEP STRAIN RATE (MECHANICAL MODEL)	-	1.300
TCCRFC	MAGNIFICATION ON CLAD CREEP STRAIN RATE (THERMAL MODEL)	-	1.000
FAIMAX	CUT OFF VALUE OF FAST NEWTRON FLUX WITHIN CLAD CREEP CAL.	N/CM2/S	1.000E+14
IPUGH	IPUGH=1 TAKES INTO ACCOUNT OF PUGH-S TURN OVER IN CLAD-CREEP CAL.	-	0
CRPEQ	OPTION FOR FORMULA OF CLAD CREEP STRAIN RATE (MECHANICAL MODEL)	-	0.000

(5) OPTION FOR PELLET CRACK. AND RELOCATION

XRELOC	RELOCATION PARAMETER IN THERMAL CALCULATION	-	0.200
FRELOC	MECHANICAL RELOCATION PARAMETER	-	0.500
EPSRLZ	AXIAL RELOCATION PARAMETER	-	0.005
FACR	OPTION FOR PELLET STIFFNESS RECOVERY IN RADIAL DIRECTION	-	1.000
FACZ	OPTION FOR PELLET STIFFNESS RECOVERY IN AXIAL DIRECTION	-	1.000
BUMIN	BURNUP AT WHICH PELLET RELOCATION STARTS	MWD/TU	5000.000
BUMAX	BURNUP AT WHICH PELLET RELOCATION CEASES	MWD/TU	20000.000
IURS	OPTION FOR PELLET GAS BUBBLE SWELLING CALCULATION	-	0
IYNG	PELLET CRACK MODEL OPTION (MECHANICAL MODEL)	-	1
ECRAC3	ELASTIC MODULUS OF PELLET AT THE TIME OF PERFECT CRACK (MECH. MODEL)	PA	2.000E+09
EFAC	MAGNIFICATION ON ELASTIC MODULUS OF PELLET (MECHANICAL MODEL)	-	1.000

(6) OPTION FOR PELLET DENSIFICATION

IDENSF	OPTION FOR FORMULA OF PELLET DESIFICATION	-	0
DMAX	MAXIMUM VOLUME SHRINKAGE RATIO BY DESIFICATION	%	0.960
SBU	BURNUP AT WHICH DESIFICATION IS 90% COMPLETED (IDENSF = 0)	MWD/TU	10000.000
TDNSF	SINTERING TEMPERATURE	K	2000.000
GG	GRAIN SIZE AFTER HEAT TREATMENT	M	1.000E-05
GGO	INITIAL GRAIN SIZE (IDENSF = 3)	M	8.000E-06
SITIM	TIME OF HEAT TREATMENT (IDENSF = 3)	HR	24.000
ADST	AJUST. FACT. (IDENSF = 4)	-	0.600

(7) OPTION FOR PELLET SWELLING MODEL

IFSWEL	OPTION FOR PELLET SWELLING MODEL	-	0
STFCP	CONTACT PRESSURE LIMIT BEYOND WHICH GAS BUBBLE CANNOT OCCUR(MECHANICAL)	PA	-3.000E+07
SPCON	CONTACT PRESSURE LIMIT BEYOND WHICH GAS BUBBLE CANNOT OCCUR(THERMAL)	PA	-1.000E+06
FACP	FACTOR MAGNIFING CONTACT PRESSURE AFFECTING BUBBLE OUTER PRESSURE	-	1.000
BQ	NUMBER OF ATOMS IN A BOUNDARY BUBBLE	ATOMS/BUBBLE	5.000E+08

(8) OPTION FOR PELLET HOTPRESS MODEL

BETAX	PELLET HOTPRESS PARAMETER	-	0.002
IHOT	OPTION FOR PELLET HOTPRESS PARAMETER	-	0

(9) OPTION FOR PLASTIC MODEL

IFY	OPTION FOR PELLET PLASTIC MODEL	-	1
ISTR	DETERMINES K OF CURVATURE OF YIELD STRESS IN ZIRCALOY	KG/MM**2	0

(10) OPTION FOR IRRADIATION GROWTH MODEL

ICAGRW	OPTION FOR FORMULA OF CLAD IRRADIATION GROWTH	-	1
CATEXF	FACTOR FZ FOR AXIAL DIRECTION (ICAGRW = 1)	-	0.050
COLDW	COLD WORK CW (ICAGRW = 1)	-	0.810

(11) OPTION FOR FP GAS RELEASE MODEL

IGASP	FISSION GAS RELEASE MODEL OPTION	-	0
IGAS	OPTION FOR TEMPERATURE ZONE MODEL	-	0
APORE	BUBBLE RADIUS IN INITIAL GRAINS	CM	0.000E+00
BFCT	MAGNIFY RESOL. RATE B FROM INTRAGRANULAR BUBBLES TO MATRIX	-	1.000
FACD	MAGNIFY EFFECTIVE INTRINSIC DIFFUSION COEFFICIENT	-	1.000
ADDF	MAGNIFY RESOLUTION RATE FROM INTERGRANULE TO INSIDE	-	9.000
FBSAT	MAGNIFY GAS SATURATION AT INTERGRANULE	-	1.000
PSAT	MAXIMUM VALUE OF PRESSURE IN INTERGRANULAR BUBBLE	PA	1.000E+08
IPEXT	OPTION FOR PRESSURE PEXT TO INTERGRANULAR BUBBLE	-	1
FGG	MAGNIFY GRAIN GROWTH CLEANUP RATIO	-	1.000
FRMIN	MINIMUM RELEASE RATE OF FP GAS RELEASE RATE	%	0.500
THEATF	INTERPOLATION PARAMETER USED IN GRAIN DIFFUSION EQUATION	-	1.000
FMULT	ADJUSTMENT FACTOR OF TIME STEP IN FP GAS RELEASE MODEL	-	1.000
NODEQ	MESH NUMBER WITHIN GRAIN IN FP GAS RELEASE MODEL	-	3
RREL	DIVIDE RATIO OF MESH WITHIN GRAIN IN GAS RELEASE MODEL	-	10.00 1.00 1.00 1.00
RB	WIDTH OF BOUNDARY LAYER (MESH FOR RESOLUTION)	CM	2.000E-06
OPORO	RATIO OF OPEN POROSITY	-	0.000
ALHOT	FACTOR MAGNIFING RELAXATION OF STRESS AFFECTING BUBBLE OUTER PRESS.	-	1.000E-04
APEXT	FACTOR MAGNIFING OF STRESS AFFECTING BUBBLE OUTER PRESS. (IPEXT=14)	-	1.000

(12) OPTION FOR UO2 GRAIN GROWTH MODEL

IGRAIN	OPTION FOR FORMULA IN UO2 GRAIN GROWTH	-	0
GR	GRAIN SIZE	MICRON	10.000
GRWF	MAGNIFY GRAIN GROWTH RATE	-	1.000
AG	FITTING PARAMETER (GRAIN GROWTH SUPPRESSION TERM)	-	1.000

(13) OPTION FOR HE GAS RELEASE MODEL

NTVHE	NUMBER OF TIME POINTS DETERMINED BY TVHE	-	0

(14) OPTION FOR GAS FLOW MODEL

GMIN	MINIMUM GAP WIDTH BETWEEN PELLET AND CLAD IN GAS FLOW MODEL	CM	0.001
THG1	INTERPOLATION PARAMETER OF VOLUME ETC. USED IN AXIAL FP GAS FLOW MODEL	-	1.000
THG2	INTERPOL. PARAM. USED IN DIFFUSION CAL. OF AXIAL FP GAS FLOW MODEL	-	1.000

AMLMX2	MAXIMUM TRANSFER MOL NUMBER IN EACH SEGMENT	MOL	1.000E-06
AMLMX3	MAXIMUM VALUE OF FP GAS RELEASE IN EACH SEGMENT	MOL	2.000E-06
DTPR	RATIO OF VOL. OF FP GAS RELEASE TO THAT OF PLENUM GAS AT EACH TIME STEP	-	0.010
ETA	CONTROL PARAMETER (USED IN DETERMINING TIME STEP WIDTH)	-	0.050

(15) OPTION FOR CORROSION MODEL

ICORRO	OPTION FOR CLAD WATERSIDE CORROSION MODEL	-	1

(16) OPTION FOR GAP CONDUCTANCE MODEL

IGAPCN	OPTION FOR GAP CONDUCTANCE MODEL	-	0
R1	ROUGHNESS OF PELLET SURFACE	CM	1.000E-04

(17) OPTION FOR LOCAL FEM MODEL

GAPLK	MAXIMAM GAP SIZE FOR GENERATING AXIAL FORCE	MICRON	0.000
AY	TILTING VALUE	MM	0.000

(18) Option for cladding anisotropy

HO(2)	Cladding anisotropy parameter	-	1.000
FO(2)	Cladding anisotropy parameter	-	1.000
GO(2)	Cladding anisotropy parameter	-	1.000

NAMELIST PARAMETERS(3)

INPUT OPTION

PARAMETER	DESCRIPTION		VALUE
(1) OPTION FOR OUTPUT/PLOTTING			
IPRINT	OUTPUT OPTION (=0;OFF ,=1;ON)		
	= 1;INPUT DATA LIST		1
	= 2;FUEL DESIGN DATA		1
	= 3;MESH AND GEOMETRY DATA		1
	= 4;PARAMETERS LIST		1
	= 5;HISTORY DATA LIST		1
	= 6;THERMAL RESULTS	(EVERY TIME STEP)	1
	= 7;MECHANICAL RESULTS	(EVERY TIME STEP)	1
	= 8;THERMAL RESULTS	(THERMAL MODEL)	1
	= 9;MECHANICAL RESULTS	(THERMAL MODEL)	1
	=10;FP GAS RESULTS	(EVERY SEGMENT)	1
	=11;FP GAS RESULTS	(WHOLE ROD)	1
	=12;FUEL-CLAD DISPLACEMENT	(MECHANICAL MODEL)	1
	=13;FUEL STRESS AND STRAIN	(MECHANICAL MODEL)	1
	=14;CLAD STRESS AND STRAIN	(MECHANICAL MODEL)	1
	=15;FINAL INFORMATION		1
	=16;THERMAL BEHAVIOR	(PLOTTER)	1
	=17;FP GAS BEHAVIOR	(PLOTTER)	1
	=18;MECHANICAL BEHAVIOR	(PLOTTER)	1
(2) OPTION FOR SEGMENT OUTPUT			
IWNOD	AXIAL SEGMENT PRINT AND PLOTTER OPTION (=0;OFF ,=1;ON)		0 0 0 1 0 0 0 0 0 0
(3) OPTION FOR OUTPUT OF THERMAL CALCULATION			

IWTHE	THERMAL INFORMATION OUTPUT OPTION (=0;OFF ,=1;ON)	
	=1;TEMPERATURE	1
	=2;GAP GAS	1
	=3;GRAIN RADIUS	1
	=4;INT. BUBBLE RADIUS	1
	=5;INT. BUBBLE DENSITY	1
	=6;DIFFUSION COEF.	1
	=7;EFFECT. DIF. COEF.	1
	=8;GRAIN ATOMS	1
	=9;BOUNDARY ATOMS	1
	=10;RELEASED ATOMS	1
	=11;GR. +BOU. ATOMS	1
	=12;GR. +BOU. +REL. ATOMS	1
	=13;PRODUCED ATOMS	1
	=14;FISSION GAS RELEASE	1
	=15;BOUNDARY DENSITY	1
	=16;BOUND. SAT. DENSITY	1
	=17;BOUNDARY PRESSURE	1
	=18;THERMAL INFORMATION	1
	=19;THERMAL GENERAL OUTPUT	1

(4) OPTION FOR OUTPUT OF LOCAL FEM CALCULATION

IWFEM	MECHANICAL INFORMATION OUTPUT CONTROL TABLE (=0;OFF ,=1;ON)	
	= 1;RADIAL STRESS	0
	= 2;AXIAL STRESSES	1
	= 3;CIRCUMFERENTIAL STRESSES	1
	= 4;SHEAR STRESSES	0
	= 5;EQUIVALENT STRESSES	1
	= 6;YIELD STRESSES	0
	= 7;RADIAL TOTAL STRAINS	0
	= 8;AXIAL TOTAL STRAINS	0
	= 9;CIRCUMFERENTIAL TOTAL STRAINS	0
	=10;SHEAR TOTAL STRAINS	0
	=11;EQUIVALENT PLASTIC STRAINS	1
	=12;RADIAL CREEP STRAINS	0
	=13;AXIAL CREEP STRAINS	0
	=14;CIRCUMFERENTIAL CREEP STRAINS	1
	=15;SHEAR CREEP STRAINS	0
	=16;EQUIVALENT CREEP STRAINS	0
	=17;RADIAL ELASTIC STRAINS	0
	=18;AXIAL ELASTIC STRAINS	0
	=19;CIRCUMFERENTIAL ELASTIC STRAINS	0
	=20;SHEAR ELASTIC STRAINS	0
	=21;RADIAL THERMAL STRAINS	0
	=22;AXIAL THERMAL STRAINS	0
	=23;STRAINS BY DENSIFICATION	0
	=24;STRAINS BY SWELLING	0
	=25;YOUNG'S MODULUS IN RADIAL DIRECTION	0
	=26;YOUNG'S MODULUS IN AXIAL DIRECTION	0
	=27;YOUNG'S MODULUS IN CIRCU. DIRECTION	0
	=28;RADIAL CREEP STRAINS RATE	0
	=29;AXIAL CREEP STRAINS RATE	0
	=30;CIRCUM. CREEP STRAINS RATE	0
	=31;SHEAR CREEP STRAINS RATE	0
	=32;EQUI. CREEP STRAINS RATE	0
	=33;RADIAL STRAINS RATE	0
	=34;AXIAL STRAINS RATE	0
	=35;CIRCUMFERENTIAL STRAINS RATE	0
	=36;SHEAR STRAINS RATE	0
	=37;EQUIVALENT STRAINS RATE	0
	=38;EQUIVALENT STRAINS ENERGY	0
	=39;RADIAL DISTRIBUTION OF TEMP.	1
	=40;PELLET/CLADDING INTERACTION	1
	=41;PELLET/PELETTE INTERACTION	1

```
                =42;DISPLACEMENT OF NODAL POINTS                    1
                =43;PCMI PLOT                                       1
                =44;CRACK/YIELD MAP                                 1
                =45;MECANICAL CALC. CONDITION                       1

(5) OPTION FOR OUTPUT OF  WHOLE ROD FEM CALCULATION

  IWROD     MECHANICAL INFORMATION OUTPUT CONTROL TABLE (=0;OFF ,=1;ON)
                = 1;RADIAL STRESS                                   0
                = 2;CIRCUM. STRESS                                  0
                = 3;AXIAL STRESS                                    0
                = 4;EQUI. STRESS                                    0
                = 5;YIELD STRESS                                    0
                = 6;RADIAL CREEP STRAIN                             0
                = 7;CIRCUM. CREEP STRAIN                            0
                = 8;AXIAL CREEP STRAIN                              0
                = 9;EQUI. HARD STRAIN                               0
                =10;EQUI. PLAS. STRAIN                              0
                =11;SWELLING STRAIN                                 0
                =12;RADIAL TOTAL STRAIN                             0
                =13;CIRCUM. TOTAL STRAIN                            0
                =14;AXIAL TOTAL STRAIN                              0
                =15;THERMAL STRAIN                                  0
                =16;ELEMENT TEMPERATURE                             0
                =17;PRESSURE                                        0
                =18;NODE DISPLACEMENT                               0

(6) OPTION FOR GETTING PLOTTER TAPE

  IPLT    DRAW UP PLOTTER TAPE OPTIONS (=0;NO ,=1;YES)              1
  IPLOPT  INTERVAL OF TIME STEP POINT FOR DRAW UP PLOTTER TAPE      -5
```

***** HISTORY DATA (1) *****

STAGE NO. (NHIST)	TIME (H: M: S)	BURNUP (MWD/TUO2)	(MWD/TU)	(GJ/KGU)	L.H.R. (W/CM)	COOLANT TEMP. (DEG.K)	COOLANT PRESS. (MPA)	COOLANT VELOSITY (M/S)	FAST NEWTRON FLUX (N/CM2.)	HISTRY OPTION (0=OFF)	PRINT OPTION (1=ON)	SS/US OPTION (1=ON)
1	0: 0: 0	0.0	0.0	0.00	0.0	555.15	13.79	6.5	5.3000+13	0	0	0
2	5: 0: 0	3.9	4.4	0.38	260.0	555.15	13.79	6.5	5.3000+13	0	0	0
3	2817:28:45	4407.2	5000.0	431.47	260.0	555.15	13.79	6.5	5.3000+13	0	0	0
4	5632:27:30	8814.5	10000.0	862.94	260.0	555.15	13.79	6.5	5.3000+13	0	0	0
5	8447:26:15	13221.7	15000.0	1294.40	260.0	555.15	13.79	6.5	5.3000+13	0	0	0
6	11262:25: 0	17628.9	20000.0	1725.87	260.0	555.15	13.79	6.5	5.3000+13	0	0	0
7	14077:23:45	22036.1	25000.0	2157.34	260.0	555.15	13.79	6.5	5.3000+13	0	0	0
8	17230:10:22	26972.2	30600.0	2640.58	260.0	555.15	13.79	6.5	5.3000+13	0	0	0
9	17235:10:22	26980.7	30609.8	2641.41	304.0	555.15	13.79	6.5	5.3000+13	-100	0	0
10	18386: 9:27	29087.7	33000.0	2847.69	304.0	555.15	13.79	6.5	5.3000+13	100	0	0
11	19830:41:11	31732.0	36000.0	3106.57	304.0	555.15	13.79	6.5	5.3000+13	100	0	0
12	21275:12:55	34376.4	39000.0	3365.45	304.0	555.15	13.79	6.5	5.3000+13	100	0	0
13	22960:29:58	37461.4	42500.0	3667.48	304.0	555.15	13.79	6.5	5.3000+13	100	0	0
14	22985:29:58	37470.1	42509.8	3668.32	269.0	555.15	13.79	6.5	5.3000+13	-100	0	0
15	24320:34:21	39865.1	45000.0	3883.21	269.0	555.15	13.79	6.5	5.3000+13	100	0	0
16	25953: 3: 4	42309.4	48000.0	4142.09	269.0	555.15	13.79	6.5	5.3000+13	100	0	0
17	27585:31:47	44953.7	51000.0	4400.97	269.0	555.15	13.79	6.5	5.3000+13	100	0	0
18	29218: 0:30	47598.1	54000.0	4659.85	269.0	555.15	13.79	6.5	5.3000+13	100	0	0
19	31122:34: 0	50683.1	57500.0	4961.88	269.0	555.15	13.79	6.5	5.3000+13	100	1	0
20	31127:34: 0	50691.2	57509.2	4962.67	269.0	555.15	13.79	6.5	5.3000+13	-100	0	0
21	31132:34: 0	50695.3	57513.8	4963.07	0.0	291.15	0.10	6.5	1.0000+09	-100	2	0

LAST STAGE NUMBER = 21

History data
(Output in the case of IPRINT(5)=1)

Time-step number, time, burnup, linear heat rate, coolant temperature, coolant pressure, coolant velocity, fast neutron flux, input option, print option, steady/unsteady manual option

***** HISTORY DATA (2) *****

STAGE (NHIST)	TIME (H: M: S)	L.H.R. (W/CM)	AXIAL NODE PEAKING FACTOR (1)	(2)	(3)	(4)	(5)	(6)	(7)	(8)	(9)	(10)	(11)	(12)
1	0: 0: 0	0.00	0.800	1.050	1.140	1.200	1.160	1.150	1.000	0.500	0	0	0	0
2	5: 0: 0	260.00	0.800	1.050	1.140	1.200	1.160	1.150	1.000	0.500	0	0	0	0
3	2817:28:45	260.00	0.800	1.050	1.140	1.200	1.160	1.150	1.000	0.500	0	0	0	0
4	5632:27:30	260.00	0.800	1.050	1.140	1.200	1.160	1.150	1.000	0.500	0	0	0	0
5	8447:26:15	260.00	0.800	1.050	1.140	1.200	1.160	1.150	1.000	0.500	0	0	0	0
6	11262:25: 0	260.00	0.800	1.050	1.140	1.200	1.160	1.150	1.000	0.500	0	0	0	0
7	14077:23:45	260.00	0.800	1.050	1.140	1.200	1.160	1.150	1.000	0.500	0	0	0	0
8	17230:10:22	260.00	0.800	1.050	1.140	1.200	1.160	1.150	1.000	0.500	0	0	0	0
9	17235:10:22	304.00	0.800	1.050	1.140	1.200	1.160	1.150	1.000	0.500	0	0	0	0
10	18386: 9:27	304.00	0.800	1.050	1.140	1.200	1.160	1.150	1.000	0.500	0	0	0	0
11	19830:41:11	304.00	0.800	1.050	1.140	1.200	1.160	1.150	1.000	0.500	0	0	0	0
12	21275:12:55	304.00	0.800	1.050	1.140	1.200	1.160	1.150	1.000	0.500	0	0	0	0
13	22960:29:56	304.00	0.800	1.050	1.140	1.200	1.160	1.150	1.000	0.500	0	0	0	0
14	22965:29:56	269.00	0.800	1.050	1.140	1.200	1.160	1.150	1.000	0.500	0	0	0	0
15	24320:34:21	269.00	0.800	1.050	1.140	1.200	1.160	1.150	1.000	0.500	0	0	0	0
16	25953: 3: 4	269.00	0.800	1.050	1.140	1.200	1.160	1.150	1.000	0.500	0	0	0	0
17	27585:31:47	269.00	0.800	1.050	1.140	1.200	1.160	1.150	1.000	0.500	0	0	0	0
18	29218: 0:30	269.00	0.800	1.050	1.140	1.200	1.160	1.150	1.000	0.500	0	0	0	0
19	31122:34: 0	269.00	0.800	1.050	1.140	1.200	1.160	1.150	1.000	0.500	0	0	0	0
20	31127:34: 0	269.00	0.800	1.050	1.140	1.200	1.160	1.150	1.000	0.500	0	0	0	0
21	31132:34: 0	0.00	0.800	1.050	1.140	1.200	1.160	1.150	1.000	0.500	0	0	0	0

FEM ANALYSIS IS APPLIED AT SEGMENT OF NUMBER 4

History of relative power profile in the axial direction

```
********** OUTPUT  ---STAGE--- 177 ********************************************************************** IFEM =  4 ****
```

THERMAL ANALYSIS INFORMATION

STAGE NO.	177	
TIME	31122.57	HR
COOLANT TEMPERATURE	555.15	DEG.K
COOLANT PRESSURE	1.38D+01	MPA

NODE	L.H.R. (W/CM)	BURN UP (MWD/TUO2)	GAP CONDUCTANCE (W/CM**2 K) TOTAL	GAS	SOLID	RAD.	TEMPERATURE (K) PC	PS	CI	CO	CLEARANCE (MICRONS)	CONTACT FORCE(MPA)	NODE
1	215.200	40546.5	0.9053	0.9013	0.0000	0.0039	1118.2	677.4	598.1	572.9	18.041	0.000	1
2	282.450	53217.3	3.8013	3.7844	0.0131	0.0038	1254.7	642.9	618.1	585.3	0.000	1.456	2
3	306.660	57778.8	4.0179	3.9682	0.0458	0.0041	1357.6	658.6	633.1	597.9	0.000	5.122	3
* 4	322.800	60819.7	4.0702	4.0228	0.0430	0.0044	1445.3	677.7	651.2	614.6	0.000	4.895	4
5	312.040	58792.4	4.1478	4.0965	0.0467	0.0046	1425.0	887.0	661.9	628.7	0.000	5.307	5
6	309.350	58285.6	4.2606	4.2108	0.0447	0.0051	1452.4	708.0	683.8	649.5	0.000	5.115	6
7	269.000	50683.1	4.1822	4.1480	0.0295	0.0047	1285.9	686.6	665.2	635.0	0.000	3.305	7
8	134.500	25341.6	0.4760	0.4716	0.0000	0.0044	962.8	707.4	613.2	597.6	42.489	0.000	8

NODE	CSFR*	PFAC*	BURN UP (FISS/CC *10**20)	THERMAL EXPANS.	PELLET DISPLACEMENT (MICRONS) CREEP	DENSIFI CATION	IRRAD. SWELL	RELOC ATION	DISPLA CEMENT	CLADDING DISPLACEMENT (MICRONS) THERMAL EXPANS.	ELASTIC DEFORM.	CREEP	DISPLA CEMENT
1	0.7968	2.0000	11.25	18.64	0.00	-31.06	43.68	15.52	46.77	1.02	0.84	-14.63	-12.77
2	0.7968	2.0000	14.76	22.51	-0.47	-31.07	57.34	15.52	63.83	1.57	0.85	-22.83	-20.41
3	0.7968	2.0000	16.03	26.37	-8.11	-31.07	82.25	15.52	66.96	2.03	0.86	-26.07	-23.17
* 4	0.7968	2.0000	16.87	29.89	-15.78	-31.07	65.53	15.52	64.09	2.62	0.87	-29.34	-25.84
5	0.7968	2.0000	16.31	29.35	-12.76	-31.07	63.34	15.52	64.39	3.01	0.88	-29.99	-26.10
6	0.7968	2.0000	16.17	30.80	-14.87	-31.07	62.80	15.52	63.17	3.77	0.89	-31.84	-27.17
7	0.7968	2.0000	14.06	24.45	-1.90	-31.07	54.61	15.52	61.60	3.21	0.88	-30.27	-26.18
8	0.7968	2.0000	7.03	14.17	0.00	-30.98	27.30	15.52	28.02	1.70	0.86	-11.63	-9.08

NODE	CLAD SURFACE TEMP. (K)	CLAD OUTER CORROSION (MICRON/O)	THICNESS(MICRON)
1	569.9	0.00985	4.43390
2	577.3	0.01729	9.25273
3	582.5	0.02891	16.27903
* 4	587.5	0.05505	27.36524
5	590.9	0.08526	37.65054
6	594.3	0.18774	58.90915
7	595.3	0.11085	48.43475
8	589.8	0.02477	19.00678

INITIAL GAS (MOL) = 5.46D-02

FISSION GAS RESULT

LOCAL FISSION GAS RELEASE FRACTION (AXIAL NODE)
1 0.00500 2 0.00953 3 0.01906 4 0.03857 5 0.02909 6 0.03113 7 0.00618 8 0.00500

ROD AVERAGE FISSION GAS RELEASE FRACTION = 0.02003

ROD GAS PRESSURE (MPA) = 8.230

FREE SPACE VOLUME(CM3) = 34.624
(GAP, PLENUM) = 4.335 30.290

TOTAL GAS (MOL) = 5.66D-02

FRACTIONS OF GAS MIXTURE (PERCENT)	AXIAL NODE 1	2	3	4	5	6	7	8
HE	95.3	95.2	95.1	95.0	95.1	95.4	96.0	96.4
N2	0.0	0.0	0.0	0.0	0.0	0.0	0.0	0.0
KR	0.6	0.6	0.6	0.6	0.6	0.6	0.5	0.5
XE	4.1	4.2	4.2	4.3	4.2	4.0	3.5	3.1

RELEASED IODINE (GRAM/CM**2) = 1.75D-05 (AVERAGE) 4.04D-05 (PEAK)

	(MOL)	HE	N2	KR	XE	TOTAL
PRODUCED GAS	. . . .	0.00D+00	0.00D+00	1.33D-02	8.89D-02	. . . . 1.02E-01
RELEASED GAS	. . . .	0.00D+00	0.00D+00	2.66D-04	1.78D-03	. . . . 2.05E-03
ROD GAS	. . . .	5.46D-02	0.00D+00	2.66D-04	1.78D-03	. . . . 5.66E-02

Thermal analysis results at each time step
(Output in the case of IPRINT(6)=1)

Time-step number, time,
coolant temperature, coolant pressure

Linear heat rate, burnup, gap conductance (total, gas, solid, radiation), temperature (pellet center, pellet surface, cladding inner surface, cladding outer surface), radial gap size, contact pressure、

Pellet inner/outer power density ratio, factor for power profile, burnup, pellet displacement (thermal expansion, swelling, densification, relocation, total), cladding displacement (thermal expansion, elasticity, creep, total)

Cladding surface temperature, oxide film growth rate, oxide film thickness

Initial gas molar number,
FP gas release rate of each axial segment,
average FP gas release rate of the rod,
fuel rod inner pressure, fuel rod space volume (gap, plenum), total gas molar number, iodine concentration (average, maximum), produced gas, released gas, gas molar number inside the fuel rod

RADIAL TEMPERATURE DISTRIBUTION AT AXIAL NODE OF 4

PELLET										/ GAP /	CLAD.		
1	2	3	4	5	6	7	8	9	10	11		1	2	3
1445	1436	1408	1361	1298	1220	1128	1024	913	796	678		651	632	615

TEMPERATURE DISTRIBUTION IN THE FUEL (DEG.C) IWTHE= 1

SEG										
8	688.31	682.88	672.05	655.91	634.59	608.24	577.05	541.28	501.22	457.22
7	1009.22	995.05	966.99	925.60	871.70	806.37	731.00	647.19	556.81	461.85
6	1174.76	1156.75	1121.10	1068.59	1000.39	918.07	823.65	719.52	608.39	493.15
5	1147.34	1129.40	1093.91	1041.68	973.88	892.12	798.45	695.26	585.27	471.38
4	1167.41	1148.81	1111.43	1058.74	985.82	900.43	802.77	695.46	581.44	463.82
3	1080.20	1063.20	1029.59	980.13	915.96	838.81	749.97	652.30	548.10	440.06
2	977.86	963.20	934.20	891.48	835.96	768.85	691.66	606.17	514.38	418.46
1	842.53	832.51	812.62	783.19	744.64	697.60	642.79	581.10	513.58	441.37

GAP GAS INFORMATION (%) IWTHE= 2

SEG	HE	N2	KR	XE
8	96.4	0.0	0.5	3.1
7	96.0	0.0	0.5	3.5
6	95.4	0.0	0.6	4.0
5	95.1	0.0	0.6	4.2
4	95.0	0.0	0.6	4.3
3	95.1	0.0	0.6	4.2
2	95.2	0.0	0.6	4.2
1	95.3	0.0	0.6	4.1

RADIUS OF GRAIN (MICRON) IWTHE= 3

SEG										
8	5.00	5.00	5.00	5.00	5.00	5.00	5.00	5.00	5.00	5.00
7	5.00	5.00	5.00	5.00	5.00	5.00	5.00	5.00	5.00	5.00
6	5.18	5.10	5.01	5.00	5.00	5.00	5.00	5.00	5.00	5.00
5	5.21	5.12	5.01	5.00	5.00	5.00	5.00	5.00	5.00	5.00
4	5.40	5.28	5.09	5.00	5.00	5.00	5.00	5.00	5.00	5.00
3	5.09	5.04	5.00	5.00	5.00	5.00	5.00	5.00	5.00	5.00
2	5.00	5.00	5.00	5.00	5.00	5.00	5.00	5.00	5.00	5.00
1	5.00	5.00	5.00	5.00	5.00	5.00	5.00	5.00	5.00	5.00

RADIUS OF INTRAGRANULAR GAS BUBBLE (ANGSTROM) IWTHE= 4

SEG										
8	3.32	3.32	3.32	3.32	3.32	3.32	3.32	3.32	3.32	3.32
7	6.59	6.07	5.17	4.14	4.36	4.36	4.36	4.36	4.36	4.36
6	10.43	9.72	8.51	6.79	5.00	4.60	4.60	4.60	4.60	4.60
5	10.64	9.94	8.43	6.64	4.91	4.62	4.62	4.62	4.62	4.62
4	11.35	10.63	9.37	7.50	5.43	4.67	4.67	4.67	4.67	4.67
3	10.06	9.35	7.88	6.02	4.40	4.58	4.58	4.58	4.58	4.58
2	7.85	7.26	6.19	4.88	3.69	4.44	4.44	4.44	4.44	4.44
1	3.15	4.00	4.00	4.00	4.00	4.00	4.00	4.00	4.00	4.00

Temperature distribution in the radial direction of the objective segment

Hereafter, items designated by IWTHE(i) are output

Temperature distribution in the pellet

Gas composition

Pellet grain size

Radius of intragranular gas bubble

DENSITY OF INTRAGRANULAR GAS BUBBLE (BUBBLES/CM**3)							IWTHE= 5			
SEG										
8	1.090D+18	1.090D+18	1.090D+18	1.090D+18	1.090D+18	1.090D+18	1.090D+18	1.090D+18	1.090D+18	1.090D+18
7	7.033D+17	7.493D+17	8.405D+17	9.674D+17	9.384D+17	9.384D+17	9.384D+17	9.384D+17	9.384D+17	9.384D+17
6	4.635D+17	4.975D+17	5.650D+17	6.866D+17	8.604D+17	9.079D+17	9.079D+17	9.079D+17	9.079D+17	9.079D+17
5	4.544D+17	4.867D+17	5.698D+17	6.990D+17	8.702D+17	9.060D+17	9.060D+17	9.060D+17	9.060D+17	9.060D+17
4	4.244D+17	4.545D+17	5.158D+17	6.321D+17	8.129D+17	8.987D+17	8.987D+17	8.987D+17	8.987D+17	8.987D+17
3	4.808D+17	5.168D+17	6.051D+17	7.537D+17	9.334D+17	9.098D+17	9.098D+17	9.098D+17	9.098D+17	9.098D+17
2	6.071D+17	6.493D+17	7.387D+17	8.743D+17	1.033D+18	9.278D+17	9.278D+17	9.278D+17	9.278D+17	9.278D+17
1	1.120D+18	9.874D+17	9.874D+17	9.874D+17	9.874D+17	9.874D+17	9.874D+17	9.874D+17	9.874D+17	9.874D+17

DIFFUSION COEFFICIENT (CM**2/SEC)							IWTHE= 6			
SEG										
8	2.000D-17	2.000D-17	2.000D-17	2.000D-17	2.000D-17	2.000D-17	2.000D-17	2.000D-17	2.000D-17	2.000D-17
7	2.891D-17	2.656D-17	2.350D-17	2.131D-17	2.000D-17	2.000D-17	2.000D-17	2.000D-17	2.000D-17	2.000D-17
6	2.261D-16	1.717D-16	1.008D-16	5.005D-17	2.737D-17	2.000D-17	2.000D-17	2.000D-17	2.000D-17	2.000D-17
5	1.488D-16	1.138D-16	6.888D-17	3.756D-17	2.409D-17	2.000D-17	2.000D-17	2.000D-17	2.000D-17	2.000D-17
4	2.020D-16	1.517D-16	8.772D-17	4.378D-17	2.535D-17	2.000D-17	2.000D-17	2.000D-17	2.000D-17	2.000D-17
3	5.764D-17	4.703D-17	3.369D-17	2.471D-17	2.103D-17	2.000D-17	2.000D-17	2.000D-17	2.000D-17	2.000D-17
2	2.448D-17	2.321D-17	2.162D-17	2.055D-17	2.012D-17	2.000D-17	2.000D-17	2.000D-17	2.000D-17	2.000D-17
1	2.015D-17	2.000D-17	2.000D-17	2.000D-17	2.000D-17	2.000D-17	2.000D-17	2.000D-17	2.000D-17	2.000D-17

EFFECTIVE DIFFUSION COEFFICIENT (CM**2/SEC)							IWTHE= 7			
SEG										
8	1.982D-17	1.982D-17	1.982D-17	1.982D-17	1.982D-17	1.982D-17	1.982D-17	1.982D-17	1.982D-17	1.982D-17
7	2.861D-17	2.629D-17	2.327D-17	2.111D-17	1.983D-17	1.983D-17	1.983D-17	1.983D-17	1.983D-17	1.983D-17
6	2.138D-16	1.640D-16	9.774D-17	4.916D-17	2.705D-17	1.983D-17	1.983D-17	1.983D-17	1.983D-17	1.983D-17
5	1.435D-16	1.105D-16	6.743D-17	3.704D-17	2.385D-17	1.983D-17	1.983D-17	1.983D-17	1.983D-17	1.983D-17
4	1.930D-16	1.462D-16	8.559D-17	4.314D-17	2.509D-17	1.983D-17	1.983D-17	1.983D-17	1.983D-17	1.983D-17
3	5.678D-17	4.641D-17	3.332D-17	2.447D-17	2.084D-17	1.983D-17	1.983D-17	1.983D-17	1.983D-17	1.983D-17
2	2.428D-17	2.302D-17	2.144D-17	2.038D-17	1.994D-17	1.983D-17	1.983D-17	1.983D-17	1.983D-17	1.983D-17
1	1.997D-17	1.982D-17	1.982D-17	1.982D-17	1.982D-17	1.982D-17	1.982D-17	1.982D-17	1.982D-17	1.982D-17

NUMBER OF GAS ATOMS IN A GRAIN (ATOMS)							IWTHE= 8			
SEG										
8	4.966D+09	1.497D+10	2.521D+10	3.582D+10	4.697D+10	5.880D+10	7.146D+10	8.511D+10	9.990D+10	1.160D+11
7	1.758D+11	1.832D+11	1.908D+11	1.904D+11	9.394D+10	1.176D+11	1.429D+11	1.702D+11	1.998D+11	2.320D+11
6	1.417D+11	1.506D+11	1.691D+11	2.034D+11	2.265D+11	1.352D+11	1.644D+11	1.958D+11	2.298D+11	2.668D+11
5	1.517D+11	1.596D+11	1.783D+11	2.072D+11	2.291D+11	1.364D+11	1.658D+11	1.975D+11	2.318D+11	2.691D+11
4	1.513D+11	1.580D+11	1.739D+11	2.021D+11	2.363D+11	1.411D+11	1.715D+11	2.043D+11	2.398D+11	2.783D+11
3	1.657D+11	1.722D+11	1.895D+11	2.171D+11	2.258D+11	1.341D+11	1.629D+11	1.941D+11	2.278D+11	2.644D+11
2	1.721D+11	1.806D+11	1.956D+11	2.040D+11	1.499D+11	1.235D+11	1.501D+11	1.787D+11	2.098D+11	2.436D+11
1	7.308D+10	2.396D+10	4.033D+10	5.732D+10	7.515D+10	9.408D+10	1.143D+11	1.362D+11	1.598D+11	1.856D+11

NUMBER OF GAS ATOMS IN A BOUNDARY (ATOMS)							IWTHE= 9			
SEG										
8	1.228D+08	3.704D+08	6.235D+08	8.861D+08	1.162D+09	1.454D+09	1.768D+09	2.105D+09	2.471D+09	2.869D+09
7	5.430D+09	5.551D+09	5.450D+09	4.980D+09	2.324D+09	2.909D+09	3.536D+09	4.211D+09	4.943D+09	5.738D+09

Density of intragranular gas bubble

Diffusion coefficient

Effective diffusion coefficient

Number of FP gas atoms in grain matrix

Number of FP gas atoms at grain boundary

6	8.682D+09	8.523D+09	8.419D+09	8.721D+09	7.123D+09	3.346D+09	4.067D+09	4.843D+09	5.685D+09	6.600D+09
5	8.939D+09	8.756D+09	8.611D+09	7.527D+09	6.571D+09	3.375D+09	4.102D+09	4.885D+09	5.734D+09	6.657D+09
4	9.488D+09	9.161D+09	8.768D+09	7.828D+09	7.052D+09	3.491D+09	4.243D+09	5.054D+09	5.932D+09	6.887D+09
3	7.632D+09	6.827D+09	6.066D+09	6.302D+09	5.839D+09	3.317D+09	4.031D+09	4.801D+09	5.635D+09	6.542D+09
2	4.318D+09	4.515D+09	5.058D+09	5.208D+09	3.689D+09	3.055D+09	3.713D+09	4.422D+09	5.190D+09	6.026D+09
1	1.757D+09	5.926D+08	9.977D+08	1.418D+09	1.859D+09	2.327D+09	2.828D+09	3.369D+09	3.954D+09	4.590D+09

NUMBER OF GAS ATOMS RELEASED TO FREE VOLUME (ATOMS)							IWTHE= 10			
SEG										
8	0.0000+00	0.0000+00	0.0000+00	0.0000+00	0.0000+00	0.0000+00	0.0000+00	0.0000+00	0.0000+00	0.0000+00
7	1.199D+10	5.535D+09	0.0000+00	0.0000+00	0.0000+00	0.0000+00	0.0000+00	0.0000+00	0.0000+00	0.0000+00
6	9.704D+10	7.835D+10	4.918D+10	1.699D+10	0.0000+00	0.0000+00	0.0000+00	0.0000+00	0.0000+00	0.0000+00
5	9.279D+10	7.391D+10	4.473D+10	1.634D+10	0.0000+00	0.0000+00	0.0000+00	0.0000+00	0.0000+00	0.0000+00
4	1.319D+11	1.066D+11	6.619D+10	2.907D+10	4.389D+08	0.0000+00	0.0000+00	0.0000+00	0.0000+00	0.0000+00
3	5.949D+10	4.740D+10	2.815D+10	3.700D+09	0.0000+00	0.0000+00	0.0000+00	0.0000+00	0.0000+00	0.0000+00
2	2.650D+10	1.884D+10	5.388D+09	0.0000+00	0.0000+00	0.0000+00	0.0000+00	0.0000+00	0.0000+00	0.0000+00
1	0.0000+00	0.0000+00	0.0000+00	0.0000+00	0.0000+00	0.0000+00	0.0000+00	0.0000+00	0.0000+00	0.0000+00

NUMBER OF GAS ATOMS IN A GRAIN AND BOUNDARY (ATOMS)							IWTHE= 11			
SEG										
8	5.089D+09	1.534D+10	2.583D+10	3.671D+10	4.813D+10	6.025D+10	7.323D+10	8.722D+10	1.024D+11	1.188D+11
7	1.813D+11	1.887D+11	1.962D+11	1.954D+11	9.626D+10	1.205D+11	1.465D+11	1.744D+11	2.047D+11	2.377D+11
6	1.504D+11	1.591D+11	1.775D+11	2.121D+11	2.336D+11	1.386D+11	1.684D+11	2.006D+11	2.355D+11	2.734D+11
5	1.606D+11	1.683D+11	1.849D+11	2.147D+11	2.357D+11	1.398D+11	1.699D+11	2.023D+11	2.375D+11	2.757D+11
4	1.608D+11	1.671D+11	1.826D+11	2.100D+11	2.433D+11	1.446D+11	1.757D+11	2.093D+11	2.457D+11	2.852D+11
3	1.733D+11	1.790D+11	1.956D+11	2.234D+11	2.316D+11	1.374D+11	1.670D+11	1.989D+11	2.334D+11	2.710D+11
2	1.764D+11	1.851D+11	2.007D+11	2.092D+11	1.536D+11	1.265D+11	1.538D+11	1.832D+11	2.150D+11	2.496D+11
1	7.484D+10	2.455D+10	4.133D+10	5.873D+10	7.701D+10	9.640D+10	1.172D+11	1.395D+11	1.638D+11	1.902D+11

NUMBER OF GAS ATOMS (GRAIN+BOUNDARY+RELEASED) (ATOMS)							IWTHE= 12			
SEG										
8	5.089D+09	1.534D+10	2.583D+10	3.671D+10	4.813D+10	6.025D+10	7.323D+10	8.722D+10	1.024D+11	1.188D+11
7	1.933D+11	1.943D+11	1.962D+11	1.954D+11	9.626D+10	1.205D+11	1.465D+11	1.744D+11	2.047D+11	2.377D+11
6	2.474D+11	2.374D+11	2.267D+11	2.291D+11	2.336D+11	1.386D+11	1.684D+11	2.006D+11	2.355D+11	2.734D+11
5	2.534D+11	2.423D+11	2.297D+11	2.311D+11	2.357D+11	1.398D+11	1.699D+11	2.023D+11	2.375D+11	2.757D+11
4	2.928D+11	2.737D+11	2.488D+11	2.390D+11	2.438D+11	1.446D+11	1.757D+11	2.093D+11	2.457D+11	2.852D+11
3	2.328D+11	2.284D+11	2.237D+11	2.271D+11	2.316D+11	1.374D+11	1.670D+11	1.989D+11	2.334D+11	2.710D+11
2	2.029D+11	2.040D+11	2.060D+11	2.092D+11	1.536D+11	1.265D+11	1.538D+11	1.832D+11	2.150D+11	2.496D+11
1	7.484D+10	2.455D+10	4.133D+10	5.873D+10	7.701D+10	9.640D+10	1.172D+11	1.395D+11	1.638D+11	1.902D+11

PRODUCED FISSION GASES IN A GRAIN (ATOMS)							IWTHE= 13			
SEG										
8	9.668D+10	9.718D+10	9.816D+10	9.964D+10	1.016D+11	1.041D+11	1.070D+11	1.105D+11	1.144D+11	1.188D+11
7	1.934D+11	1.944D+11	1.963D+11	1.993D+11	2.032D+11	2.081D+11	2.141D+11	2.209D+11	2.288D+11	2.377D+11
6	2.476D+11	2.375D+11	2.268D+11	2.292D+11	2.337D+11	2.394D+11	2.462D+11	2.541D+11	2.632D+11	2.734D+11
5	2.536D+11	2.424D+11	2.298D+11	2.312D+11	2.357D+11	2.414D+11	2.483D+11	2.563D+11	2.654D+11	2.757D+11
4	2.929D+11	2.739D+11	2.490D+11	2.391D+11	2.439D+11	2.498D+11	2.569D+11	2.651D+11	2.746D+11	2.852D+11
3	2.329D+11	2.286D+11	2.238D+11	2.272D+11	2.317D+11	2.373D+11	2.440D+11	2.519D+11	2.609D+11	2.710D+11
2	2.030D+11	2.041D+11	2.061D+11	2.092D+11	2.134D+11	2.186D+11	2.248D+11	2.320D+11	2.403D+11	2.496D+11
1	1.547D+11	1.555D+11	1.571D+11	1.594D+11	1.626D+11	1.665D+11	1.712D+11	1.768D+11	1.831D+11	1.902D+11

Number of FP gas atoms released

Sum of the number of FP gas atoms in a grain and at a grain boundary

Sum of the number of FP gas atoms in a grain, at a grain boundary and released

Number of FP gas atoms produced

FISSION GAS RELEASE RATE IN A RING (%)							IWTHE= 14			
SEG										
8	0.50	0.50	0.50	0.50	0.50	0.50	0.50	0.50	0.50	0.50
7	6.34	2.98	0.50	0.50	0.50	0.50	0.50	0.50	0.50	0.50
6	39.22	33.00	21.69	7.42	0.50	0.50	0.50	0.50	0.50	0.50
5	36.62	30.51	19.47	7.20	0.50	0.50	0.50	0.50	0.50	0.50
4	45.07	38.94	26.60	12.29	0.50	0.50	0.50	0.50	0.50	0.50
3	25.69	21.07	12.72	1.78	0.50	0.50	0.50	0.50	0.50	0.50
2	13.19	9.37	2.78	0.50	0.50	0.50	0.50	0.50	0.50	0.50
1	0.50	0.50	0.50	0.50	0.50	0.50	0.50	0.50	0.50	0.50

FP gas release rate

DENSITY OF GAS ATOMS IN A BOUNDARY (ATOMS/CM**2)							IWTHE= 15			
SEG										
8	3.910D+13	1.179D+14	1.985D+14	2.820D+14	3.698D+14	4.629D+14	5.626D+14	6.701D+14	7.865D+14	9.131D+14
7	1.728D+15	1.767D+15	1.735D+15	1.585D+15	7.397D+14	8.260D+14	1.125D+15	1.340D+15	1.573D+15	1.827D+15
6	2.573D+15	2.605D+15	2.672D+15	2.776D+15	2.267D+15	1.065D+15	1.294D+15	1.542D+15	1.810D+15	2.101D+15
5	2.622D+15	2.656D+15	2.725D+15	2.396D+15	2.092D+15	1.074D+15	1.306D+15	1.555D+15	1.825D+15	2.119D+15
4	2.586D+15	2.620D+15	2.690D+15	2.492D+15	2.245D+15	1.111D+15	1.351D+15	1.609D+15	1.888D+15	2.192D+15
3	2.342D+15	2.141D+15	1.931D+15	2.006D+15	1.859D+15	1.056D+15	1.283D+15	1.528D+15	1.794D+15	2.083D+15
2	1.374D+15	1.437D+15	1.610D+15	1.658D+15	1.174D+15	9.724D+14	1.182D+15	1.408D+15	1.652D+15	1.918D+15
1	5.594D+14	1.886D+14	3.176D+14	4.513D+14	5.917D+14	7.407D+14	9.003D+14	1.072D+15	1.259D+15	1.461D+15

FP gas density at grain boundary

SATURATION DENSITY OF GAS ATOMS IN A BOUNDARY (ATOMS/CM**2)							IWTHE= 16			
SEG										
8	5.100D+15	5.100D+15	5.100D+15	5.100D+15	5.100D+15	5.100D+15	5.100D+15	5.100D+15	5.100D+15	5.100D+15
7	2.905D+15	2.937D+15	3.004D+15	3.107D+15	5.068D+15	5.068D+15	5.068D+15	5.068D+15	5.068D+15	5.068D+15
6	2.573D+15	2.605D+15	2.672D+15	2.776D+15	2.925D+15	4.861D+15	4.861D+15	4.861D+15	4.861D+15	4.861D+15
5	2.622D+15	2.656D+15	2.725D+15	2.833D+15	2.987D+15	5.003D+15	5.003D+15	5.003D+15	5.003D+15	5.003D+15
4	2.586D+15	2.620D+15	2.690D+15	2.801D+15	2.959D+15	5.054D+15	5.054D+15	5.054D+15	5.054D+15	5.054D+15
3	2.752D+15	2.787D+15	2.859D+15	2.972D+15	3.132D+15	5.223D+15	5.223D+15	5.223D+15	5.223D+15	5.223D+15
2	2.977D+15	3.013D+15	3.085D+15	3.198D+15	3.358D+15	5.386D+15	5.386D+15	5.386D+15	5.386D+15	5.386D+15
1	3.339D+15	5.213D+15	5.213D+15	5.213D+15	5.213D+15	5.213D+15	5.213D+15	5.213D+15	5.213D+15	5.213D+15

Maximum allowable FP gas density at grain boundary

EXTERNAL STRESS IN A BOUNDARY (MPA)							IWTHE= 17			
SEG										
8	8.23	8.23	8.23	8.23	8.23	8.23	8.23	8.23	8.23	8.23
7	8.23	8.23	8.23	8.23	8.23	8.23	8.23	8.23	8.23	8.23
6	8.23	8.23	8.23	8.23	8.23	8.23	8.23	8.23	8.23	8.23
5	8.23	8.23	8.23	8.23	8.23	8.23	8.23	8.23	8.23	8.23
4	8.23	8.23	8.23	8.23	8.23	8.23	8.23	8.23	8.23	8.23
3	8.23	8.23	8.23	8.23	8.23	8.23	8.23	8.23	8.23	8.23
2	8.23	8.23	8.23	8.23	8.23	8.23	8.23	8.23	8.23	8.23
1	8.23	8.23	8.23	8.23	8.23	8.23	8.23	8.23	8.23	8.23

External force imposed on the grain boundary

MECHANICAL ANALYSIS INFORMATION	IFEM= 4
STAGE NO.	177
TIME	31122.57 HR

Mechanical analysis results at each time step (Output in the case of IPRINT(7)=1)

LINEAR HEAT RATING	322.80	W/CM
FAST NEUTRON FLUX	5.30D+13	N/CM**2-S
FISSION RATE	1.48D+13	FISSIONS/CM**3-S
BURNUP	6.08D+04	MWD/TUO2

RADIAL TEMPERATURE DISTRIBUTION (DEG.C) IWFEM= 39

PELLET									GAP	CLADDING	
1170.42	1148.71	1117.08	1053.93	993.55	894.95	811.76	687.85	590.71	454.89	370.02	348.86

PELLET/CLADDING MECHANICAL INTERATION STATUS IWFEM= 40

NODAL COMBINATION FUEL-CLAD	CONTACT SURFACE STATUS	PELLET INCREMENTAL STRESS(PA) RADIAL	PELLET INCREMENTAL STRESS(PA) AXIAL	PELLET TOTAL STRESS(PA) RADIAL	PELLET TOTAL STRESS(PA) AXIAL	CLADDING INCREMENTAL STRESS(PA) RADIAL	CLADDING INCREMENTAL STRESS(PA) AXIAL	CLADDING TOTAL STRESS(PA) RADIAL	CLADDING TOTAL STRESS(PA) AXIAL	RADIAL GAP (MICRONS)
62- 69	FIXD	-5.6948D+04	-2.3195D+04	-3.8299D+06	-1.3358D+06	5.6948D+04	2.3195D+04	3.8299D+06	1.3358D+06	2.4286D-13
61- 68	FIXD	-3.2487D+04	5.8664D+03	-2.9186D+06	1.9630D+05	3.2487D+04	-5.8664D+03	2.9186D+06	-1.9630D+05	-4.1633D-13
60- 67	SLIP	-1.8034D+04	-7.2135D+03	-2.2167D+06	-8.8668D+05	1.8034D+04	7.2135D+03	2.2167D+06	8.8668D+05	1.3878D-13
59- 66	FIXD	-3.4597D+04	-1.3253D+04	-3.0449D+06	-6.3241D+05	3.4597D+04	1.3253D+04	3.0449D+06	6.3241D+05	-1.0408D-13
58- 65	FIXD	-3.3616D+04	-8.7091D+03	-3.1612D+06	-3.4037D+05	3.3616D+04	8.7091D+03	3.1612D+06	3.4037D+05	2.1684D-13
57- 64	FIXD	-3.6851D+04	-4.7898D+03	-3.2150D+06	-2.8536D+05	3.6851D+04	4.7898D+03	3.2150D+06	2.8536D+05	1.6480D-13
56- 63	FIXD	-3.8358D+04	0.0000D+00	-3.3796D+06	0.0000D+00	3.8358D+04	0.0000D+00	3.3796D+06	0.0000D+00	8.6736D-14

PELLET/PELLET MECHANICAL INTERATION STATUS IWFEM= 41

NODAL POINT	CONTACT STATUS	AXIAL STRESS (PA) INCREMENTAL	AXIAL STRESS (PA) TOTAL	AXIAL DISPLACEMENT (CM) DISP.	AXIAL DISPLACEMENT (CM) CONTACT	AXIAL DISPLACEMENT (CM) DISTANCE	RADIAL GAP (MICRONS) MINIMUM	RADIAL GAP (MICRONS) BOUNDARY
7	OPEN	0.0000D+00	0.0000D+00	7.5127D-01	7.6914D-01	1.7871D-02	-4.1633D-13	3.0000D+00
11	OPEN	0.0000D+00	0.0000D+00	7.5187D-01	7.6914D-01	1.7272D-02	-4.1633D-13	3.0000D+00
18	OPEN	0.0000D+00	0.0000D+00	7.5118D-01	7.6914D-01	1.7957D-02	-4.1633D-13	3.0000D+00
22	OPEN	0.0000D+00	0.0000D+00	7.5120D-01	7.6914D-01	1.7943D-02	-4.1633D-13	3.0000D+00
29	OPEN	0.0000D+00	0.0000D+00	7.5263D-01	7.6914D-01	1.6513D-02	-4.1633D-13	3.0000D+00
33	OPEN	0.0000D+00	0.0000D+00	7.5547D-01	7.6914D-01	1.3674D-02	-4.1633D-13	3.0000D+00
40	OPEN	0.0000D+00	0.0000D+00	7.5941D-01	7.6914D-01	9.7296D-03	-4.1633D-13	3.0000D+00
44	OPEN	0.0000D+00	0.0000D+00	7.6386D-01	7.6914D-01	5.2844D-03	-4.1633D-13	3.0000D+00
51	FIXD	-2.2959D+05	-8.5680D+06	7.6914D-01	7.6914D-01	0.0000D+00	-4.1633D-13	3.0000D+00
55	FIXD	-4.8645D+04	-2.6245D+06	7.6914D-01	7.6914D-01	0.0000D+00	-4.1633D-13	3.0000D+00
62	OPEN	0.0000D+00	0.0000D+00	7.6899D-01	7.6914D-01	1.5412D-04	-4.1633D-13	3.0000D+00

DISPLACEMENT OF NODES (MICRON) IWFEM= 42

(R-DIRECTION)									GAP		
0.0	17.4	31.6	38.2	44.5	50.1	54.3	56.8	63.1	69.1	72.01	-11.0	-9.1	-7.6
0.0		4.0		18.7		33.9		53.2		69.91	-13.1		-9.5

Time-step number, time, linear heat rate, fast neutron flux, fission rate, burnup, coolant temperature, coolant pressure
Hereafter, items designated by IWFEM (i) are output

Temperature distribution in the radial direction

Pellet/cladding contact status

Contact state, radial and axial components of the contact stress increment, radial and axial components of the contact stress, radial gap

Pellet/pellet contact states

Contact states, stress increment in the axial direction, axial stress, axial displacement, contact boundary, distance to the contact boundary

Displacement of node in the radial and axial directions

0.0	3.6	9.8	14.8	21.6	31.2	41.6	49.2	55.7	62.2	67.4I	-15.6	-13.6	-11.8
0.0		10.0		26.8		41.3		56.7		67.9I	-15.1		-11.6
0.0	6.5	14.0	20.9	28.1	37.7	46.4	52.6	58.3	64.3	69.6I	-13.4	-11.6	-10.0
0.0		13.1		31.7		46.6		60.8		71.1I	-11.9		-8.8
0.0	7.7	15.9	22.8	30.0	39.6	48.7	55.3	61.0	66.6	71.6I	-11.4	-9.7	-8.2

(Z-DIRECTION)

										GAP			
252.7	253.4	230.8	204.5	181.8	162.5	143.6	118.8	91.4	91.4	89.9I	46.9	46.9	46.9
229.2		192.4		146.9		110.0		83.4		75.2I	40.2		38.9
184.4	152.5	139.3	122.8	110.6	99.1	88.4	78.2	72.6	66.3	63.9I	32.4	32.0	31.7
110.2		96.6		79.1		66.0		54.2		47.5I	23.9		24.4
65.2	66.4	60.2	55.2	50.4	46.7	42.8	39.1	35.6	33.3	31.7I	15.8	16.1	16.5
30.4		29.2		25.0		20.7		17.6		16.0I	7.9		8.3
0.0	0.0	0.0	0.0	0.0	0.0	0.0	0.0	0.0	0.0	0.0I	0.0	0.0	0.0

AXIAL STRESSES IN THE FUEL AND THE CLADDING (MN/M**2) IWFEM= 2

SIG(Z)

										GAP		
-0.5	-0.1	-0.4	-0.2	-0.5	-0.2	-0.7	-2.9	-3.8	-3.1	I	-20.0	-18.9
-1.0	-1.8	-0.8	-1.7	-0.9	-2.2	-1.8	-1.7	-2.2	-1.6	I	-18.2	-21.4
-2.7	-1.7	-2.5	-1.6	-2.5	-1.7	-2.2	-2.3	-1.8	-1.9	I	-16.0	-21.1
-2.7	-2.9	-2.6	-2.6	-2.5	-2.6	-2.4	-2.4	-2.2	-2.3	I	-16.3	-18.2
-3.1	-3.1	-2.9	-3.0	-2.8	-2.8	-2.8	-2.5	-2.5	-2.0	I	-16.6	-16.8
-3.3	-3.2	-3.2	-3.0	-3.0	-3.0	-2.9	-2.8	-2.5	-2.3	I	-16.3	-15.8

CIRCUMFERENTIAL STRESSES IN THE FUEL AND THE CLADDING (MN/M**2) IWFEM= 3

SIG(T)

										GAP		
-1.1	-0.9	-1.3	-1.2	-1.7	-1.6	-2.2	-3.5	-4.0	-4.2	I	-31.6	-34.6
-2.2	-3.1	-2.2	-3.2	-2.3	-3.3	-2.8	-2.5	-3.1	-3.2	I	-32.1	-36.1
-3.5	-2.6	-3.5	-2.7	-3.6	-2.6	-3.1	-3.3	-3.0	-3.9	I	-31.8	-36.9
-3.3	-3.5	-3.4	-3.5	-3.4	-3.5	-3.2	-3.4	-3.3	-4.0	I	-31.7	-35.6
-3.6	-3.6	-3.5	-3.7	-3.5	-3.5	-3.6	-3.4	-3.6	-3.7	I	-31.3	-34.3
-3.7	-3.7	-3.7	-3.7	-3.7	-3.6	-3.6	-3.5	-3.5	-3.9	I	-30.6	-33.7

EQUIVALENT STRESSES IN THE FUEL AND THE CLADDING (MN/M**2) IWFEM= 5

EQ.SIG

										GAP		
0.6	0.9	1.1	1.4	1.6	2.1	2.3	3.0	1.2	1.3	I	17.2	19.1
1.3	1.5	1.6	1.9	2.0	2.3	2.1	2.0	1.8	1.8	I	18.1	20.4
1.1	1.0	1.3	1.4	1.6	1.4	1.5	1.5	1.8	2.1	I	18.7	20.7
0.9	1.0	1.1	1.2	1.2	1.3	1.4	1.4	1.5	1.9	I	18.1	20.3
0.9	1.0	1.0	1.1	1.1	1.1	1.2	1.3	1.4	1.8	I	17.5	19.7
0.9	0.9	1.0	1.0	1.0	1.0	1.0	1.1	1.2	1.6	I	17.0	19.2

Stress in the axial direction

Stress in the circumferential direction

Equivalent stress

```
|        EQUIVALENT PLASTIC STRAINS IN THE FUEL AND CLADDING     (0.01%)        IWFEM= 11      |
```

EPSP										GAP		
0.0	0.0	0.0	0.0	0.0	0.0	0.0	0.0	0.0	0.0	I	0.0	0.0
0.0	0.0	0.0	0.0	0.0	0.0	0.0	0.0	0.0	0.0	I	0.0	0.0
0.0	0.0	0.0	0.0	0.0	0.0	0.0	0.0	0.0	0.0	I	0.0	0.0
0.0	0.0	0.0	0.0	0.0	0.0	0.0	0.0	0.0	0.0	I	0.0	0.0
0.0	0.0	0.0	0.0	0.0	0.0	0.0	0.0	0.0	0.0	I	0.0	0.0
0.0	0.0	0.0	0.0	0.0	0.0	0.0	0.0	0.0	0.0	I	0.0	0.0

Equivalent plastic strain

```
|        CIRCUMFERENTIAL CREEP STRAINS IN THE FUEL AND CLADDING   (0.01%)       IWFEM= 14      |
```

EPSC(T)										GAP		
-21.4	-43.3	-50.6	-46.5	-40.7	-34.7	-29.5	-12.3	3.4	16.1	I	-44.9	-37.3
-213.9	-192.7	-166.8	-126.3	-100.6	-67.8	-48.2	-24.5	-8.4	7.4	I	-50.2	-42.0
-162.7	-131.5	-109.2	-84.2	-65.4	-44.4	-29.3	-13.1	-3.7	7.0	I	-52.4	-44.1
-120.6	-100.5	-83.2	-60.8	-46.7	-31.1	-21.2	-8.3	-0.1	9.7	I	-49.9	-42.0
-98.3	-83.9	-68.4	-47.5	-34.9	-20.7	-12.4	-2.1	5.2	13.3	I	-46.7	-39.3
-81.9	-70.8	-58.4	-40.8	-29.0	-16.2	-7.6	2.6	9.0	16.4	I	-44.4	-37.2

Creep strain in the circumferential direction

```
|        PCMI PLOT                                                              IWFEM= 43      |
0   ***STAGE*** 177     TIME   31122.57 (HR)    POWER     322.80(W/CM)
        PCMI PLOT(MM)
          Z        0.000          0.020          0.040          0.060          0.080          0.100
                   I--------------I--------------I--------------I--------------I--------------I
 7       7.60      X                                                     X
 6       6.33      I                                                    X
 5       5.07      I                                                  X
 4       3.80      I                                                   X
 3       2.53      X                                                    X
 2       1.27      I                                                     X
 1       0.00      I                                                     X
```

Diagram of pellet/cladding contact states

C:Radial position of cladding inner surface
P:Radial position of pellet outer surface
X:Position of cladding-pellet contact
G:Gap width. In this case, all the node couples are in contact state.

```
|        CRACK AND YIELD MAP  (*=YES)                                           IWFEM= 44      |
0   CRACK(R)                    CRACK(Z)                    CRACK(T)                    YIELD
    PELLET        CLADDING      PELLET        CLADDING      PELLET        CLADDING      PELLET        CLADDING
    +--+--+--+--+--+ +--+       +--+--+--+--+--+ +--+       +--+--+--+--+--+ +--+       +--+--+--+--+--+ +--+
    I  I  I  I  I  I I  I       I  I  I  I  I  I I  I       I  I  I  I  I  I I  I       I  I  I  I  I  I I  I
    I  I  I  I  I  I I  I       I  I  I  I  I  I I  I       I  I  I  I  I  I I  I       I  I  I  I  I  I I  I
    +--+--+--+--+--+ +--+       +--+--+--+--+--+ +--+       +--+--+--+--+--+ +--+       +--+--+--+--+--+ +--+
    I  I  I  I  I  I I  I       I  I  I  I  I  I I  I       I  I  I  I  I  I I  I       I  I  I  I  I  I I  I
    I  I  I  I  I  I I  I       I  I  I  I  I  I I  I       I  I  I  I  I  I I  I       I  I  I  I  I  I I  I
    +--+--+--+--+--+ +--+       +--+--+--+--+--+ +--+       +--+--+--+--+--+ +--+       +--+--+--+--+--+ +--+
    I  I  I  I  I  I I  I       I  I  I  I  I  I I  I       I  I  I  I  I  I I  I       I  I  I  I  I  I I  I
    I  I  I  I  I  I I  I       I  I  I  I  I  I I  I       I  I  I  I  I  I I  I       I  I  I  I  I  I I  I
    +--+--+--+--+--+ +--+       +--+--+--+--+--+ +--+       +--+--+--+--+--+ +--+       +--+--+--+--+--+ +--+
```

Crack and yield point map

The asterisks indicate the Gauss points at which cracking or yielding occurred. In this case, neither yielding nor cracking took place.

An example of PCMI plot when pellet and cladding are not in contact state

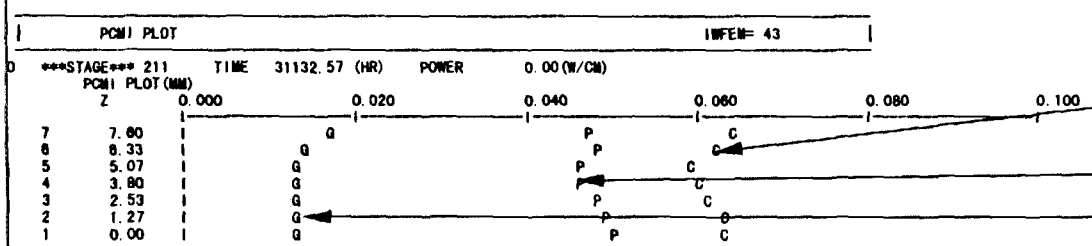

PCMI Figure

C: Radial position of cladding inner surface.

P: Radial position of pellet surface.

X: Position of cladding – pellet contact.

An example of plot when cracking and yielding occurred.

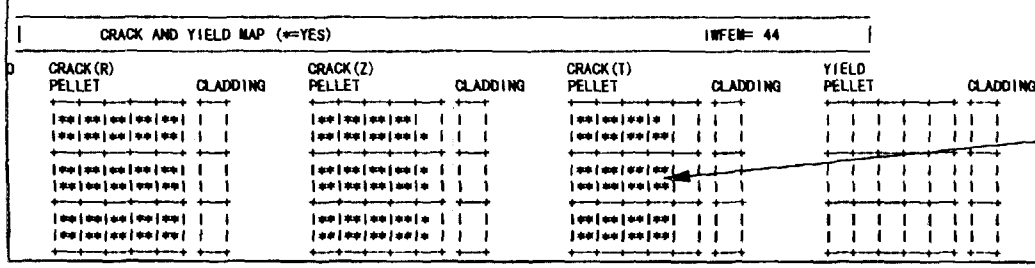

Cracking and yielding figure

Asterisks indicate the Gauss points at which either cracking or yielding occurred.

RESULTS OF THERMAL ANALYSIS / THERMAL INFORMATION (SEGMENT NUMBER 4)

POWER HISTORY				THERMAL INFORMATION												
				TEMPERATURE				GAP CONDUCTANCE								
STEP NO.	TIME (HR)	LINEAR HEAT RATE (W/CM)	BURNUP (MWD/ TUO2)	FUEL CENTER (DEG. C)	FUEL SURFACE (DEG. C)	CLAD INNER (DEG. C)	CLAD OUTER (DEG. C)	TOTAL (W/CM2 /C)	GAS (W/CM2 /C)	SOLID (W/CM2 /C)	RADIAL GAP SIZE (MIC)	CONTACT PRESSURE (MPA)	PRODUCE GAS (XE+KR) (10-3MOL)	FISSION GAS RELEASE (%)	IODINE RELEASE (10-5 G/CM2)	CPU TIME (SEC)
1	0.0	0.0	0.0	282.0	282.0	282.0	282.0	0.3410	0.3384	0.0000	62.07	0.00	0.00	0.50	0.000	1
33	5.0	312.0	4.7	1231.7	489.0	349.8	313.5	0.7465	0.7415	0.0000	30.17	0.00	0.00	0.50	0.000	23
45	2817.5	312.0	5288.7	1249.8	513.4	350.6	314.5	0.6393	0.6339	0.0000	36.48	0.00	1.33	0.50	0.046	34
56	5632.5	312.0	10577.3	1235.0	505.3	351.0	314.9	0.6742	0.6689	0.0000	33.94	0.00	2.66	0.67	0.121	43
67	8447.4	312.0	15866.0	1208.7	486.6	351.2	315.1	0.7684	0.7634	0.0000	28.49	0.00	4.00	1.01	0.277	65
78	11262.4	312.0	21154.7	1178.6	464.5	351.4	315.3	0.9195	0.9147	0.0000	22.42	0.00	5.33	1.14	0.417	80
89	14077.4	312.0	26443.4	1147.2	441.6	351.6	315.5	1.1558	1.1513	0.0000	16.33	0.00	6.66	1.09	0.498	94
101	17230.2	312.0	32386.7	1114.5	417.3	354.0	318.0	1.6436	1.6393	0.0000	9.53	0.00	8.15	0.99	0.554	108
107	17235.2	364.8	32376.9	1269.2	415.3	366.1	324.2	2.4693	2.4649	0.0000	4.31	0.00	8.15	1.03	0.575	116
114	18386.2	364.8	34905.2	1261.6	408.7	367.5	325.6	2.9481	2.9438	0.0000	1.11	0.00	8.79	2.63	1.579	126
121	19830.7	364.8	38078.4	1258.1	403.5	369.6	327.8	3.5833	3.5763	0.0027	0.00	0.29	9.59	3.31	2.173	136
128	21275.2	364.8	41251.7	1268.2	405.6	371.8	330.2	3.6052	3.5891	0.0117	0.00	1.29	10.39	3.98	2.816	145
136	22960.5	364.8	44953.7	1282.5	409.3	374.7	333.1	3.5199	3.4982	0.0172	0.00	1.92	11.32	4.72	3.656	156
141	22965.5	322.8	44964.1	1129.0	395.8	364.5	327.5	3.4325	3.4270	0.0013	0.00	0.15	11.33	4.72	3.656	162
148	24320.6	322.8	47598.1	1130.6	394.2	366.3	329.3	3.8526	3.8397	0.0087	0.00	0.97	11.99	4.49	3.679	170
155	25953.1	322.8	50771.3	1137.8	395.2	368.6	331.7	4.0447	4.0187	0.0217	0.00	2.42	12.79	4.24	3.706	175
162	27585.5	322.8	53944.5	1146.9	397.2	371.2	334.4	4.1413	4.1041	0.0330	0.00	3.70	13.59	4.02	3.737	182
169	29218.0	322.8	57117.7	1157.6	400.1	374.2	337.4	4.1593	4.1150	0.0399	0.00	4.51	14.39	3.88	3.820	187
177	31122.6	322.8	60819.7	1172.1	404.5	378.1	341.4	4.0702	4.0228	0.0430	0.00	4.89	15.32	3.86	4.041	196
178	31127.6	322.8	60829.5	1172.6	404.7	378.3	341.6	4.0704	4.0229	0.0431	0.00	4.90	15.32	3.86	4.042	197
211	31132.6	0.0	60834.3	18.0	18.0	18.0	18.0	0.5161	0.5157	0.0000	18.66	0.00	15.32	3.86	4.042	227

Summary of thermal analysis of the objective segment
(Output in the case of IPRINT(8)=1)

Time-step number, time, linear heat rate, burnup, temperature (pellet center, pellet surface, inner surface and outer surface of cladding), gap conductance (total, gas, solid), radial gap width, contact pressure, amount of gas produced, FP gas release ratio, iodine concentration, computation time

RESULTS OF THERMAL ANALYSIS / MECHANICAL INFORMATION (SEGMENT NUMBER 4)

POWER HISTORY			FUEL						FUEL - CLAD		CLAD			
STEP NO.	TIME (HR)	LINEAR HEAT RATE (W/CM)	BURNUP (MWD/TUO2)	THERMAL EXPAN-SION (MIC)	CREEP (MIC)	DENSIFI-CATION (MIC)	SWELL-ING (MIC)	RELOCA-TION (MIC)	RADIAL DISPLA-CEMENT (MIC)	RADIAL GAP (MIC)	CONTACT PRESSURE (MPA)	THERMAL EXPAN-SION (MIC)	ELASTIC DEFORM-ATION (MIC)	CREEP (MIC)	RADIAL DISPLA-CEMENT (MIC)
1	0.0	0.0	0.0	0.0	0.0	0.0	0.0	15.5	15.5	62.1	0.0	0.0	0.0	0.0	0.0
33	5.0	312.0	4.7	33.9	0.0	0.0	0.0	15.5	49.4	30.2	0.0	1.7	0.6	-0.3	1.9
45	2817.5	312.0	5288.7	35.1	0.0	-21.9	5.7	15.5	34.4	36.5	0.0	1.7	0.5	-8.9	-6.7
56	5632.5	312.0	10577.3	34.3	0.0	-28.3	11.4	15.5	32.9	33.9	0.0	1.7	0.5	-12.9	-10.7
67	8447.4	312.0	15866.0	33.0	0.0	-30.3	17.1	15.5	35.3	28.5	0.0	1.7	0.5	-16.0	-13.8
78	11262.4	312.0	21154.7	31.4	0.0	-30.8	22.8	15.5	38.8	22.4	0.0	1.7	0.5	-18.6	-16.3
89	14077.4	312.0	26443.4	29.7	0.0	-31.0	28.5	15.5	42.8	16.3	0.0	1.7	0.5	-20.8	-18.5
101	17230.2	312.0	32366.7	28.1	0.0	-31.0	34.9	15.5	47.4	9.5	0.0	1.8	0.6	-23.1	-20.8
107	17235.2	364.8	32376.9	33.6	0.0	-31.0	34.9	15.5	53.0	4.3	0.0	2.1	0.6	-23.1	-20.3
114	18386.2	364.8	34905.2	33.2	0.0	-31.1	37.6	15.5	55.3	1.1	0.0	2.2	0.7	-24.0	-21.2
121	19830.7	364.8	38078.4	33.0	-0.1	-31.1	41.0	15.5	58.3	0.0	0.3	2.2	0.7	-25.2	-22.3
128	21275.2	364.8	41251.7	33.4	-1.5	-31.1	44.4	15.5	60.8	0.0	1.3	2.3	0.8	-26.2	-23.1
136	22960.5	364.8	44953.7	34.0	-5.4	-31.1	48.4	15.5	61.5	0.0	1.9	2.4	0.8	-27.0	-23.8
141	22965.5	322.8	44964.1	28.1	-5.4	-31.1	48.4	15.5	55.6	0.0	0.1	2.2	0.8	-27.0	-24.1
148	24320.6	322.8	47598.1	28.2	-5.7	-31.1	51.3	15.5	58.2	0.0	1.0	2.2	0.8	-27.8	-24.8
155	25953.1	322.8	50771.3	28.4	-6.8	-31.1	54.7	15.5	60.8	0.0	2.4	2.3	0.8	-28.5	-25.4
162	27585.5	322.8	53944.5	28.8	-8.8	-31.1	58.1	15.5	62.6	0.0	3.7	2.4	0.8	-28.9	-25.7
169	29218.0	322.8	57117.7	29.3	-11.7	-31.1	61.5	15.5	63.6	0.0	4.5	2.5	0.8	-29.1	-25.8
177	31122.8	322.8	60819.7	29.9	-15.8	-31.1	65.5	15.5	64.1	0.0	4.9	2.6	0.9	-29.3	-25.8
178	31127.6	322.8	60829.5	29.9	-15.8	-31.1	65.5	15.5	64.1	0.0	4.9	2.8	0.9	-29.3	-25.8
211	31132.6	0.0	60834.3	0.0	-15.8	-31.1	65.5	15.5	34.2	18.7	0.0	0.0	4.6	-29.3	-24.7

Summary of thermal analysis and mechanical information for the objective segment
(Output in the case of (IPRINT(9)=1)

Time-step number, time, linear heat rate, burnup

Pellet:
thermal expansion, creep, densification, swelling, relocation, total amount of radial displacement

Pellet-cladding:
radial gap width, contact pressure

Cladding:
thermal expansion, elastic deformation, creep, total amount of radial displacement

RESULTS OF THERMAL ANALYSIS / FISSION GAS INFORMATION (SEGMENT NUMBER 4)

POWER HISTORY				FUEL CENTER									FUEL-CLAD		
STEP NO.	TIME (HR)	LINEAR HEAT RATE (W/CM)	BURNUP (MWD/ TUO2)	FUEL CENTER TEMP. (DEG.C)	GRAIN RADIUS (MIC)	BUBBLE RADIUS (ANGST)	BUBBLE DENSITY (10D17 BU/CM3)	DIFFUS. COEFF. (10D-16	DIFFUS. COEFF. /EFFECT CM2/S)	GAS DENS.AT BOUND. (10D13	SATURA -TION DENS. AT/CM2)	LOCAL FGR AT CENTER (%)	FISSON GAS RELASE (%)	AMOUNT OF GAS IN GAP (10-3MOL)	XE+KR PERCENT IN GAP (%)
1	0.0	0.0	0.0	282.0	5.00	0.00	19.35	0.2	0.20	0.0	567.7	0.50	0.50	1.31	0.00
33	5.0	312.0	4.7	1231.7	5.00	0.06	19.12	0.2	0.20	0.0	430.2	0.50	0.50	0.67	0.00
45	2817.5	312.0	5288.7	1249.8	5.40	5.45	8.11	6.6	5.18	138.5	228.2	0.50	0.50	0.71	0.19
56	5632.5	312.0	10577.3	1235.0	5.40	6.46	7.14	5.3	4.41	230.0	230.0	8.52	0.67	0.69	0.32
67	8447.4	312.0	15866.0	1208.7	5.40	6.55	7.07	3.6	3.14	235.0	235.0	17.24	1.01	0.64	0.52
78	11262.4	312.0	21154.7	1178.6	5.40	6.55	7.07	2.2	2.07	241.4	241.5	19.84	1.14	0.60	0.63
89	14077.4	312.0	26443.4	1147.2	5.40	6.55	7.07	1.4	1.32	248.5	248.6	19.21	1.09	0.55	0.72
101	17230.2	312.0	32366.7	1114.5	5.40	6.55	7.07	0.9	0.84	256.5	256.6	16.65	0.99	0.50	0.86
107	17235.2	364.8	32376.9	1269.2	5.40	11.30	4.26	8.6	7.19	232.8	232.8	17.92	1.03	0.48	1.37
114	18386.2	364.8	34905.2	1261.6	5.40	11.35	4.24	7.8	6.57	236.3	236.3	34.53	2.63	0.49	7.58
121	19830.7	364.8	38078.4	1258.1	5.40	11.35	4.24	7.4	6.28	238.4	238.4	41.00	3.31	0.50	7.15
128	21275.2	364.8	41251.7	1268.2	5.40	11.35	4.24	8.5	7.11	238.3	238.3	46.52	3.96	0.50	7.40
138	22960.5	364.8	44953.7	1282.5	5.40	11.35	4.24	10.5	8.41	237.9	237.9	52.64	4.72	0.50	8.50
141	22965.5	322.8	44964.1	1129.0	5.40	11.35	4.24	1.1	1.03	231.6	262.6	52.63	4.72	0.53	8.23
148	24320.6	322.8	47598.1	1130.6	5.40	11.35	4.24	1.1	1.06	170.6	262.7	49.74	4.49	0.53	4.94
155	25953.1	322.8	50771.3	1137.8	5.40	11.35	4.24	1.2	1.17	217.7	262.0	46.67	4.24	0.53	4.03
162	27585.5	322.8	53944.5	1146.9	5.40	11.35	4.24	1.4	1.34	261.0	261.0	44.39	4.02	0.53	3.83
169	29218.0	322.8	57117.7	1157.6	5.40	11.35	4.24	1.6	1.56	259.9	259.9	44.17	3.88	0.52	4.07
177	31122.6	322.8	60819.7	1172.1	5.40	11.35	4.24	2.0	1.93	258.6	258.6	45.07	3.86	0.52	5.00
178	31127.6	322.8	60829.5	1172.6	5.40	11.35	4.24	2.0	1.94	258.5	258.5	45.07	3.86	0.52	5.00
211	31132.6	0.0	60834.3	18.0	5.40	11.35	4.24	0.2	0.20	244.9	755.8	45.07	3.86	0.90	4.27

Summary of thermal analysis and FP gas information for the objective segment
(Output in the case of IPRINT(10)=1)

Time-step number, time, linear heat rate, burnup

Pellet center:

temperature, grain size, bubble radius, bubble density, diffusion coefficient, effective diffusion coefficient, FP gas density at grain boundary, FP gas density limit, FP gas release ratio

The objective segment:

FP gas release ratio, gas molar number in gap, percentage of Xe + Kr in gap gas

RESULTS OF THERMAL ANALYSIS / FISSION GAS INFORMATION (WHOLE FUEL ROD)

POWER HISTORY					FUEL ROD											
STEP NO.	TIME (HR)	LINEAR HEAT RATE (W/CM)	BURNUP (MWD/TU02)	(10020 FISS/CC)	AMOUNT OF GAS PRODUCE (XE+KR)	PELEASE (XE+KE)	PLENUM (10D-3 MOLE)	GAP	TOTAL IN FUEL ROD	FRACTION OF GAS MIXTURE HE (%)	N2 (%)	KR (%)	XE (%)	FISSION GAS RELEASE (%)	INNER GAS PRESSURE (MPA)
1	0.0	0.0	0.0	0.00	0.00	0.00	44.11	10.47	54.57	100.00	0.00	0.00	0.00	0.50	6.58
33	5.0	312.0	4.7	0.00	0.01	0.00	48.34	6.23	54.57	100.00	0.00	0.00	0.00	0.50	7.67
45	2817.5	312.0	5288.7	1.47	8.88	0.04	48.09	6.52	54.62	99.92	0.00	0.01	0.07	0.50	7.48
56	5632.5	312.0	10577.3	2.93	17.76	0.09	48.21	6.46	54.67	99.83	0.00	0.02	0.15	0.53	7.46
67	8447.4	312.0	15866.0	4.40	26.64	0.16	48.49	6.25	54.73	99.71	0.00	0.04	0.26	0.61	7.50
78	11262.4	312.0	21154.7	5.87	35.52	0.23	48.82	5.98	54.80	99.58	0.00	0.05	0.36	0.65	7.57
89	14077.4	312.0	26443.4	7.34	44.40	0.28	49.17	5.68	54.85	99.49	0.00	0.07	0.45	0.63	7.64
101	17230.2	312.0	32366.7	8.98	54.35	0.33	49.58	5.33	54.90	99.40	0.00	0.08	0.53	0.61	7.73
107	17235.2	364.8	32376.9	8.98	54.37	0.34	50.00	4.91	54.91	99.38	0.00	0.08	0.54	0.62	7.81
114	18386.2	364.8	34905.2	9.68	58.61	0.85	50.58	4.84	55.42	98.47	0.00	0.20	1.33	1.44	7.91
121	19830.7	364.8	38078.4	10.56	63.94	1.15	50.91	4.82	55.72	97.94	0.00	0.27	1.79	1.80	7.98
128	21275.2	364.8	41251.7	11.44	69.27	1.43	51.19	4.82	56.00	97.44	0.00	0.33	2.23	2.07	8.04
136	22960.5	364.8	44953.7	12.47	75.49	1.81	51.56	4.82	56.38	96.79	0.00	0.42	2.79	2.40	8.12
141	22965.5	322.8	44964.1	12.47	75.50	1.81	51.33	5.05	56.38	96.79	0.00	0.42	2.79	2.40	8.07
148	24320.6	322.8	47598.1	13.21	79.93	1.83	51.35	5.06	56.40	96.75	0.00	0.42	2.82	2.29	8.09
155	25953.1	322.8	50771.3	14.09	85.25	1.86	51.39	5.04	56.43	96.71	0.00	0.43	2.86	2.18	8.11
162	27585.5	322.8	53944.5	14.97	90.58	1.88	51.44	5.02	56.46	96.66	0.00	0.43	2.90	2.08	8.14
169	29218.0	322.8	57117.7	15.85	95.91	1.93	51.52	4.98	56.50	96.59	0.00	0.44	2.97	2.01	8.18
177	31122.8	322.8	60819.7	16.87	102.13	2.05	51.68	4.94	56.62	96.39	0.00	0.47	3.14	2.00	8.23
178	31127.8	322.8	60829.5	16.88	102.14	2.05	51.68	4.93	56.62	96.39	0.00	0.47	3.14	2.00	8.23
211	31132.6	0.0	60834.3	16.88	102.15	2.05	48.74	7.88	56.62	96.39	0.00	0.47	3.14	2.00	3.84

Summary of thermal analysis and FP gas information for whole fuel rod
(Output in the case of IPRINT(11)=1)

Time-step number, time, linear heat rate, burnup

Whole fuel rod:
amount of FP gas produced, amount of FP gas released, gas molar number in the plenum, gas molar number in the gap, total gas molar number, gas composition, FP gas release rate, inner pressure of the fuel rod

RESULTS OF FEM MECHANICAL ANALYSIS / FUEL AND CLAD DEFORMATIONS (ANALYZED SEGMENT NUMBER 4)

POWER HISTORY				TOP OF FUEL				FUEL - CLAD AT TOP			CLADDING			DIAMETRAL RIDGE	
STEP NO.	TIME (HR)	LINEAR HEAT RATE (W/CM)	BURNUP (MWD/ TUO2)	AXIAL DIPS. CENTER (MIC)	AXIAL DIPS. SURFACE (MIC)	RADIAL DIPS. INNER (MIC)	RADIAL DIPS OUTER (MIC)	RADIAL GAP AT TOP (MIC)	CONTACT PRESS. AXIAL (MPA)	CONTACT PRESS. RADIAL (MPA)	AXIAL DISP. AT TOP (MIC)	RADIAL DISP. OUT/TOP (MIC)	RADIAL DISP. OUT/MID (MIC)	RIDGE HEIGHT (MAX) (MIC)	RIDGE HEIGHT (TOP-MID) (MIC)
1	0.0	0.0	0.0	0.00	0.00	0.00	0.00	39.74	0.00	0.00	0.00	0.00	0.00	0.00	0.00
33	5.0	312.0	4.7	67.69	43.27	0.00	78.17	2.27	0.00	0.00	2.33	3.63	3.63	0.00	0.00
45	2817.5	312.0	5288.7	48.87	11.91	0.00	47.00	6.42	0.00	0.00	13.03	-17.03	-17.03	0.00	0.00
56	5632.5	312.0	10577.3	51.47	9.54	0.00	47.73	0.71	0.00	0.00	17.77	-26.68	-26.68	0.00	0.00
67	8447.4	312.0	15866.0	56.02	13.81	0.00	43.65	0.00	1.52	3.80	21.41	-31.77	-33.72	2.36	1.95
78	11262.4	312.0	21154.7	65.46	17.60	0.00	43.57	0.00	3.11	7.78	24.15	-31.74	-33.59	4.21	1.65
89	14077.4	312.0	26443.4	81.79	21.87	0.00	46.59	0.00	3.83	9.58	26.55	-28.89	-31.09	4.81	2.20
101	17230.2	312.0	32366.7	105.73	26.74	0.00	51.79	0.00	4.99	12.48	29.50	-24.04	-26.28	6.03	2.24
107	17235.2	364.8	32376.9	114.95	28.70	0.00	59.22	0.00	5.37	23.53	31.46	-17.10	-21.50	7.83	4.40
114	18386.2	364.8	34905.2	141.34	28.27	0.00	58.81	0.00	5.30	14.94	31.03	-17.57	-19.99	7.90	2.42
121	19830.7	364.8	38078.4	159.48	29.23	0.00	58.19	0.00	4.69	11.72	31.94	-18.16	-20.33	8.23	2.16
128	21275.2	364.8	41251.7	175.60	30.16	0.00	57.57	0.00	3.95	9.88	32.81	-18.72	-20.77	8.46	2.05
136	22960.5	364.8	44953.7	192.72	31.15	0.00	56.63	0.00	3.24	8.11	33.75	-19.56	-21.53	8.57	1.97
141	22965.5	322.8	44964.1	185.57	30.42	0.00	52.54	0.00	1.10	2.76	32.90	-23.43	-24.95	7.89	1.52
148	24320.6	322.8	47598.1	185.55	31.51	0.00	50.44	0.00	0.70	1.79	33.95	-25.32	-26.44	7.56	1.12
155	25953.1	322.8	50771.3	187.52	32.59	0.00	49.08	0.00	0.31	2.15	35.04	-26.49	-27.59	7.63	1.10
162	27585.5	322.8	53944.5	191.08	33.70	0.00	48.18	0.00	0.86	2.76	36.14	-27.26	-28.43	7.80	1.16
169	29218.0	322.8	57117.7	195.42	34.78	0.00	47.50	0.00	1.15	3.29	37.23	-27.83	-29.01	8.01	1.19
177	31122.6	322.8	60819.7	201.28	36.04	0.00	46.93	0.00	1.34	3.83	38.48	-28.28	-29.49	8.29	1.20
178	31127.6	322.8	60829.5	201.33	36.05	0.00	46.97	0.00	1.36	3.87	38.49	-28.24	-29.45	8.29	1.21
211	31132.6	0.0	60834.3	145.21	6.00	0.00	-3.23	16.76	0.00	0.00	27.88	-48.05	-49.13	7.93	1.08

Summary of mechanical analysis and deformation information for the objective segment
(Output in the case of IPRINT(12)=1)

Time-step number, time, linear heat rate, burnup

Pellet:
- axial displacement at the center,
- axial displacement at the surface,
- radial displacement at the center hole,
- radial displacement at the surface

Gap:
- radial gap width, contact pressure (axial and radial directions)

Cladding:
- axial displacement,
- radial displacement (ridge, center),
- ridge height (maximum, ridge-center)

RESULTS OF FEM MECHANICAL ANALYSIS / STRESSES AND STRAINS IN FUEL (ANALYZED SEGMENT NUMBER 4)

POWER HISTORY				TOP AND INNER OF FUEL											
STEP NO.	TIME (HR)	LINEAR HEAT RATE (W/CM)	BURNUP (MWD/ TUO2)	CIRCUM. TOTAL STRAIN (0.01%)	AXIAL TOTAL STRAIN (0.01%)	RADIAL TOTAL STRAIN (0.01%)	CIRCUM. CREEP STRAIN (0.01%)	AXIAL CREEP STRAIN (0.01%)	RADIAL CREEP STRAIN (0.01%)	EQUIVA. CREEP STRAIN (0.01%)	EQUIVA. PLASTIC STRAIN (0.01%)	CIRCUM. STRESS (MPA)	AXIAL STRESS (MPA)	RADIAL STRESS (MPA)	EQUIVA. STRESS (MPA)
1	0.0	0.0	0.0	104.	71.	104.	0.	0.	0.	0.	0.	0.0	0.0	0.0	0.0
33	5.0	312.0	4.7	226.	176.	225.	0.	0.	0.	0.	0.	3.0	-0.4	2.8	3.4
45	2817.5	312.0	5288.7	204.	117.	201.	19.	-35.	16.	35.	0.	-0.1	-0.4	-0.1	0.3
56	5632.5	312.0	10577.3	211.	107.	208.	24.	-45.	21.	45.	0.	0.0	-0.2	0.0	0.2
67	8447.4	312.0	15866.0	213.	115.	210.	23.	-43.	19.	43.	0.	-0.5	-0.2	-0.5	0.3
78	11262.4	312.0	21154.7	212.	132.	209.	17.	-32.	13.	32.	0.	-1.3	-0.5	-1.3	0.8
89	14077.4	312.0	26443.4	210.	153.	207.	9.	-17.	5.	17.	0.	-1.8	-0.7	-1.8	1.2
101	17230.2	312.0	32366.7	210.	180.	206.	0.	0.	-4.	7.	0.	-2.4	-0.8	-2.4	1.6
107	17235.2	364.8	32376.9	228.	199.	224.	0.	1.	-4.	7.	0.	-7.1	-3.9	-7.4	3.8
114	18386.2	364.8	34905.2	232.	202.	226.	-2.	1.	-8.	18.	0.	-2.0	-1.8	-2.0	0.5
121	19830.7	364.8	38078.4	230.	210.	222.	-5.	7.	-12.	23.	0.	-1.7	-1.4	-1.7	0.5
128	21275.2	384.8	41251.7	228.	218.	220.	-9.	13.	-17.	30.	0.	-1.4	-1.2	-1.4	0.4
136	22960.5	364.8	44953.7	227.	225.	218.	-12.	18.	-22.	36.	0.	-1.1	-1.0	-1.1	0.3
141	22965.5	322.8	44964.1	216.	205.	207.	-12.	18.	-22.	36.	0.	1.4	-0.1	1.5	1.6
148	24320.6	322.8	47598.1	211.	203.	202.	-11.	15.	-20.	34.	0.	0.0	-0.1	0.0	0.1
155	25953.1	322.8	50771.3	208.	207.	198.	-12.	18.	-22.	36.	0.	-1.1	-0.2	-1.1	0.9
162	27585.5	322.8	53944.5	206.	214.	196.	-16.	24.	-25.	40.	0.	-1.1	-0.4	-1.1	0.8
169	29218.0	322.8	57117.7	204.	220.	195.	-18.	29.	-28.	44.	0.	-1.1	-0.4	-1.1	0.7
177	31122.6	322.8	60819.7	203.	228.	194.	-21.	35.	-31.	49.	0.	-1.1	-0.5	-1.1	0.6
178	31127.6	322.8	60829.5	203.	228.	194.	-21.	35.	-31.	49.	0.	-1.1	-0.5	-1.1	0.6
211	31132.6	0.0	60834.3	122.	114.	113.	-21.	35.	-31.	49.	0.	6.9	0.8	7.0	6.2

Summary of mechanical analysis and pellet stress/strain information for the objective segment

(Output in the case of IPRINT(13)=1)

Time-step number, time, linear heat rate, burnup

Pellet center:

total strain in the circumferential, axial and radial directions;

creep strain in the circumferential, axial and radial directions;

equivalent creep strain; equivalent plastic strain; stress in the circumferential, axial and radial directions;

equivalent stress

RESULTS OF FEM MECHANICAL ANALYSIS / STRESSES AND STRAINS IN CLAD (ANALYZED SEGMENT NUMBER 4)

POWER HISTORY				TOP AND INNER OF CLADDING											
STEP NO.	TIME (HR)	LINEAR HEAT RATE (W/CM)	BURNUP (MWD/TUO2)	CIRCUM. TOTAL STRAIN (0.01%)	AXIAL TOTAL STRAIN (0.01%)	RADIAL TOTAL STRAIN (0.01%)	CIRCUM. CREEP STRAIN (0.01%)	AXIAL CREEP STRAIN (0.01%)	RADIAL CREEP STRAIN (0.01%)	EQUIVA. CREEP STRAIN (0.01%)	EQUIVA. PLASTIC STRAIN (0.01%)	CIRCUM. STRESS (MPA)	AXIAL STRESS (MPA)	RADIAL STRESS (MPA)	EQUIVA. STRESS (MPA)
1	0.0	0.0	0.0	11.3	11.1	20.8	0.0	0.0	0.0	0.0	0.0	-71.3	-33.2	-8.3	54.9
33	5.0	312.0	4.7	14.8	14.1	25.5	-0.9	0.1	0.8	1.0	0.0	-69.5	-34.2	-9.4	52.3
45	2817.5	312.0	5288.7	-8.1	28.2	45.4	-25.5	3.5	21.9	26.9	0.0	-58.9	-27.4	-8.8	43.8
56	5632.5	312.0	10577.3	-18.9	34.4	54.4	-36.3	5.3	31.0	38.5	0.0	-58.3	-26.8	-8.8	43.4
67	8447.4	312.0	15866.0	-24.9	38.0	60.4	-43.2	6.0	37.2	46.2	0.0	-53.0	-30.6	-10.5	37.0
78	11262.4	312.0	21154.7	-25.4	40.5	61.9	-46.1	5.9	40.2	49.6	0.0	-34.1	-27.0	-13.6	18.5
89	14077.4	312.0	26443.4	-22.4	42.5	60.5	-46.2	5.7	40.5	50.1	0.0	-9.0	-21.0	-15.5	10.6
101	17230.2	312.0	32366.7	-17.3	44.6	57.5	-43.9	4.7	39.2	52.4	0.0	14.4	-9.5	-18.0	29.2
107	17235.2	364.8	32376.9	-10.0	46.0	53.5	-43.8	4.7	39.2	52.5	0.0	71.3	15.6	-25.2	84.1
114	18386.2	364.8	34905.2	-10.6	45.2	53.5	-38.6	3.7	34.9	58.1	0.0	19.7	-7.4	-19.7	35.1
121	19830.7	364.8	38078.4	-11.2	46.2	53.9	-37.3	3.4	34.0	59.4	0.0	3.4	-11.0	-17.5	18.6
128	21275.2	364.8	41251.7	-11.9	47.2	54.6	-37.0	3.2	33.7	59.7	0.0	-6.4	-14.1	-16.2	9.2
136	22960.5	364.8	44953.7	-12.8	48.3	55.6	-36.9	3.2	33.7	59.8	0.0	-16.6	-17.7	-15.0	3.1
141	22965.5	322.8	44964.1	-16.9	47.9	57.2	-36.9	3.2	33.7	59.8	0.0	-44.8	-27.1	-11.5	28.9
148	24320.6	322.8	47598.1	-18.9	49.4	59.0	-38.9	3.4	35.5	62.0	0.0	-44.9	-24.0	-10.8	29.8
155	25953.1	322.8	50771.3	-20.3	50.8	60.7	-40.9	3.7	37.2	64.2	0.0	-40.8	-23.1	-11.0	26.0
162	27585.5	322.8	53944.5	-21.2	52.1	61.9	-42.4	3.9	38.6	65.9	0.0	-37.2	-21.9	-11.3	22.5
169	29218.0	322.8	57117.7	-21.9	53.3	63.0	-43.7	4.0	39.7	67.2	0.0	-34.4	-20.9	-11.7	19.8
177	31122.6	322.8	60819.7	-22.5	54.7	64.1	-44.9	4.2	40.7	68.5	0.0	-31.8	-20.0	-12.0	17.2
178	31127.6	322.8	60829.5	-22.5	54.8	64.1	-44.9	4.2	40.7	68.5	0.0	-31.6	-19.9	-12.0	17.0
211	31132.6	0.0	60834.3	-40.2	41.1	37.0	-44.9	4.2	40.7	68.5	0.0	40.4	25.1	-2.5	37.6

Summary of results of mechanical analysis and cladding stress/strain information for individual segment
(Output in the case of IPRINT(14)=1)

Time-step number, time, linear heat rate, burnup

Ridge inner surface of cladding:
total strain in the circumferential, axial and radial directions; creep strain in the circumferential, axial and radial directions; equivalent creep strain; equivalent plastic strain; stress in the circumferential, axial and radial directions; equivalent stress

TITLE

ZORITA-1 GROUP A < Z001P > NOMINAL IFEM 4

FINAL INFORMATION

STAGE		211	CALC. TIMES		692
MAX. TIME	(HR)	31132.6	MAX. DELOR	(MIC)	3.6
MAX. LHR	(W/CM)	364.8	MAX. DELDM	(MIC)	3.6
INI. GAP	(MIC)	168.0	MAX. DELR	(MIC)	0.0
BURNUP	(MWD/TUO2)	60834.3	R. MAXEQSIG	(MPA)	84.1
MAX. TEMP	(DEG. C)	1282.5	R. MAXSIGZ	(MPA)	25.1
F. G. R.	(%)	2.0	R. MAXSIGT	(MPA)	71.3
IOD(10-5 GRAM/CM2)		1.7	MAX. EQSIG	(MPA)	85.7
CR. DOWN(AV.)	(MIC)	-52.4	MAX. SIGZ	(MPA)	51.1
CR. DOWN(MAX)	(MIC)	-48.0	MAX. SIGT	(MPA)	71.3
DEL. DR	(MIC)	-48.0	AV. GAP	(MIC)	27.5
DEL. DM	(MIC)	-49.1	R. GAP	(MIC)	33.5
DEL. RIGDE	(MIC)	1.1	CONTACT LHR	(W/CM)	312.0

Summary of final results of major items
(Output in the case of IPRINT(15) = 1)

Title, segment number

Total number of time steps, irradiation time, maximum linear heat rate, initial gap width, maximum burnup, maximum temperature, iodine concentration, creep down (average) at a designated time step, creep down (maximum) at a designated time step, displacement at ridge of cladding after irradiation, displacement at center of cladding after irradiation, ridge height of cladding after irradiation

Total number of time steps, maximum displacement at ridge of cladding, maximum displacement at center of cladding, ridge height at the time of maximum displacement of cladding, maximum equivalent stress at ridge of cladding, maximum axial stress at ridge of cladding, maximum circumferential stress at ridge of cladding, maximum equivalent stress of cladding, maximum axial stress of claddings, maximum circumferential stress of cladding, average diametral gap width at a designated time step, ridge gap width at a designated time step (diameter), linear heat rate at starting time of contact.

国際単位系 (SI) と換算表

表1　SI基本単位および補助単位

量	名称	記号
長さ	メートル	m
質量	キログラム	kg
時間	秒	s
電流	アンペア	A
熱力学温度	ケルビン	K
物質量	モル	mol
光度	カンデラ	cd
平面角	ラジアン	rad
立体角	ステラジアン	sr

表2　SIと併用される単位

名称	記号
分，時，日	min，h，d
度，分，秒	°，′，″
リットル	l，L
トン	t
電子ボルト	eV
原子質量単位	u

1 eV = 1.60218 × 10^{-19} J

1 u = 1.66054 × 10^{-27} kg

表3　固有の名称をもつSI組立単位

量	名称	記号	他のSI単位による表現
周波数	ヘルツ	Hz	s^{-1}
力	ニュートン	N	$m \cdot kg/s^2$
圧力，応力	パスカル	Pa	N/m^2
エネルギー，仕事，熱量	ジュール	J	N·m
工率，放射束	ワット	W	J/s
電気量，電荷	クーロン	C	A·s
電位，電圧，起電力	ボルト	V	W/A
静電容量	ファラド	F	C/V
電気抵抗	オーム	Ω	V/A
コンダクタンス	ジーメンス	S	A/V
磁束	ウェーバ	Wb	V·s
磁束密度	テスラ	T	Wb/m^2
インダクタンス	ヘンリー	H	Wb/A
セルシウス温度	セルシウス度	℃	
光束	ルーメン	lm	cd·sr
照度	ルクス	lx	lm/m^2
放射能	ベクレル	Bq	s^{-1}
吸収線量	グレイ	Gy	J/kg
線量当量	シーベルト	Sv	J/kg

表4　SIと共に暫定的に維持される単位

名称	記号
オングストローム	Å
バーン	b
バール	bar
ガル	Gal
キュリー	Ci
レントゲン	R
ラド	rad
レム	rem

1 Å = 0.1 nm = 10^{-10} m

1 b = 100 fm^2 = 10^{-28} m^2

1 bar = 0.1 MPa = 10^5 Pa

1 Gal = 1 cm/s^2 = 10^{-2} m/s^2

1 Ci = 3.7 × 10^{10} Bq

1 R = 2.58 × 10^{-4} C/kg

1 rad = 1 cGy = 10^{-2} Gy

1 rem = 1 cSv = 10^{-2} Sv

表5　SI接頭語

倍数	接頭語	記号
10^{18}	エクサ	E
10^{15}	ペタ	P
10^{12}	テラ	T
10^{9}	ギガ	G
10^{6}	メガ	M
10^{3}	キロ	k
10^{2}	ヘクト	h
10^{1}	デカ	da
10^{-1}	デシ	d
10^{-2}	センチ	c
10^{-3}	ミリ	m
10^{-6}	マイクロ	μ
10^{-9}	ナノ	n
10^{-12}	ピコ	p
10^{-15}	フェムト	f
10^{-18}	アト	a

（注）

1. 表1－5は「国際単位系」第5版，国際度量衡局 1985年刊行による。ただし，1 eVおよび1 uの値はCODATAの1986年推奨値によった。
2. 表4には海里，ノット，アール，ヘクタールも含まれているが日常の単位なのでここでは省略した。
3. barは，JISでは流体の圧力を表わす場合に限り表2のカテゴリーに分類されている。
4. EC閣僚理事会指令ではbar，barnおよび「血圧の単位」mmHgを表2のカテゴリーに入れている。

換算表

力	N(=10^5 dyn)	kgf	lbf
	1	0.101972	0.224809
	9.80665	1	2.20462
	4.44822	0.453592	1

粘度　1 Pa·s(N·s/m^2) = 10 P(ポアズ)(g/(cm·s))

動粘度　1 m^2/s = 10^4 St(ストークス)(cm^2/s)

圧力	MPa(=10 bar)	kgf/cm^2	atm	mmHg(Torr)	lbf/in^2(psi)
	1	10.1972	9.86923	7.50062×10^3	145.038
	0.0980665	1	0.967841	735.559	14.2233
	0.101325	1.03323	1	760	14.6959
	1.33322×10^{-4}	1.35951×10^{-3}	1.31579×10^{-3}	1	1.93368×10^{-2}
	6.89476×10^{-3}	7.03070×10^{-2}	6.80460×10^{-2}	51.7149	1

エネルギー・仕事・熱量	J(=10^7 erg)	kgf·m	kW·h	cal(計量法)	Btu	ft·lbf	eV
	1	0.101972	2.77778×10^{-7}	0.238889	9.47813×10^{-4}	0.737562	6.24150×10^{18}
	9.80665	1	2.72407×10^{-6}	2.34270	9.29487×10^{-3}	7.23301	6.12082×10^{19}
	3.6×10^6	3.67098×10^5	1	8.59999×10^5	3412.13	2.65522×10^6	2.24694×10^{25}
	4.18605	0.426858	1.16279×10^{-6}	1	3.96759×10^{-3}	3.08747	2.61272×10^{19}
	1055.06	107.586	2.93072×10^{-4}	252.042	1	778.172	6.58515×10^{21}
	1.35582	0.138255	3.76616×10^{-7}	0.323890	1.28506×10^{-3}	1	8.46233×10^{18}
	1.60218×10^{-19}	1.63377×10^{-20}	4.45050×10^{-26}	3.82743×10^{-20}	1.51857×10^{-22}	1.18171×10^{-19}	1

1 cal = 4.18605 J(計量法)
= 4.184 J (熱化学)
= 4.1855 J (15 °C)
= 4.1868 J(国際蒸気表)

仕事率　1 PS(仏馬力)
= 75 kgf·m/s
= 735.499 W

放射能	Bq	Ci
	1	2.70270×10^{-11}
	3.7×10^{10}	1

吸収線量	Gy	rad
	1	100
	0.01	1

照射線量	C/kg	R
	1	3876
	2.58×10^{-4}	1

線量当量	Sv	rem
	1	100
	0.01	1

(86年12月26日現在)

LIGHT WATER REACTOR FUEL ANALYSIS CODE FEMAXI-IV(VER.2)—DETAILED STRUCTURE AND USER'S MANUAL—